AD-A087 475 QUEEN'S UNIV KINGSTON (ONTARIO) F/6 17/9
PERFORMANCE CHARACTERISTICS OF LEAKY COAXIAL CABLES.(U)
APR 80 J L MASON F19628-77-C-0249
UNCLASSIFIED RADC-TR-79-340 NL

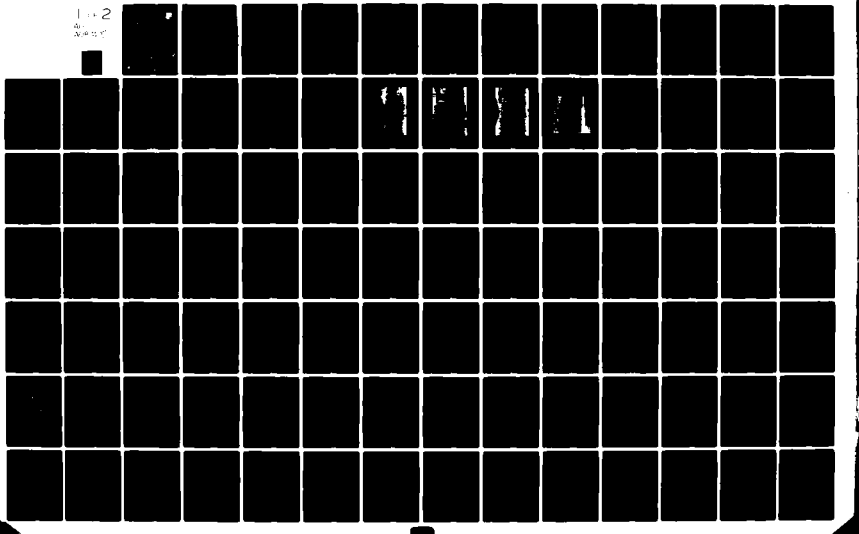

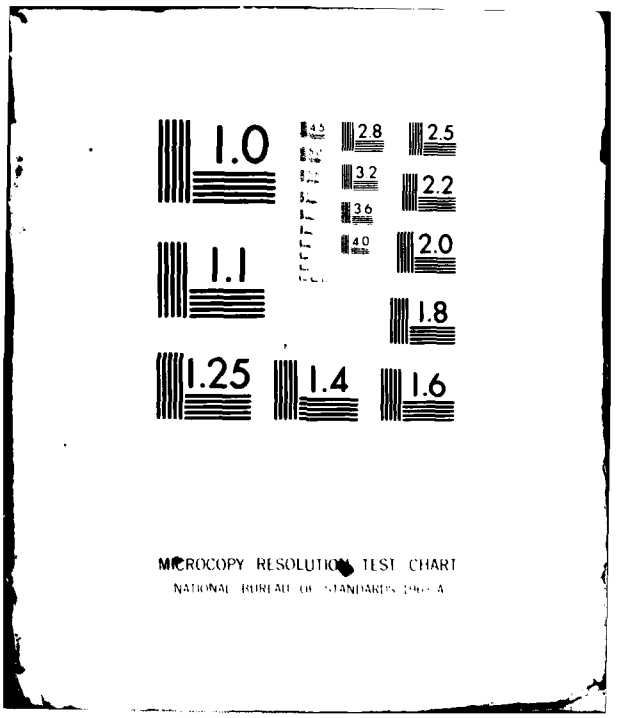
1.0
1.1
1.25
1.4
1.6
1.8
2.0
2.2
2.5
2.8
3.2
3.6
4.0
MICROCOPY RESOLUTION TEST CHART
NATIONAL BUREAU OF STANDARDS 1963-A

RADC-TR-79-340
Final Technical Report
April 1980

LEVEL II

(12)

PERFORMANCE CHARACTERISTICS OF LEAKY COAXIAL CABLES

Queens University

Dr. James L. Mason

ROME AIR DEVELOPMENT CENTER
Air Force Systems Command
Griffiss Air Force Base, New York 13441

This report has been reviewed by the RADC Public Affairs Office (PA) and is releasable to the National Technical Information Service (NTIS). At NTIS it will be releasable to the general public, including foreign nations.

RADC-TR-79-340 has been reviewed and is approved for publication.

APPROVED: Nicholas V. Karas

NICHOLAS V. KARAS
Project Engineer

APPROVED: Allan C. Schell

ALLAN C. SCHELL
Chief, Electromagnetic Sciences Division

FOR THE COMMANDER: John P. Huss

JOHN P. HUSS
Acting Chief, Plans Office

If your address has changed or if you wish to be removed from the RADC mailing list, or if the addressee is no longer employed by your organization, please notify RADC (EEC) Hanscom AFB MA 01731. This will assist us in maintaining a current mailing list.

Do not return this copy. Retain or destroy.

UNCLASSIFIED

SECURITY CLASSIFICATION OF THIS PAGE (When Data Entered)

REPORT DOCUMENTATION PAGE	READ INSTRUCTIONS BEFORE COMPLETING FORM
1. REPORT NUMBER: RADC-TR-79-340	2. GOVT ACCESSION NO.: AD-A087475	3. RECIPIENT'S CATALOG NUMBER
4. TITLE (and Subtitle): PERFORMANCE CHARACTERISTICS OF LEAKY COAXIAL CABLES	5. TYPE OF REPORT & PERIOD COVERED: Final Technical Report, Nov 77 — Jun 79
	6. PERFORMING ORG. REPORT NUMBER: N/A
7. AUTHOR(s): Dr. James L. Mason	8. CONTRACT OR GRANT NUMBER(s): F19628-77-C-0249
9. PERFORMING ORGANIZATION NAME AND ADDRESS: Queens University, Kingston, Ontario, Canada	10. PROGRAM ELEMENT, PROJECT, TASK AREA & WORK UNIT NUMBERS: 62702F, 46001523
11. CONTROLLING OFFICE NAME AND ADDRESS: Deputy for Electronic Technology (RADC/EEC), Hanscom AFB MA 01731	12. REPORT DATE: Apr 80; 13. NUMBER OF PAGES: 163
14. MONITORING AGENCY NAME & ADDRESS (if different from Controlling Office): Same	15. SECURITY CLASS. (of this report): UNCLASSIFIED; 15a. DECLASSIFICATION/DOWNGRADING SCHEDULE: N/A

16. DISTRIBUTION STATEMENT (of this Report)

Approved for public release; distribution unlimited.

17. DISTRIBUTION STATEMENT (of the abstract entered in Block 20, if different from Report)

Same

18. SUPPLEMENTARY NOTES

RADC Project Engineer: Nicholas V. Karas (EEC)

19. KEY WORDS (Continue on reverse side if necessary and identify by block number)

target signature	environmental effects
guided radar	intrusion sensor
leaky coaxial cable	RF sensor
ported cable	microwave sensor
signature analysis	

20. ABSTRACT (Continue on reverse side if necessary and identify by block number)

This work deals with guided radar and reports on the experiments and analysis that were performed to obtain information on the function of leaky coaxial cables used as radio frequency intrusion sensors. Four subjects were investigated: (1) environmental effects on the leaky coaxial cable and the guided radar system, (2) use of doppler shift caused by an intruder to determine the velocity and direction of the intruder, (3) target identification, classification and signature, AND

DD FORM 1 JAN 73 1473 EDITION OF 1 NOV 65 IS OBSOLETE

UNCLASSIFIED

SECURITY CLASSIFICATION OF THIS PAGE (When Data Entered)

293000

4) a single leaky coaxial cable intrusion detection system. The most important environmental factor was moisture, either rain or snow. Results have demonstrated that the velocity of a target moving longitudinally between the leaky cable sensors can be measured, based on the doppler shift in the return signal. Rudimentary target classification has been demonstrated based on a defined target signature-the log-magnitude of the Fourier transform of the target vector. A single cable intrusion detection system was investigated which incorporated a modulation technique which allowed the intruder to be located.

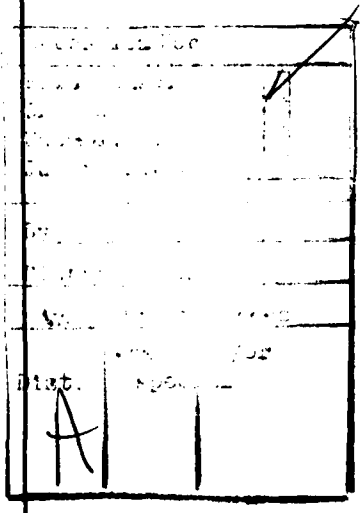

TABLE OF CONTENTS

List of Figures

List of Tables

EVALUATION

Because of the increasing costs of resources, the increasing attempts at sabotage or destruction of these resources by individuals or small groups, whose methods have become more sophisticated, and the increasing costs of security personnel, the development of intruder detection systems has become a prime objective of USAF, of DoD, and of many other government agencies. One intruder detection concept, which has many possible system configurations, uses a leaky coaxial cable as the primary sensor. To properly use this type of cable, the properties of the cable should be understood and the cable performance known under a wide variety of conditions and situations. The work in this contract deals with determining analytically and experimentally the properties and performance of leaky coaxial cables.

Nuisance alarms plague most, if not all, intruder detection systems. A nuisance alarm is one generated at the sensor by any source that exhibits signatures similar to those of personnel, vehicles or craft (e.g. wildlife, or fish). The ability to identify an intrusion from the intruder characteristic signature would decrease the nuisance alarm rate, thereby increasing the effectiveness of the intrusion system. Results indicate that it is possible, in principle, to obtain a library of target signatures, and from these determine criteria for identifying an intrusion.

Leaky coaxial cables, used as sensors, lay on the ground or are buried. In either instance, the weather affects their performance, and this, in turn, affects vital system parameters such as target sensitivity, cable profile, and false alarm rate. Experiments investigated the relationship between changes in

the environmental medium and changes in the various parameters of the intrusion system. Knowing this relationship greatly helps in designing leaky coaxial cable sensor systems that will operate effectively in all kinds of weather.

The work described in this report adds significantly to the knowledge that is needed to design a leaky coaxial cable sensor system that meets government requirements.

Nicholas V. Karas

NICHOLAS V. KARAS
Contract Monitor

Performance Characteristics
of
Leaky Coaxial Cables

1.1 Introduction

This is the final report required under USAF contract No. F19628-77-C-0249. It deals, in the main, with the subject of guided radar and discusses a number of experiments, analytical procedures and finally, conclusions, of a project designed to update the scientific information available on this topic.

Queen's University has been in the forefront of research devoted to obstacle detection techniques using guided radar, and various staff members have played an important role in the development of this field. A bibliography containing many of the publications of interest is provided at the end of this report.

The first successful attempt to detect an obstacle using guided radar was performed by Mackay in 1973 and a reliable technique to perform the task was reported by Penstone and Mackay in 1974. A joint effort by Queen's University and Computing Devices Company resulted in the development of the first field equipment in 1977 under a contract with the Canadian Penitentiary Services. Further development of the equipment together with extensive field trials, laboratory experiments and analytical studies has continued under various contracts with the USAF, the Canadian National Research Council and other government agencies in Canada and the U.S. This report adds to the general body of knowledge that is steadily growing in this area and provides new insights to problems of target detection and identification.

The report is mainly concerned with the following aspects:

(a) Environmental studies

(b) Velocity measurements

(c) Target identification, classification and signature analysis

(d) Development of a single-cable technique for relatively short perimeters.

The study of various phenomena related to guided radar is fraught with difficulties. In a general sense, a reasonable model of the propagation of energy along the medium (i.e. via leaky coaxial cable and through the immediate surroundings of the cable) has been hypothesized by Beal [1,2] which appears to match observation more closely than other workers [3]. Indeed, the results of well-controlled labora-

tory experiments agree very well with theory for relatively short lengths of cable [4]. There has been some difficulty, however, in trying to expand the theory to fully meet the practical situation, in which very long lines are used and the environment is relatively uncontrollable. The problem, essentially, is not that the theory is incorrect, but rather that it is extremely difficult to characterize the environment of a long perimeter through various soil formations and climatic conditions. General statements as to the performance of guided radar systems in various environments have indeed been made, but the ability to reliably verify the conclusions is limited by the means available to accurately identify the environment surrounding a buried cable. Continuous and long-term experimentation is therefore necessary to provide much-needed data to compare with hypothesis. With this in mind, therefore, this project has concentrated in the main on providing a good data base for further study. Many of the experiments performed required considerable sophistication of equipment and deployment of personnel and were designed to provide data on a number of aspects of the project; results for each particular purpose were often obtained by processing the general data base in a particular manner.

While the theory of propagation via guided radar has received much attention, often because of its application to the communications field, little is yet known of the interaction of a target with the detection zone. General information, concerning the reflected power expected from various targets, the influence of a target on the incident field and the region of detection around the cables has been reported in the past.[5] However, little work has been done on precisely what constitutes a target for guided radar. This information could be very useful for developing target classification schemes which would allow a reduction in the false alarm rate in a deployed system. A start has been made on this problem and the results are presented in this report.

At the present time, a number of field models of guided radar instruments are being deployed on a trial basis. In addition, it appears likely that further commercial development of several single-cable techniques will continue over the next few years. The success of many of these attempts to develop reliable systems for various purposes will still depend on a proper understanding of the pehnomena involved and on the interaction between various targets and the detection procedure. This report is intended to assist these attempts in providing reliable up-to-date data on several important items.

1.2 Outline of Report

Section 2 of this report is a description of the guided radar research facility at Queen's University. Included is a summary of the characteristics of the leaky coaxial cables used in the experiments. A brief description is given of the signal processing equipment and automated data logging system.

Much more detailed information on the system is available in theses by Vinnins [6] and Patterson [7].

Section 3 presents the results of the experiments designed to assess the effect of changing weather conditions on the performance of a guided radar system. This work was carried out during the winter and early spring of 1979.

The work presented in Section 4 demonstrates that a guided radar system can be used to measure the velocity of targets within the detection zone. Experiments are also reported in which the velocities of two targets simultaneously within the detection zone were independently measured.

Section 5 describes target classification experiments performed using a variety of different targets including human beings, a dog, a car and a wooden trolley. An explanation is given of some of the distinctive features of these signatures.

One approach to analysing target signatures is to simulate the expected signal return from targets based upon a knowledge of their motion dynamics and the characteristics of the guided radar system. Some preliminary work has been done using this approach and is reported in Section 6.

Section 7 deals with a novel single-cable guided radar suitable for relatively short perimeters. A technique is described which allows not only detection but also location of targets even though the system operates in a continuous wave mode.

Section 8 summarizes the results obtained during the contract period and also contains suggestions for possible future research in guided radar.

2. System Description

2.1 Field Site

The experimental work described in this report was carried out at the Queen's University test site situated approximately eight kilometers northeast of Kingston. The facility consists of a 15 m long trailer and a large grass covered field. The trailer can be either air conditioned or heated to maintain the inside temperature at 18° C.

A plan view of the field site is shown in figure 2.1. Along the western edge of the site there is a fence line and a gravel road. Between these, the ground slopes downward towards the road and is tree and bush covered. Trees also line the northern boundary of the site. There is also a 65 metre long section of normal gravel railroad bed 3 metres wide and 30 cm deep. Standard wooden ties and tracks are installed on the gravel bed according to railroad practice.

The leaky coaxial cables were normally laid on the ground or suspended at various heights in the air on wooden stakes. All the cable installations were in the open part of the field site a minimum of 8 metres away from any trees.

Figure 2.2 is a photograph of the trailer which housed all the signal processing and data logging equipment. A section of the railway track is also visible in the photograph as is the wooden moveable platform or trolley which was used as a target in some of the experiments described in this report. The trolley was propelled by a rope and pulley arrangement driven by a 3 h.p. dc motor. Figure 2.3 is a photograph of the central cable run which allowed experiments to be performed using a variety of cable spacings and heights above the ground. Figure 2.4 is a photograph taken inside the trailer at the operator's console of the data logging computer. The operator had a good view of the test track through the front window and of the other cable runs through the side window. The photograph in figure 2.5 shows the analogue equipment which made up the guided radar system.

2.2 Cables

All of the leaky coaxial cables used in the tests described in this report were manufactured by Andrew Antenna Company Ltd., Ontario Canada and were of the RADIAX type. These cables are constructed in an identical manner to standard HELIAX coaxial cable with the exception that slots have been milled in the solid outer conductor prior to the plastic sheath being applied. It is these slots that cause the cables to be "leaky".

A family of RADIAX cable types are manufactured by Andrews, differing only in the size of the slots in the outer conductor. These have been named by the manufacturer RX4-1, RX4-2 and RX4-3, in ascending order of slot size and consequently "leakiness". All three cable types were used at the field site. Manufacturer's specifications for these cables are given in Table 2.1. A photograph showing the cable construction is given in figure 2.6.

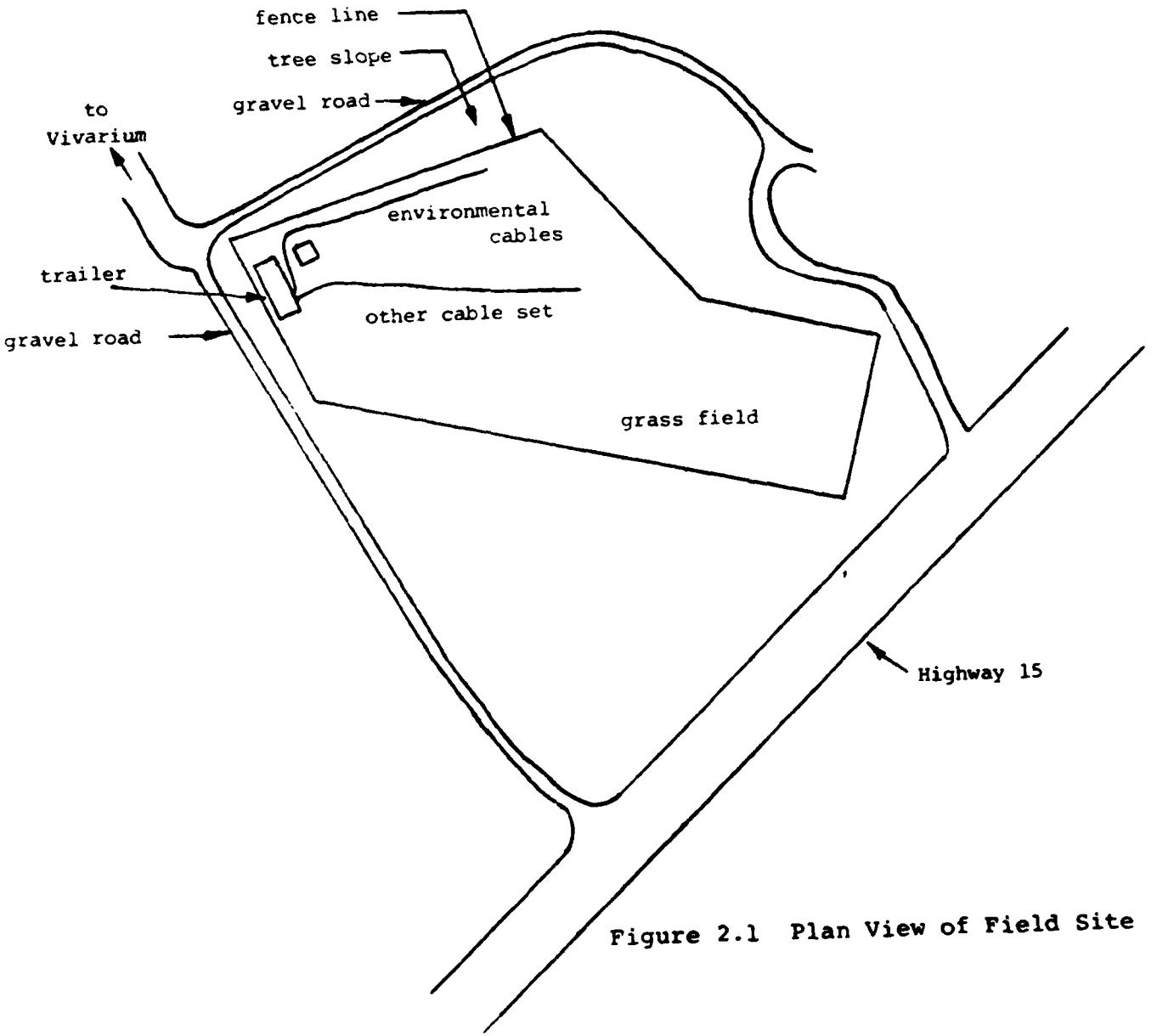

Figure 2.1 Plan View of Field Site

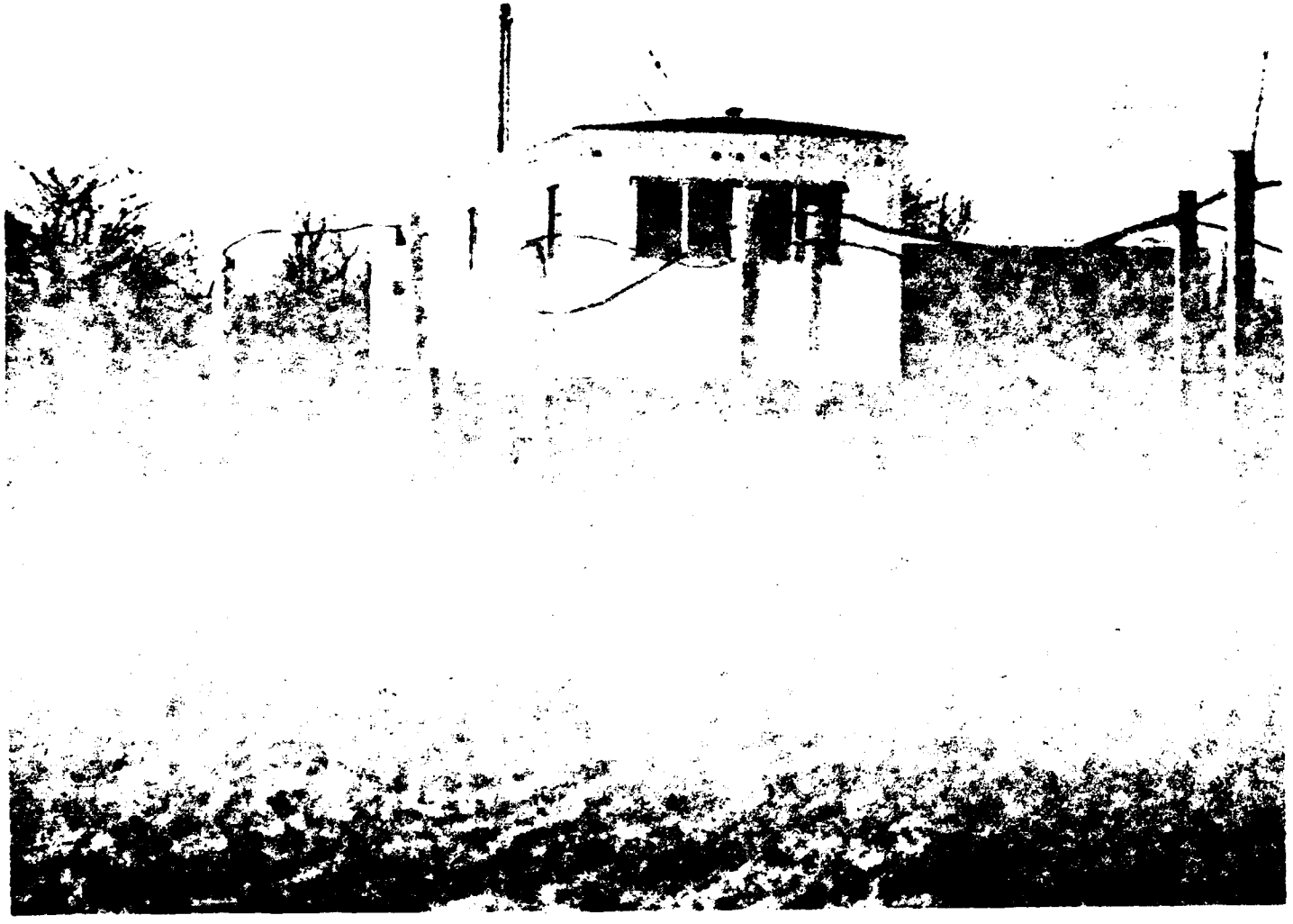

Figure 2.2: Trailer, Railway Track and Trolley

Figure 2.3: Central Cable Run

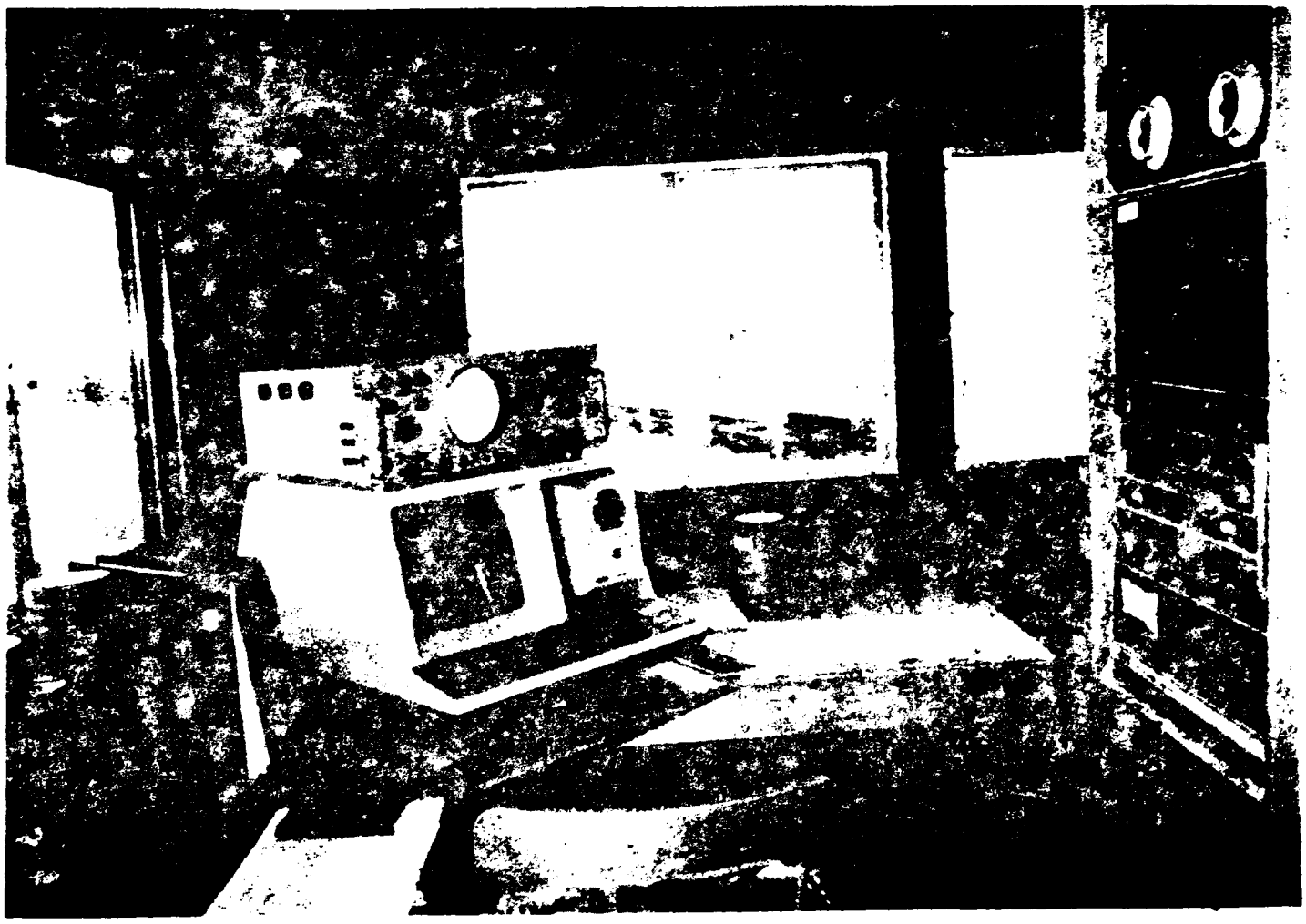

Figure 2.4: Operator's Console

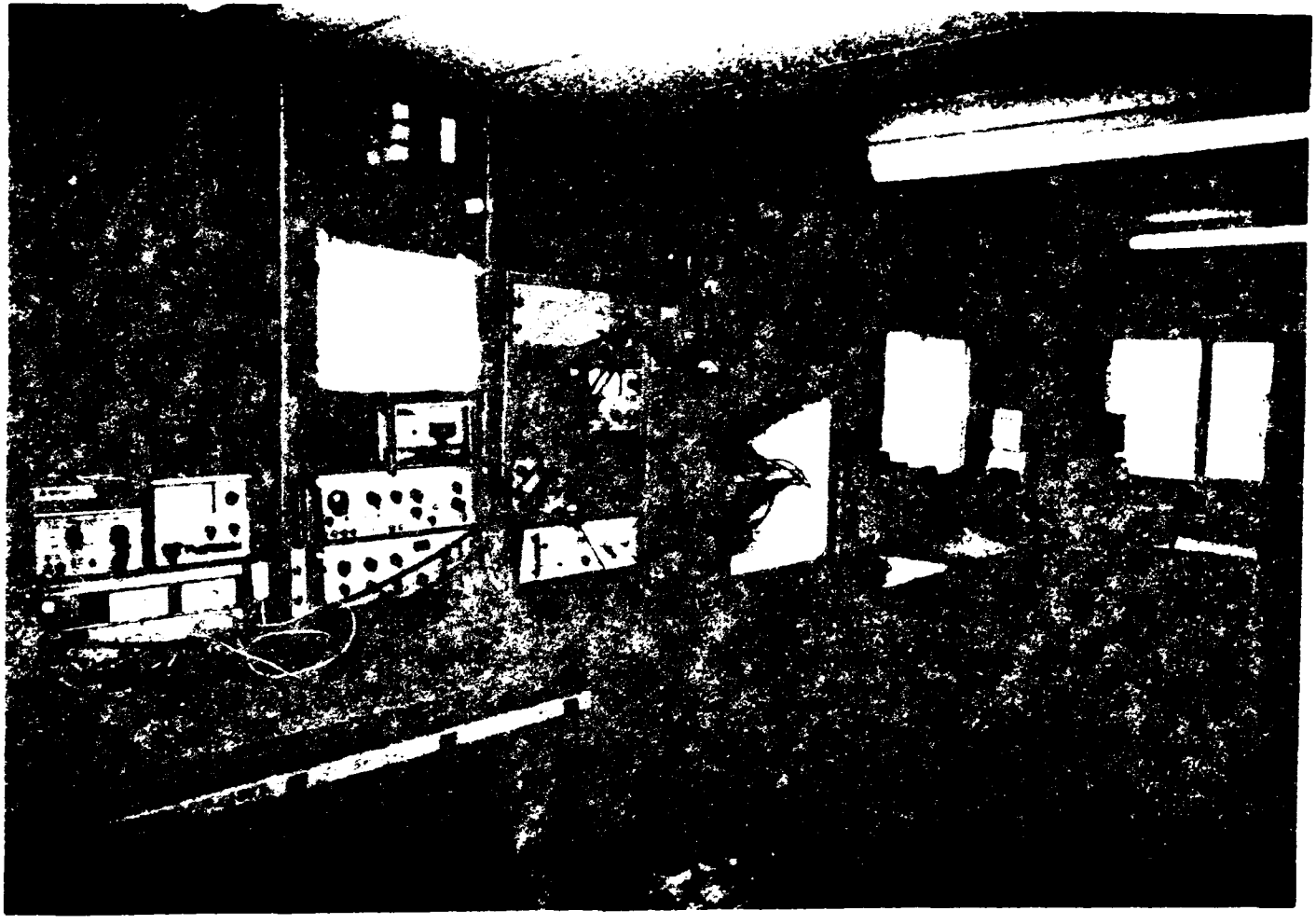

Figure 2.5: Guided Radar Analogue System

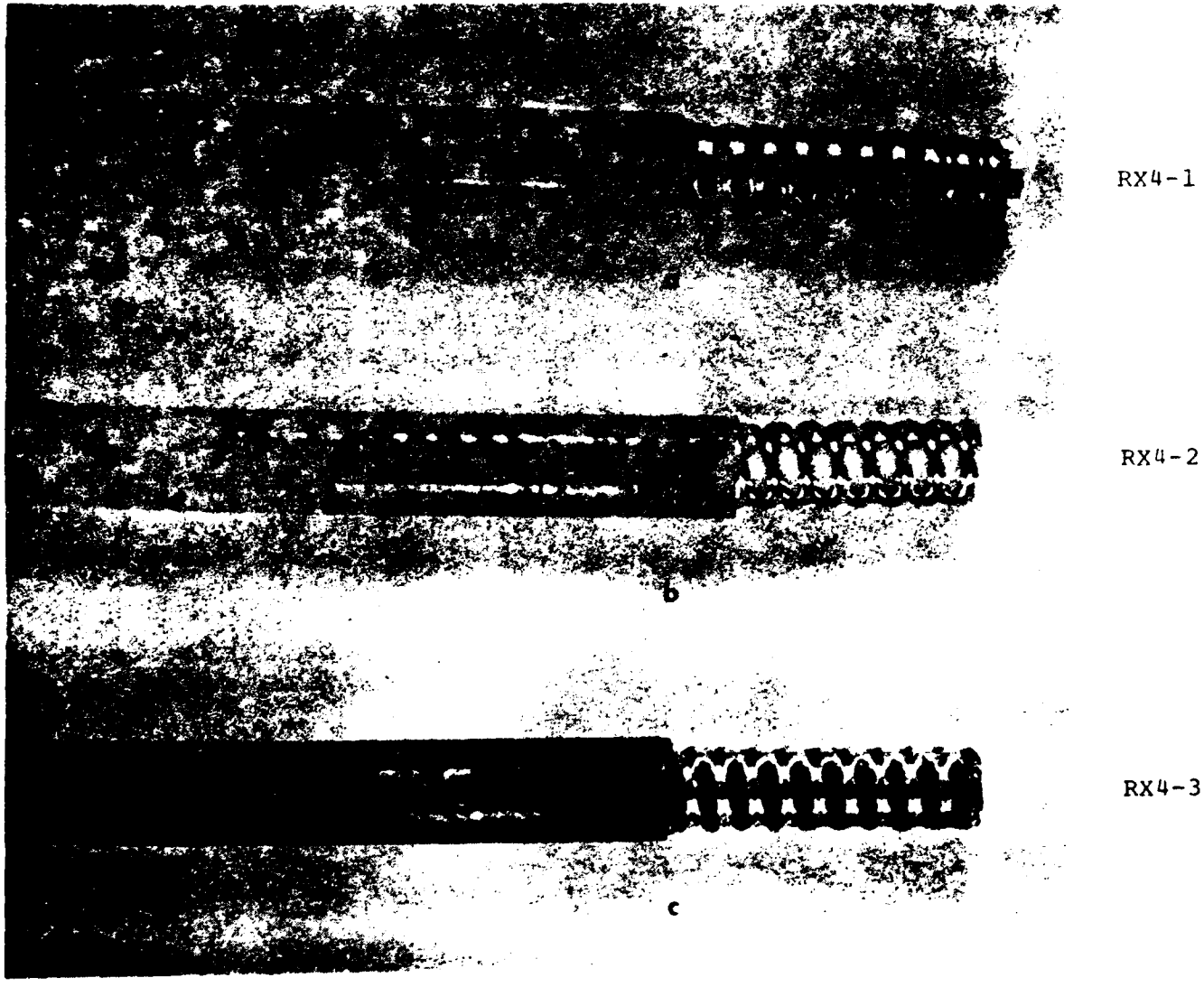

Figure 2.6: Leaky Coaxial Cables

Table 2.1

SPECIFICATIONS FOR LEAKY CABLES AT 60 MHz

	RX4-1	RX4-2	RX4-3
Nominal size	1/2"	1/2"	1/2"
Impedance, ohms	50	50	50
Velocity, percent of velocity of light in free space	79	79	79
Typical VSWR	1.3	1.3	1.3
Attenuation, in free space (dB/100 ft)	0.6	0.75	1.1
Coupling Loss (dB at 20 ft.)	83	76	71

The standard cables used were a total of 470 feet in length and were made up of a lead-in section 200 ft. long, 350 ft. of radiating cable and a 20 ft. long termination section. The lead-in and termination sections were non-radiating HELIAX. The centre conductor and dielectric were continuous throughout the total length of the cables and no connectors were necessary between the HELIAX and RADIAX portions. N-type connectors were installed in both ends of the cables.

The cables were either laid on the surface of the ground or suspended in the air on wooden stakes. A variety of cable runs were installled which allowed the cables to be placed at different heights ranging from 0 feet to 6 feet and at different spacings from 5 feet to 12 feet.

2.3 Analog Hardware

2.3.1 Introduction

The guided radar transmitter and the analog portion of the receiver is built up of commercially available processing blocks which can be configured as either a pulsed or continuous wave system. The interconnection of the various units is made through coaxial relays which can be controlled by the data logging computer. This allows the system to operate unattended for long periods of time with system reconfiguration occurring, as appropriate, under software control.

2.3.2 Pulse Mode

Short bursts of an RF carrier are transmitted. Three crystal controlled frequencies are available; 30, 60, 120 MHz. The pulse width is manually controlled and was normally set to 60 ns for the experiments described in this report. The pulse repetition rate is controlled by the PDP-11 computer and was normally 2.2 μsec.

The receiver consists of a broadband preamplifier, followed by a synchronous detector and a 7 MHz bandpass amplifier. The local oscillator could be phase shifted by 90° under computer control allowing either the in-phase (I) or quadrature (Q) component of the return signal to be monitored.

A block diagram of the pulse system is shown in figure 2.7.

2.3.3 CW Mode

In the CW mode a continuous carrier is transmitted at the selected frequency. The receiver consists of a hybrid, to provide the required quadrature local oscillator, a pair of mixers, a pair of chopper stablized amplifiers with switch selected gains and a computer controlled electronic switch to select which received signal component is to be monitored. The continuous wave system is shown in block form in figure 2.8.

A summary of some of the important characteristics of the analog portion of the system is given in Table 2.2.

2.4 Digital Hardware

2.4.1 Introduction

The digital portion of the guided radar system consists of three sections: 1) Sampler and digital preprocessor, 2) preset and timing logic and 3) PDP-11/10 minicomputer. These will be briefly described in the following subsections. A block diagram of the system is given in figure 2.9.

2.4.2 Sampler and Digital Preprocessor

The sampler and preprocessor section of the system performs the digitization of the base-band return signal.

Band-limited components of the return signal are multiplexed, and fed by the R.F. hardware into a high speed, sample and hold module which, in turn, feeds the analog sampled values into a high speed 8-bit successive approximation analog-to-digital converter. In order to increase the signal-to-noise ratio of the return signal, many successive samples of each component are added together. Due to speed limitations, the PDP 11/10 cannot perform this operation in a reasonable time and hence a preprocessor unit is required to sum consecutive samples of the components in each phase. Upon completion of the required number of integrations, the integrated data is passed on to the computer, ready for storage on the magnetic tape. Figure 2.10 is a block diagram of the organization of the preprocessor.

Table 2.2

GUIDED RADAR SYSTEM SPECIFICATIONS

General	
Carrier Frequency	1 MHz to 450 MHz variable 30, 60, 120 MHz crystal controlled
Output Power	10 watts peak
RF Bandwidth	50 MHz
Receiver noise figure	6 dB
Pulse Mode	
Pulse width	40 ns min, manually controlled
Pulse repetition rate	450 KHz max, computer controlled
Resolution	$\geq$ 8 ft in RADIAX
Baseband Bandwidth	7 MHz
CW Mode	
Baseband Bandwidth	32 Hz

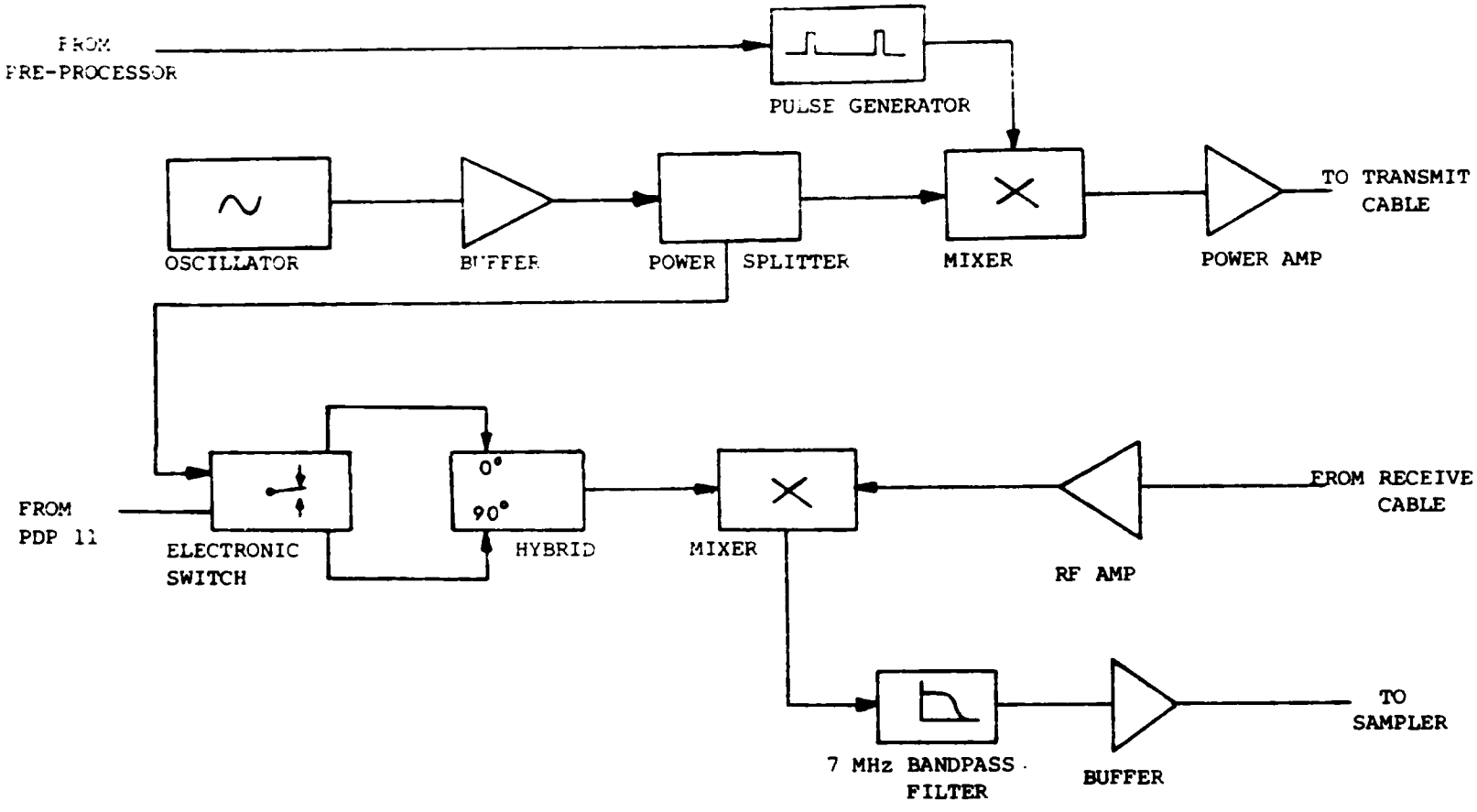

Figure 2.7 Pulse Analog System

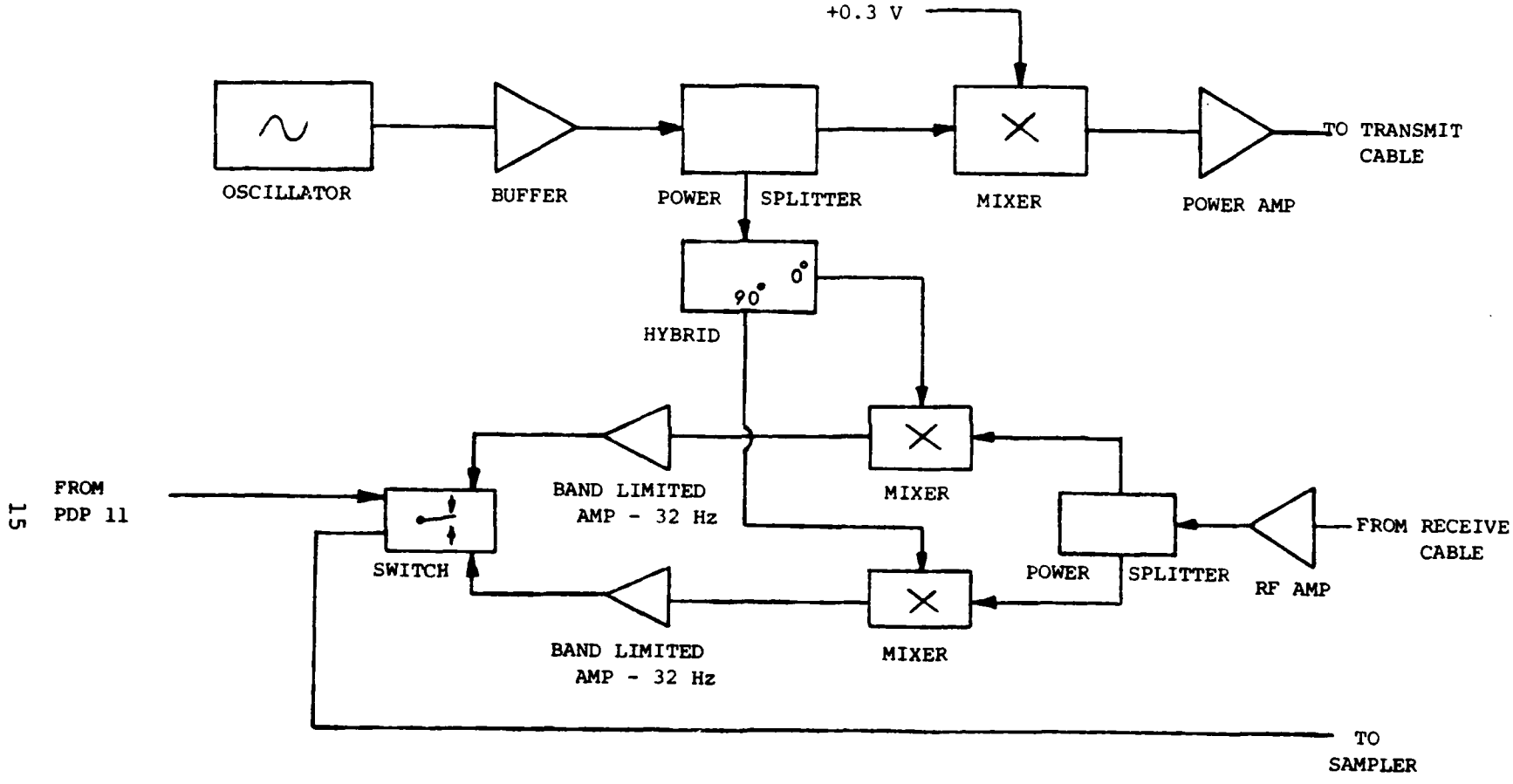

Figure 2.8 CW Analog System

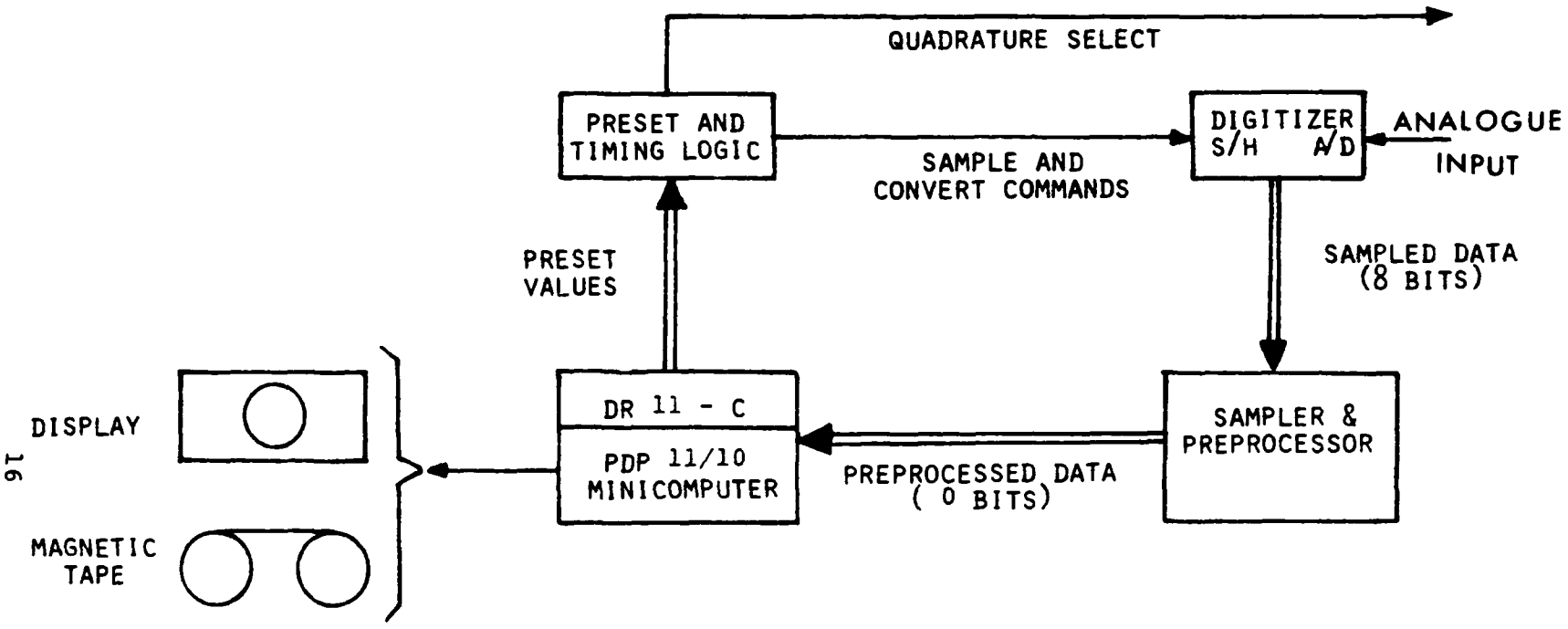

Figure 2.9 Digital Hardware

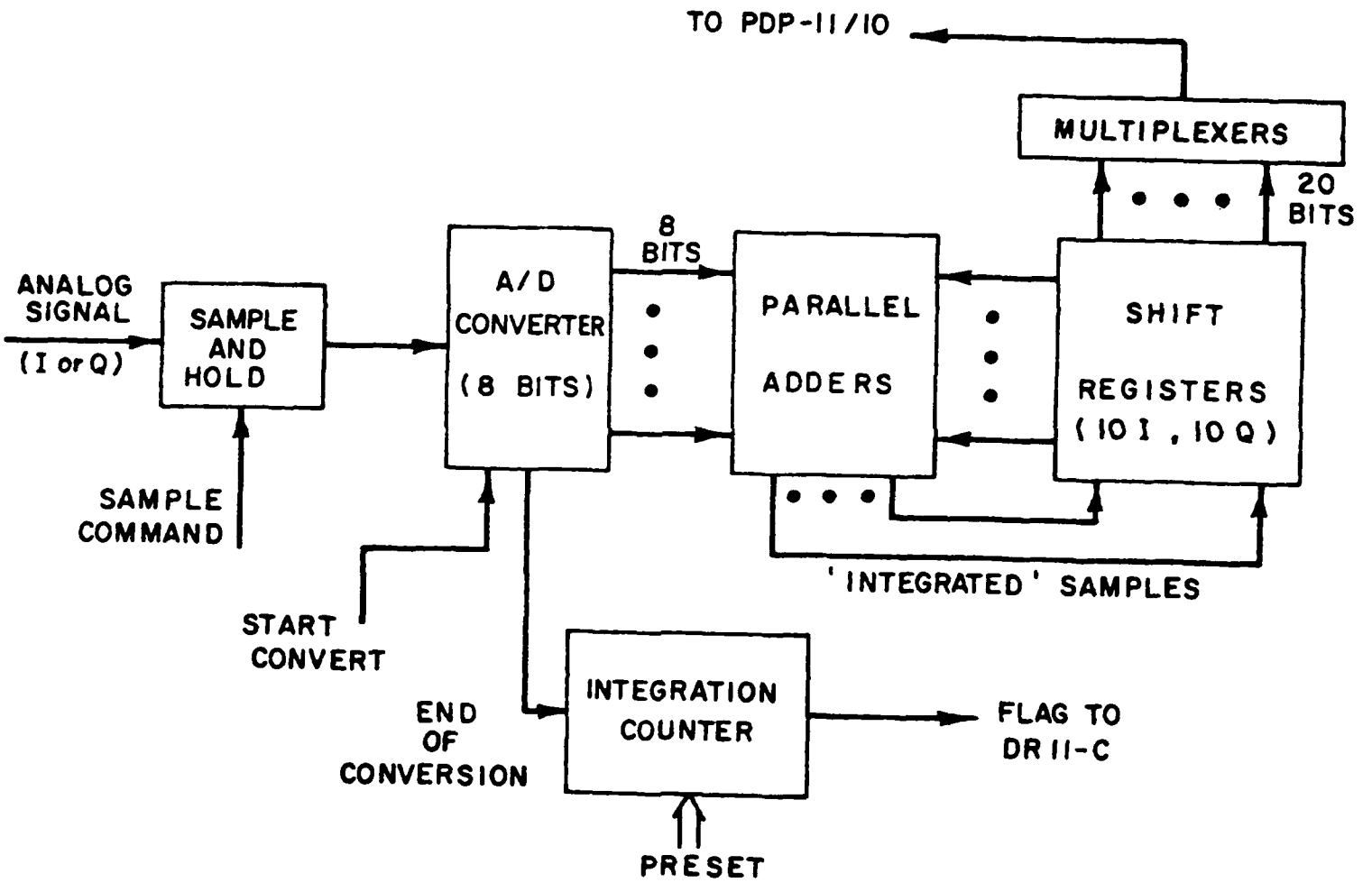

Figure 2.10 Preprocessor

2.4.3 Preset and Timing Logic

The preset and timing logic section controls the events within the system in accordance with the system control parameters. The timing logic works on an internal 50 MHz TTL clock from which it synchronizes the events in the system. Thus, on command from the timing logic the selection of either the in-phase or quadrature phase by the electronic switch, the issuing of the sample commands to the sample and hold, and the start conversion to the ADC, take place, in the proper sequence. The preset logic also stores the required number of integrations and keeps track of the number of integrations performed by the preprocessor, flagging the computer on completion.

2.4.4 The PDP 11/10 Minicomputer

The minicomputer serves as the control centre and performs the function of managing the operation of the guided radar system. Operating parameters are entered through a teletype system. Operating parameters are entered through a teletype terminal. The relevant information, in turn, is conveyed to the different sections within the system. Upon completion of all operations, including the preprocessing of the data, the computer is flagged by the preprocessor and reads the data through a DR-11 digital interface. This data can be processed in real time and the results displayed on an oscilloscope through a digital-to-analog converter (DAC), or alternatively, can be stored on DEC-tape for later analysis on a larger PDP-15 computer located at the University.

2.5 System Parameters

2.5.1 Introduction

The guided radar system has an inherent flexibility of operation wherein the adjustment of certain system parameters is possible, either manually or by program control through the computer. This is necessary because the system is designed to be a scientific tool rather than an operational detection system.

The relevant parameters of the system are the following:

1. Sampling frequency rate
2. Number of integrations
3. R.F. carrier frequency
4. Transmit power.

2.5.2 Sampling Frequency Rate

The sampling frequency rate is computer controlled. The doppler frequency in the return signal is a measure of the velocity of a target. Under Nyquist's criterion, the sampling frequency rate should be at least twice the maximum frequency to be measured. Hence the selection of the sampling rate will be determined by the range of velocities of the targets to be detected. For this system, the rate can be varied between 24 KHz and 450 kHz. As will be seen in the next section, the combination of this parameter and the number of integrations will determine the fastest detectable target velocity.

2.5.3 Number of Integrations

To increase the signal-to-noise ratio of the system, successive sampled values are integrated. While integration of the sampled data improves the signal-to-noise ratio, it also decreases the effective sampling frequency rate of the system.

Thus, in any experiment, an optimum choice of the two parameters is necessary. The number of integrations performed on each component can be selected within the range of 1 to 4096.

2.5.4 R.F. Carrier Frequency

The R.F. carrier frequency can be manually selected to be either 30 MHz, 60 MHz or 120 MHz. Several parameters affect the particular choice of operating frequency. The cables have a useful performance range of 20 MHz to 400 MHz. Reduction in leakage at low frequencies and attenuation effects at higher frequencies limit their usefulness outside this range. In the study of moving targets, the choice of a particular frequency is determined by the maximum expected target velocity. Since the doppler frequency shift is directly proportional to target velocity and carrier frequency, the use of a higher carrier frequency provides a better resolution in the detection and measurement of the velocity of slower moving targets, while a lower carrier frequency is more apt for faster targets that might otherwise have been outside the system bandwidth as determined by the effective sampling rate.

2.5.5 Transmit Power

The maximum continuous transmit power of the system is 5 watts. However, the return signal power varies from experiment to experiment depending upon factors such as the size of the slots in the outer conductor, the separation between the cables, and the prevailing environmental and weather conditions. Thus for each experiment, the transmit power is chosen to be the highest possible, consistent with the dynamic range of the receiver.

3 Environmental Effects

3.1 Introduction

From past experience it is known that the type of ground upon which leaky cables are laid affects their performance in a guided radar system. Furthermore the condition of the ground -- whether it is frozen, wet, moist, dry -- also has considerable influence on system parameters such as target sensitivity, cable profile and false alarm rate. The purpose of the experiments described in this chapter was to investigate the relationship between changes in the environmental conditions and changes in various parameters of a guided radar system. The work was carried out during the winter and early spring seasons when the most significant changes in ground conditions would be expected to occur.

An automated data logging system was set up which allowed a variety of measurements to be made on both a pulse and CW guided radar system at regular intervals. The details of the operation of the system are given in Section 3.2 and the measurements made are described in Section 3.3. The results and a discussion of them is given in Sections 3.4 to 3.9 Section 3.10 is a summary of this phase of the project.

3.2 Data Logging Facility

A pair of RADIAX RX4-2 cables, 350 feet in length were used for the monitoring of the effect of weather conditions on the guided radar system. These cables were laid parallel to each other, approximately 6 feet apart along the western boundary of the field site. Their location has been marked on figure 2.1 , the plan view of the site. The cables were laid on the surface of the ground several months before monitoring began.

Six soil moisture cells and three soil temperature cells were also installed near the trailer end of the cables. A detailed schematic of the cable placement is given in figure 3.1.

The computer based data recording facility is shown in figure 3.2. The data was recorded on DECtape on the PDP/11 minicomputer and transferred to the main university campus for processing on a PDP/15. Mode selection hardware consisting of a group of coaxial relays and a logic block allowed either the CW hardware or the pulse system hardware to be selected under software control. The CW and pulse hardware were described in Section 2.3.3 and 2.3.2 respectively, of this report. A computer controlled stepping relay allowed the soil moisture and temperature cells to be sequentially sampled when desired.

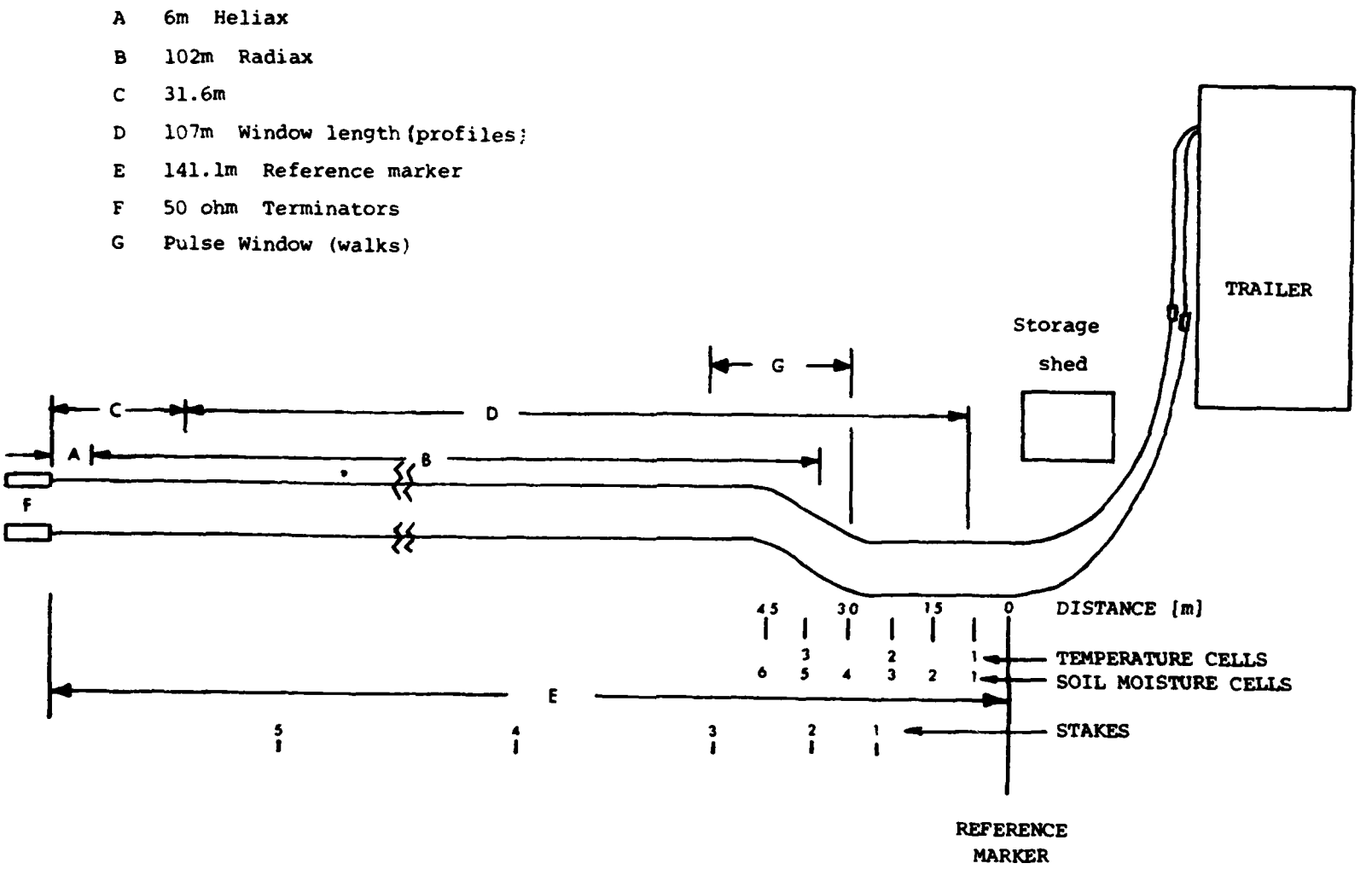

Figure 3.1: Cable Placement

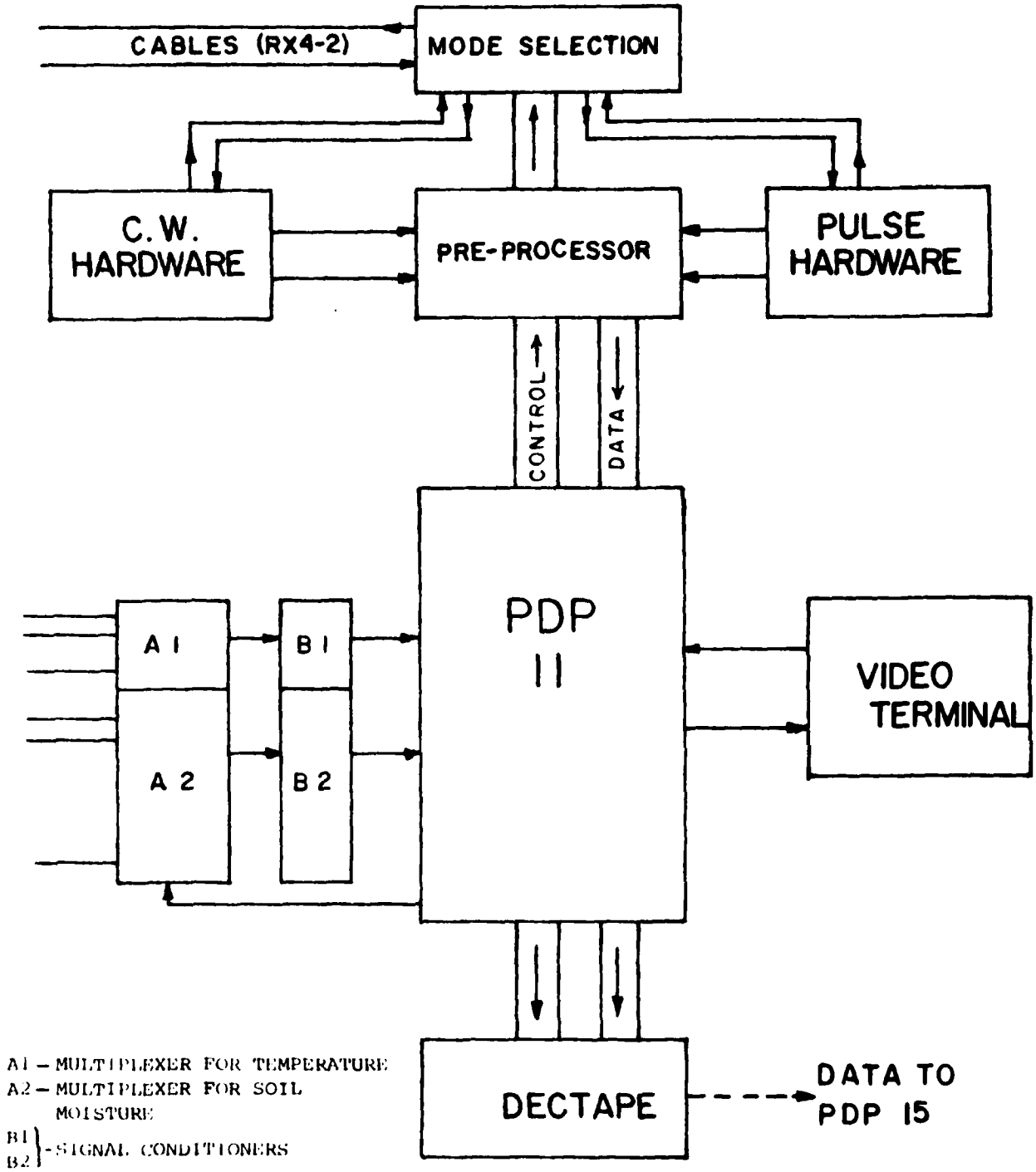

Figure 3.2: Environmental Data Recording Facility

3.3 Measurements

3.3.1 CW Profile

The system components were configured as shown in figure 2.8 . Each time a CW profile measurement was made 250 samples of both the I and Q components of the return signal were recorded. Each sample of a particular component was the sum of 4096 individual readings and the time taken for measurement was 4.5 seconds. The effective profile sampling rate was 27 Hz.

3.3.2 Pulse Profile

Figure 2.7 shows the pulse guided radar system used for these measurements. A window, consisting of 50 range cells, a total of 107 metres long was monitored. The window started 35 metres from the transmitter end of the cables and was positioned as shown in figure 3.1.

Five complete profiles were recorded during an interval of 4.5 seconds. Therefore, the effective sampling rate was 1.1 Hz.

3.3.3 Sensitivity

The system sensitivity was measured at various times by means of a standard walk. The target, a human, moved down the length of the cables midway between them and the resulting target response was used as an indication of system sensitivity. A standard walk was carried out every three or four days between February 14th and April 1st. More frequent walks were taken during rapid changes in environmental conditions.

3.3.3.1 Data Format

The system response during the standard walk was recorded using the pulsed guided radar system described in Section 2.3.2.

The system parameters were:

Pulse width	60 ns
Repetition rate	456 kHz
Number of integrations	4096
Number of range cells	10
Range cell length	8 ft.
Window length	80 ft.
Window position	350 ft. from transmit end of the cables

A complete profile consisted of 4096 x 10 samples of each return signal component (I and Q). Therefore the effective profile sampling rate was $\frac{456 \times 10^3}{4096 \times 10 \times 2} = 5.6$ Hz. The data was recorded directly onto DECtape at the field site and then transferred to the departmental computer system for processing. Figure 3.3 shows the format in which the data was recorded at the field site.

3.3.3.2 Method of Walking

The return signal was recorded for a period of approximately 34 seconds before the target entered the detection zone. The target then positioned himself between the cables at the point marked in figure 3.1 and proceeded to walk at a velocity of 0.9 m/sec. The track of the target was approximately midway between the two cables.

The walk started 30 metres before the observation window and continued for 15 metres past the window. The target stopped at marked locations every 27 m for a period of five seconds.

The walks were done under a variety of weather conditions; consequently there were variations in how the target moved from one walk to another. The target took small steps (<0.3 m) if possible, to minimize the influence of leg motion on the results. The feet remained as close to the ground as possible. However, when there were large accumulations of snow it was impossible to maintain this style of walk. Consequently, a number of different walk styles were used.

When the snow was deep and uncompacted the target still took small steps but had to lift his feet a considerable distance above the ground for each step. Since all walks were taken along the same route footprints became well defined in the snow and were used as guides for subsequent walks. In very deep powder snow, snowshoes were used.

At various times during the winter a thick ice crust formed on the accumulated snow base. This crust was thick enough to support the weight of the target and, therefore, the target walked above the ground at a height equal to the snow depth.

Although the exact conditions of the target's walk varied throughout the measurement period, the differences in style would not be expected to greatly influence the results.

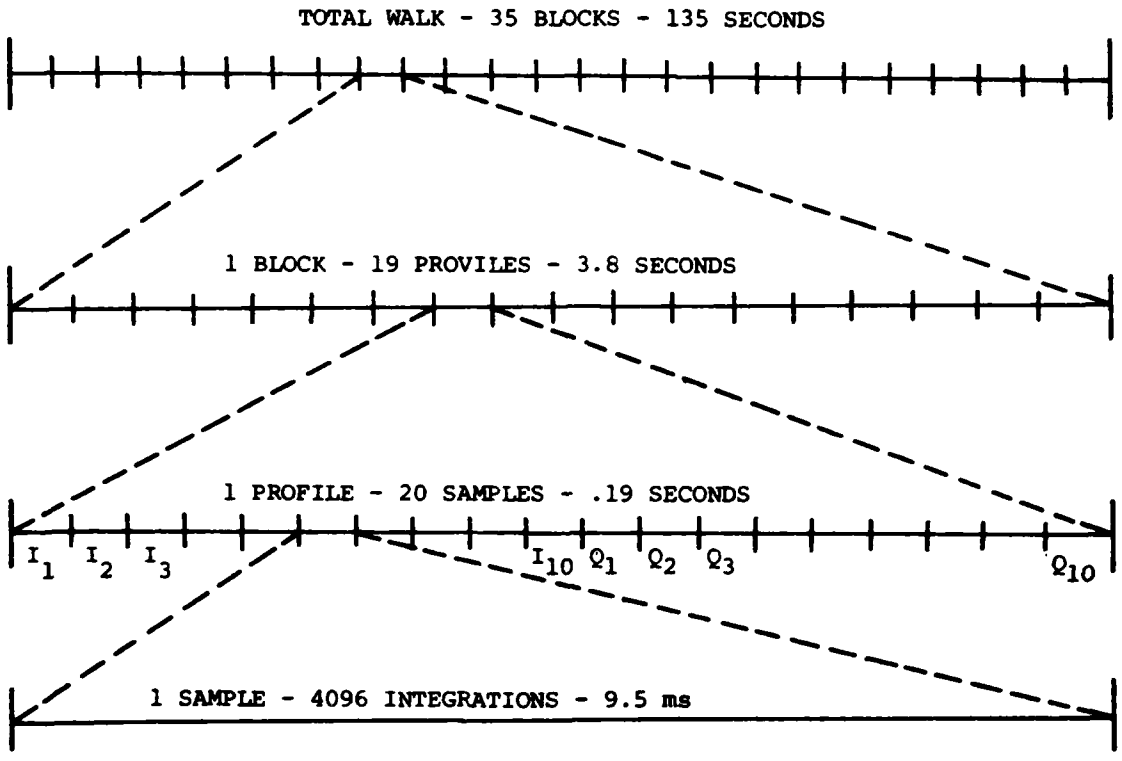

Figure 3.3: Format of Data from Field Site

3.3.4 Environmental Data

The soil moisture and soil temperature cells were sampled each time an automated profile measurement was made. The resulting data was recorded on DECtape.

A log of the environmental conditions was made for each visit to the field site. The data recorded included air temperature, general weather conditions and snow depth at six selected positions along the length of the cable.

More detailed environmental data was available from the Environment Canada weather office at Norman Rogers airport. This office is located approximately five miles south-west of the field site. Monthly summaries from Environment Canada contain hourly air temperature readings, average snow depth on the ground, wind velocity and direction, information concerning the onset of rain or snow and general weather conditions

3.4 General weather conditions

The majority of the experiments dealing with the effect of weather conditions on the leaky cable sensor were performed between January 8, 1979 and April 25, 1979. This period of time includes the portion of the winter season when snowfall is heaviest and snow cover is most variable as well as the spring thaw and early spring conditions. An overview of the weather conditions can be obtained from the records maintained at Environment Canada, Kingston Weather Office. Based upon the weather summaries kept there, the conditions for the relevant months in 1979 were typical of those occurring in other years.

Monthly summaries, for January to April 1979, provided by Environment Canada for the Kingston Airport Weather Office, are attached to this report as Appendix A. Relevant data from these summaries have been plotted in figures 3.4 and 3.5. Figure 3.4 is a plot of the daily maximum and minimum temperatures. Also plotted is the daily rainfall. Figure 3.5 is a plot of the snow on the ground and the daily snowfall.

The temperature ranged from -32°C on February 10 to +19°C on April 20. There were several periods of warm weather during the winter when the ground was snow covered and when the temperature was above 0°C and precipitation, in the form of rain, occurred. These were separated by cold spells. Snow on the ground ranged from 0 cm to 45 cm with the largest snowfalls being in January. The snow cover dropped rapidly at the beginning of March, disappearing completely on March 13. There was also considerable rain during this period. The end of March and beginning of April was also a period of generally warm weather and heavy rainfall.

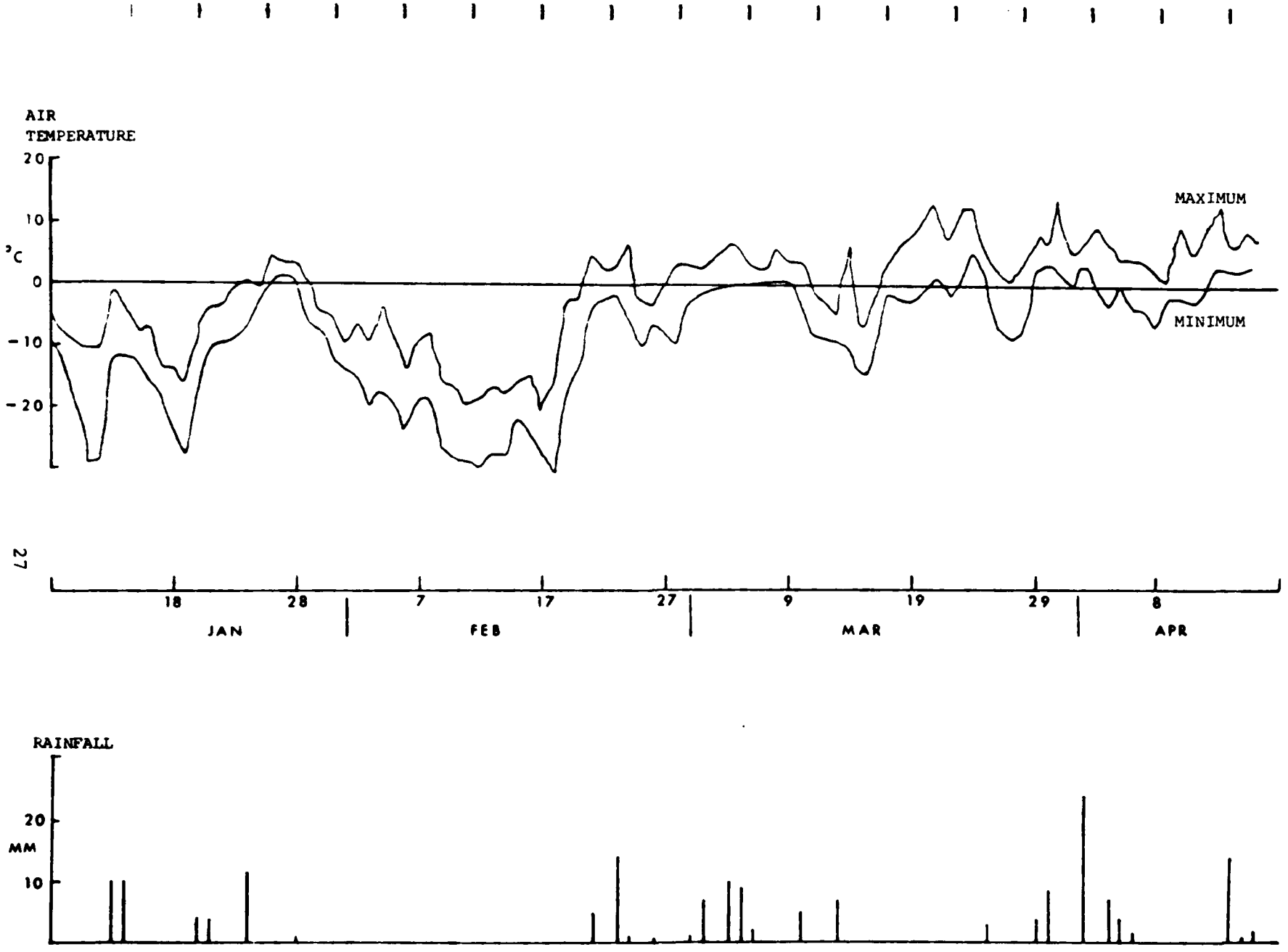

Figure 3.4 Daily Temperature Range and Rainfall

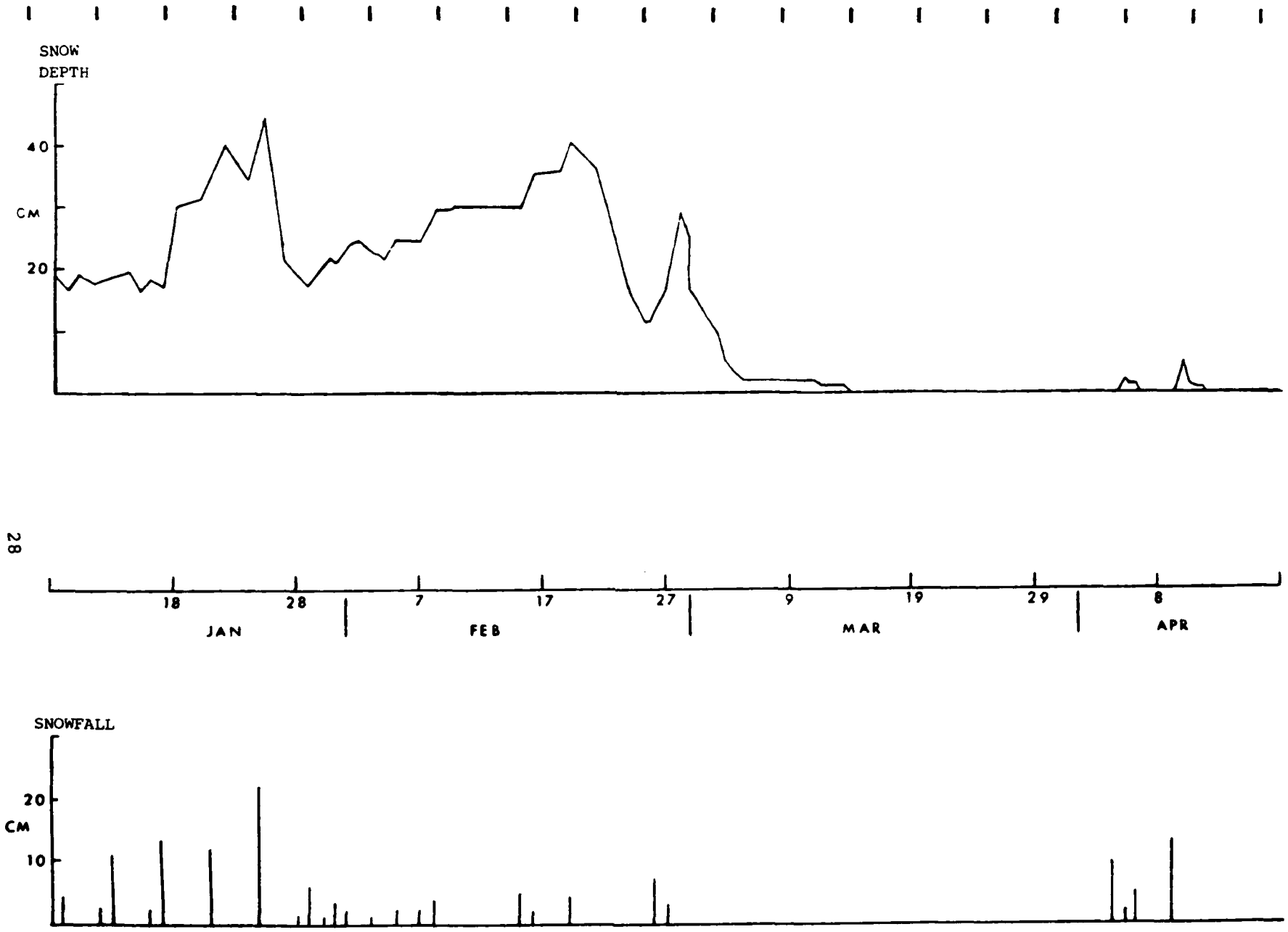

Figure 3.5 Snow Depth and Daily Snowfall

3.5 Field Site Data

Between January 31 and March 3 the snow depth at six positions along the length of the cables was measured each time a standard walk was performed. These results are plotted in figure 3.6. Due to drifting of the snow there are variations in the accumulated snow cover from one position to the next. The average snow cover at the field site is compared to the snow depth data obtained from the weather office in figure 3.7. The two measurements are in general agreement indicating that weather office data can be used when average field site data is unavailble or unreliable because of rapidly changing conditions.

An informal log was kept of the air temperature and the general weather conditions each time the field site was visited.

A reading was made of the soil moisture and soil temperature sensors each time a system profile measurement was made. The sensors, however, had been installed in the ground many months before the winter freeze-up. Unfortunately, most of the sensors had failed during the early winter and could not be removed from the ground to be repaired and recalibrated. Since the data obtained from these sensors could not be considered to be reliable it will not be referred to further in this report.

3.6 System Noise

The effect of the environmental conditions on the system noise was assessed from two different types of data, namely; 1) the initial blocks of data recorded during standard walks when no target was within the sensor detection zone, and 2) the 250 profile samples taken during each CW profile measurement.

3.6.1 Standard Walks

During the recording of the first twelve blocks of data for each standard walk no target was present within the detection zone of the sensors. These data consist of 190 samples of each component of the profile for each of the 10 cells recorded over a period of 41 seconds. The effective sampling rate was 1.1 Hz. The standard deviation of these samples is an indication of the system noise.

Table 3.1 gives the standard deviation of the magnitude (M_{SD}) of the profile for cells 1, 5 and 8 at the time of each standard walk. This data is plotted in figure 3.8 along with the snow depth data. The noise appears to be independent of the snow depth and the weather conditions.

Figure 3.9 is a plot of M_{SD} versus cell number for three different dates. A typical profile is also plotted in this figure. The noise from a particular cell is not related to the profile magnitude for that cell. In fact, the noise magnitude appears to be constant throughout the length of the data window.

Table 3.1

SUMMARY OF NOISE MEASUREMENTS

DATE	TIME	M_{SD} (mV)			WEATHER CONDITIONS
		Cell 1	Cell 5	Cell 8	
Feb. 21	5 p.m.	3.9	3.2	5.0	rain
25	12 p.m.	4.4	4.5	4.4	crusty snow
26	4 p.m.	5.1	4.8	5.3	heavy snow with driftin
28	5 p.m.	4.0	4.3	4.1	sunny
Mar. 3	3 p.m.	3.6	4.0	3.8	sunny
5	11 a.m.	3.9	3.8	4.8	showers, snow cover almost gone
6	10 a.m.	3.6	3.8	5.6	rain
7	5 p.m.	3.8	3.9	4.9	cloudy, warm, traces of snow on ground
10	7 a.m.	3.7	4.9	7.2	raining
12	11 a.m.	4.3	6.4	7.4	light snow, showers
15	5 p.m.	5.4	5.7	6.7	clear
26	4 p.m.	5.1	6.0	10	snow, rain showers
Apr. 5	4 p.m.	5.1	4.9	5.6	light snow overnight
6	5 p.m.	4.2	4.6	7.9	heavy snow overnight, stormy conditions, light cover of snow
9	5 p.m.	4.3	5.0	4.8	snowing all day
10	1 a.m.	3.9	5.3	6.1	snow
10	3 p.m.	3.7	5.2	6.4	
13	3 p.m.	4.1	3.5	5.7	overcast
15	2 p.m.	18	17	21	cloudy
17	4 p.m.	5.7	4.6	5.8	sunny

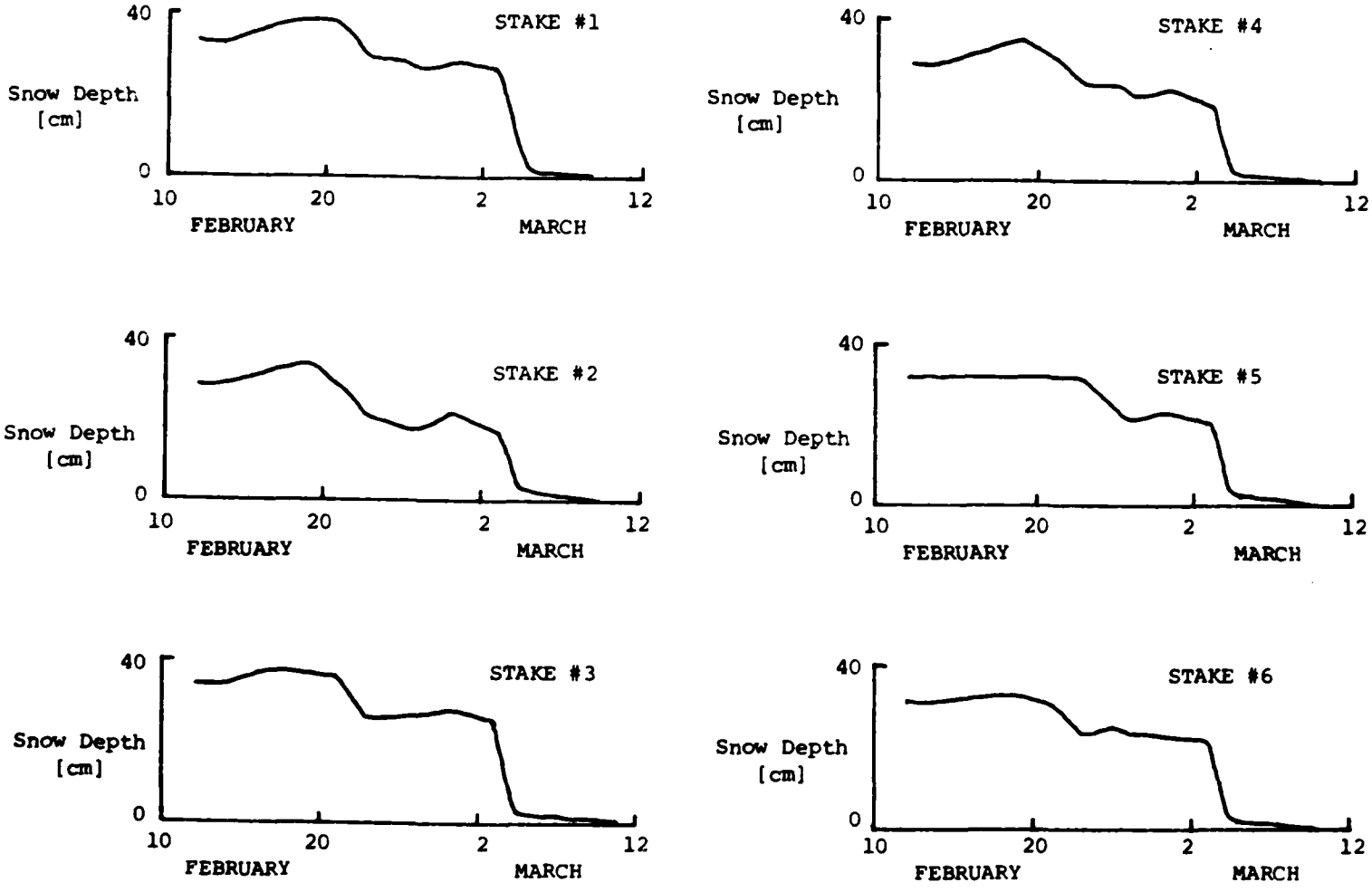

Figure 3.6 Snow Depth Measured at Field Site

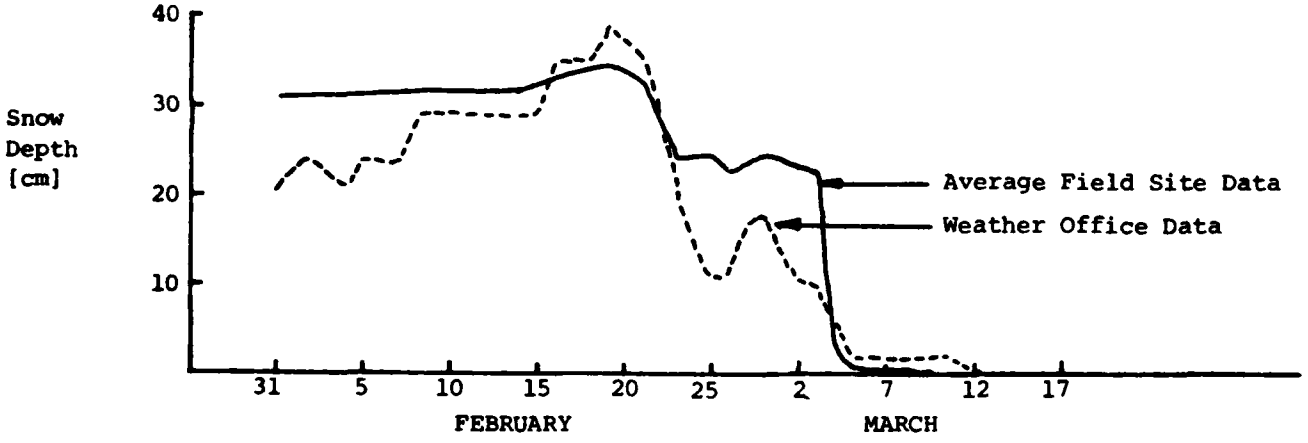

Figure 3.7 Snow Depth Comparison

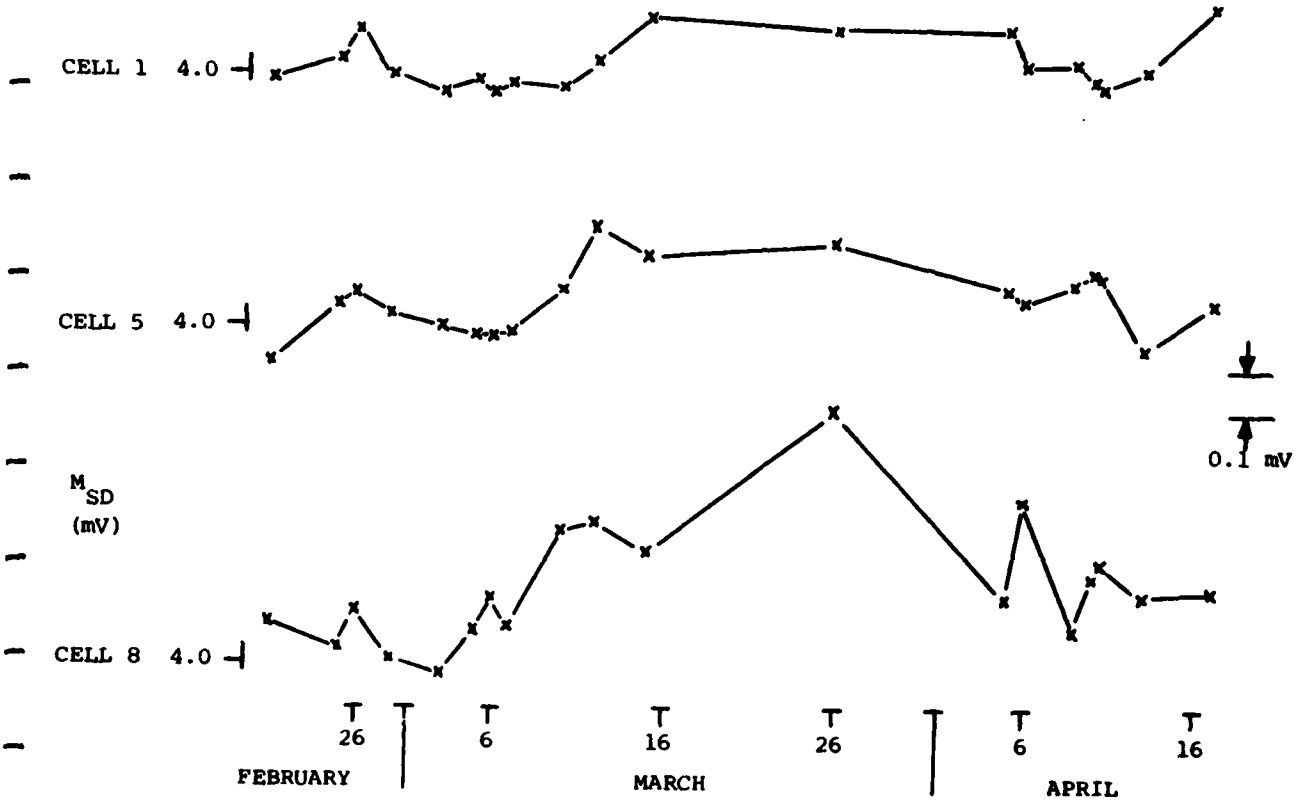

Figure 3.8 M_{SD} versus Date

Figure 3.9 M_{SD} versus Cell Number

Typical noise plots are given in figures 3.10 and 3.11. Figure 3.10 is a plot of I, Q, and M for cells 1 and 8 on February 25. Figure 3.11 is a plot of M for cells 1 and 8 on three different dates.

3.6.2 CW Profile

Each time a CW profile was recorded 250 readings of I and Q were made at a profile sampling rate of 27 Hz. The total time taken for each record was 4.5 seconds. The standard deviation of the 250 samples was calculated.

From this data the noise on the CW profile appeared to be unrelated to the weather conditions, snow depth or ground conditions.

3.6.3 Receiver Noise

Two types of receiver noise tests were performed. In the first type the noise generated within the receiver itself was measured by terminating the input with a standard 50Ω load and recording the CW profile once per hour for 66 hours. In the second test the cable was left connected to the receiver input but the transmitter was turned off. The CW profile was again measured once per hour for 66 hours. In this case the data includes not only receiver noise but also any noise in the environment picked up by the receive sensor.

The data was processed in the standard fashion to yield

I - the average of 250 samples of the in-phase component
Q - the average of 250 samples of the quadrature component
M - the average magnitude
I_{SD} - the standard deviation of the 250 I samples
Q_{SD} - the standard deviation of the 250 Q samples

Figure 3.12 is a plot of I, Q and M with the receiver input terminated and figure 3.13 is a plot of the results with the receive cable connected. They are essentially the same. The stability of the Q channel is considerably poorer than that of the I channel.

The maximum value of I_{SD} and Q_{SD} was the same whether or not the receive cable was connected indicating that the majority of the noise was generated within the receiver rather than being caused by external sources of electromagnetic energy.

A summary of the receiver noise tests is given in Table 3.2.

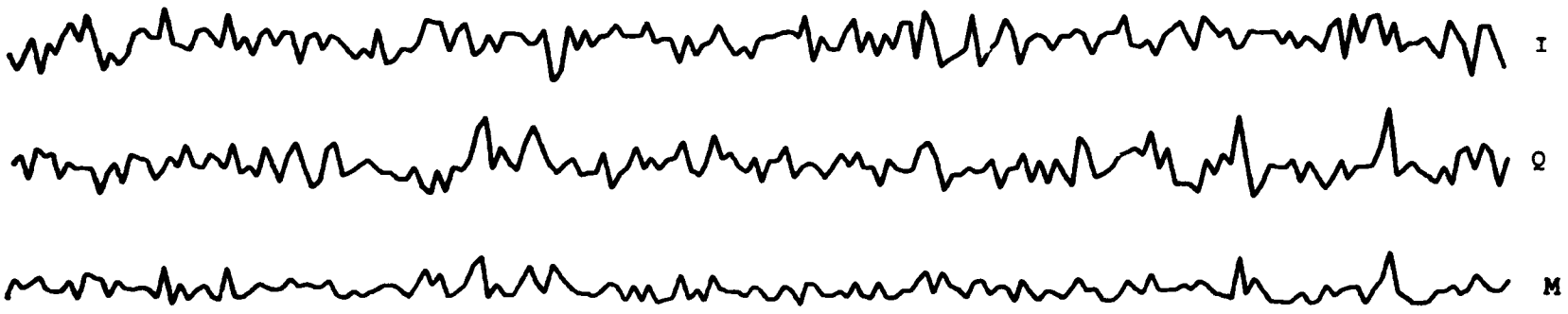

RANGE CELL 8

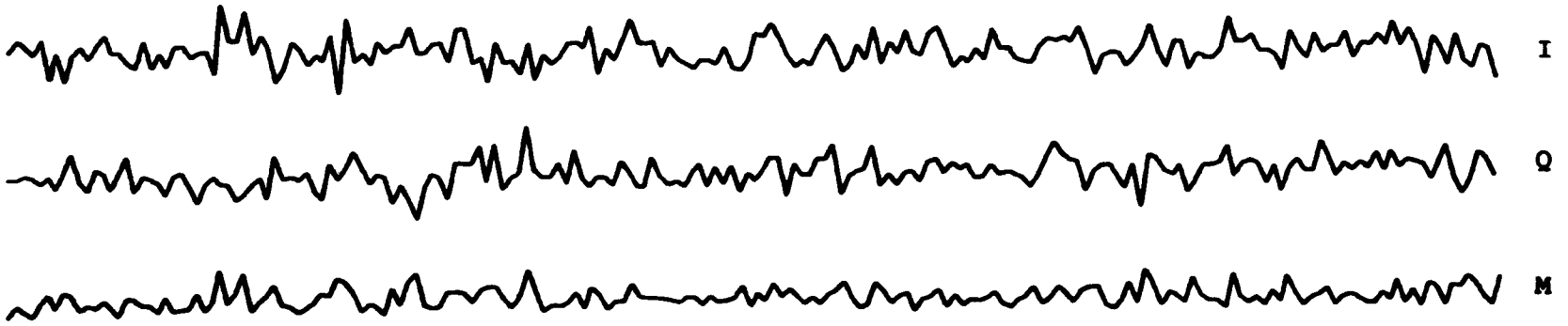

RANGE CELL 1

5 sec

10 mV

Figure 3.10 System Noise - February 25

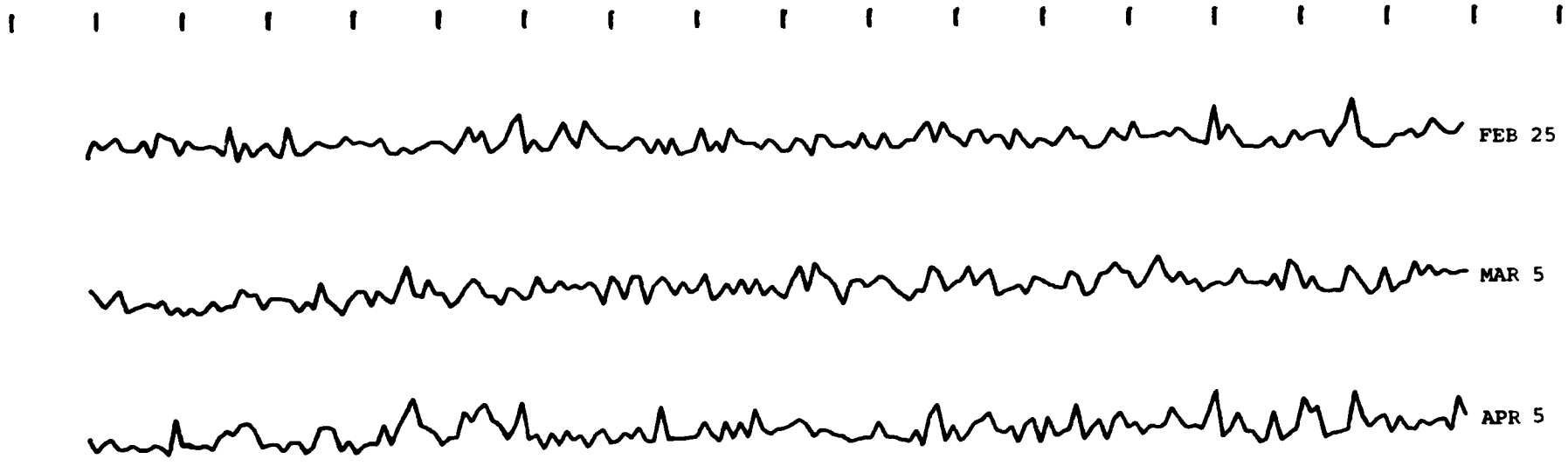

RANGE CELL 8

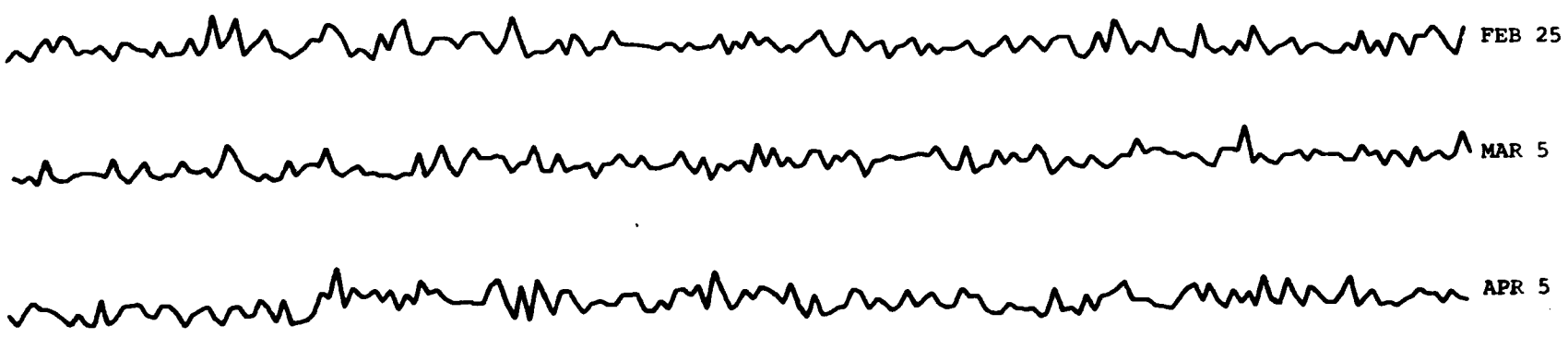

RANGE CELL 1

10 mV

5 sec

Figure 3.11 System Noise Magnitude

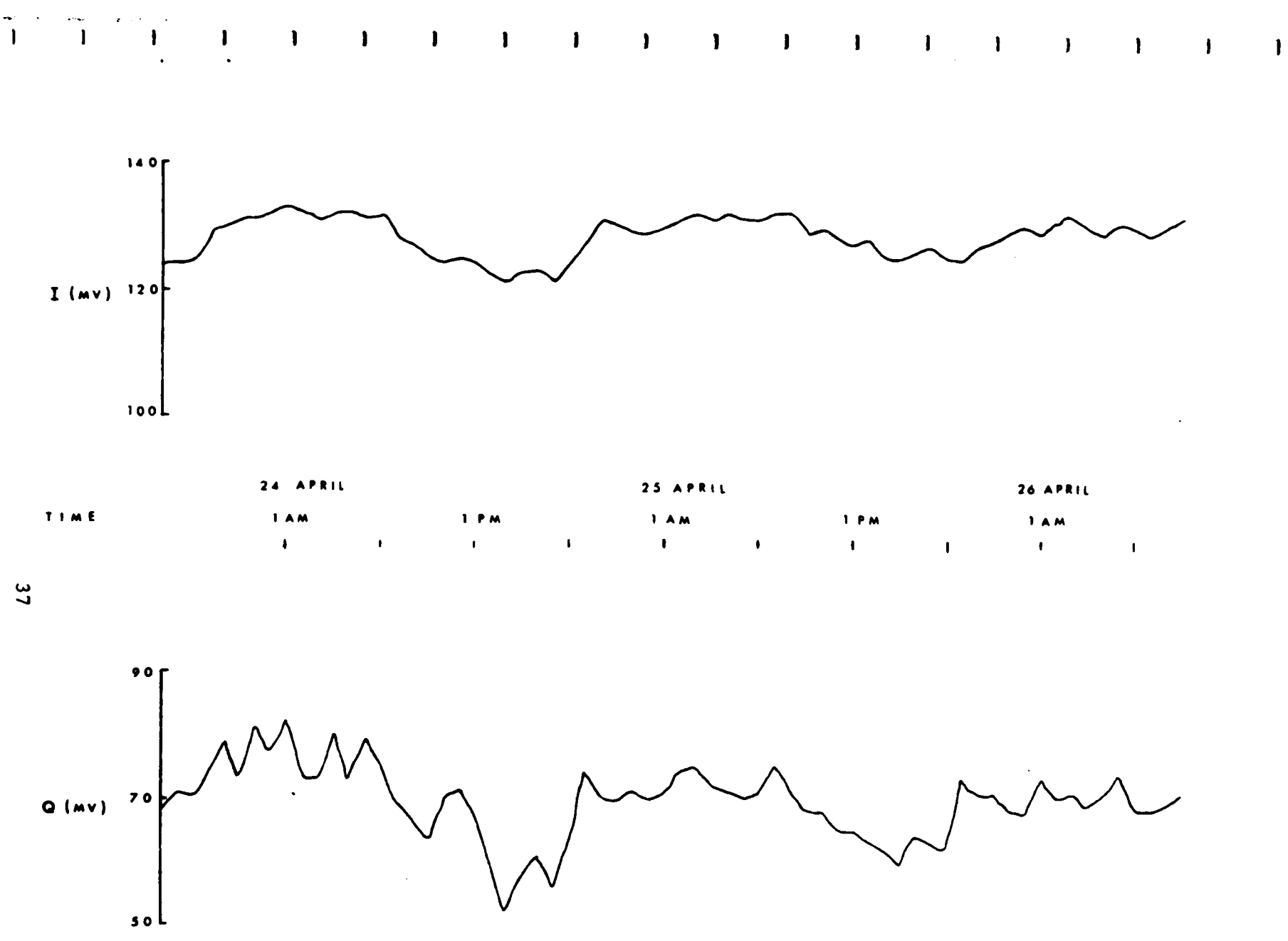

Figure 3.12 CW Receiver Stability - input terminated

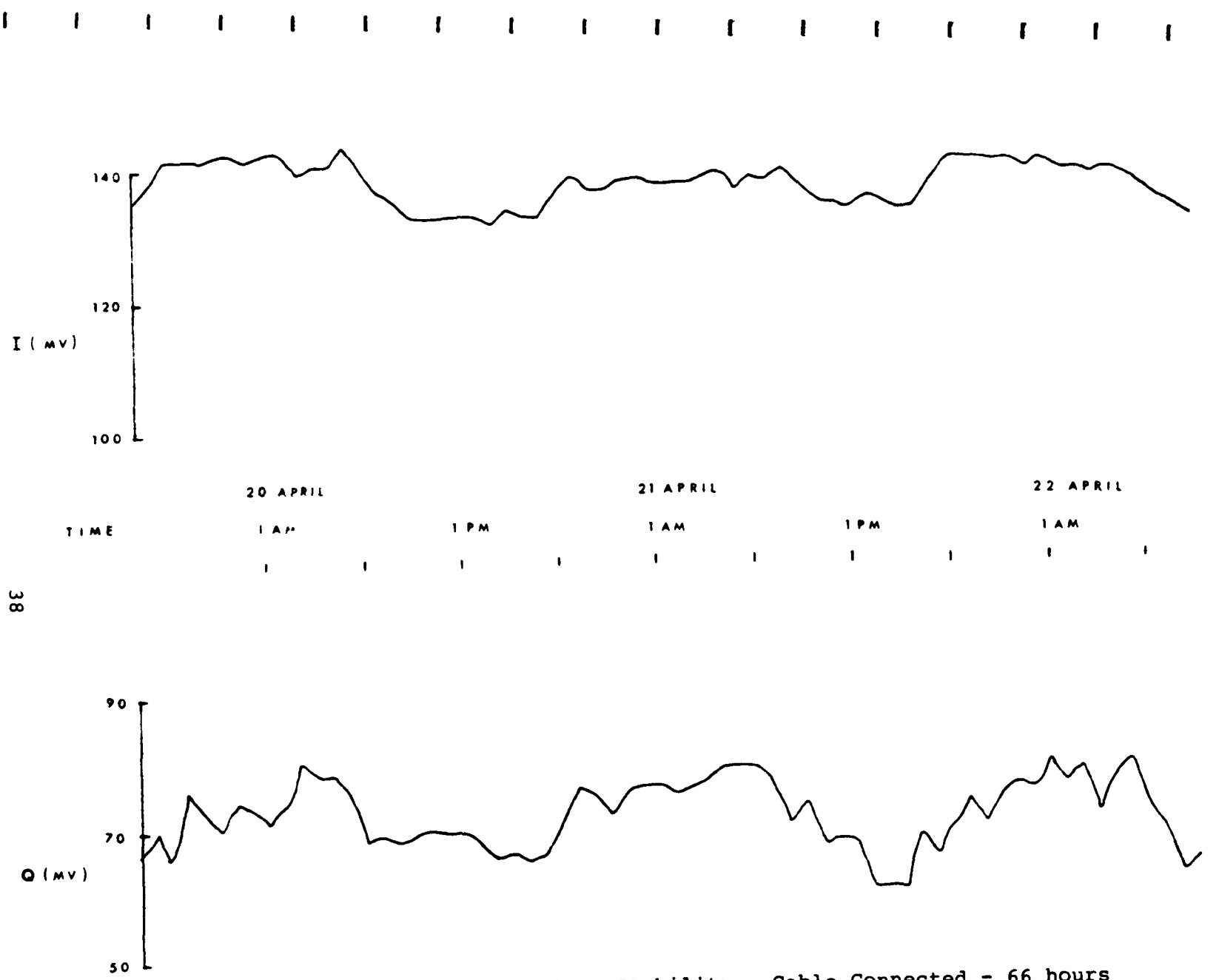

Figure 3.13 Receiver Stability - Cable Connected - 66 hours

Table 3.2

RECEIVER NOISE TESTS

	Receive Cable Connected	Receiver Input Terminated
STABILITY (mV)		
$I_{MAX} - I_{MIN}$	12	12
$Q_{MAX} - Q_{MIN}$	20	22
$M_{MAX} - M_{MIN}$	26	15
NOISE (mV)		
I_{SD} (max)	3.2	3.3
Q_{SD} (max)	2.9	3.1

3.6.4 Conclusions

The majority of the noise within the system is generated in the receiver itself. The environmental conditions do not add appreciably to the high frequency noise. At the Queen's University field site externally generated electromagnetic fields do not significantly increase the noise level. Since the noise is receiver generated, it is uniform in magnitude along the length of the sensors and is not related to the profile or sensitivity at a particular location.

3.7 Sensitivity

3.7.1 Typical Results

Table 3.3 is a summary of the date and time when each standard walk was performed. Included in the table is a brief description of the weather conditions at the time.

Figure 3.14 is a plot of the I component of the profile during a typical standard walk for each of the ten range cells; figure 3.15 is a plot of the corresponding magnitude response for each cell during the same walk. In these plots the abscissa variable is time and the ordinate variable is target response. Each curve is the response from a different range cell. The profile magnitude is also plotted on this figure for reference. During this walk there was 11 cm of snow on the ground. Although the snow had a thick ice crust on top the footprints from previous walks were distinct. Therefore, the target lifted his feet a considerable distance above the ground during each step. This is the probable cause of the rapid variations seen in the sensitivity plots.

An alternate presentation of the data recorded during the same standard walk is given in figure 3.16. In this figure target response is plotted versus the cell number (distance along the cable) at equal time intervals during the walk. The width of the target response remains constant as the target walks through the data "window" implying that the distance resolution of the system also remains constant. This fact was true for all standard walks, independent of the weather conditions.

3.7.2 Sensitivity Variation with Weather Conditions

The maximum magnitude of the target response in each cell was used as a measure of system sensitivity. The sensitivity for each cell during each walk, relative to the sensitivity for the corresponding cell on the reference date of February 25, is plotted in figure 3.17. The curves for all ten cells are plotted on the same ordinate scale. However for clarity they have been shifted vertically relative to each other. The absolute sensitivity of each cell is marked at the beginning of each curve. The rainfall data from the weather office is also plotted in this figure.

Table 3.3

SUMMARY OF STANDARD WALKS

DATE	TIME	SNOW DEPTH (cm)	TEMPERATURE (cm)	WEATHER CONDITIONS
Feb. 21	5 p.m.	35	+1	rain
25	12 p.m.	11		crusty snow
26	4 p.m.	11		heavy snow with drifting
28	5 p.m.	18	+3	sunny
Mar. 3	3 p.m.	6	+6	sunny
5	11 a.m.	2	+3	showers, snow cover almost gone
6	10 a.m.	2	+3	rain
7	5 p.m.	2	+3	cloudy, warm, traces of snow on ground
10	7 a.m.	2	-1	raining
12	11 a.m.	1	0	light snow, showers
15	5 p.m.	0	-10	clear
26	4 p.m.	0	-3	snow, rain showers
Apr. 5	4 p.m.	2	+5	light snow overnight
6	5 p.m.	1	0	heavy snow overnight, stormy conditions, light cover of snow
9	5 p.m.	0	0	snowing all day
10	1 a.m.	5	-1	snow
10	3 p.m.	5	+16	
13	3 p.m.	0	+13	overcast
15	2 p.m.	0	+10	cloudy
17	4 p.m.	0	+15	sunny

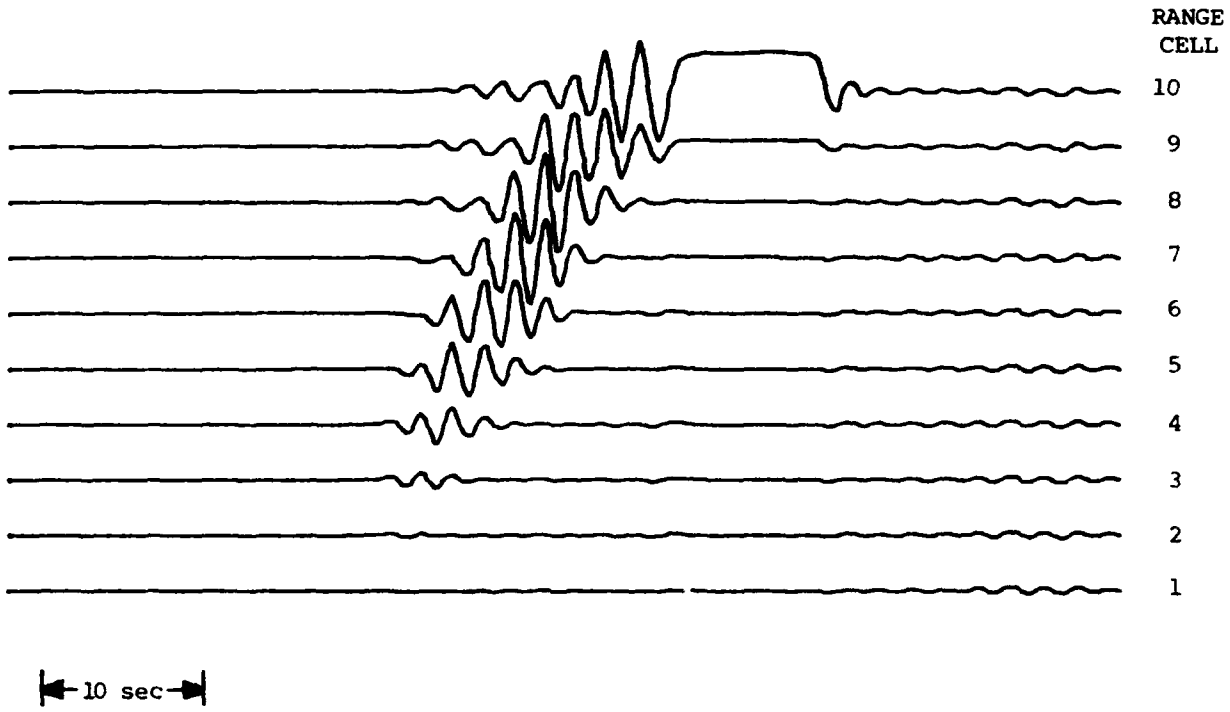

Figure 3.14 I Component During Standard Walk - February 21

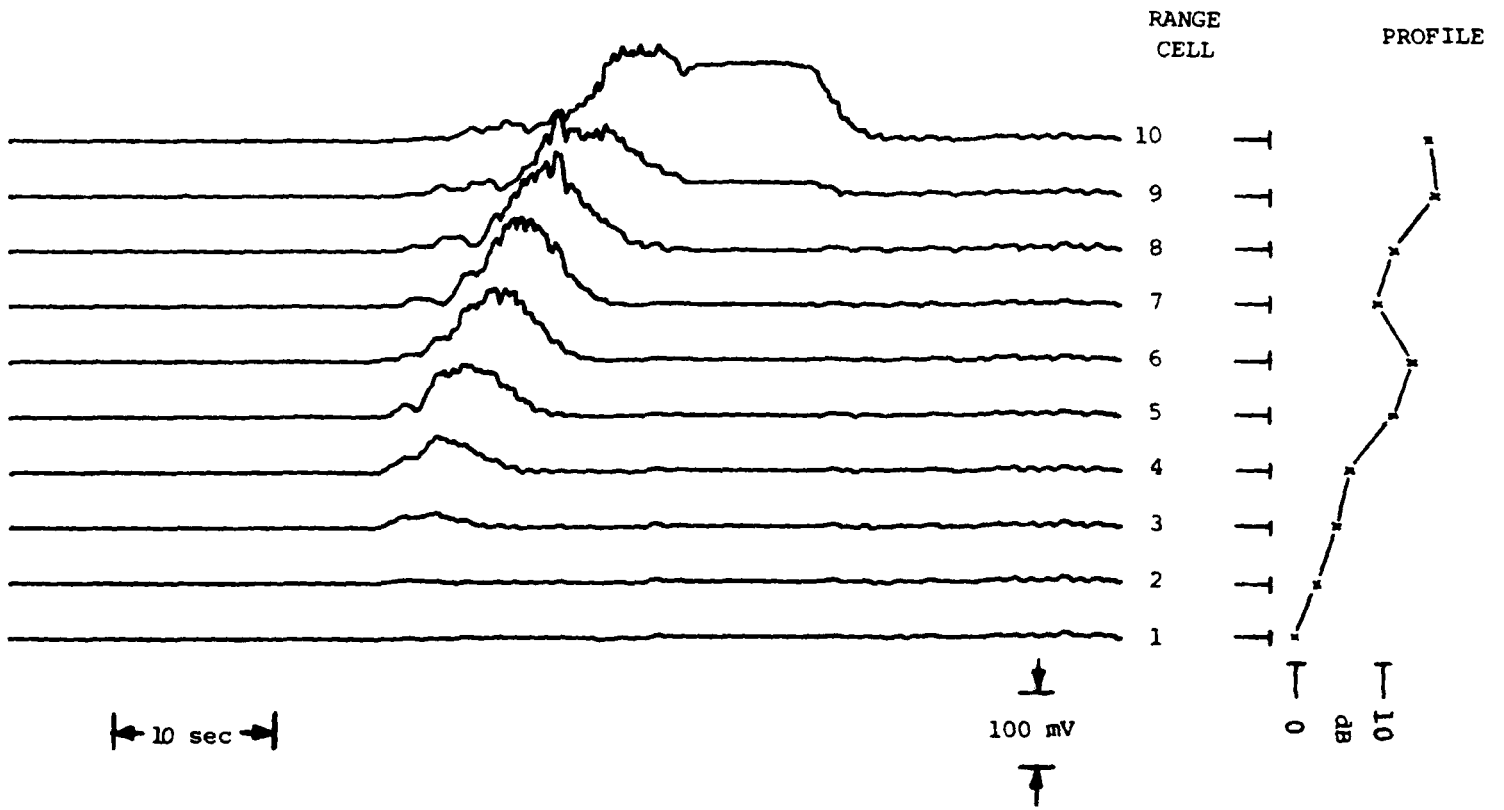

Figure 3.15 Magnitude Response During Standard Walk - February 21

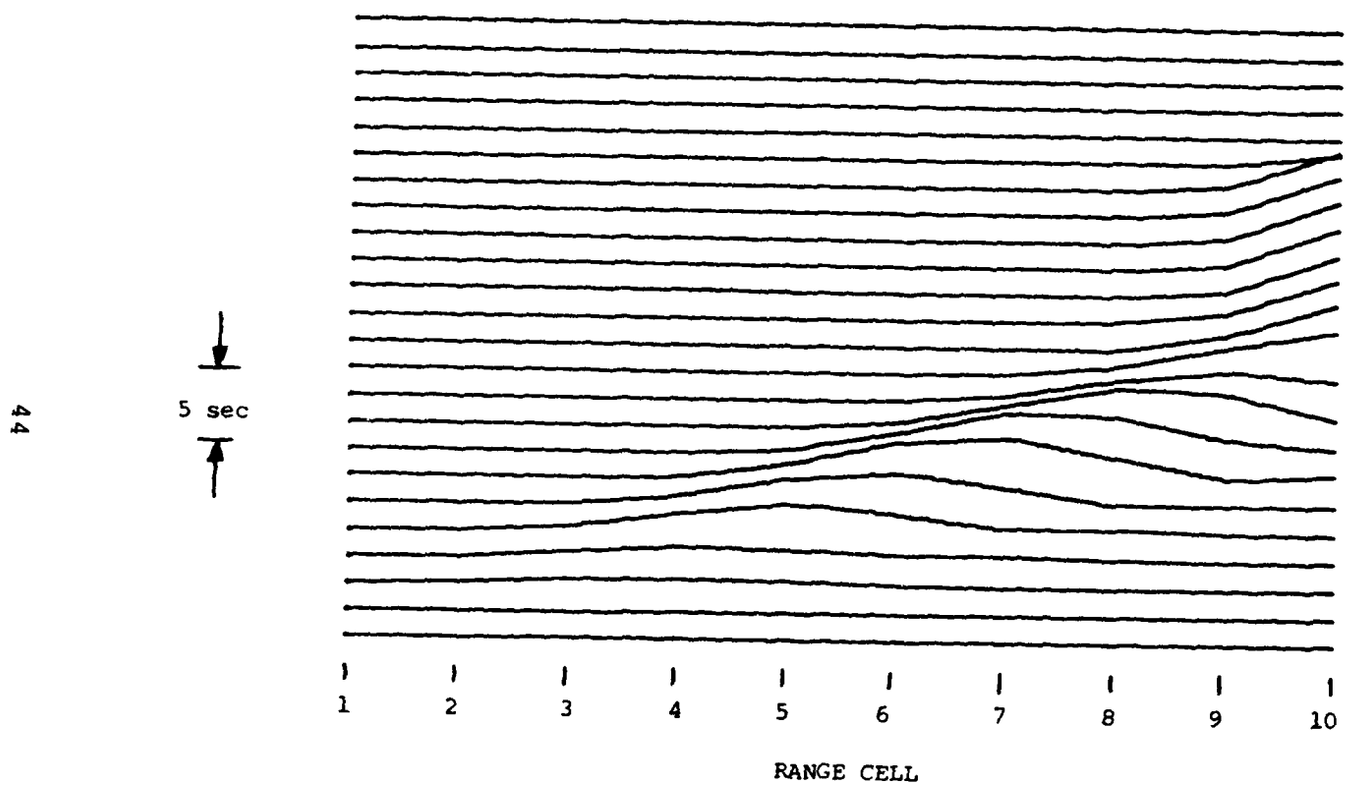

Figure 3.16 System Response - Standard Walk

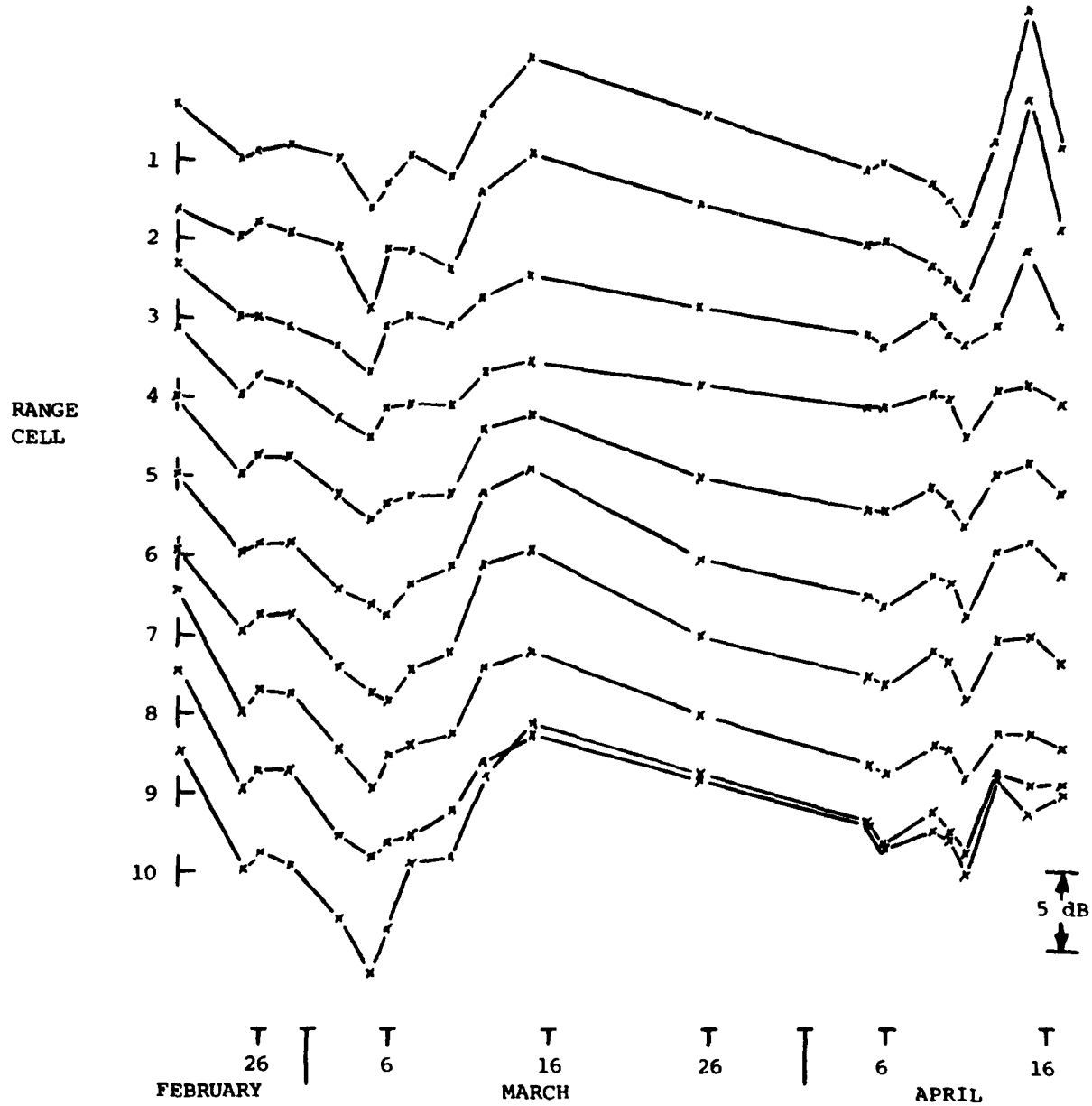

Figure 3.17 Sensitivity Variation - Each Cell

The sensitivity varies in a similar fashion for each range cell in response to changes in the weather conditions. Moisture either on the ground or saturating the snow above the cables has the greatest effect on sensitivity.

Between February 21 and February 24 a total of 20.8 mm of rain fell and the snow depth decreased from 35 cm to 15 cm. By the 25th the snow was well saturated with moisture. The sensitivity decreased by 5 to 7 dB during this period of time. Between March 2 and March 6 rain and warm temperatures caused the rapid disappearance of the remaining snow cover. The sensitivity was reduced by a further 5 dB. From the 7th of March to the 14th of March the ground was clear of snow and was gradually drying out although the surface was still moist. The sensitivity rose by approximately 10 dB to a maximum on March 15th. More complete drying of the surface after March 15th resulted in a gradual decline in sensitivity.

3.7.3 Sensitivity Variation from Cell to Cell

The variation in sensitivity in response to changing weather conditions along the length of the cable was relatively uniform. This is demonstrated by figure 3.18. For this plot, the sensitivity on February 25th was used as a reference for each cell. Only the change in sensitivity from the February 25th reference value for each cell is plotted in figure 3.18. The greatest difference in the change in sensitivity occurred on April 17 between cell 1 and cell 10. The difference was 6.2 dB.

Table 3.4 is a summary of the sensitivity changes during the experimental period. The change in sensitivity at a particular point on the cable appears to be unrelated to the absolute sensitivity at that point.

3.7.4 Summary

The sensitivity is most clearly influenced by moisture in the vicinity of the cables, either in the surface soil beneath the cables or in the form of moist snow above the cables. Under very wet conditions (rapidly melting snow) a large decrease in sensitivity was noted averaging 9.1 dB. With the ground moist but clear of snow and surface water (March 16) the sensitivity appeared to be 2 or 3 dB greater than when the ground was dry. Changes in sensitivity were relatively uniform along the length of the observation window.

3.8 Pulse Profile

Two types of measurement were made of pulse profile. The first series of measurements was made immediately prior to each standard walk. These results will be discussed in sub sections 3.8.1 to 3.8.3. Pulse profile was also recorded at hourly intervals for certain periods of time (See section 3.3.2). These results, along with the corresponding CW profile will be discussed in section 3.9.

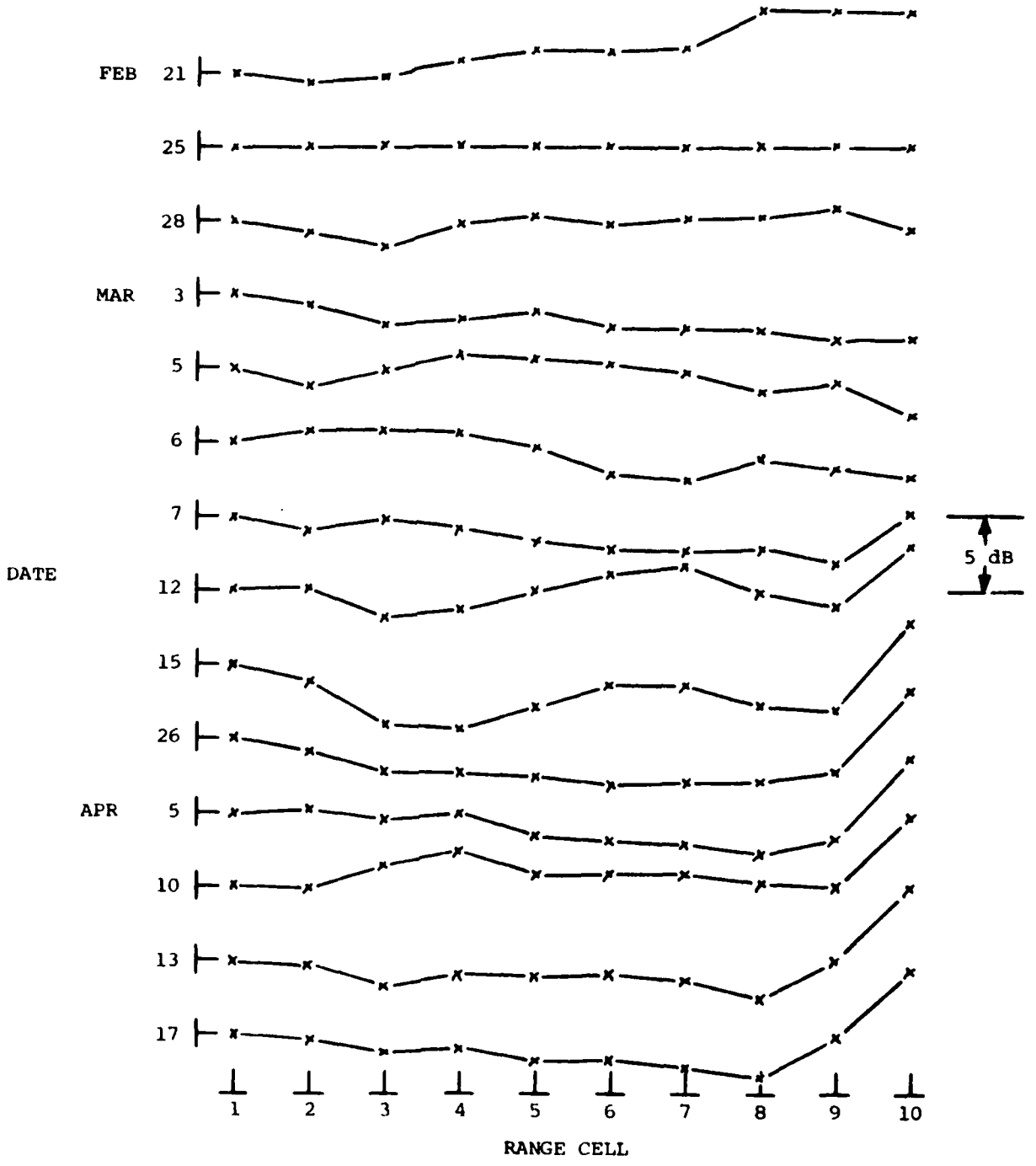

Figure 3.18: Sensitivity Variations along the Sensor with Weather

Table 3.4

VARIATION IN SENSITIVY

RANGE CELL	SENSITIVITY MAX (dB)	SENSITIVITY MIN (dB)	SENSITIVITY VARIATION (dB)	ABSOLUTE SENSITIVITY Feb. 25
1	9.5	-4.1	13.6	0
2	8.9	-4.5	13.4	.63
3	4.1	-3.5	7.6	5.4
4	4.2	-2.6	6.8	11.8
5	5.0	-3.4	8.4	14.0
6	5.2	-3.9	9.1	16.7
7	5.2	-4.1	9.3	18.3
8	7.8	-4.9	12.7	16.4
9	7.6	-4.3	11.9	15.2
10	9.3	-6.5	15.8	16.7

Note: All sensitivities are calculated relative to the sensitivity for a particular range cell on February 25.

3.8.1 Profile Variation with Weather Conditions

The recordings of pulse profile were made immediately prior to each standard walk. Figure 3.19 is a plot of the profile in each cell with the profile on February 21st being chosen as the reference for each cell. The rainfall data is also plotted in this figure. The three symbols x . and ∘ are used in the plots of the response of the different range cells merely for clarity.

The pattern of profile variation is similar for all cells during most of the measurement period. The largest profile changes occurred in response to rain and melting snow.

3.8.2 Profile Variation from Cell to Cell

Figure 3.20 is a plot of the change in profile along the cable on various dates when standard walks were performed. The profile in each cell has been normalized to the corresponding profile on February 21st.

The change in profile is relatively uniform along the cable. Cells #4 and #8 have anomolously low profiles on some of the dates when an experiment was performed. The reason for this is unknown although it could result from very localized differences in ground moisture (puddle formation perhaps, caused by a local ground depression).

Table 3.5 summarizes the changes in profile in each range cell. Also given is the reference profile on February 21, normalized to cell 1.

3.8.3 Sensitivity versus cell profile

A question which has arisen in the past concerning guided radar is whether sensitivity and profile are directly related in a particular range cell. A comparison of figures 3.17 and 3.19 indicates that both these parameters respond in a similar fashion to changes in the environmental conditions although there does not appear to be a direct correlation between them. This is further illustrated by figure 3.21 in which profile is plotted versus sensitivity for cell 1 and cell 5.

3.9 Automated Profile Monitoring

3.9.1 Results

At various times between December 21, 1978 and April 9, 1979 the guided radar system was configured for automated sampling of CW profile and pulse profile. Measurements of the profile were made at a pre-selected rate, usually once per hour. At times more frequent measurements were made. Table 3.6 is a summary of the dates and weather conditions during these measurements.

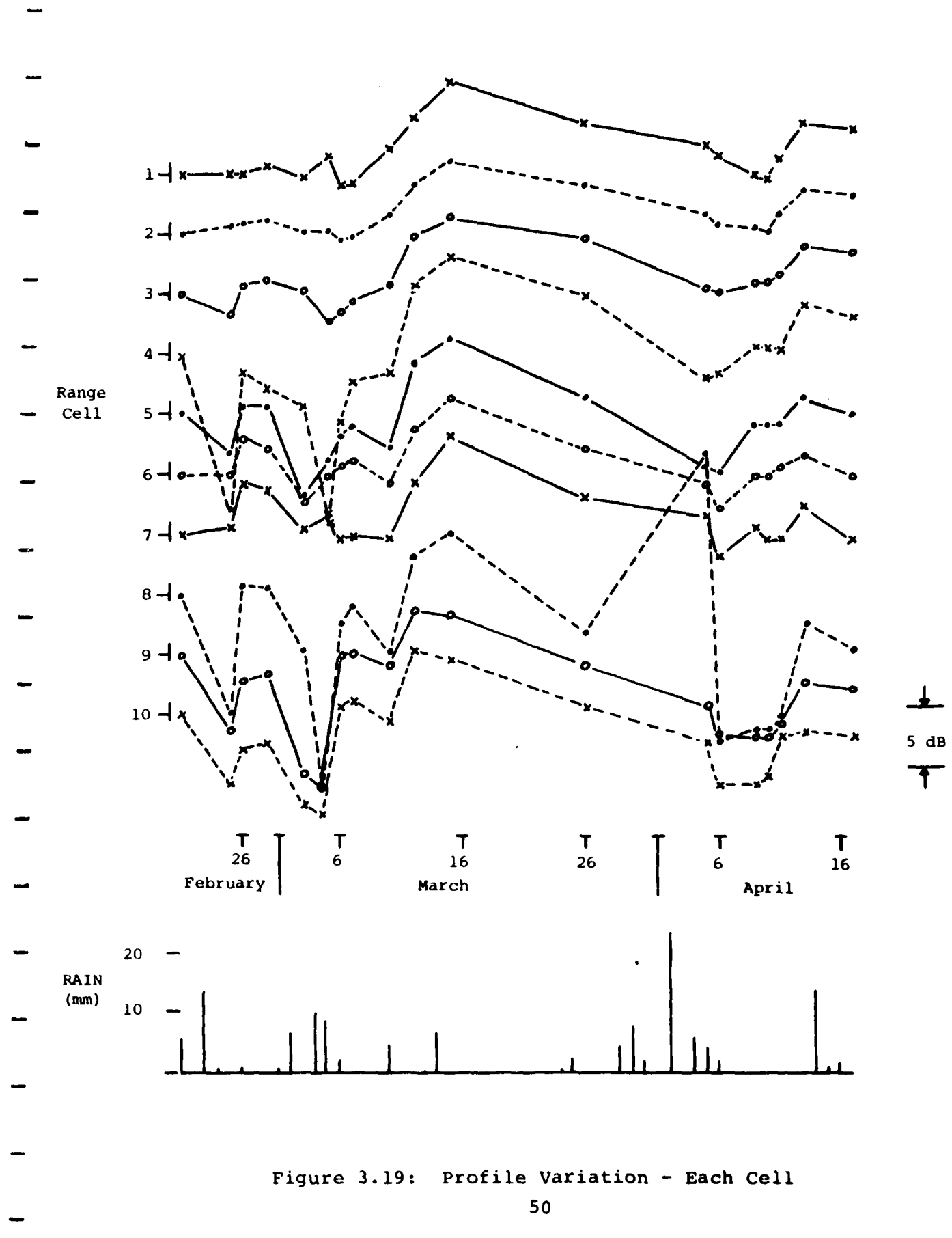

Figure 3.19: Profile Variation - Each Cell

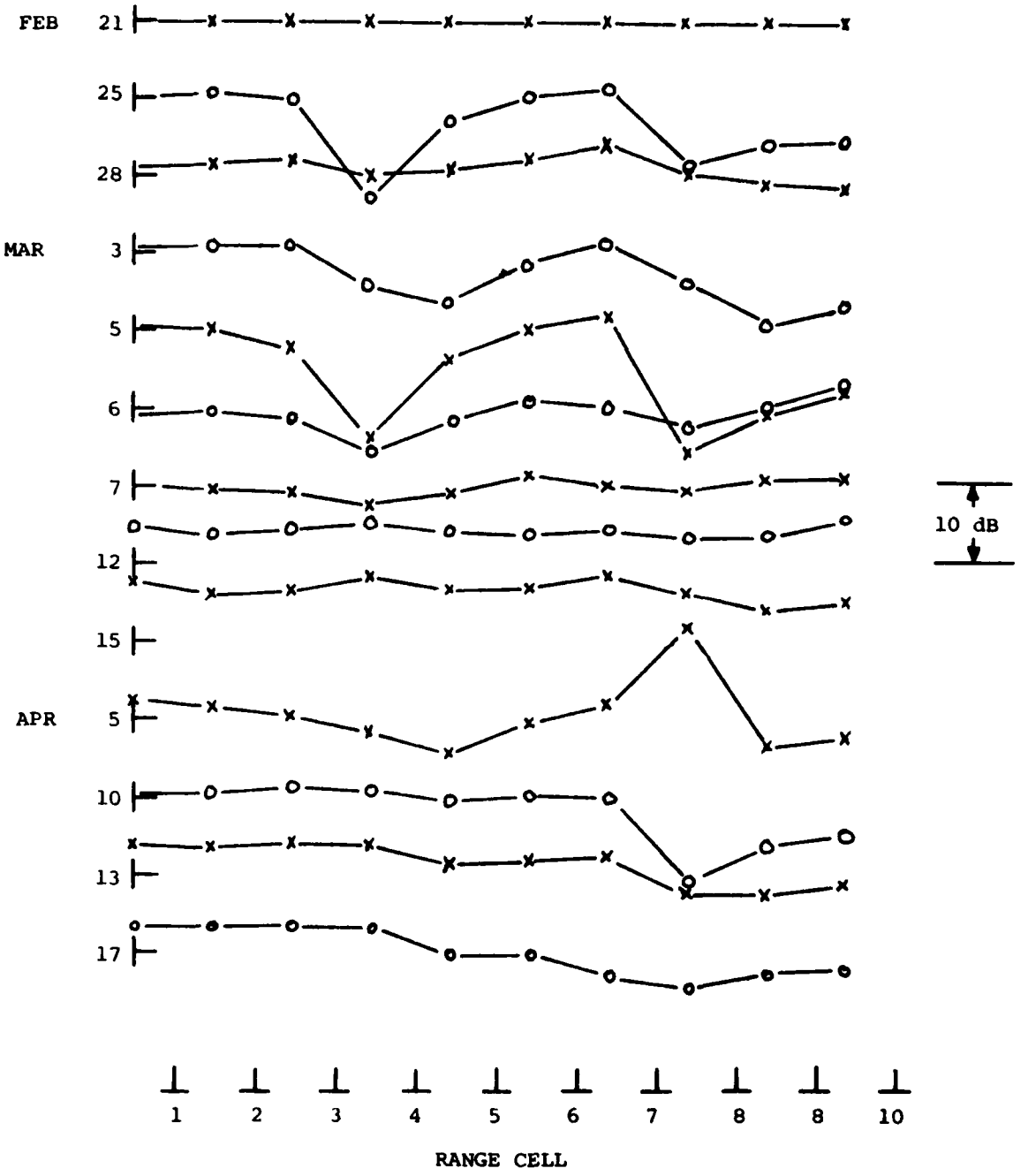

Figure 3.20: Profile Variation along the Sensor

Table 3.5

PULSE PROFILE VARIATION

RANGE CELL	PROFILE MAGNITUDE MAX (dB)	MIN (dB)	VARIATION (dB)	REFERENCE PROFILE Feb. 21
1	7.7	- .92	8.6	0
2	6.1	- .45	6.6	2.5
3	6.5	-1.5	8.0	4.8
4	8.2	-14	22.2	6.3
5	6.4	- 6.8	13.2	11.3
6	6.3	- 2.9	9.2	13.4
7	8.1	- .29	8.4	9.5
8	5.2	-16	21.2	11.3
9	3.7	-11	14.7	16.0
10	5.5	- 7.5	13.0	15.1

Note: All profiles are calculated relative to the profile for a particular range cell on February 21.

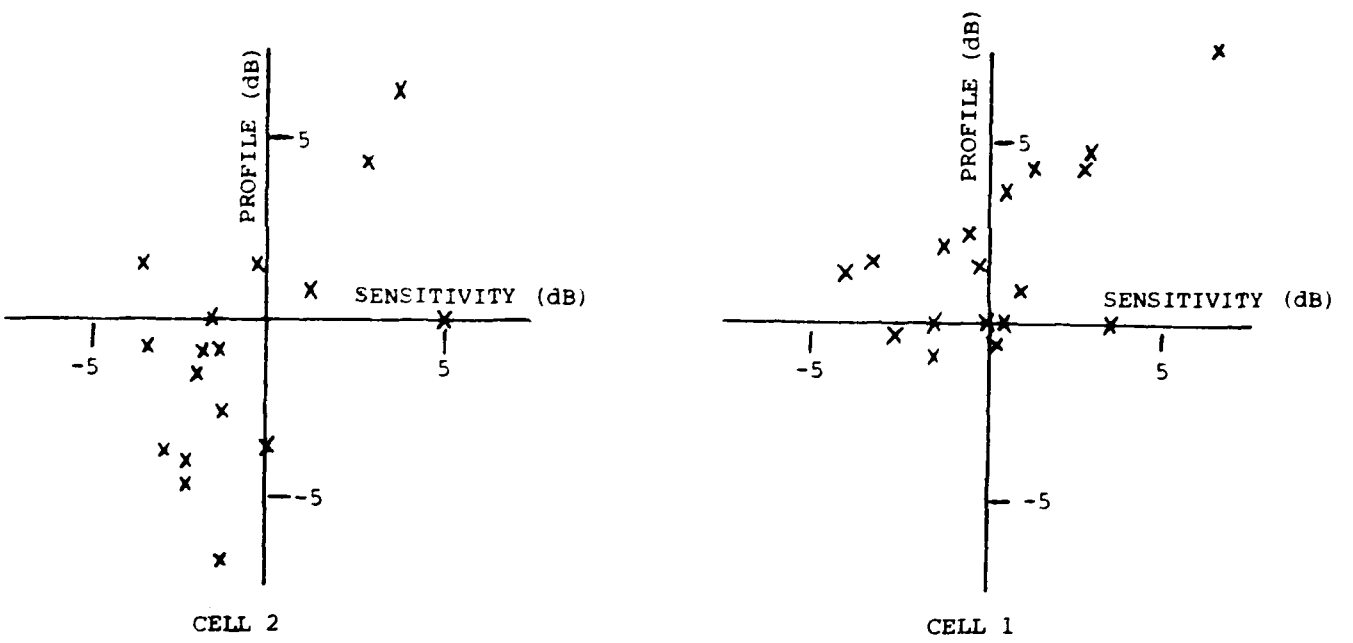

Figure 3.21: Sensitivity versus Profile

Table 3.6

SUMMARY OF AUTOMATED PROFILE RECORDINGS

START			LENGTH (hours)	RATE (per hour)	WEATHER
Dec.	21	12:49 p.m.	66	1	
Jan.	6	1:05 a.m.	51	1	sunny, cold
	10	3:30 p.m.	26	1	overcast, cold
	17	3:55 a.m.	45	1	very cold, heavy snow
	19	6:15 p.m.	8	1	very cold, overcast
	20	9:15 a.m.	33	1	rain
	27	6:28 p.m.	33	1	warm, overcast
	30	5:42 a.m.	20	10	cold, overcast
	30	3:25 p.m.	33	10	light snow
	30	9:38 p.m.	20	1	light snow
Feb.	1	7:34 a.m.	33	1	clear, sunny, cold
	3	1:02 p.m.	66	1	clear, cold
	6	6:31 a.m.	33	1	clear, very cold
	9	12:51 p.m.	55	1	clear, very cold
	12	1:15 a.m.	64	1	overcast, cold
	16	9:30 p.m.	66	1	light dry snow
	23	8:00 p.m.	33	1	warm, heavy rain
	28	6:30 a.m.	50	1	clear, warm
Mar.	7	9:30 a.m.	50	2	overcast, warm
	8	10:40 p.m.	33	1	overcast, warm
	14	10:26 p.m.	33	1	rain
	18	4:36 p.m.	33	2	clear, warm
Apr.	2	1:05 a.m.	19	1	warm, heavy rain
	6	1:00 a.m.	66	1	rain and snow
	9	5:19 p.m.	7	2	heavy wet snow

The large amount of data can most conveniently be displayed graphically. Figure 3.22 is an example of a plot of the pulse profile each hour for a period of 33 hours starting at 9 p.m. on December 22. What is of interest in this data is the change in profile in response to changes in the weather. To make the changes more evident the first profile in the sequence can be selected as a reference and only the difference between a profile and the reference plotted. This has been done to produce figure 3.23. The weather conditions are marked on the plots. Figure 3.24 is the CW profile (I, Q and M) for the same period of time.

At the beginning of this time period the ground was frozen at the surface and there was a trace of snow on the ground. Overnight temperatures reached a low of -4°C. The profile was stable until the morning of the 23rd. Temperatures of +2°C caused the snow to disappear and the ground surface to melt. The CW profile magnitude dropped by 2.1 dB due to the ground moisture. The profile rose back to its former level when the temperature again fell below the freezing point. This effect was seen several times during December.

Figures 3.25 and 3.26 show the pulse and CW profile changes during clear stable weather. The temperature was below -10°C throughout and 19 cm of snow covered the cables. The maximum CW profile variation was 0.7 dB.

Rain on previously dry ground had a large effect on both the CW and pulse profiles. This is illustrated in figures 3.27 and 3.28. Approximately 1 mm of rain and 5 cm of snow fell overnight on the 6th of April with the sky clearing in the early morning. The CW profile rose by 9 dB during the precipitation and dropped by 6.2 dB as the ground dried during the warm sunny day. Rain during the evening of the 7th caused the profile to rise again.

The effect of rain saturating previously dry snow is shown in figures 3.29 and 3.30. Initially, in these figures, a light drizzle was falling. This changed to moderate rain around noon of the 23rd followed by gradual clearing. Approximately 20 cm of snow was on the ground on the 23rd which decreased to 15 cm during the rainfall. There is a delay between the onset of the rain and an effect being seen in the profiles as might be expected. Once the moisture had percolated through the snow cover to the vicinity of the cables significant changes were evident in both the pulse and CW profiles.

3.10 Summary

The weather conditions obviously significantly affect the performance of a guided radar system. From the data collected it is possible to draw general conclusions as to the nature of these effects. However, since the

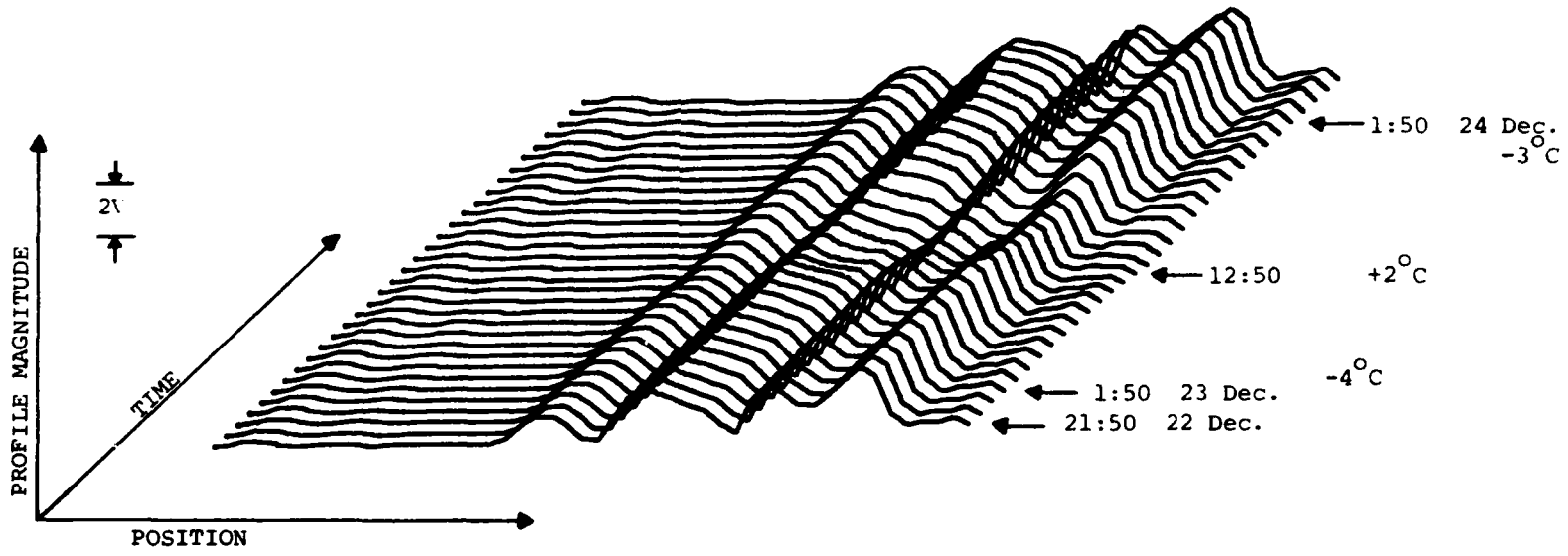

Figure 3.22: Pulse Profile - December 22

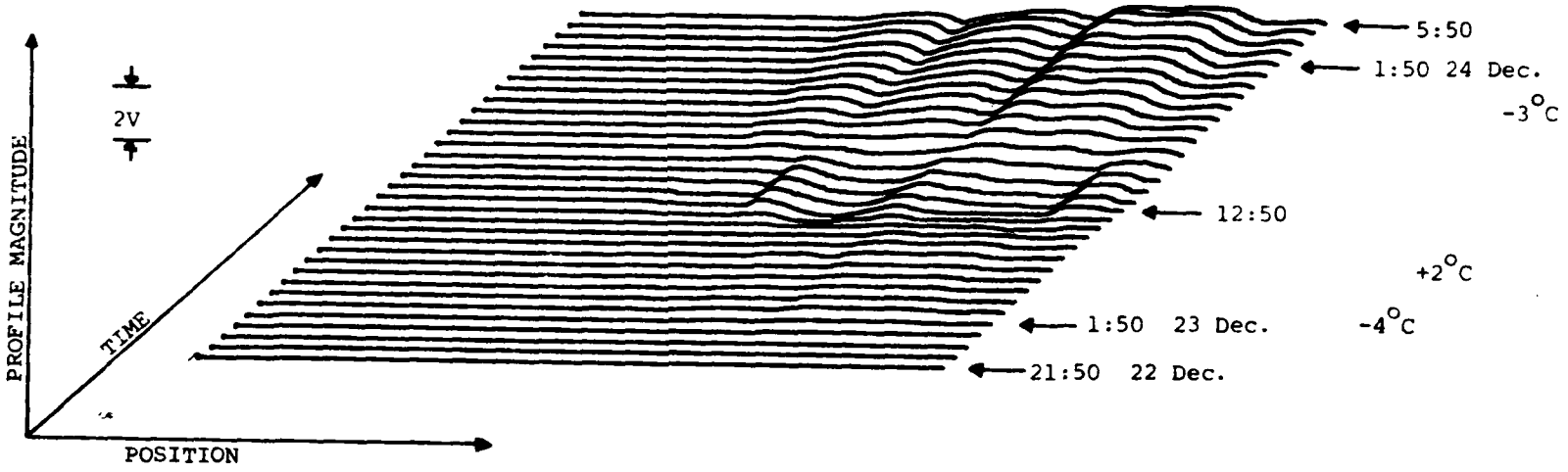

Figure 3.23: Pulse Profile Change - December 22

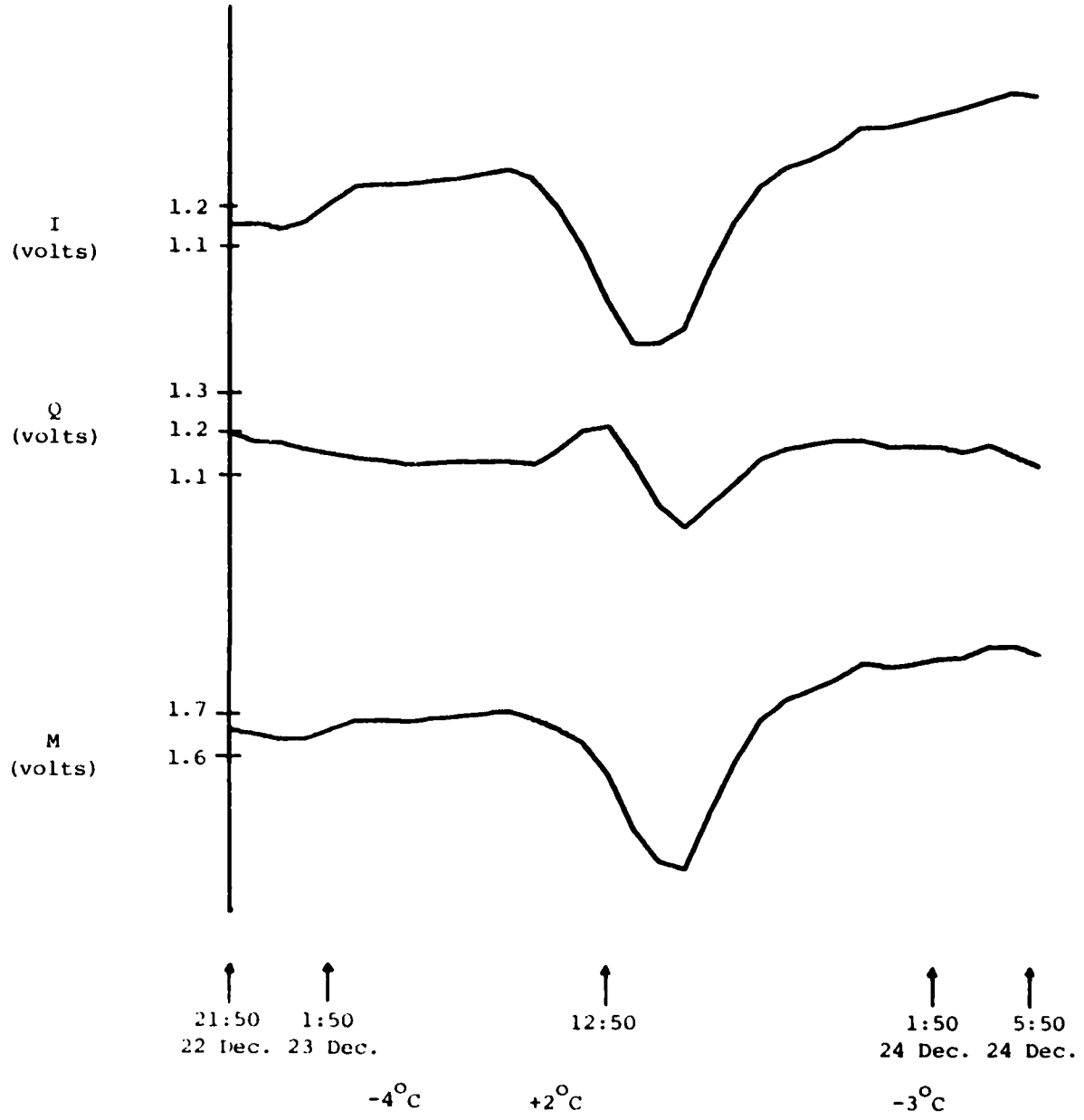

Figure 3.24: CW Profile - December 22

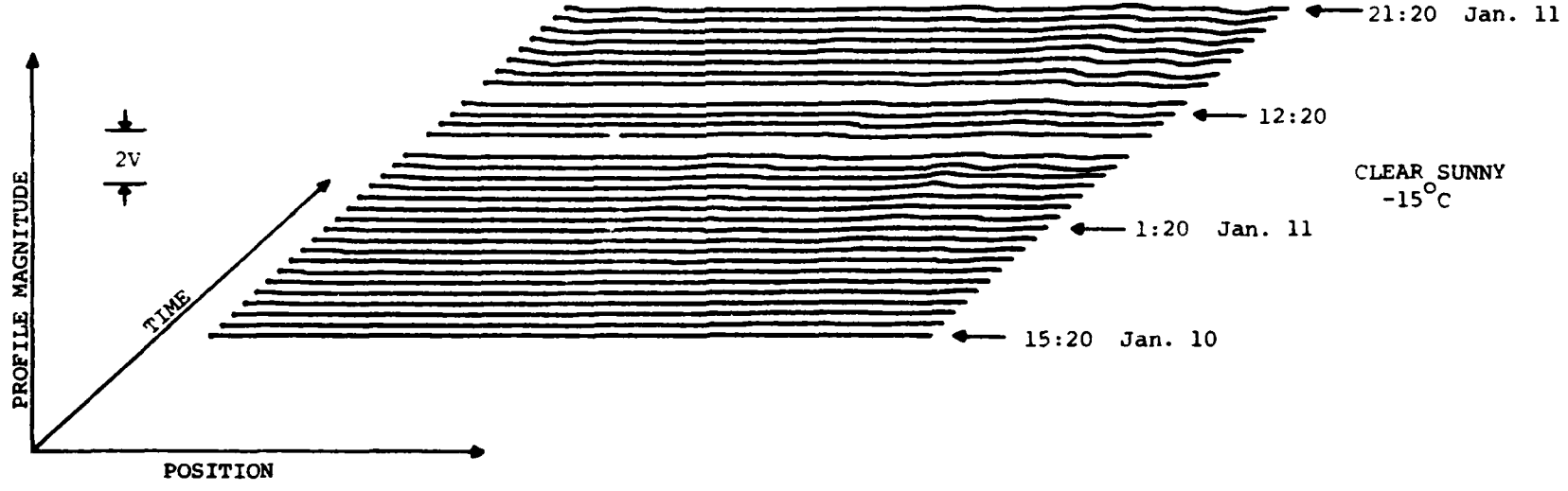

Note: Blank lines indicate missed data

Figure 3.25: Pulse Profile Change - clear weather

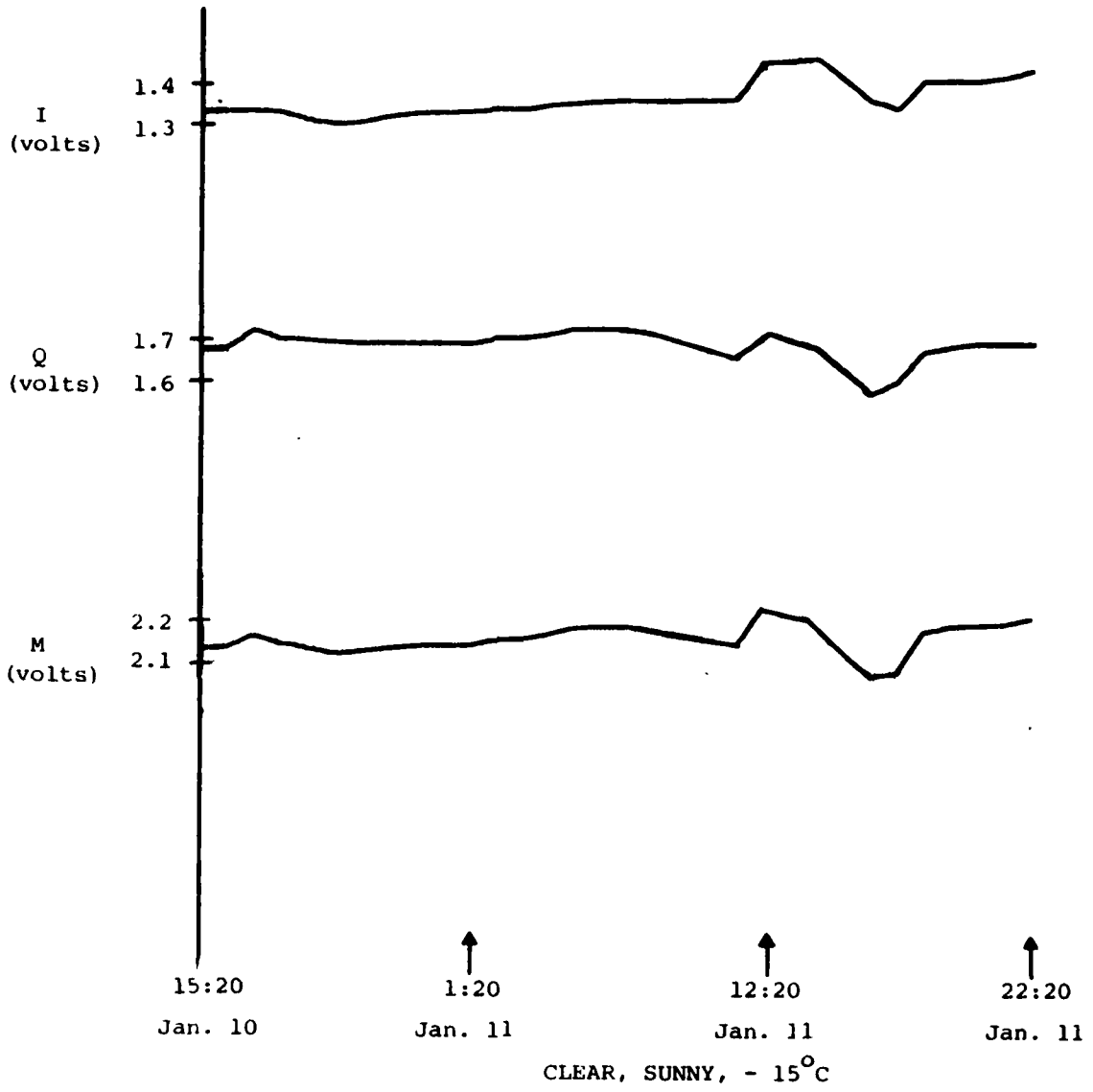

Figure 3.26: CW Profile - clear weather

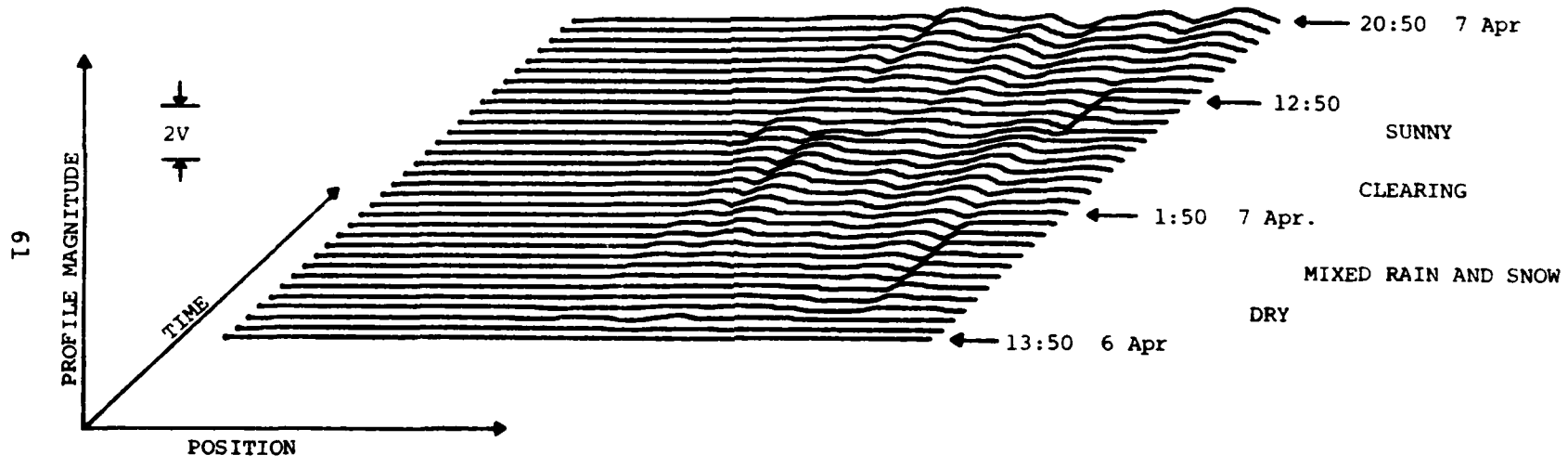

Figure 3.27: Pulse Profile Change - rain on dry ground

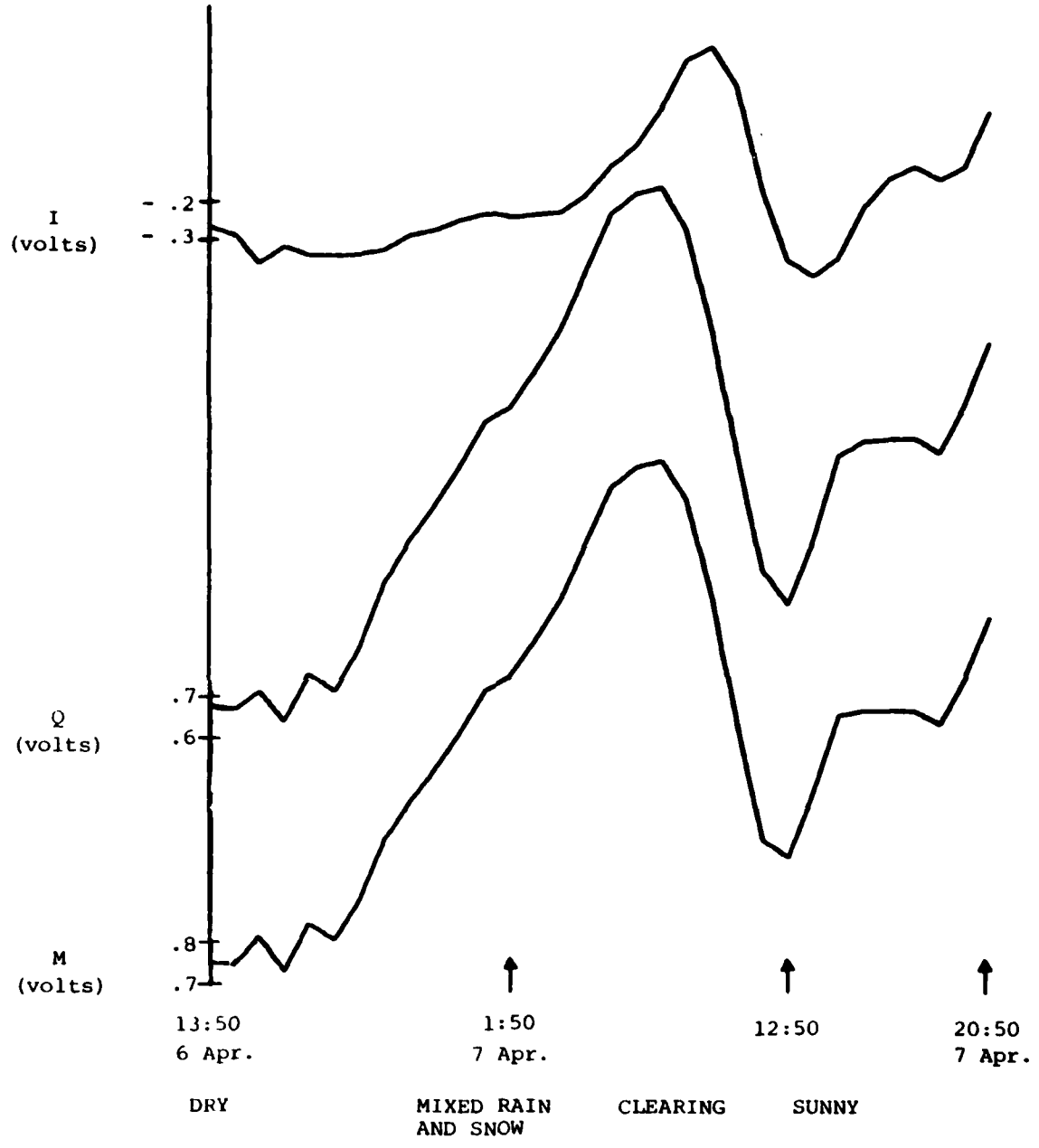

Figure 3.28: CW Profile - rain on dry ground

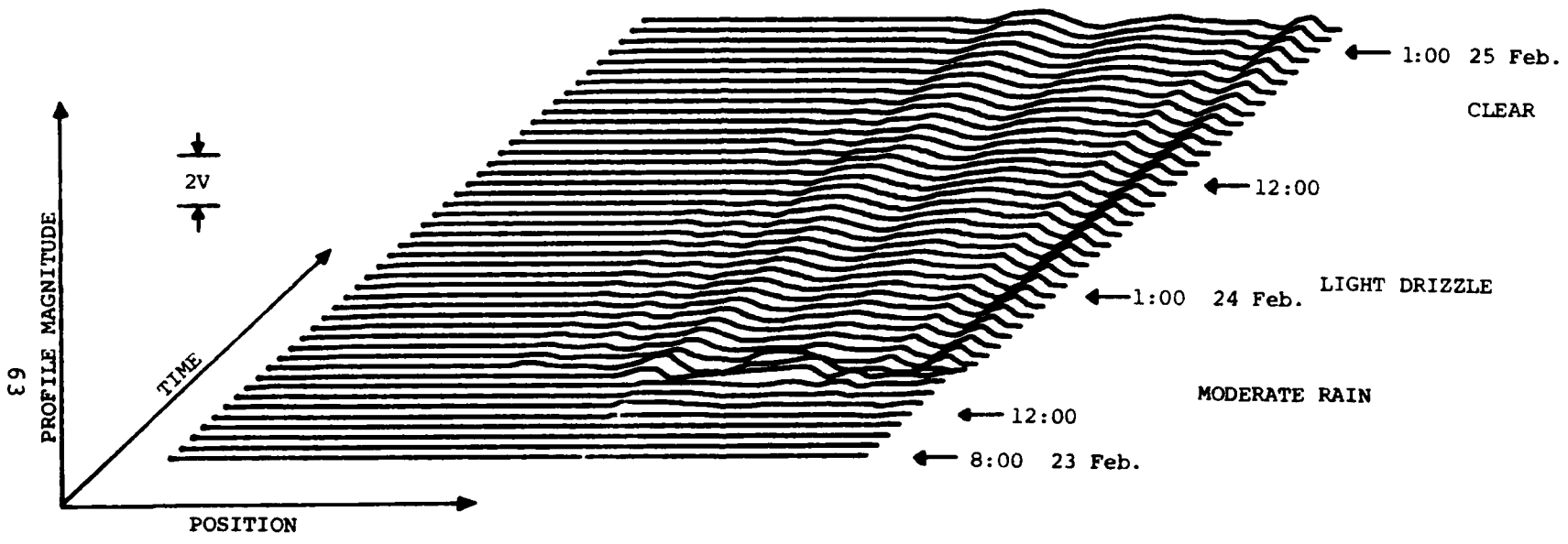

Figure 3.29: Pulse Profile Change - rain on snow

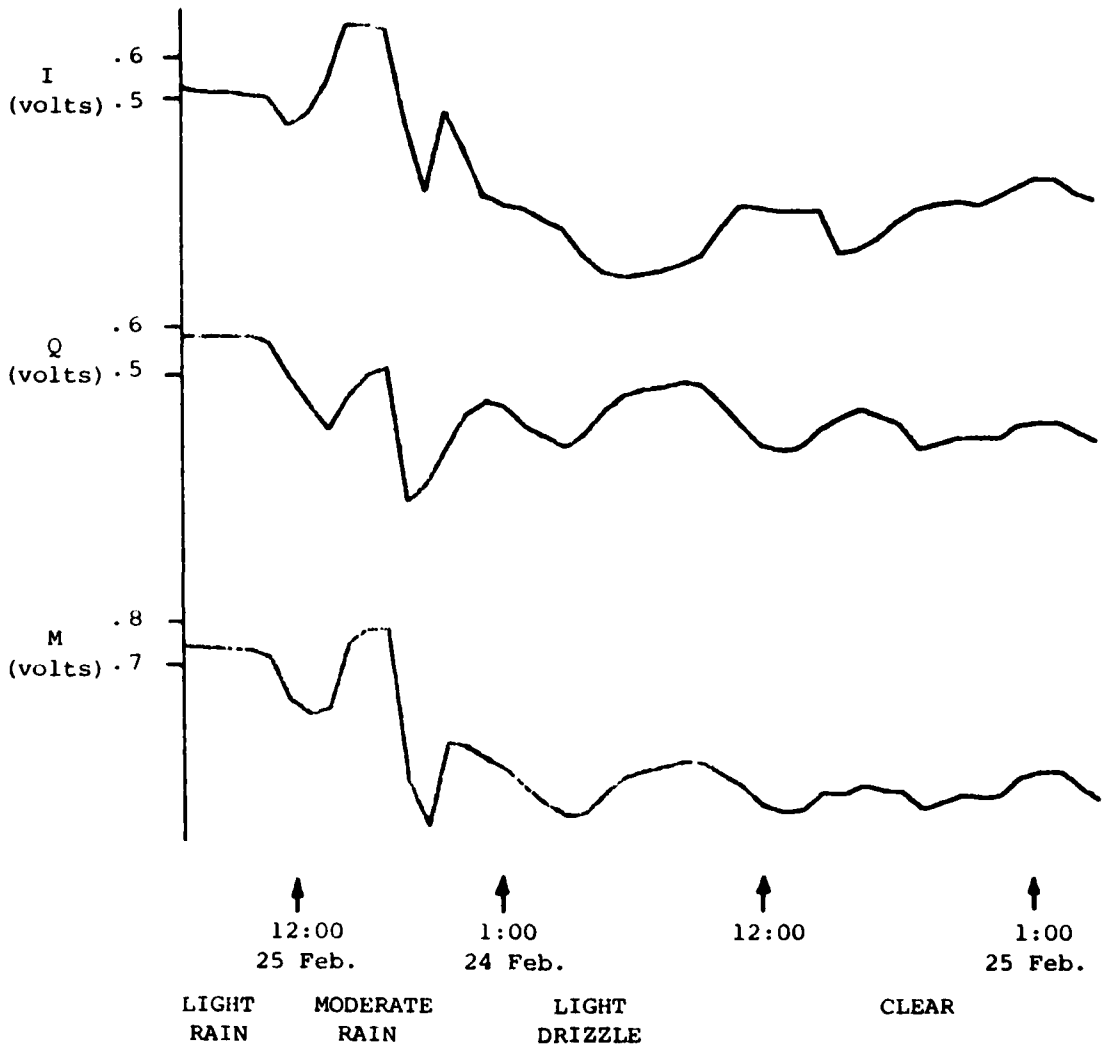

Figure 3.30: CW Profile - rain on snow

monitoring was done throughout only one winter season and since a particular combination of weather conditions occurs only once or twice during a season, in an uncontrolled fashion, it is not possible to be precise about the relation between the magnitude of an effect. The following general conclusions can be made.

- The presence of large amounts of moisture either in the snow above the cables or on the ground beneath has the most significant effect on profile and sensitivity. A decrease of up to 10 dB in the sensitivity can occur in any particular range cell. Similar variations in the profile in any range cell can also be expected.
- The sensitivity is enhanced by 2 to 3 dB when the ground is only slightly moist. The pulse profile also increases under the same conditions.
- The change in sensitivity in any range cell is unrelated to the absolute sensitivity in the same cell.
- Profile variations of up to 22 dB were measured during the experimental period although 10 dB was a more normal figure.
- The profile and sensitivity in a particular range cell appear to be only loosely correlated.
- Rapid changes in CW profile can be expected when rain falls on previously dry ground. An increase of 9 dB at a rate of 0.6 dB/hr. was noted. A decrease of 1 dB/hr was seen when the ground was drying out.
- Thawing of the ground surface causes a decrease of about 2 dB in the CW profile.
- Noise in the system is generated principally within the receiver. Weather conditions do not affect the noise appreciably.

4. VELOCITY MEASUREMENT

4.1 Introduction

A target moving longitudinally between the two sensors in a ported coaxial cable intrusion detection system causes a doppler shift in the frequency of the return signal. The purpose of the experiments described in this section was to demonstrate that the magnitude of the doppler shift could be used to measure the target velocity and furthermore, that the direction of motion of the target with respect to the transmitter could also be determined from the return signal.

The principle upon which the measurement technique is based can be conveniently described with the aid of a vector model of the return signal in the presence of a target shown in figure 4.1. Synchronous detection is used to obtain the in-phase (I) and quadrature (Q) components of the return signal. The reference profile, the return signal in the absence of a target, is represented in the figure by vector $\overline{R}$. With a target present, the profile changes to vector $\overline{P}_T$. The vector difference between $\overline{R}$ and $\overline{P}_T$ is referred to as the target profile $\overline{T}$. The phase $\phi(t)$ of $\overline{T}$ is calculated from the relation

$$\phi(t) = \tan^{-1}(\Delta Q/\Delta I) \qquad (4.1)$$

where

$$\Delta I = I_{\overline{P}_T} - I_{\overline{R}}$$

and

$$\Delta Q = Q_{\overline{P}_T} - Q_{\overline{R}}$$

The magnitude of $\overline{T}$ is

$$M_{\overline{T}} = [\,(\Delta I)^2 + (\Delta Q)^2\,]^{1/2} \qquad (4.2)$$

As a target moves down the cable the target profile $\overline{T}$ rotates about the centre of the circle in figure 4.1 with an angular velocity which is directly proportional to the linear velocity of the target.

The magnitude of the target profile $\overline{T}$ is determined by the magnitude of the field in the detection zone and the cross-section of the target. The cross-section is assumed to be constant for a particular target in a particular orientation. The phase of $\overline{T}$ depends upon the time taken for the electromagnetic energy to propagate from the transmitter to the target and back again. As the target moves

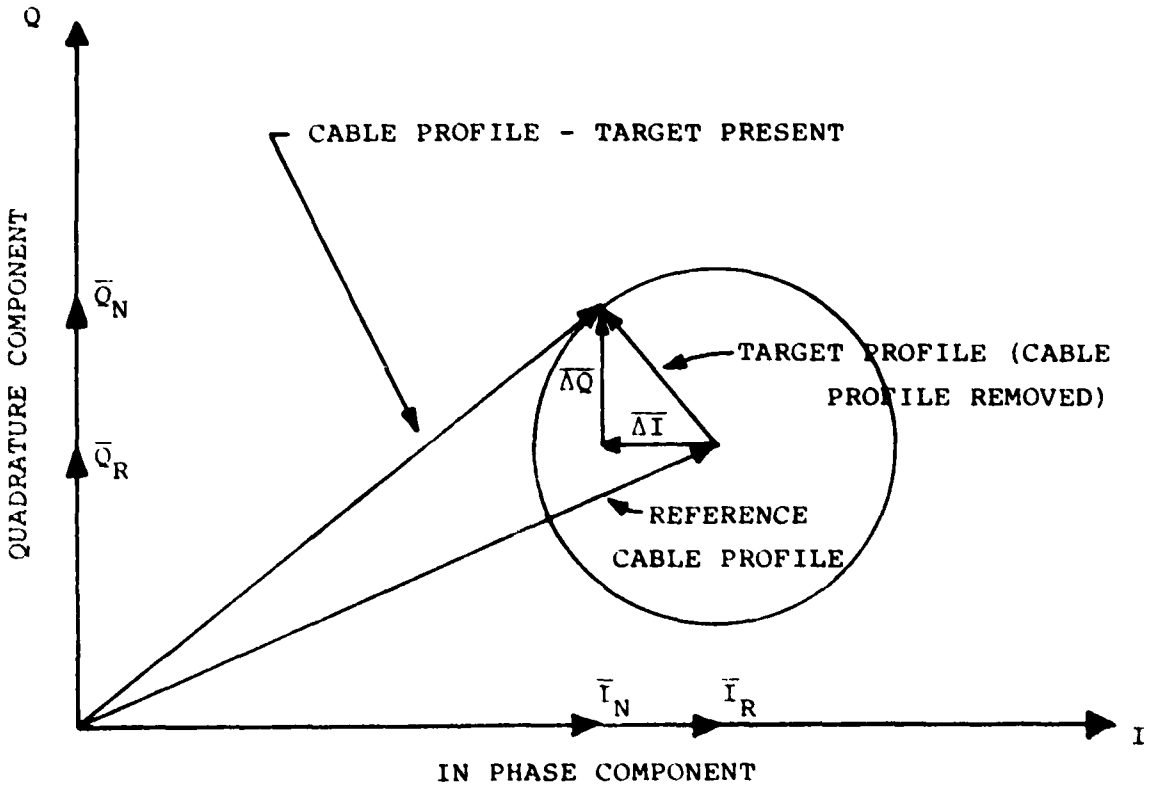

Figure 4.1: Vector Model of the Return Signal

away from the transmit end of the cables this path length increases and hence, so does the phase of $\bar{T}$. As the target moves towards the transmitter the path length and consequently, the phase of T decreases.

A 360 degree phase shift, or one complete rotation of target profile $\bar{T}$ in the vector diagram, corresponds to the target moving a distance of half the wavelength of the RF signal within the leaky co-axial cable. If a target moves at a constant velocity, $\bar{T}$ rotates at a constant angular velocity, and $\Delta\bar{I}$ and $\Delta\bar{Q}$ (the projections of $\bar{T}$ on the orthogonal axes) will vary sinusoidally. The frequency of these sinusoids will be directly proportional to the velocity of the target, and the direction of rotation of $\bar{T}$ will be an indication of the direction of motion of the target.

4.2 Processing

The overall processing scheme for the measurement of velocity from the return signal is shown in Figure 4.2. The recorded experimental data consists of two discrete sampled time sequences corresponding to the in-phase and quadrature components of the return signal. Let these two sequences be $\{I_n\}$ and $\{Q_n\}$, where

I_n = n^{th} sample in the in-phase sampled time sequence of the return signal

Q_n = n^{th} sample in the quadrature sampled time sequence of the return signal

$n = \{0, 1, 2, \ldots, N-1\}$

N = number of samples taken in each array.

The reference cable profile is first removed from the two arrays. If:

I_R = in-phase component of the reference cable profile, and,

Q_R = quadrature component of the reference cable profile

then

$$\left\{\Delta I_n\right\}_{n=0}^{N-1} = \left\{\Delta I_n + j\ Q_n\right\}_{n=0}^{N-1} \qquad (4.5)$$

The result of the transform operation is a complex spectrum $F\{x(n)\}$, where

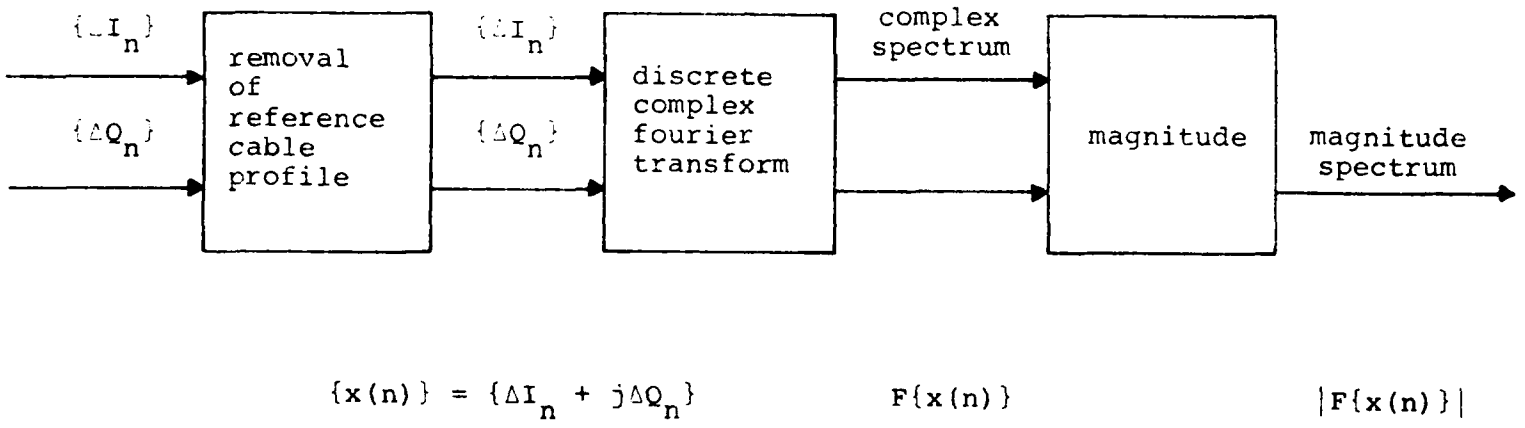

Figure 4.2: Velocity Measurement Processing Scheme

$$F\left\{x(n)\right\}_{n=0}^{N-1} = F\left\{\Delta I_n + j\,\Delta Q_n\right\}_{n=0}^{N-1}$$

$$= \sum_{n=0}^{N-1} (\Delta I_n + j\,\Delta Q_n)\exp(-j\,\frac{2\pi n}{N}\,k) \quad (4.6)$$

If f_s is the sampling frequency, k takes on discrete values that are integer multiples of f_s/N. The value of f_s/N is the frequency resolution of the spectrum. The magnitudes of the elements of the complex array form the power spectrum P(k), where

$$P(k) = \left|\sum_{n=0}^{N-1} (\Delta I_n + j\,\Delta Q_n)\exp(-j\,\frac{2\pi n}{N}\,k)\right| \quad (4.7)$$

Using this power spectrum, the average velocity v of the target can be calculated from the frequency of the largest spectral component by the relation:

$$v = \frac{1}{2} \times f_t \times \frac{v_{coax}}{f_c} \quad (4.8)$$

where,

f_t = frequency of the principal spectral component in the spectrum

v_{coax} = velocity of propagation of the electromagnetic wave in the leaky cable

f_c = carrier frequency

4.3 Experimental Procedure

A series of experiments was performed to verify the analysis presented in the previous section of this report. In each experiment the target moved along the cables at a velocity that was roughly constant. The total distance covered by the target and the time taken were each measured and the average velocity was calculated.

The return signal from a variety of different targets, moving at different speeds in both directions was recorded. The target moved either midway between the cables or just outside the receive cable. In all the experiments the sampling rate was high enough and the target velocity was low enough that no aliasing occurrred.

The cables were either suspended in the air at approximately 1.5 metres or laid on the ground. Targets used included a human walking, running or bicycling, a dog trotting, a car and a wooden cart. The cart travelled on a standard railroad track and bed which had been installed at the Queen's University field site for other experiments. It was propelled by a D.C. motor through a rope and pulley system.

The normal sequence of events in each experiment was as follows:

1) the return signal was recorded for 5 seconds with no target in the detection zone. This was done to establish a reference profile
2) the target entered the detection zone and remained at the starting point for 5 seconds
3) the target moved down the cables at the desired rate

Obviously, this procedure was impractical when either the trolley or the dog were used as targets. In the experiments involving either of these targets an estimate of the reference profile was obtained by averaging all the samples in each component array during the whole experiment.

4.4 Return Signal

Figure 4.3 is a plot of the I and Q components of the target profile recorded while a target (the trolley) moved between the cables at a velocity of 6.3 metres/sec. For this experiment the cables were in the air on wooden poles just outside the railway tracks. This signal is typical of those recorded in all the experiments dealing with velocity measurement.

An inspection of each component of the profile reveals the following features:

a) a basic sinusoidal signal
b) a low frequency overall envelope
c) a gradual decrease in the peak value of the envelope
d) a small amount of high frequency noise.

The frequency of the basic sinusoid is proportional to the velocity of the target. The slowly changing magnitude envelope results from non-uniform sensitivity of the system at different locations along the path due to interference between two different modes of propagation of energy along the sensor [16]. It transforms to a low frequency in the spectrum and does not hinder the velocity measurement

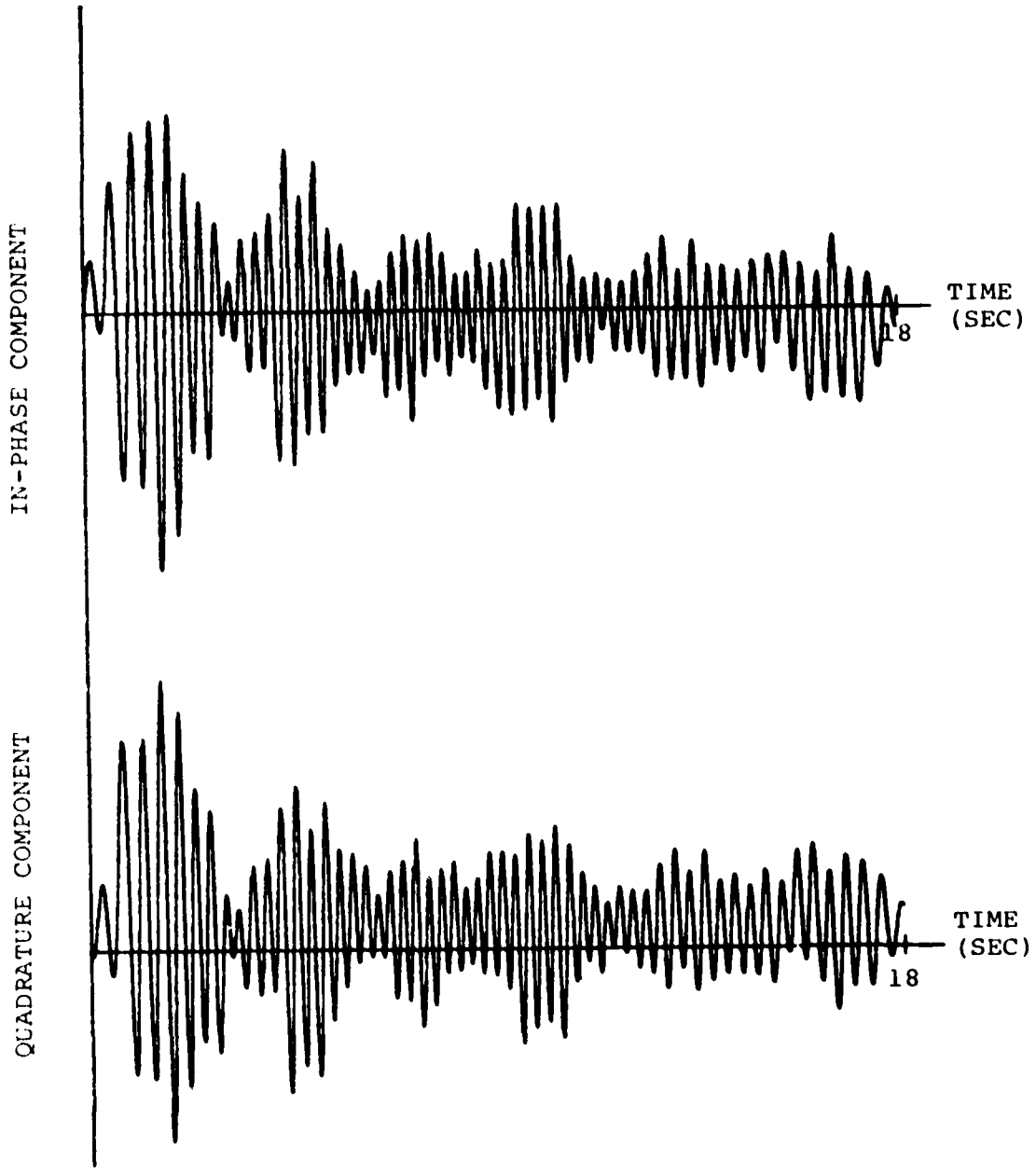

Figure 4.3: The Return Signal - ΔI and ΔQ

process. The gradual decrease in the peak value of the envelope as the target moves away from the transmit end of the sensor is due to cable attenuation. The high frequency noise can be attributed to the cables vibrating in the wind, grass in the vicinity of the cables, noise in the receiver and quantization noise.

4.5 Velocity Measurement

Table 4.1 summarizes the different combinations of target, target speed and cable placement used in these experiments.

Figure 4.4 shows the magnitude of the power spectra obtained in two different experiments. In each case the trolley moved along the track at a speed of 0.3 metres/sec. but in different directions. For the purposes of this report, all velocities toward the transmit/receive end of the cables will be considered to be positive, while all velocities away from the transmit/receive end are negative. Since the sampling rate of the system is 52.8 Hz, the power spectrum covers a range of ± 26.4 Hz. However, only the portion of the spectrum that contains the major frequency components of the baseband signal is plotted. A total of 1024 samples of the return signal were used in the transform implying that the sample points in the transform are .052 Hz apart.

Since, in all experiments, the velocities of the targets were fairly constant, the longitudinal axis can be considered to be a linear measure of doppler frequency or velocity, with a range of ± 0.5 Hz or ± 1.0 metres/sec. The vertical axis is the magnitude of the complex fourier transform. Although dimensionless, this magnitude is directly proportional to the energy at each discrete frequency in the baseband signal. In Figure 4.4 the frequencies of the largest peaks in the power spectra correspond to the doppler frequencies of the moving targets. The velocities are computed using equation 4.8.

The velocities computed from the spectra of Figure 4.4 were found to be in agreement with the measured values, indicating that the technique was effective for targets moving in both directions.

The power spectra in Figure 4.5 are computed from the return signals of five experiments in which a human walked down the cable at different speeds between 0.5 metres/sec. and 2.5 metres/sec. at intervals of 0.5 metre/sec.

The graph of Figure 4.6 shows the relationship between the velocities computed from the spectra of Figure 4.5 and the corresponding velocities measured during the experiment. It is seen that over this range of velocities, the computed and measured values are in good agreement.

The spectrum shown in Figure 4.7 was obtained from a human running at an average velocity of 6.6 m/sec. The cables were laid on the ground. The main spectral component occurs at a frequency indicating the average velocity of the target. As well, secondary peaks occur on either side of the main component. These secondary peaks are believed to be related to the motion of the legs and will be discussed in detail in the next chapter.

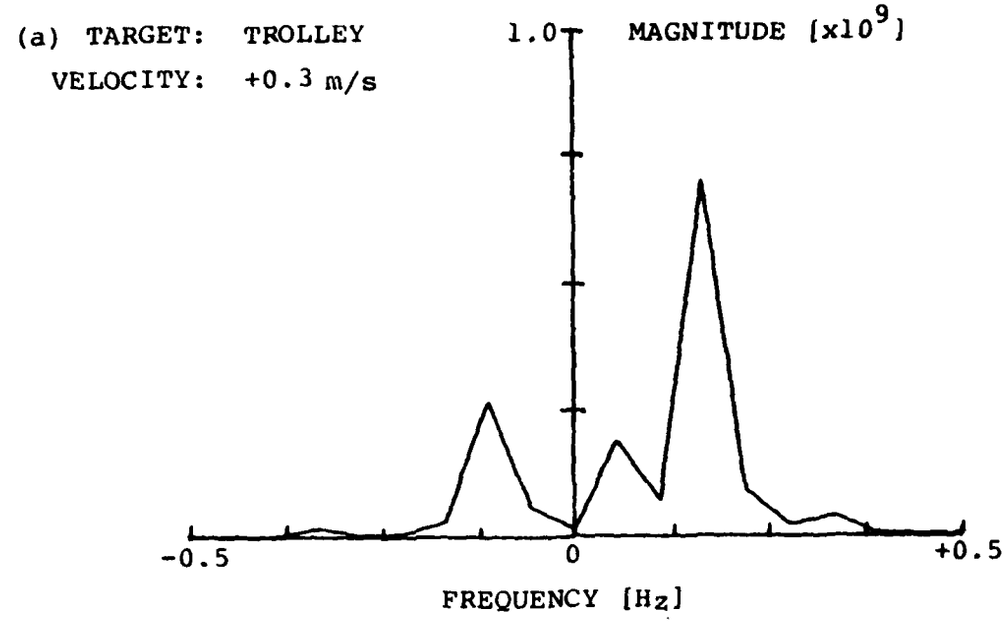

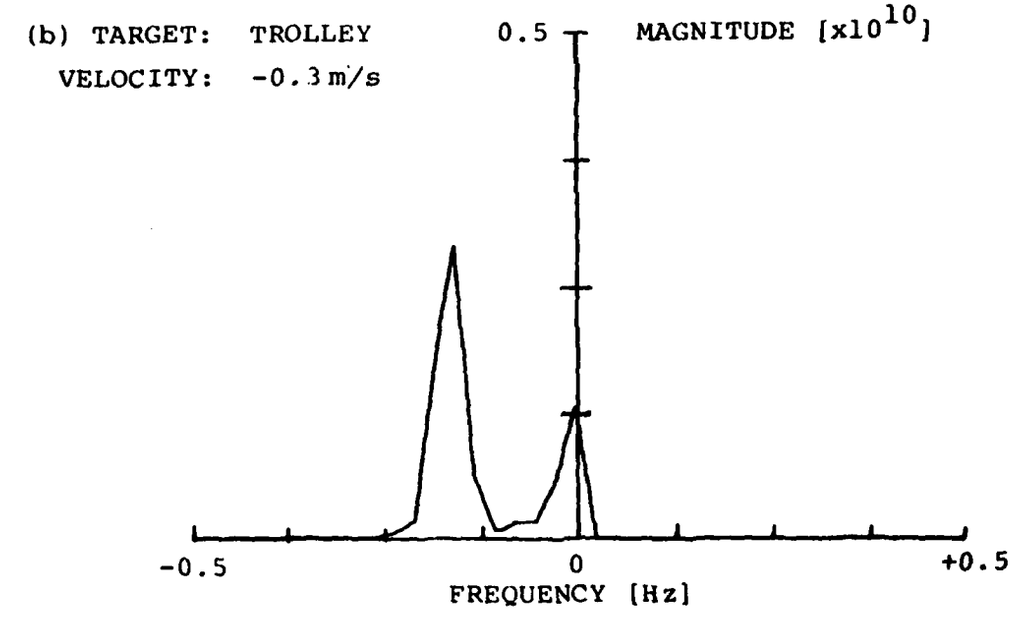

Figure 4.4: Spectra for Measurement of Velocity of Trolley

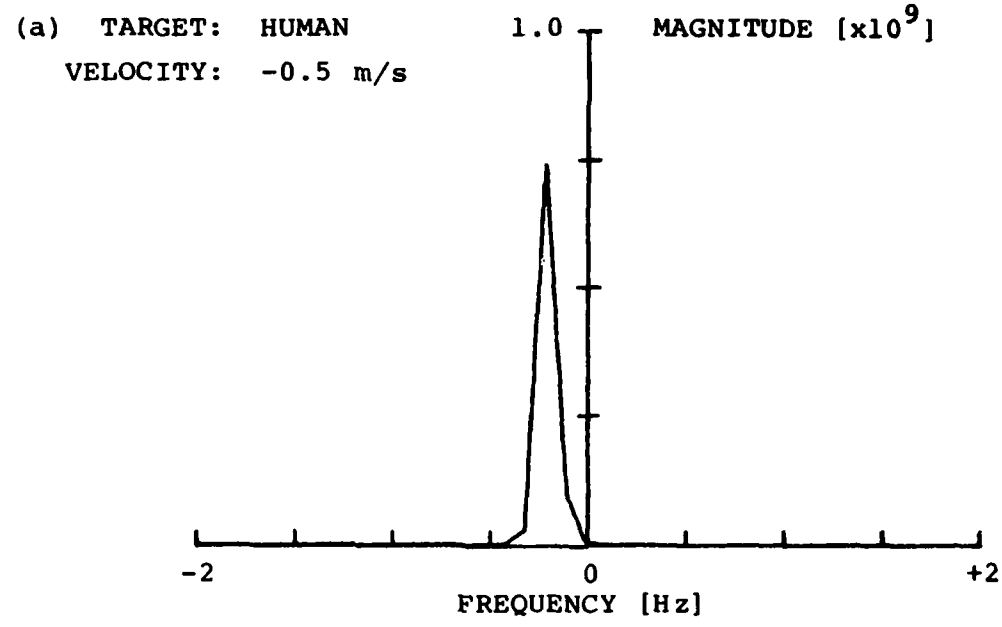

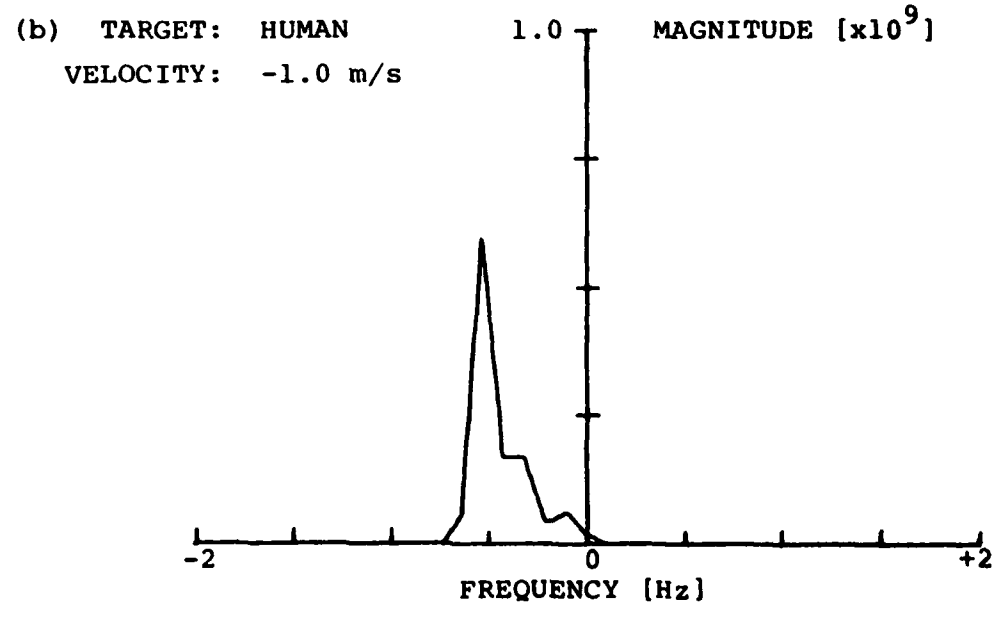

Figure 4.5: Spectra for Measurement of Velocity of Human

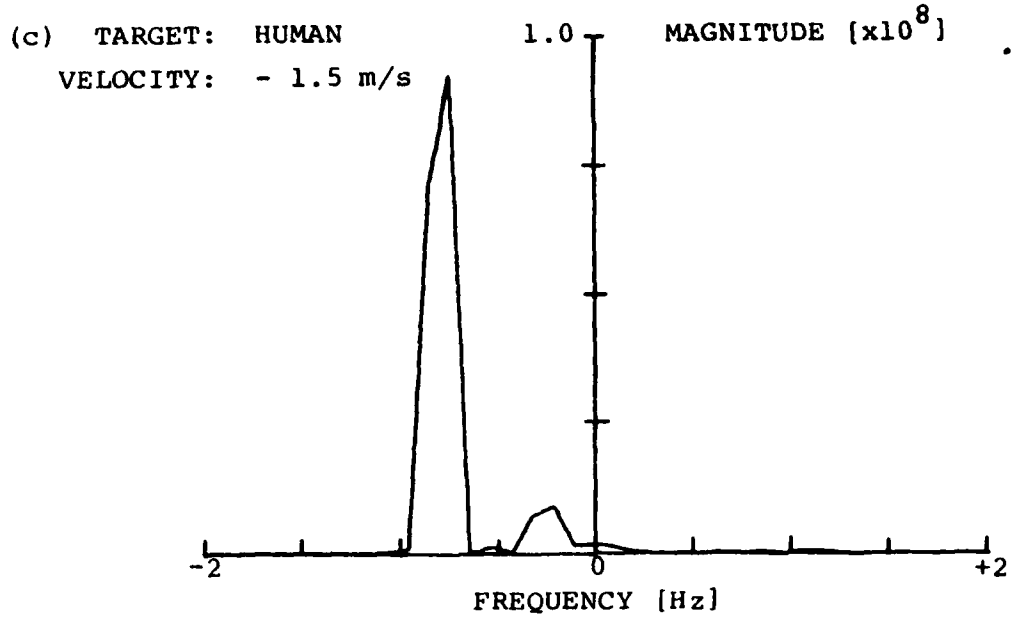

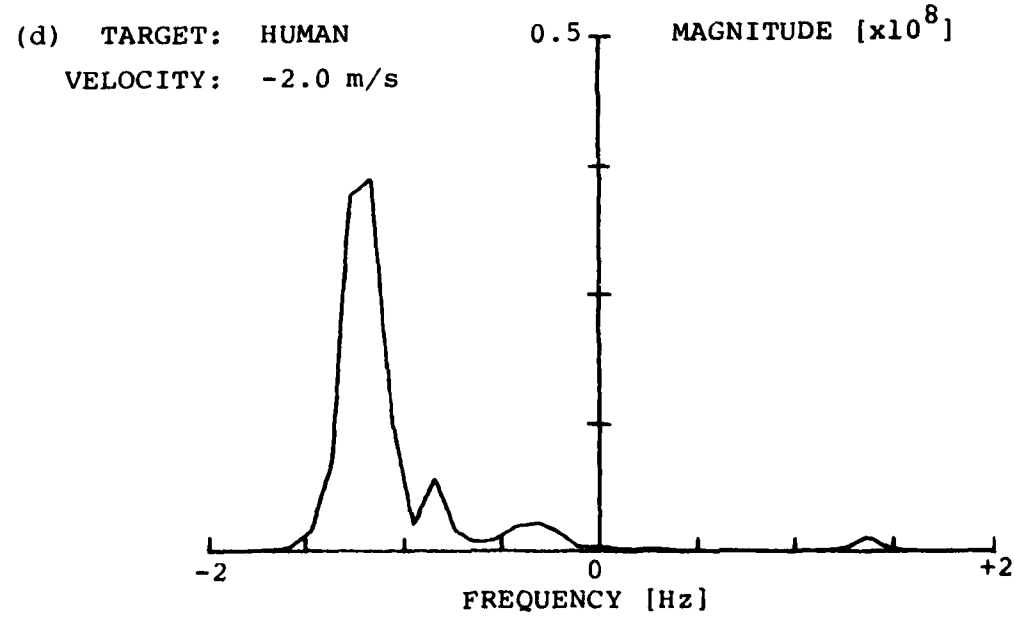

Figure 4.5: Spectra for Measurement of Velocity of Human

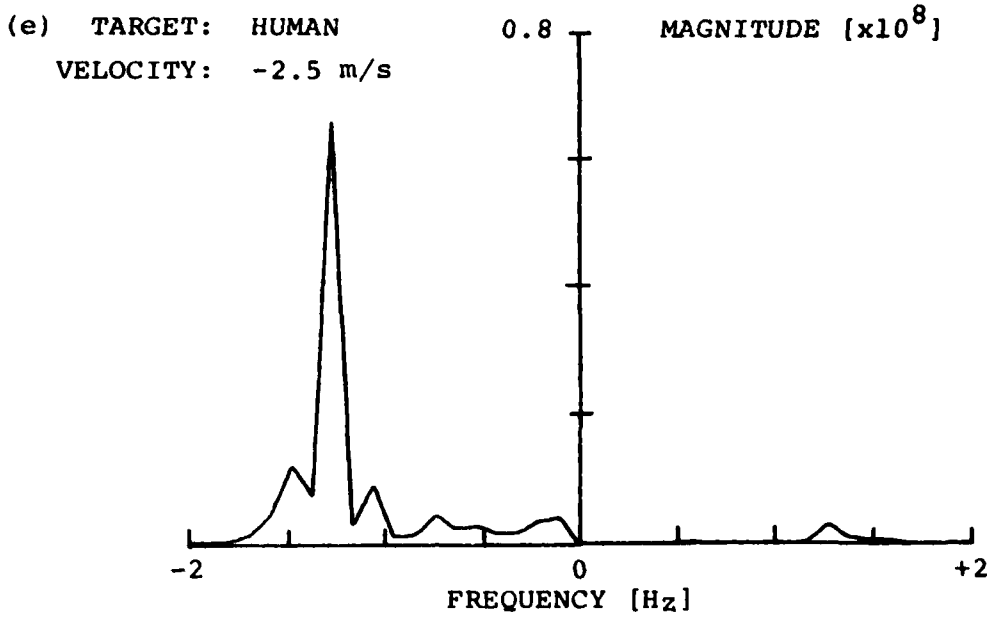

Figure 4.5: Spectra for Measurement of Velocity of Human

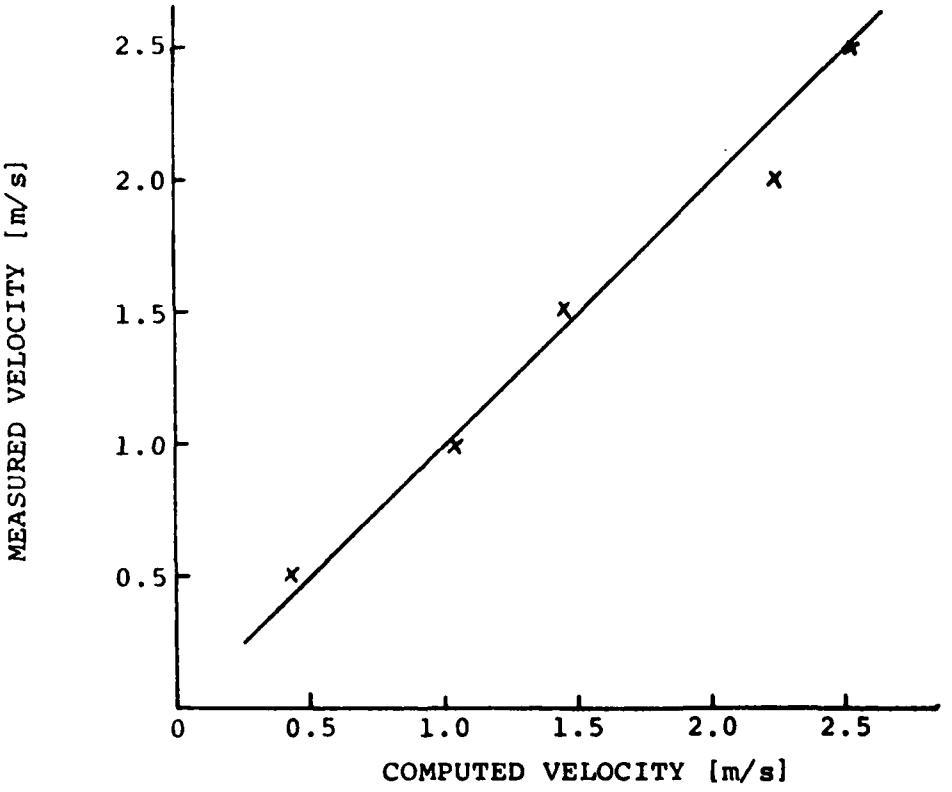

Figure 4.6: Relation Between Observed and Computed Velocity

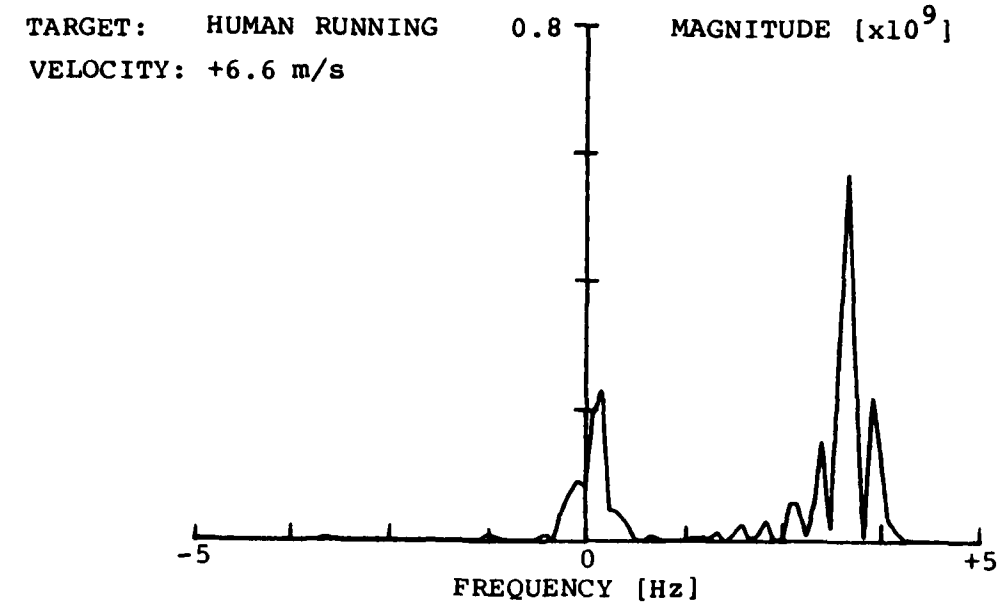

Figure 4.7: Spectrum for a Human Running

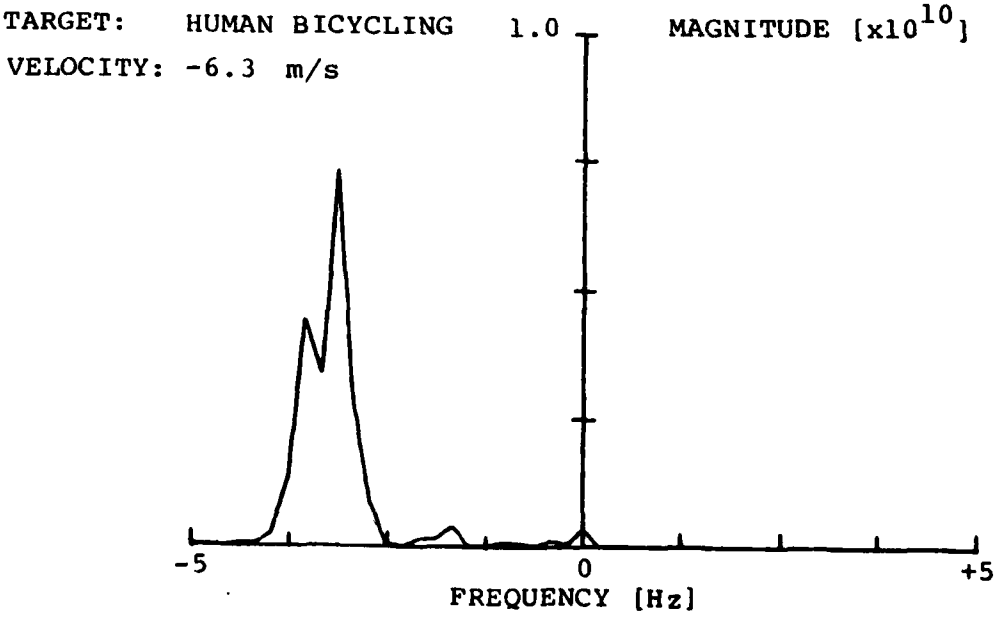

Figure 4.8: Spectrum for a Human Bicycling

Figure 4.8 is the spectrum for a human bicycling, and Figure 4.9 for a dog running between the cables. Figure 4.10 is the result obtained for a car travelling down the sensor just outside the cables.

In all cases the target velocity calculated from equation 4.8 corresponded to the measured target velocity. Neither the position of the cables with respect to the ground nor the location of the target with respect to the cables influenced the accuracy of the velocity measurement.

4.6 Multiple Targets

A number of experiments were conducted in which two targets moved along the sensor simultaneously.

To obtain the results shown in Figure 4.11 a human walked at + 0.85 m/sec in front of the trolley which was moving in the same direction at 0.2 m/sec. Spectral components are clearly visible corresponding to the average velocity of each target. In a different experiment two humans walked at the same speed in opposite directions. The spectrum of the return signal for the situation is shown in Figure 4.12. Again, a peak occurs in the spectrum corresponding to each target.

4.7 Conclusions

A C.W. guided radar system using leaky coaxial cables as the sensor can be used to measure the velocity of targets within the detection zone by calculating the doppler shift in the return signal. In this analysis the doppler frequency was calculated by means of a discrete complex fourier transform of a sequence of samples of the return signal. If, however, only a single target is in the detection zone and only a measurement of velocity is required (rather than "target signature" discussed in the next chapter) a much simpler processing scheme is possible. Either the I or Q components of the target profile $\overline{T}$ could be passed through an infinite clipper followed by a zero crossing detector. The zero crossing frequency would be directly related to target velocity.

The velocities of multiple targets within the detection zone can be independently measured using a C.W. system if they differ from each other (either in speed or direction) by an amount greater than the resolution of the system in frequency space. This property would allow the detection of multiple targets with a C.W. system, assuming, of course, that their velocities differ. If the targets are separated in space but have the same velocity then a pulsed guided radar must be used to resolve the targets. However, if the targets are resolvable in space with the pulsed system then the velocities of each target can be independently measured.

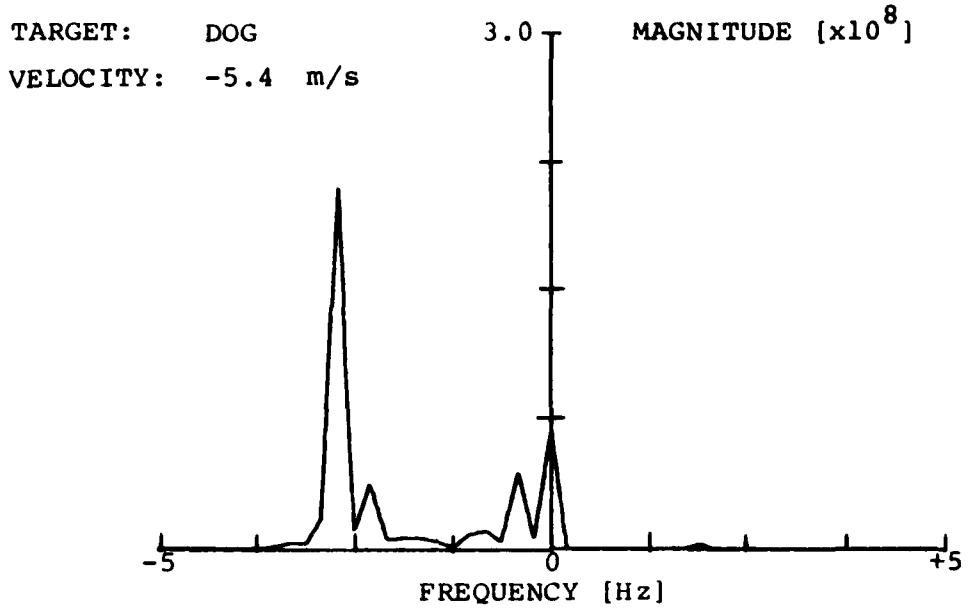

Figure 4.9: Spectrum for a Dog Running

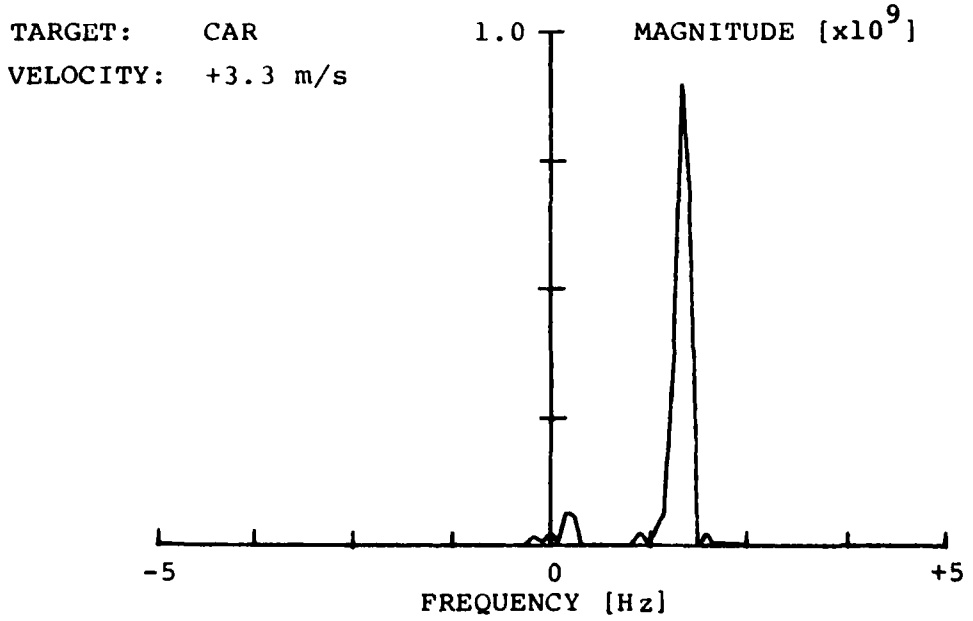

Figure 4.10: Spectrum for a Car

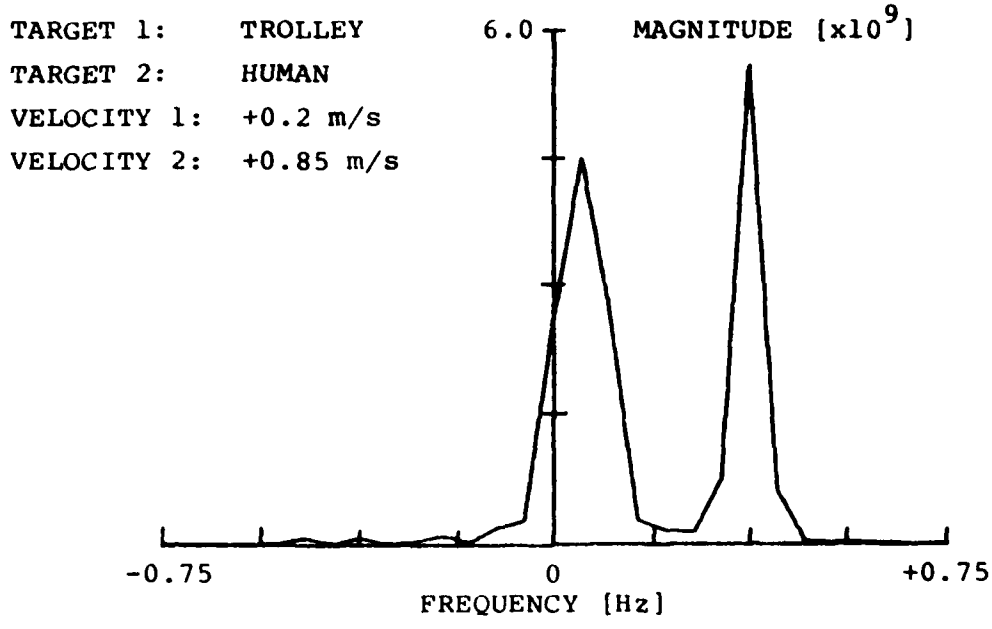

Figure 4.11: Spectrum for Two Targets - same direction

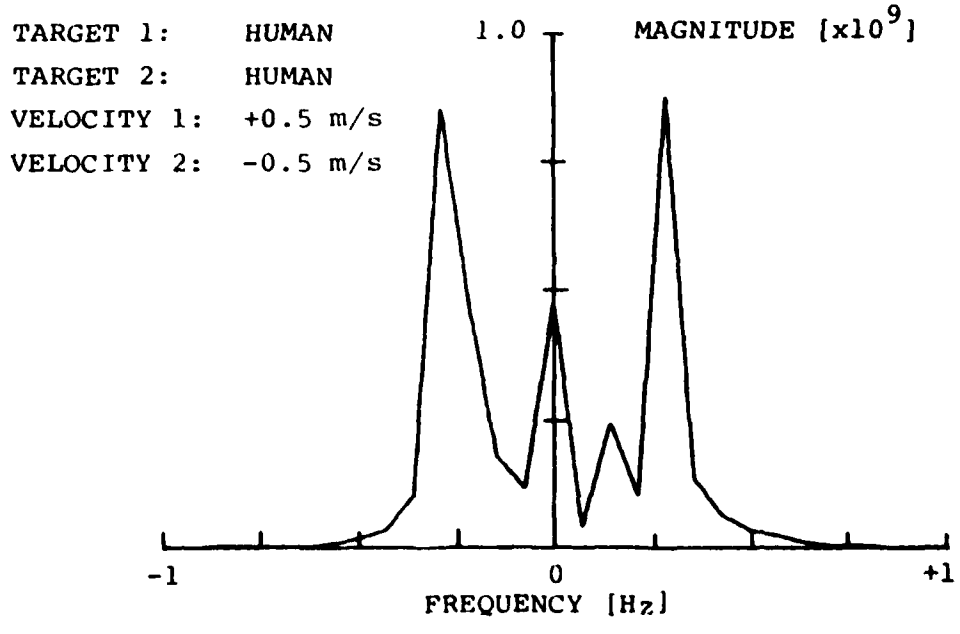

Figure 4.12: Spectrum for Two Targets - opposite direction

5. Target Classification

5.1 Introduction

After transforming the return signal from a leaky coaxial sensor into frequency space it is possible to identify components in the calculated spectrum which result from the doppler shift due to the average target velocity. The demonstration of this fact has been described in the previous chapter. The spectrum, however, should contain more information than simply the average velocity of a target; it should also contain information about the characteristic motion of individual parts of the target if they move at a velocity other than the average velocity. For instance, in the case of a human walking, although the body moves at a relatively constant velocity, the arms and legs do not. In addition, the body and each of the appendages have different effective radar cross-sections that are determined by their individual shape, size and location relative to the sensors. The overall return signal will be some combination of the return signal from each body part and hence will reflect the motion characteristics of the target components. The spectrum should also contain detailed information about target characteristics.

The purpose of the experiments described in this chapter was to demonstrate that the spectrum of the return signal contains information which could be useful for target classification.

5.2 Processing

The processing required for the analysis of the return signal for this application is an extension of that used in the measurement of target velocity. The scheme is shown in block form in figure 5.1. As was described in section 4.1, the recorded data consists of the arrays $\{I_n\}$ and $\{Q_n\}$, (the in-phase and quadrature components of the return signal), from which the target vector arrays $\{\Delta I_n\}$ and $\{\Delta Q_n\}$ are generated.

For performing a discrete fourier transform the finite duration sampled time sequence is assumed to be periodic with a period equal to the observation interval. The transformation then yields a discrete spectrum. However, when the data recorded consists of a non-integer number of cycles of a quasi-periodic waveform, phase jumps or discontinuities are caused at either end of the time sequence when the time sequence is assumed to be periodic. Spurious spectral components are produced by these discontinuities. The application of a digital "window" to the time sequences before transformation aids in ridding the frequency domain spectrum of some of this spectral leakage and smooths the spectral samples in the fourier transform.

Extensive literature exists concerning the selection of an appropriate filter or window for particular applications [8, 9]. Harris [10] provides a good summary of the use of various windows for harmonic analysis. Two important criteria for the selection of a window are the detectability of single frequency tones and the resolvability of neighbouring tones of similar strength. The 6 dB bandwidth of the central lobe of

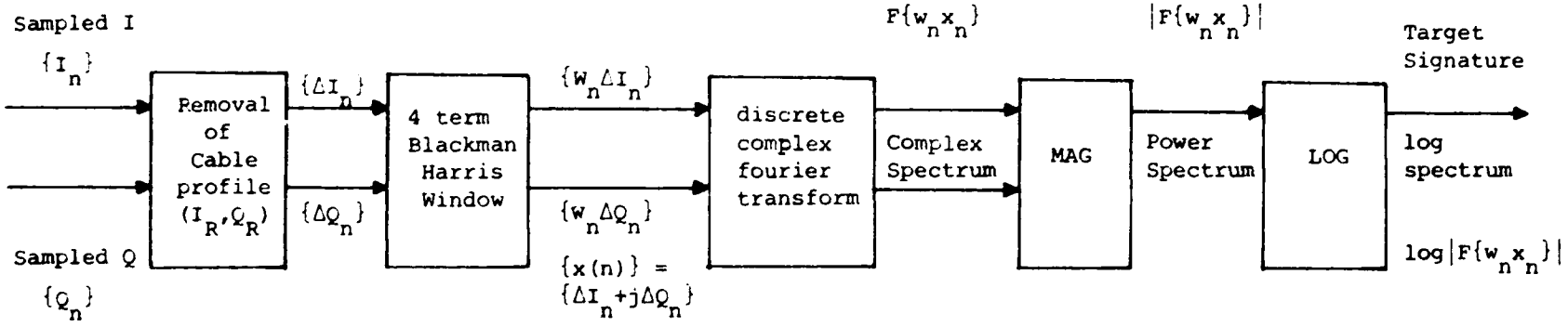

Figure 5.1: Target Signature Processing Scheme

AD-A087 475 QUEEN'S UNIV KINGSTON (ONTARIO) F/6 17/9
PERFORMANCE CHARACTERISTICS OF LEAKY COAXIAL CABLES.(U)
APR 80 J L MASON F19628-77-C-0249
UNCLASSIFIED RADC-TR-79-340 NL

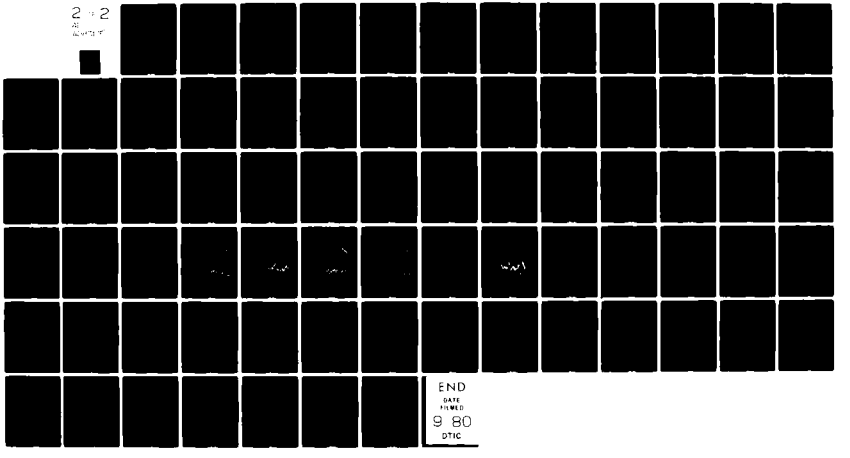

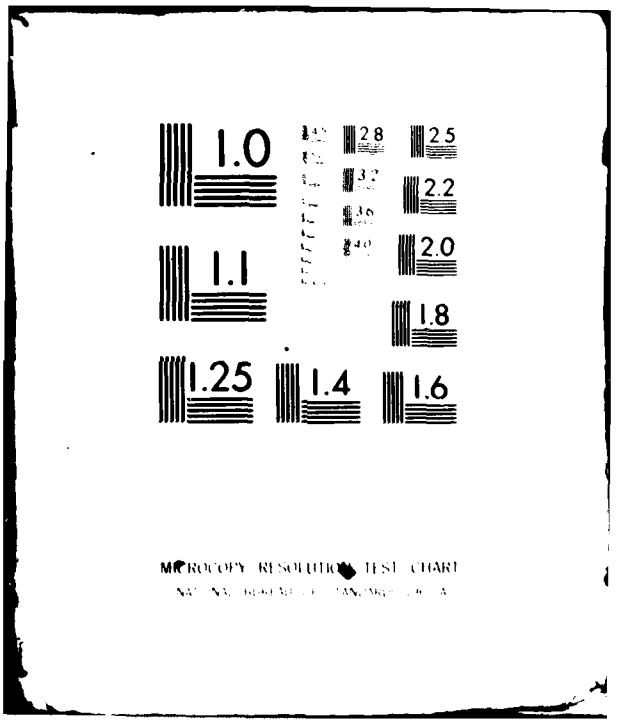
1.0
1.1
1.25
1.4
1.6
1.8
2.0
2.2
2.5
2.8
3.2
3.6
4.0
MICROCOPY RESOLUTION TEST CHART

the transform of the window is a measure of the resolvability. A low sidelobe level increases the detectability of weak tones in the presence of strong ones. Choice of a window usually entails a trade-off between the highest sidelobe level and the 6 dB bandwidth.

The window employed in the processing scheme for target classification was the so-called Blackman-Harris window. The weighting functions w_n for this window are generated by the relation:

$$\left\{w_n\right\}_{n=0}^{N-1} = \left\{a_0 - a_1 \cos(\frac{2\pi}{N} n) + a_2 \cos(\frac{2\pi}{N} 2n) - a_3 \cos(\frac{2\pi}{N} 3n)\right\}_{n=0}^{N-1} \quad (5.1)$$

where

N = number of samples taken,

and

a_0, a_1, a_2, a_3 are constants selected in accordance with desired window properties.

The Blackman Harris window was selected because it possessed properties suitable for use in harmonic analysis, and in addition was simple to implement digitally. In the trade-off between the sidelobe level and the 6 dB bandwidth, a sidelobe level of - 74 dB was chosen, commensurate with the dynamic range of the system. The coefficients of the window were:

$a_0 = 0.40217$

$a_1 = 0.49703$

$a_2 = 0.09392$

$a_3 = 0.00183$

The window had the following properties:

highest sidelobe level = - 74 dB

sidelobe fall off rate = - 6 dB/octave

6.0 dB bandwidth - 2.44 bins[1]

3.0 dB bandwidth = 1.74 bins.

[1]In a discrete spectrum the distance between adjacent discrete frequencies is called a bin.

Figure 5.2(a) shows the envelope of the window, and Figure 5.2(b) the log magnitude of its transform in dB, normalized to its peak value.

The data arrays $\{\Delta I_n\}$ and $\{\Delta Q_n\}$ are windowed using this Blackman-Harris window and modified to arrays $\{w_n\ \Delta I_n\}$ and $\{w_n\ \Delta Q_n\}$ respectively.

The windowed time sequences are the real and imaginary inputs to a discrete complex fourier transform. If the complex input sequence is $\{x(n)\}$, then:

$$\left\{x(n)\right\}_{n=0}^{N-1} = \left\{w_n\ \Delta I_n + j\ w_n\ \Delta Q_n\right\}_{n=0}^{N-1} \tag{5.2}$$

These sequences are then transformed into complex frequency space. Hence:

$$F\left\{x(n)\right\}_{n=0}^{N-1} = F\left\{w_n\ I_n + j\ w_n\ Q_n\right\}_{n=0}^{N-1}$$

$$= \sum_{n=0}^{N-1} (w_n\ \Delta I_n + j\ w_n\ \Delta Q_n)\exp(-j\frac{2\pi n}{N}\ k) \tag{5.3}$$

where N is the total number of samples.

f_s is the sampling frequency, and k takes on discrete frequency values that are integer multiples of f_s/N.

The power spectrum P(k) is:

$$P(k) = \left|\sum_{n=0}^{N-1} (w_n\ \Delta I_n + J\ w_n\ \Delta Q_n)\exp(-j\frac{2\pi n}{N}\ k)\right| \tag{5.4}$$

The base 10 logarithm of this power spectrum generates the log spectrum referred to as the target signature. Hence the target signature T(k) is:

$$T(k) = 20\ \log_{10}\left|\sum_{n-0}^{N-1}(w_n\ \Delta I_n + j\ w_n\ \Delta Q_n)\exp(-j\frac{2\pi n}{N}\ k)\right| \tag{5.5}$$

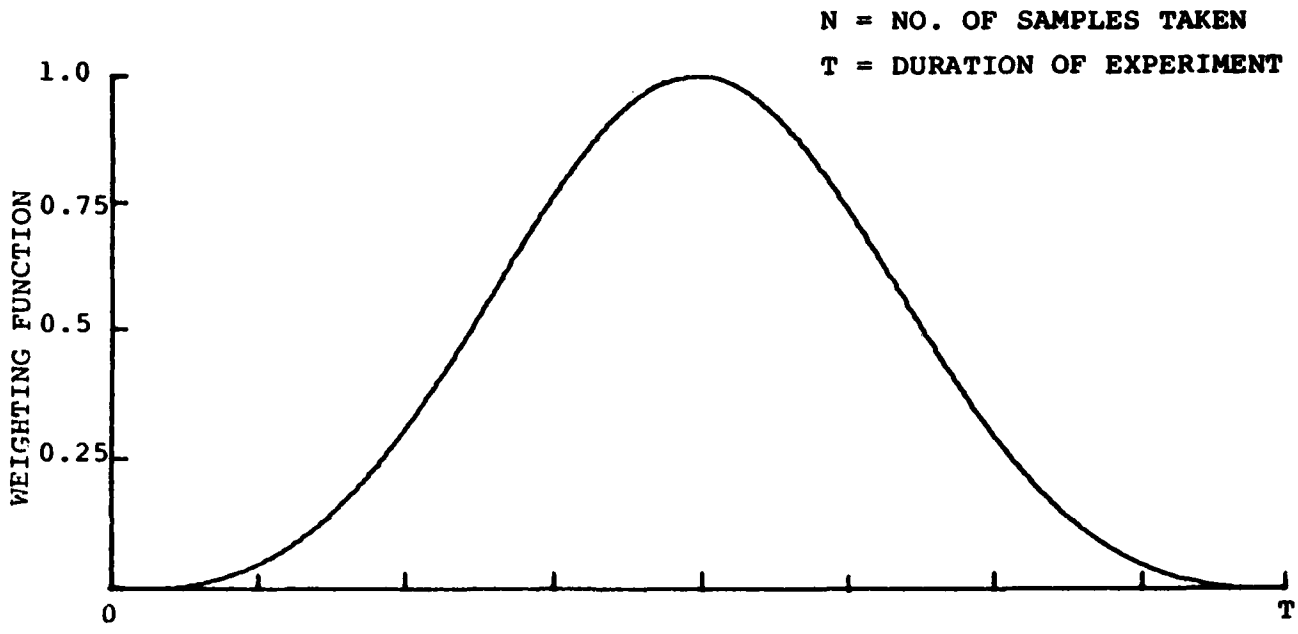

(a) ENVELOPE OF WINDOW

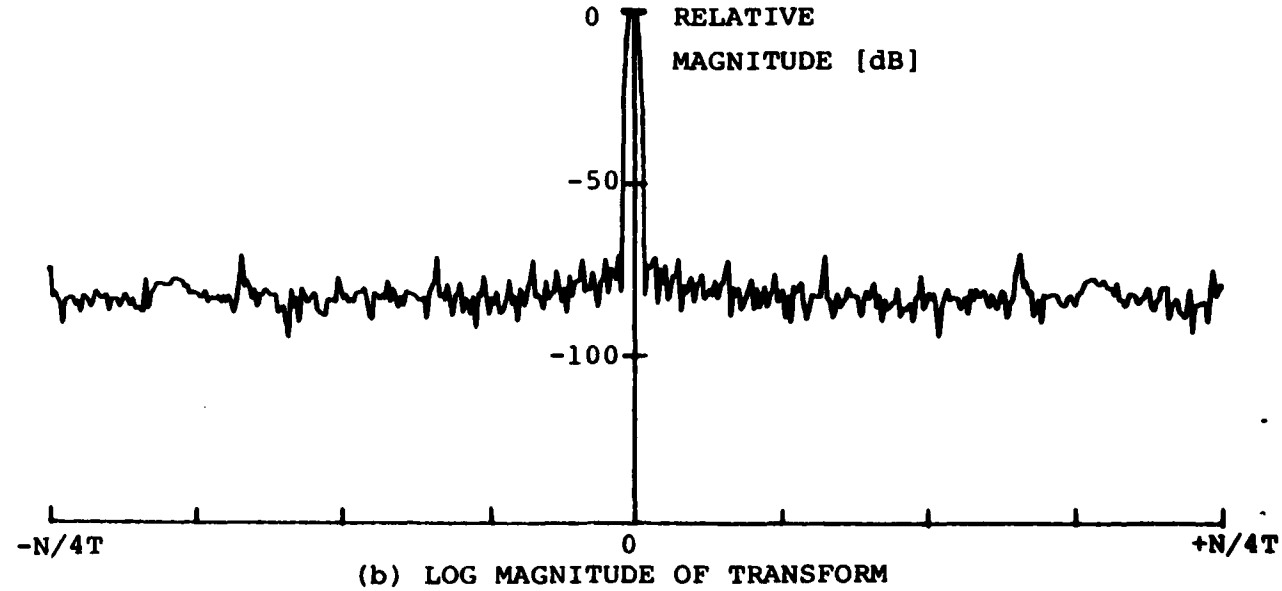

(b) LOG MAGNITUDE OF TRANSFORM

Figure 5.2: Blackman-Harris Window

This target signature is the principal tool that is used to demonstrate the feasibility of rudimentary target classification using a guided radar system.

5.3 Experiments

A variety of different types of targets were used in the experiments. Since the purpose was to demonstrate that certain characteristics of the way in which different targets moved would be reflected in the target signature, targets were chosen with kinematics of locomotion as different from each other as possible. These included humans walking, running and bicycling; a dog running; the trolley on a railroad track; and a car being driven along the sensor just outside the cables.

A series of experiments was also performed using a human target with the cables at various heights above the ground from 0 m to 2 m. These experiments were designed to demonstrate the variation in target signature which occurs because of the non uniform distribution of the field around the leaky cable sensor.

5.4 Results

5.4.1 Human Targets, normal walk

The first series of experiments all involved a human as the target, walking midway between the cables. The walk however, was not a natural one. To reduce the complexity of the observed signature the target maintained his arms stationary with respect to his body at all times.

The experimental series is summarized in Table 5.1 and typical signatures are given in figures 5.3 to 5.5.

Figure 5.3 demonstrates the effect of cable height on the sidelobe structure of the signatures. The walk which resulted in figure 5.3(a) was done at - 1 m/sec while the other two walks were at - 0.5 m/sec. As might be expected a large spectral component occurs in all signatures corresponding to the average velocity of the target. There is also considerable structure in the signatures at other frequencies particularly when the cables were on the ground. In particular, in figure 5.3(a) it is seen that the primary peak is located at -0.5 Hz, while secondary peaks occur at -4.0 Hz, -2.2 Hz, +0.5 Hz, +1.1 Hz, +2.9 Hz and +4.6 Hz. For the present, if the peak at +0.5 Hz is ignored, then all other peaks are found to occur at frequencies that are integer multiples of the primary frequency component. In addition, the distance (in frequency space) between neighbouring peaks is approximately three times the primary frequency. The first sidelobe was typically 18 dB lower than the central peak and the second sidelobes were approximately 38 dB lower.

Table 5.1

SUMMARY OF HUMAN TARGET SIGNATURE EXPERIMENTS

Speed (m/s)	Direction	Cable Height (m)	
1.5	+	0	
0.5	-	0	
1.0	-	0	
1.5	-	0	
2.0	-	0	
2.5	-	0	
0.5	-	1	
1.5	-	1	
0.5	-	2	
1.0	+	2	
0		0	Marking Time
0		0	Swinging arms

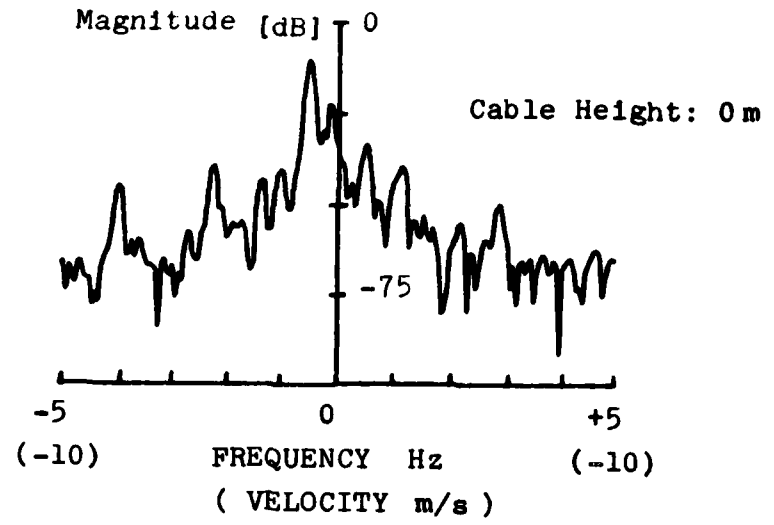

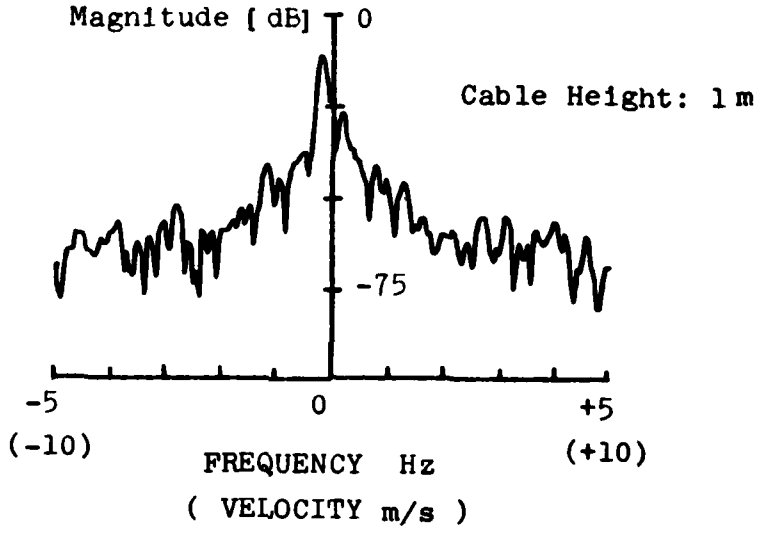

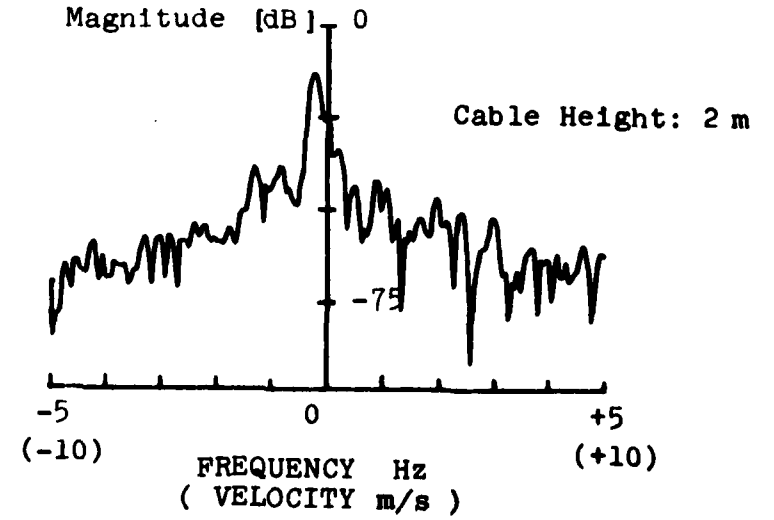

Figure 5.3: Effect of Cable Height on Human Target Signatures

The signature for the human walk with the cables 1 m in the air is shown in figure 5.3(b). Again sidelobes are evident in the signatures although they are considerably less distinct than they were with the cables on the ground. When the cables were 2 m in the air (figure 5.3(c)) the signature was basically similar to that obtained with the cables 1 m high. In both these figures the position of the discernable sidelobes is related to the position of the main peak in the same fashion as was noted above.

The existence of the secondary peaks in the signatures for a human walk and their particular position in frequency space with respect to the main peak are due to the motion of the legs and feet of the target and the cyclic manner with which they move.

When the cables are on the ground the effects of leg motion are more clearly seen in the signature because the coupled field strength in the vicinity of the legs increases. The energy seen in the return signal at any given doppler frequency would be expected to be the product of an effective "cross-section" for the portion of the target concerned and the field strength in that region.

The position of the sidelobes with respect to the central peak is determined by the normal pattern of leg motion. For a walking human target, these secondary peaks appear in the vicinity of a frequency

$$f_n = f_o + 3nf_o \qquad 5.6$$

where f_o = frequency representing the average walking speed

n = an integer

This relation holds true over a considerable range of walking speeds. This is demonstrated by the signatures shown in figure 5.4 and the data from a series of experiments summarized in Table 5.2. The validity of equation 5.6 reflects the fact that increased walking speed is normally accomplished by humans by increasing step frequency rather than step length.

The return signal and consequent signature for a human target walking between the sensors has been simulated based upon a study of the kinematics of leg motion during normal locomotion. The relationship between sidelobe position in the signature and the peak representing average velocity will be discussed more fully in the Section 6 of this report.

In addition to the secondary peaks in the signature which have been identified as resulting from leg motion, for each principal spectral component an image component occurs, 15 to 25 dB lower, at the corresponding frequency on the opposite side of the zero frequency axis. This effect is clearly visible in the signatures shown in figure 5.5. These peaks occur because of inaccuracies in the quadrature oscillator and in the I and Q channel gains in the synchronous detector. They will be more fully discussed in Section 5.5.

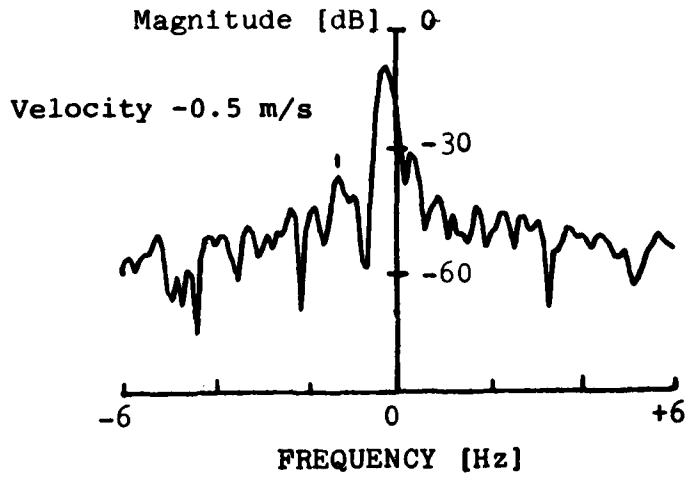

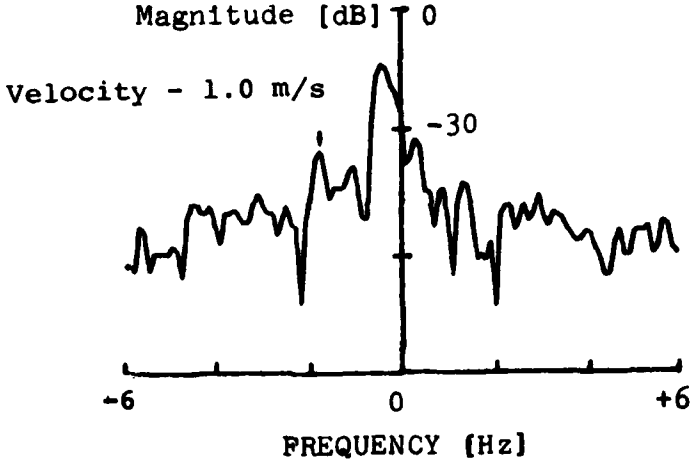

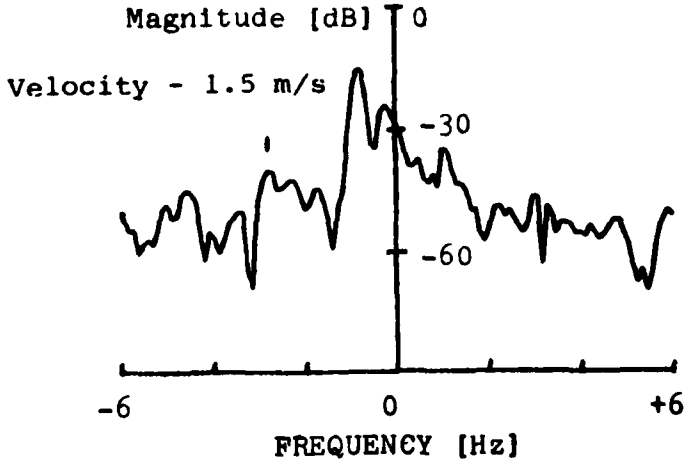

Figure 5.4: Signatures of Human Targets

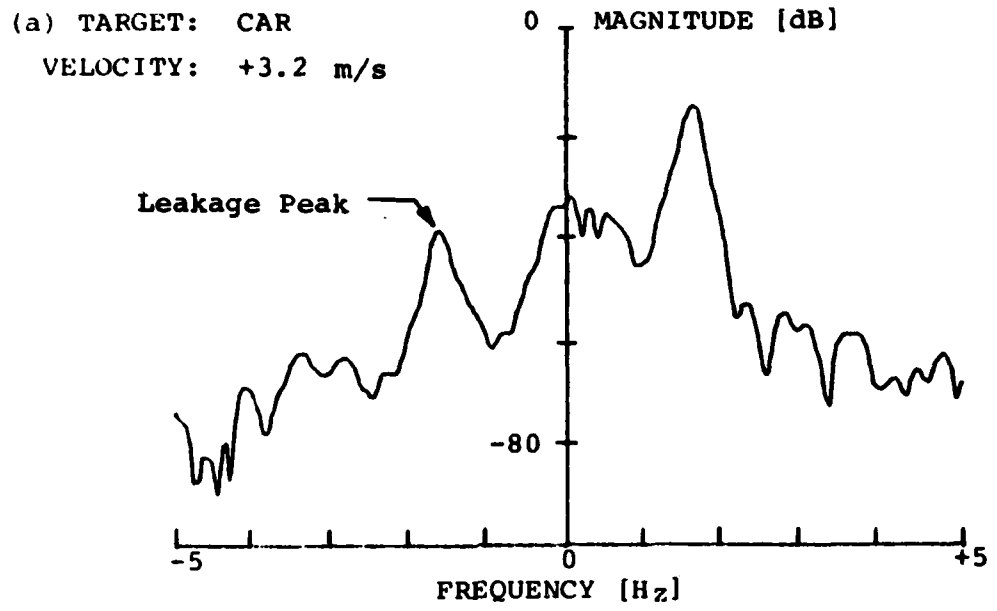

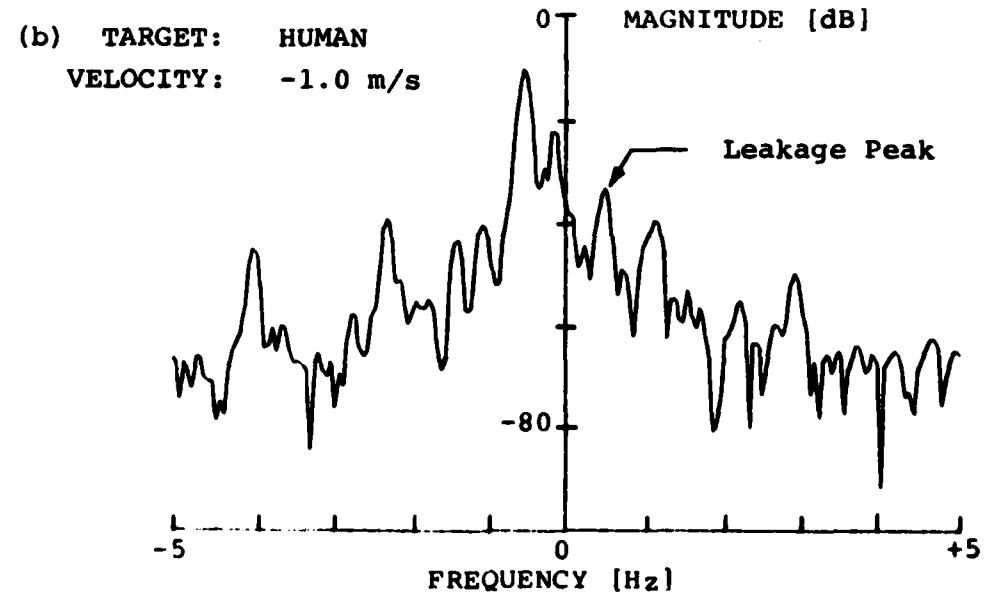

Figure 5.5 Signatures Demonstrating Spectral Leakage

5.4.2 Human Target, other motions

Signatures were also obtained for human targets a) marking time (figure 5.6) and b) swinging his arms parallel to the cables (figure 5.7). In the first case the cables were on the ground and in the second case were 1 metre off the ground. In both cases the cyclic motion of the appropriate appendage produces a distinct sideband structure. Since the average velocity is 0 m/sec the largest spectral component occurs at zero Hz.

5.4.3 Other Targets

Four other targets with motion dynamics considerably different from those of a human walking were also used. These were

a) a car - figure 5.8
b) the trolley on the railroad track - figure 5.9
c) a human bicycling - figure 5.10
d) a dog running between the cables - figure 5.11

For both the car and the trolley the target signatures were composed of the main spectral peak corresponding to the average velocity of the target with few other distinct features in the sidebands. The "leakage" of energy from one frequency to the corresponding frequency on the opposite side of the zero frequency axis is clear in these signatures.

The signatures for the bicycle target, shown in figure 5.10, have some structure in the sidebands but the regularity of the sidelobes that occurred in the signatures of walking targets is not present. Although there is some motion of the legs in the horizontal plane when riding a bicycle, the speed of travel of the legs, with respect to the average velocity, is less than when walking due to the gearing on the bicycle. Also, the amplitude of motion in the horizontal plane, again with respect to the bicycle, is also less then when walking.

Figure 5.11 shows the target signature of a dog running down the cables. Here, as in the signature of the human walk, secondary peaks are visible, and are caused by the motion of the dog's feet. In frequency space, the position of the secondary peaks relative to the principal peak differs from that of the human target signature. This is due to the fact that dogs have different kinematics of motion than humans.

5.5 System Inaccuracies

Certain inaccuracies in the system hardware components cause the spectral components in the signatures to be reflected about the zero frequency axis. Measurements were performed on the system components to establish the magnitude of various system errors on the target signature. These errors were:

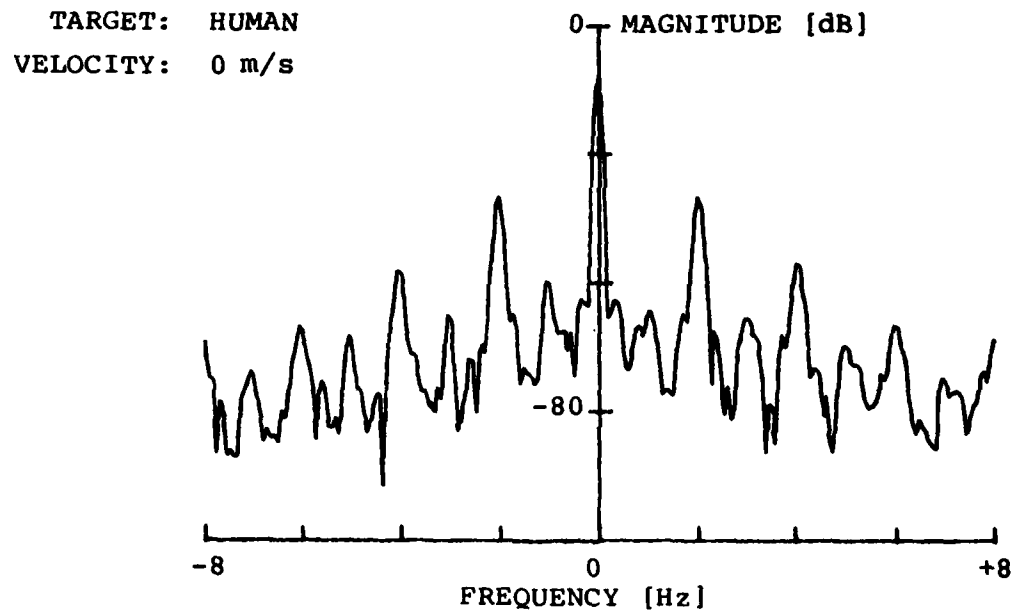

Figure 5.6: Human Marking Time

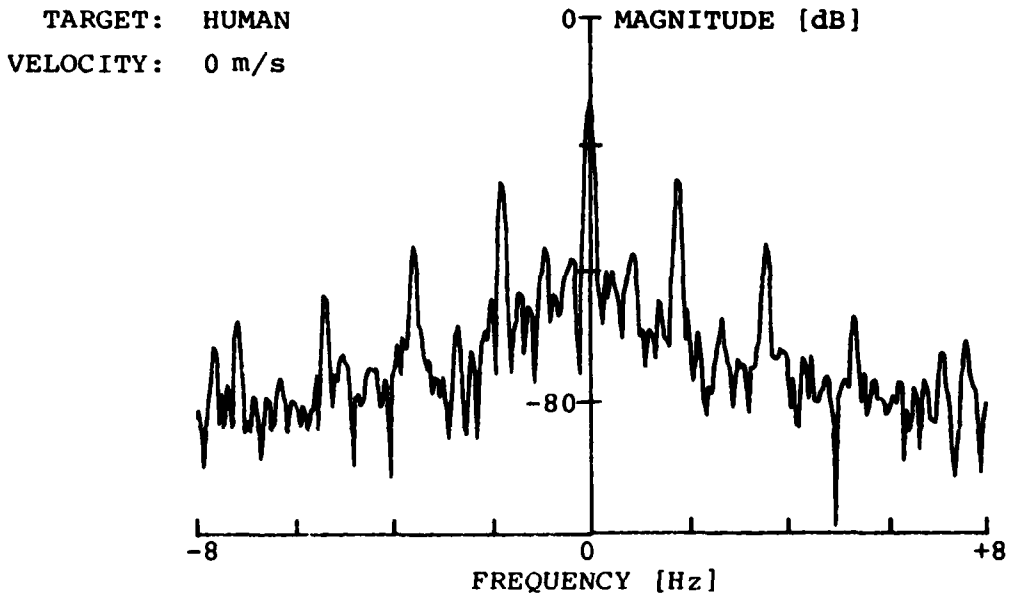

Figure 5.7: Human Swinging Arms Parallel to Cables

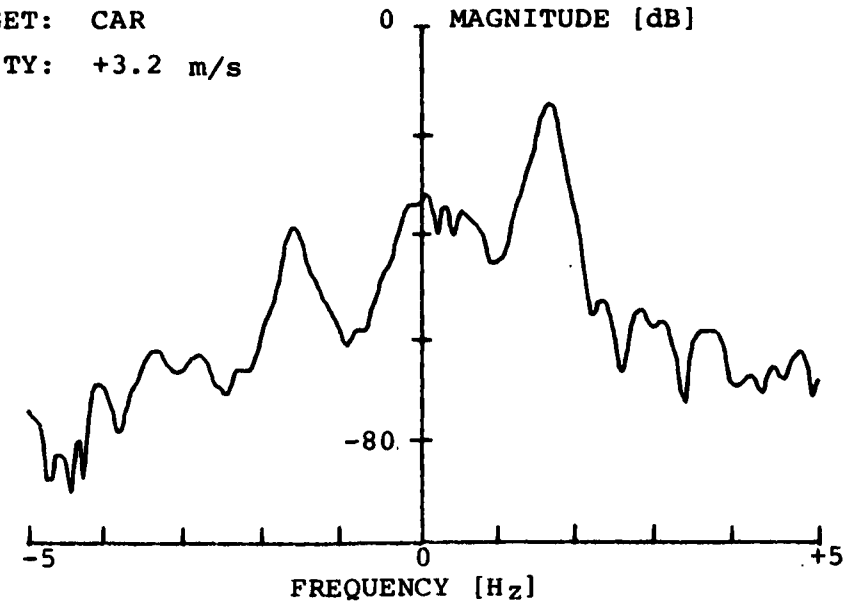

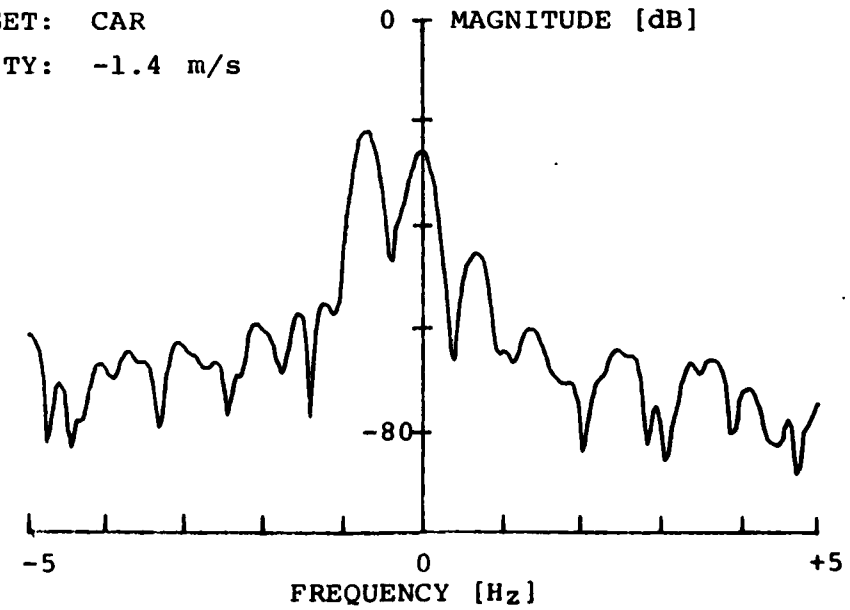

Figure 5.8: Target Signatures of Car

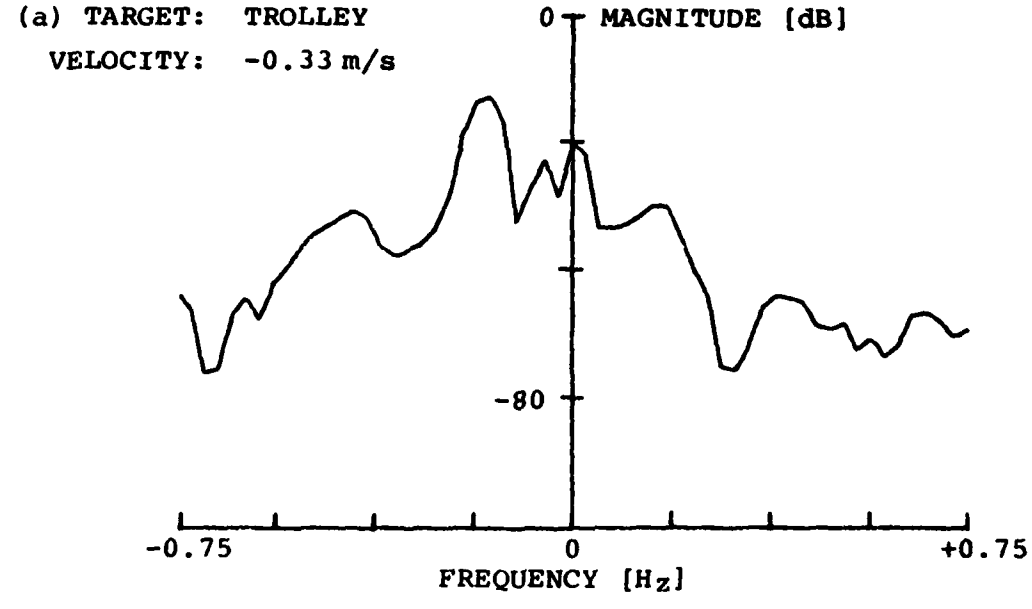

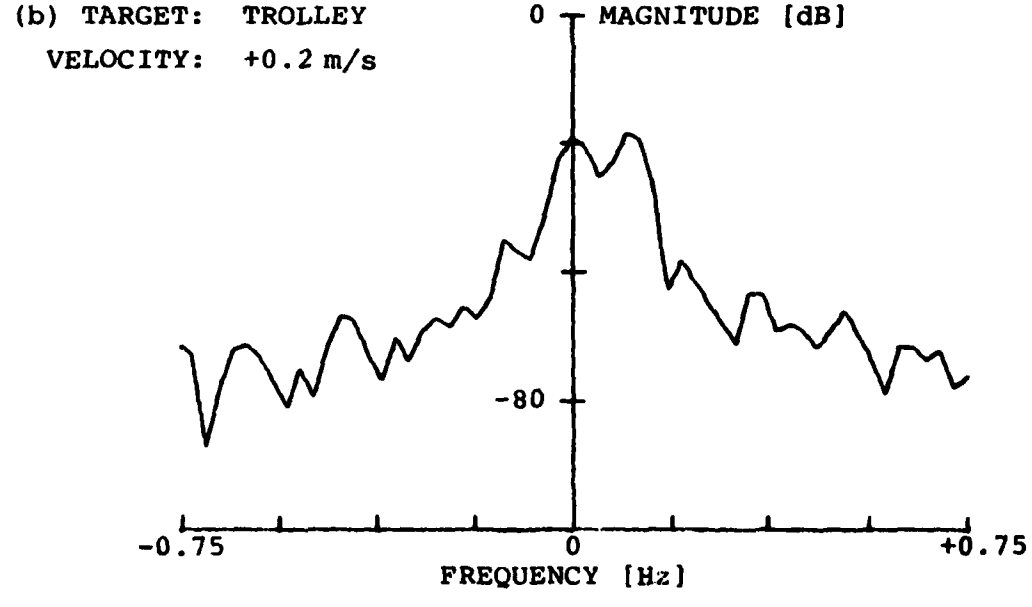

Figure 5.9: Target Signatures of the Trolley

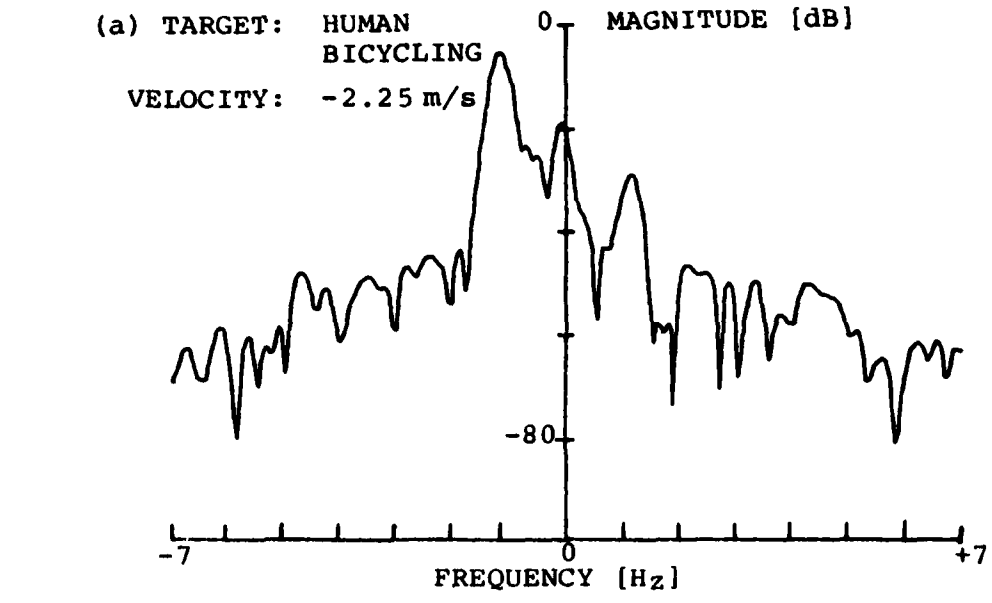

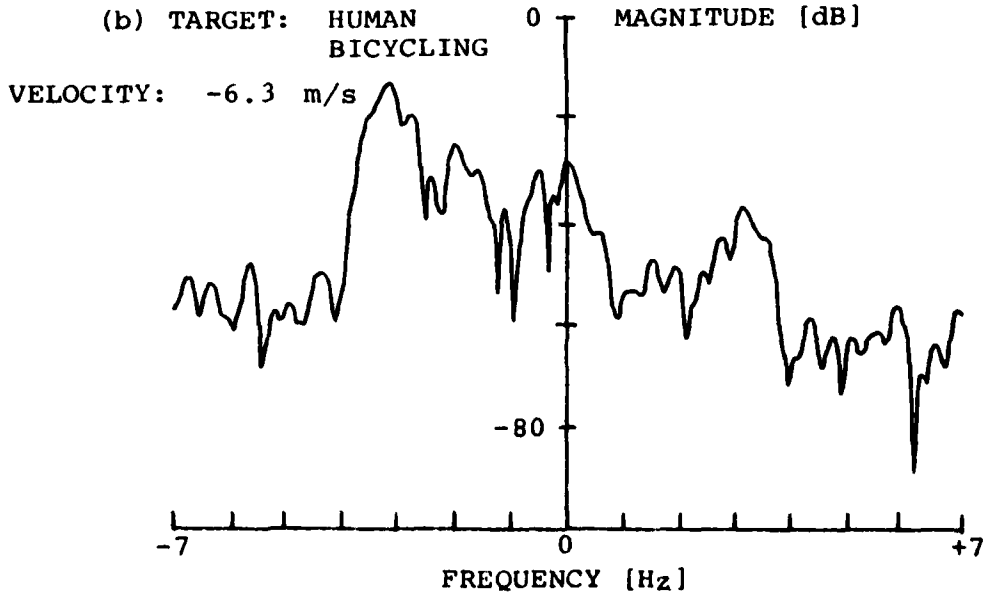

Figure 5.10: Target Signatures of a Human Bicycling

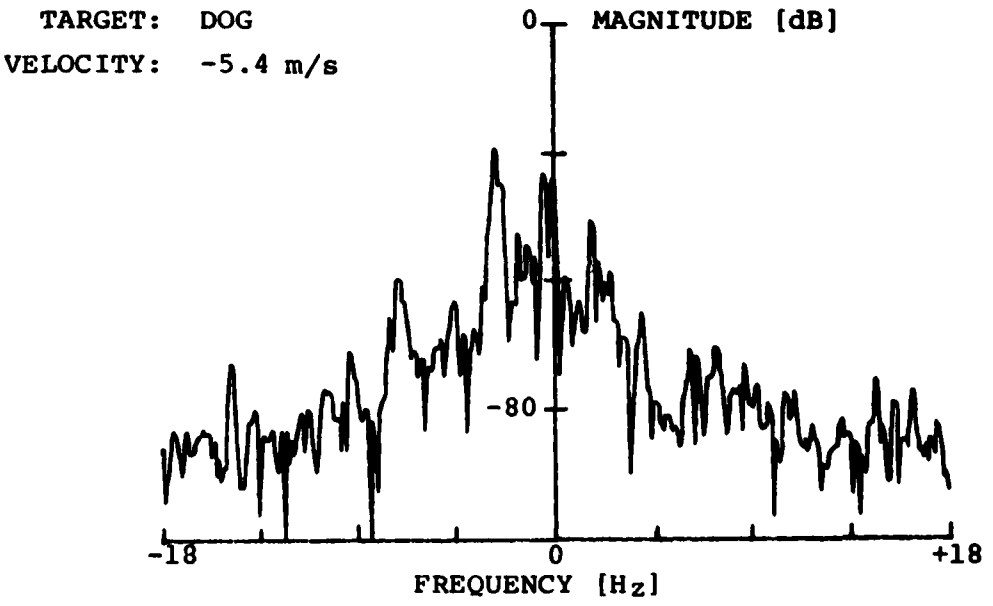

Figure 5.11: Target Signature of Dog Running

1. Deviation from quadrature: The deviation from quadrature of the ANZAC JH-10-4 broadband, 90 degree hybrid was measured with a vector voltmeter. It was found to be 3.0 degrees, which is within the worst case specifications at 60 MHz, as quoted by the manufacturer.

2. Amplitude imbalance: The difference in gain between the I channel and the Q channel, measured at 60 MHz was 1 dB.

The influence of these errors on the target signature, can be demonstrated analytically for the simple case of the return signal consisting of a single spectral component. Errors in amplitude or in phase, change a spectral component by transferring some of the energy at that frequency to its image frequency.

It will be assumed for the purposes of this analysis that the observation interval is of duration equal to the time required by the target to move a distance corresponding to half the wavelength of the RF signal in the coaxial cable. This corresponds to a baseband return signal of a single cycle in each component. The fourier transform of this signal places the corresponding spectral peak at the first discrete frequency in the calculated spectrum (bin 1).

The sampled complex return signal after removal of the cable profile, as before, is

$$\left\{x(n)\right\}_{n=0}^{N-1} = \left\{\Delta I_n + j\ \Delta Q_n\right\}_{n=0}^{N-1}$$

where

$n = \{0, 1, 2, \ldots, N-1\}$

N = number of samples taken.

For a target moving at constant velocity the return signal is sinusoidal.

Hence

$$\left\{x(n)\right\}_{n=0}^{N-1} = \left\{\cos\frac{2\pi n}{N} + j\ \cos\left(\frac{2\pi n}{N} + \theta\right)\right\}_{n=0}^{N-1} \qquad (5.7)$$

where

θ = phase difference between the two channels; ideally, θ = 90 degrees

In addition, if there is an amplitude imbalance between channels

$$\left\{x(n)\right\}_{n=0}^{N-1} = \left\{\alpha \cos\frac{2\pi n}{N} + j \cos(\frac{2\pi n}{N} + \theta\right\}_{n=0}^{N-1} \quad (5.8)$$

where

α = magnitude of the real (in-phase) part of the return signal

β = magnitude of the imaginary (quadrature) part of the return signal, ideally, $\alpha = \beta$.

The transformation to frequency space yields:

$$F\left\{x(n)\right\}_{n=0}^{N-1} = \sum_{n=0}^{N-1} x(n) \exp(-j \frac{2\pi}{N} nk)$$

$$= \sum_{n=0}^{N-1} [\alpha \cos \frac{2\pi n}{N} + j\beta \cos(\frac{2\pi n}{N} + \theta)]$$

$$\cdot \exp(-j \frac{2\pi n}{N} k) \quad (5.9)$$

Substituting the realtion $\cos \phi = \frac{1}{2}\left[\exp(j\phi) + \exp(-j\phi)\right]$ yields

$$F\left\{x(n)\right\}_{n=0}^{N-1} = \frac{\alpha}{2} \sum_{n=0}^{N-1} \exp(-j \frac{2\pi n}{N}(k-1)) + \frac{\alpha}{2} \sum_{n=0}^{N-1} \exp(-j\frac{2\pi N}{n}(k+1))$$

$$+ \frac{j\beta}{2} \exp(j\theta) \sum_{n=0}^{N-1} \exp(-j \frac{2\pi n}{N} (k-1))$$

$$+ \frac{j\beta}{2} \exp(-j\theta) \sum_{n=0}^{N-1} \exp(-j \frac{2\pi n}{N} (k+1))$$

$$= \frac{\alpha}{2}\,\delta(k-1) + \frac{\alpha}{2}\,\delta(k+1) + \frac{j\beta}{2}\exp(j\theta)\;\delta(k-1)$$

$$+ \frac{j\beta}{2}\exp(-j\theta)\;\delta(k+1) \qquad (5.10)$$

Gathering terms gives;

$$F\left\{x(n)\right\}_{n=0}^{N-1} = \delta(k-1)\left[\frac{\alpha}{2} + \frac{j\beta}{2}\exp(j\theta)\right]$$

$$+ \delta(k+1)\left[\frac{\alpha}{2} + \frac{j\beta}{2}\exp(-j\theta)\right]$$

$$= \frac{1}{2}\,\delta(k-1)[\alpha - \beta\sin\theta + j\beta\cos\theta]$$

$$+ \frac{1}{2}\,\delta(k+1)[\alpha + \beta\sin\theta + j\beta\cos\theta] \qquad (5.11)$$

Let γ = ratio of magnitudes of the positive and negative frequency components

Then $\gamma = \dfrac{|\alpha - \beta\sin\theta + j\beta\cos\theta|}{|\alpha + \beta\sin\theta + j\cos\theta|}$

or, in dB,

$$\gamma = 10\log_{10}\left|\frac{\alpha^2 + \beta^2 - 2\alpha\beta\sin\theta}{\alpha^2 + \beta^2 + 2\alpha\beta\sin\theta}\right| \qquad (5.12)$$

In the Queen's guided radar system the measured errors of amplitude (1 dB) and phase (3.0 degrees) give a γ of -27 dB. The approximate value of γ seen in the signatures in figures 5.3 through 5.11 is -25 dB.

5.6 Summary

It has been demonstrated that the target return signal contains information about the kinematics of motion of the target. This information could be useful for classifying targets. It is contained in the portions of the return signal

which are doppler shifted due to the instantaneous velocity of each physical section of the target.

The appropriately filtered and windowed fourier transform of the return signal is referred to as the target signature. In all signatures a large peak was evident which corresponded to the average velocity of the target. In addition, secondary peaks were observed due to motion of the legs or arms of a human target. The position of these side lobes, with respect to the main peak representing average velocity, reflects characteristics of normal human locomotion. The target signature of a dog is quite different from that of a human because of the different pattern of motion of the four legs of the dog.

A simple target such as an automobile or the wooden trolley produced a signature which had no noticeable features other than the principal peak.

Some inaccuracies in the receiver were observed to introduce spectral leakage to the image frequency giving rise to anomalous peaks in the target signature. However, these inaccuracies could be compensated for with slightly more sophisticated signal processing techniques.

Much work has been done on target signature analysis for other types of detection systems. The signal processing techniques that have been developed could well be applied to the guided radar case. However, the signal processing would have to be extended to deal with significant differences between the field configuration in normal radar and that in guided radar.

The return signal and therefore the target signature is a result of the interaction of the complex target with the electromagnetic field produced by the radar system. In a normal radar this field is spatially uniform. In guided radar the target is interacting with a distinctly non-uniform field distribution. The contribution of each section of the target to the total signature is highly dependent upon its exact position with respect to the sensors. More experimental and theoretical analysis would be required to determine the appropriate techniques to deal with the added complications of the non-uniform field. One approach would be to simulate the target return signal and the target signature based upon known field configuration data and the kinematics of motion of the target. Initial experiments have been performed using this approach and are discussed in the next section.

6 Simulation of Target Signatures

6.1 Introduction

An attempt was made to reproduce the form of the target signatures obtained experimentally for human targets by modelling the human as a collection of targets all moving with the same average velocity but each having a different cross section and instantaneous velocity. The model was intended to demonstrate the characteristics of human locomotion which produce the distinctive features in the signature described in the previous chapter.

6.2 Return Signal, single component target

Initially, the target was assumed to be a single point object moving uniformly along the cables in the x direction. The orientation of the spatial axes with respect to the leaky cable sensor is shown in figure 6.1 and is:

x axis: parallel to the cables
y axis: perpendicular to the cables
z axis: perpendicular to the plane of the cables

The point target is assumed to have a reflectivity σ and to be at position (x_o, y_o, z_o) at time $t = 0$. At any other time t, the target position is (x,y,z) and its instantaneous velocity is $\bar{v}(\underline{t})$. If v_x, v_y and v_z are the x, y, and z components of $\bar{v}$, respectively, the equations of motion of the point object can be written:

$$x(t) = x_o + \int_0^t v_x dt \qquad (6.1)$$

$$y(t) = y_o + \int_0^t v_y dt \qquad (6.2)$$

$$z(t) = z_o + \int_0^t v_z dt \qquad (6.3)$$

Both the I and Q components of the target vector are a sinusoidal function of $\frac{2\pi f_c x}{v_{coax}}$

where: f_c = carrier frequency

v_{coax} = velocity of propagation of the carrier in the coaxial cable.

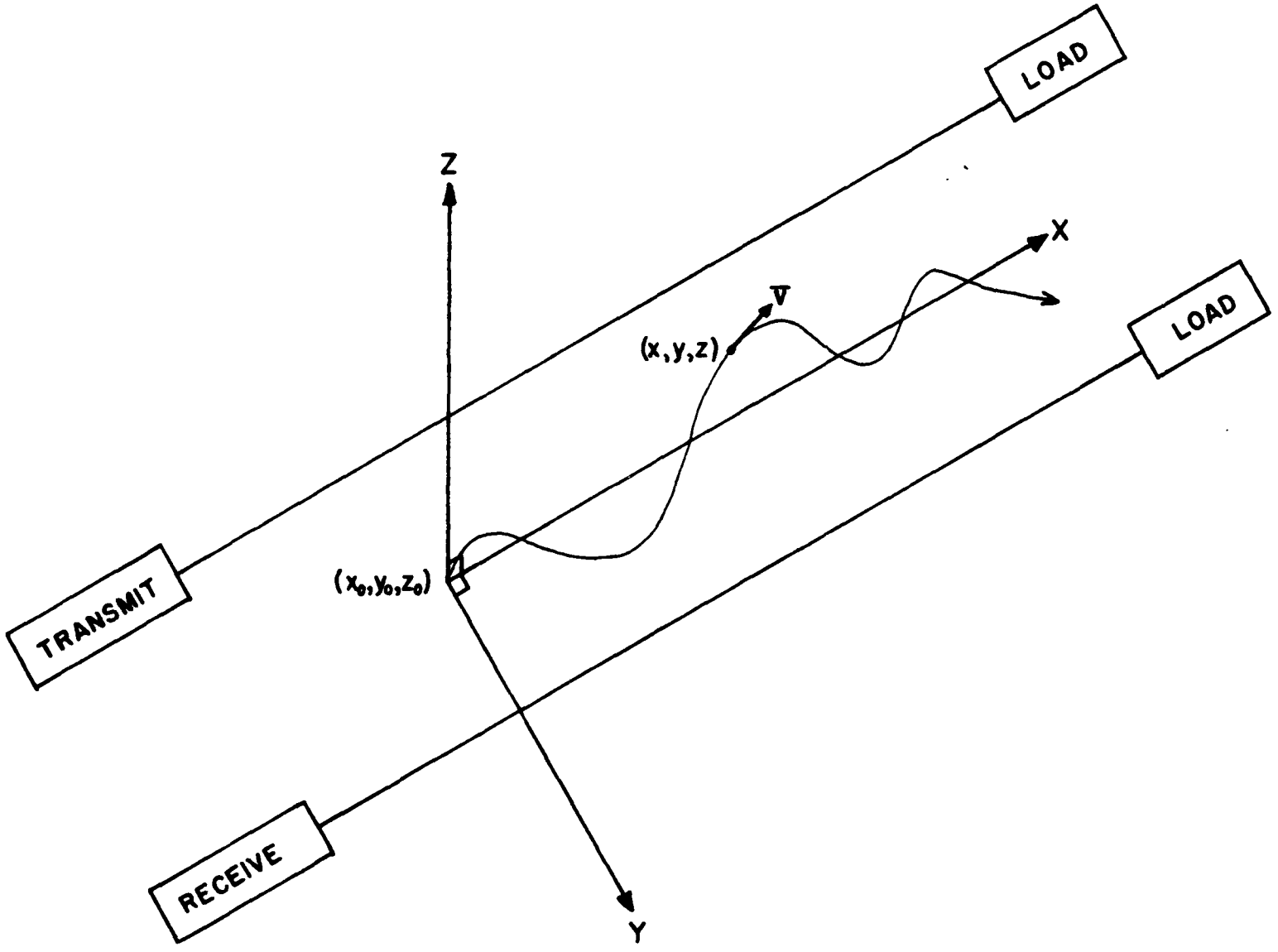

Figure 6.1: Orientation of Axes with Respect to Cables

In addition, each component will be amplitude modulated by a function of position which represents the varying sensitivity of the sensor in the three spatial directions. For convenience this function will be divided into two components: one, S(x) representing the sensitivity variation along the length of the cables, and the other, S(y,z), representing the sensitivity in the other two dimensions.

From field site experiments it is known that S(x) is, in general, a slowly varying function of x. The magnitude of S(x) depends upon the position of the cables with respect to the ground as does the spatial frequency. The variation of S(x) would not be expected to greatly influence the target signature since it would transform to a low value in frequency space. S(x) will be assumed to be a constant.

The sensitivity in the plane perpendicular to the length of the cables is distinctly non-uniform. The response is determined by factors such as the distance between the cables, the type of cable and its position relative to the ground, and the frequency of operation of the system. The sensitivity contours in the y-z plane have been measured [11] and have also been roughly estimated from the theoretical power density distribution for a 2 wire d.c. transmission line. Initially, the sensitivity in the transverse plane will be assumed to be constant. Thus the model will not include effects due to the lifting of the feet during each step or due to deviation of the target in the y direction from the midline between the cables.

The complete analog baseband signal produced by a single point object is:

$$I(t) = \sigma\, S(x)S(y,z)\, \sin\left(\frac{2\pi f_c}{v_{coax}}\, x\right) \qquad (6.4)$$

$$Q(t) = \sigma\, S(x)S(y,z)\, \cos\left(\frac{2\pi f_c}{v_{coax}}\, x\right) \qquad (6.5)$$

6.3 Multiple Component Targets

Consider a target consisting of n distinct components having target cross-sections $\{\sigma_1, \sigma_2, \ldots, \sigma_n\}$ respectively. In addition let the instantaneous velocity of these components at time t be $\{\bar{v}_1, \bar{v}_2, \ldots, \bar{v}_n\}$ respectively. Since all n components are part of one composite body, they all have the same average velocity. Each component will be considered to be a point object. At time t = 0 let the position of the n^{th} component be (x_{no}, y_{no}, z_{no}). Equations 6.4 and 6.5 can now be used to model the contribution of each component of the target to the total return signal.

Thus,

$$I(t) = \sigma_1 \, S(x_1) \, S(y_1 z_1) \, \sin \frac{2\pi f_c}{v_{coax}} \, x_1$$

$$+ \sigma_2 \, S(x_2) \, S(y_2, z_2) \, \sin \frac{2\pi f_c}{v_{coax}} \, x_2 + \ldots,$$

$$+ \sigma_n \, S(x_n) \, S(y_n, z_n) \, \sin \frac{2\pi f_c}{v_{coax}} \, x_n \qquad (6.6)$$

$$Q(t) = \sigma_1 \, S(x_1) \, S(y_1, z_1) \, \cos \frac{2\pi f_c}{v_{coax}} \, x_1$$

$$+ \sigma_2 \, S(x_2) \, S(y_2, z_2) \, \cos \frac{2\pi f_c}{v_{coax}} \, x_2 + \ldots,$$

$$+ \sigma_n \, S(x_1) \, S(y_n, z_n) \, \cos \frac{2\pi f_c}{v_{coax}} \, x_n \qquad (6.7)$$

Hence

$$I(t) = \sum_{i=1}^{n} \sigma_i \, S(x_i) \, S(y_i, z_i) \, \sin \frac{2\pi f_c}{v_{coax}} \, x_i \qquad (6.8)$$

$$Q(t) = \sum_{i=1}^{n} \sigma_i \, S(x_i) \, S(y_i, z_i) \, \cos \frac{2\pi f_c}{v_{coax}} \, x_i \qquad (6.9)$$

where

$$x_i = x_{io} + \int_o^t v_{ix} \, dt \qquad (6.10)$$

$$y_i = y_{io} + \int_o^t v_{iy} \, dt \qquad (6.11)$$

$$z_i = z_{io} + \int_o^t v_{iz}\, dt \qquad (6.12)$$

Equations 6.8 through 6.12 form the complete simulation of an ideal return signal from a target with known motion-characteristics. In a practical system this basic return signal, along with extraneous noise caused by terrain and weather conditions, and system noise, will determine the actual return signal.

Once the baseband return signal is generated on the basis of the above model and the kinematics of motion of the target, it is processed in a fashion identical to that used to obtain a target signature from an experimentally obtained return signal (see figure 5.1).

6.4 Results

6.4.1 Simple Target

Figure 6.2(a) shows the signature for a single component simulated target moving at a uniform velocity of 0.7 m/sec. This would represent the signature of a human target when the trunk, moving at the average velocity, is the major body part causing the target vector. It would correspond to the situation when the leaky cables are raised above the ground so that the motion of the legs would have little or no influence on the return signal and when the arms are held stationary with respect to the body. For comparison figure 6.2(b) shows the signature for a human target when the cables were at a height of 2 m, well away from the leg motion. In both cases there is a large peak in the signature corresponding to the average target velocity but little other distinct structure.

6.4.2 Three Component Target

To include the effects of the motion of the legs in the simulated target signature a three component target was used. One component of the target moved at a uniform velocity and represented the trunk and upper limbs of the human. Each of the other two components represented the lumped effect of one leg and foot. Naturally, they moved at the same average velocity as the first component; however, they had an instantaneous velocity which varied with time in the same manner as the instantaneous velocity of the human heel during normal walking. The legs were assumed to be 180 degrees out of phase with each other.

The velocity time curves used in the model to represent the leg motion are shown in figure 6.3. They were obtained in a study by Winter [12] of the kinematics of normal human locomotion. The curves, in fact, are for the motion of the heel of the foot.

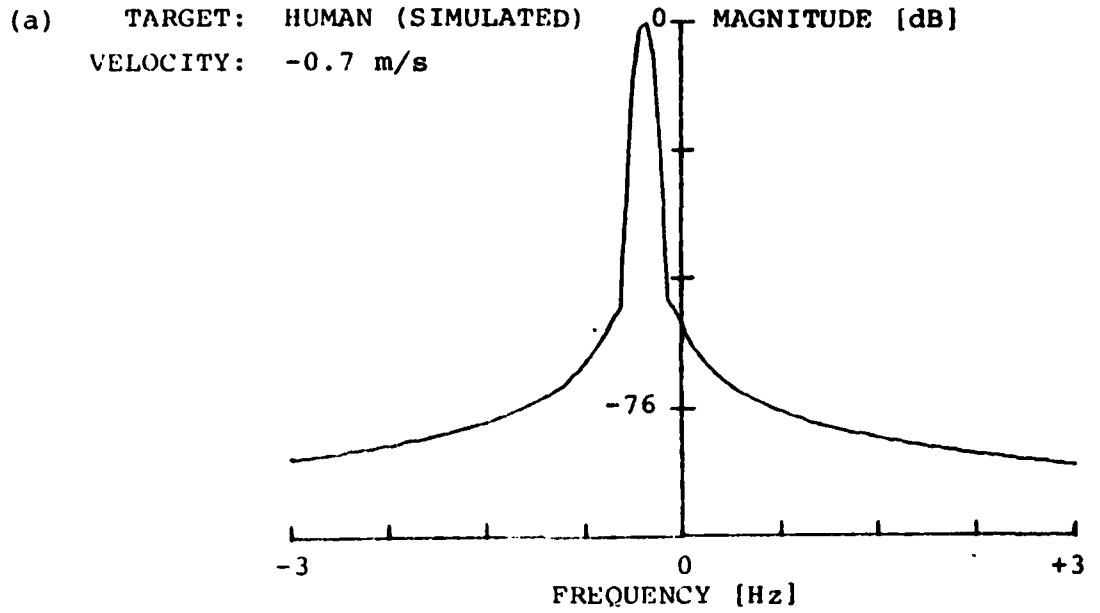

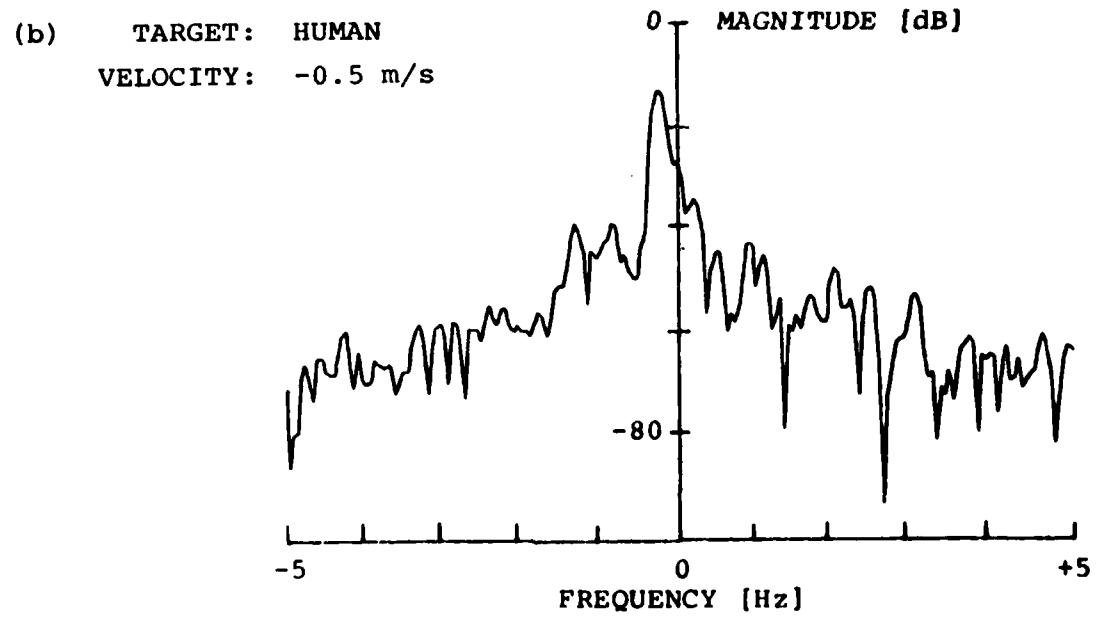

Figure 6.2: Target Signatures - Human Target - Cables in Air

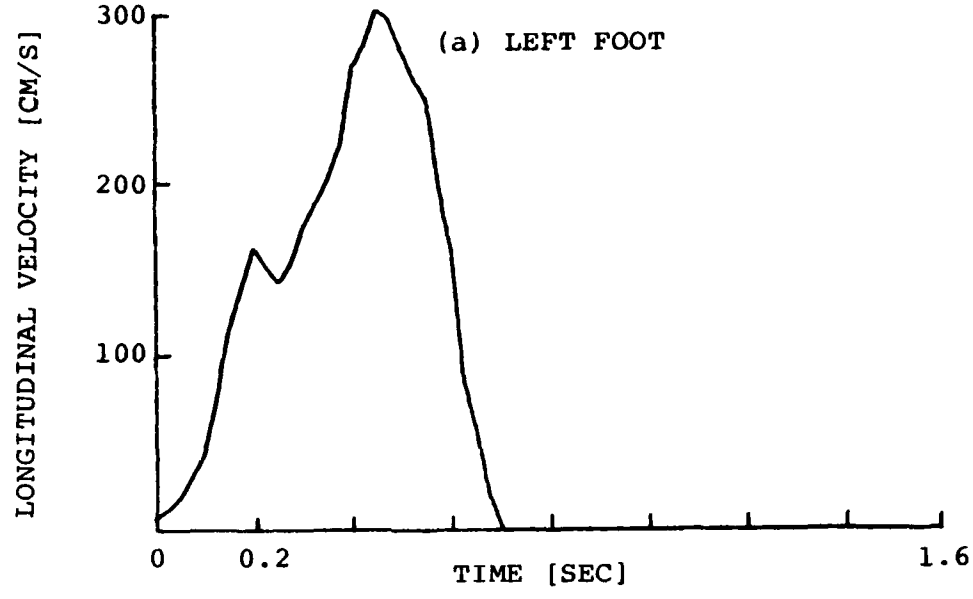

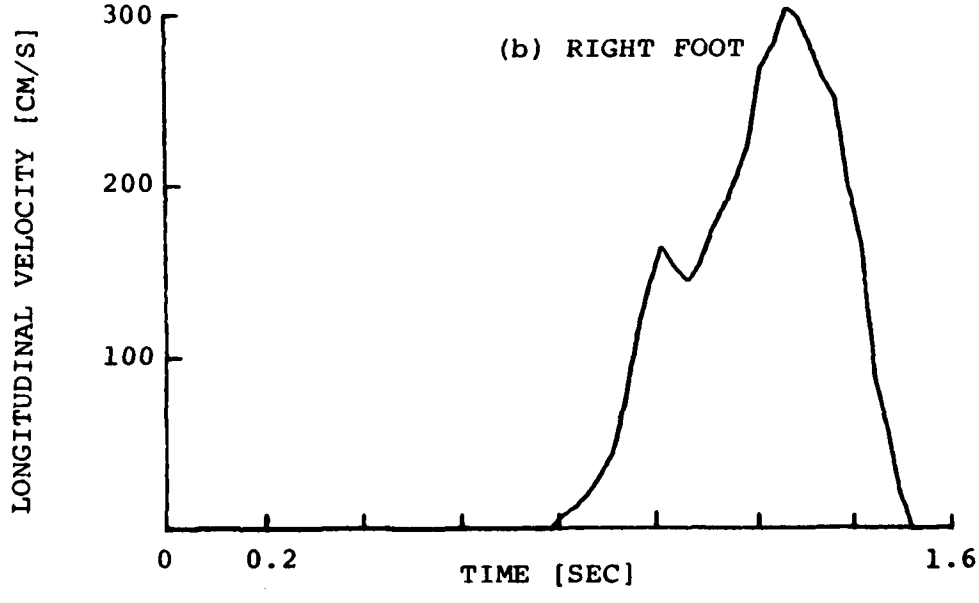

Figure 6.3: Motion Characteristics of Heel

A signature for a walking human target, modelled as three lumped components, is shown in figure 6.4(a). Figure 6.4(b) is a corresponding signature experimentally obtained with the cables on the ground. A comparison of the two signatures reveals that the simulated target signature shows some features characteristic of the experimentally obtained signature. In particular, the distance in frequency space between adjacent peaks is approximately three times the frequency resulting from the average velocity in both signatures.

To produce the simulated signature the reflection coefficient (or cross-section 6) of the legs was arbitrarily chosen to be 1/10 that of the body and no attempt was made to match the peak heights in the simulated signature to those in the experimentally obtained one. Also the system inaccuracies discussed in section 5.5 which cause extra peaks to occur in the experimental signature were not included in the simulation.

6.5 Conclusions

A very simplified model of the human body as a target gives signatures which correspond in gross detail to those obtained experimentally. The use of the motion characteristics of the feet as representative of those of the legs may explain some of the difference between the synthesized and experimentally obtained signatures. A more exact model would incorporate target components (with appropriate motion characteristics) corresponding to the different sections of the leg. Details of the field distribution ($S(y,z)$) and target component motion in the y and z directions should also be included in a complete simulation of a target signature.

These initial results indicate that it should be possible, in principle, to create a library of target signatures on the basis of which general target classification could be performed. A knowledge of the dynamics of target motion could be used to predict distinctive features of expected signatures. The experiments in which the signature for human targets was measured, reported in Section 5, were conducted in a variety of different weather conditions including both clear dry weather and heavy rain. Even though the system response changes under different environmental conditions, the changes are such that they do not greatly affect major features of the signatures.

Naturally, humans can dramatically change the dynamics of their locomotion (walking upright, crawling etc). Animals on the other hand are not likely to do so. Therefore, the recommended approach to reducing false alarms caused by animals would be to identify those characteristics of motion of animals which are distinct and relatively constant and which result in clear patterns in the target signatures. A signature simulation technique could be useful in identifying these distinctive signature patterns.

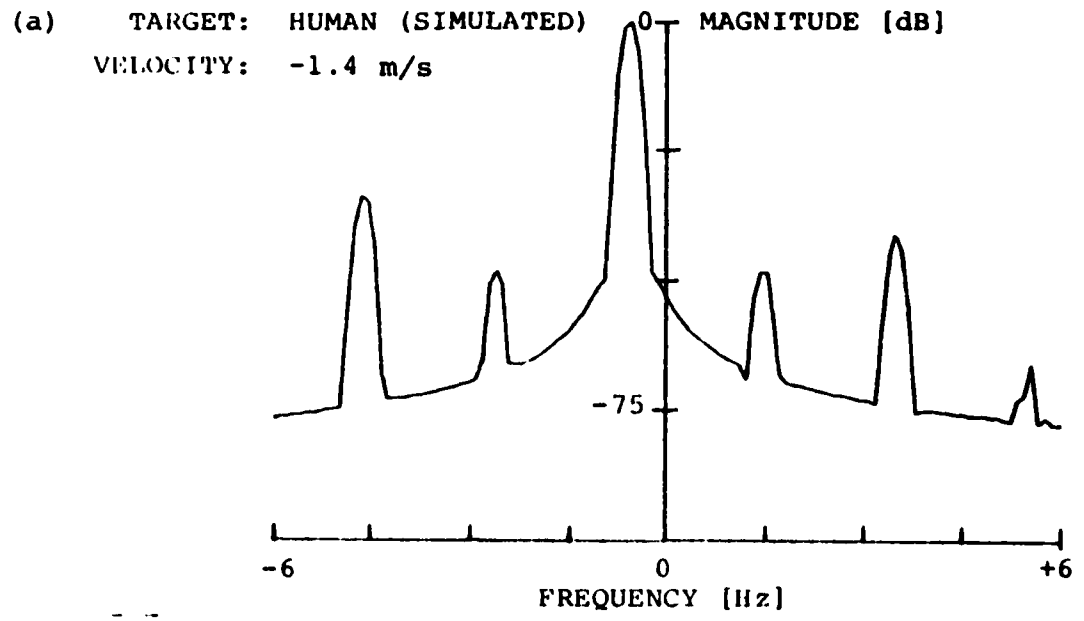

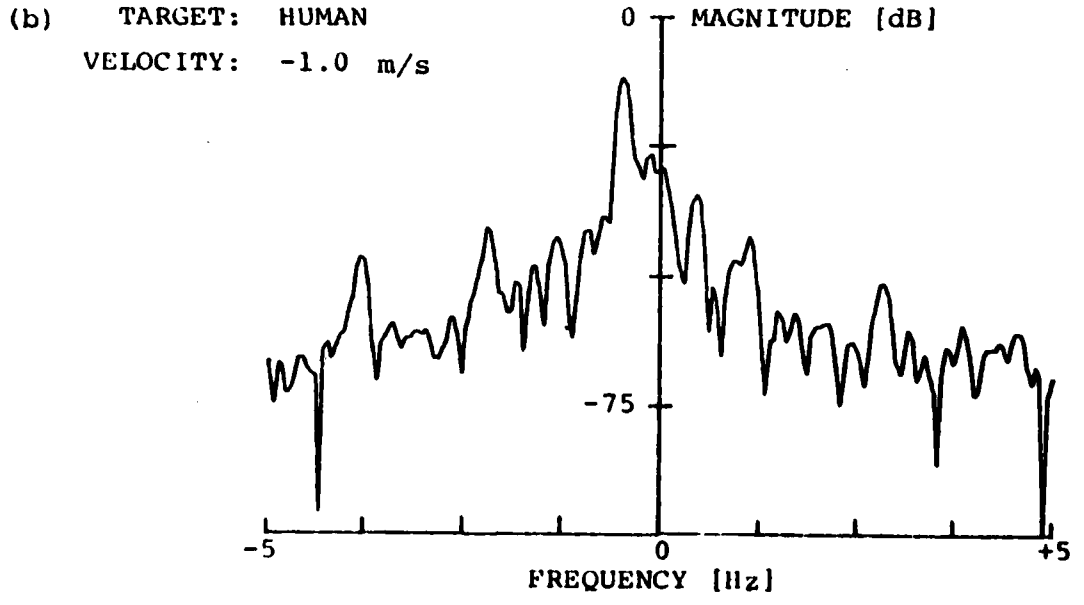

Figure 6.4: Target Signatures - Human Target - Cables on the Ground

Signature simulation could also be a useful method for assessing the effective cross-section of various parts of the human body. This would require a knowledge of the field distribution $\delta(x)$ and $\delta(y,z)$.

Although comments in this report have been mainly limited to longitudinal motion of the target distinct target signatures should also be produced by transverse crossings of the sensors. The characteristics of these signatures would result from the interaction of the target with the changing field strength in the y direction rather than from an actual doppler frequency shift in the return signal.

7 Single Cable System

7.1 Introduction

In all the work discussed so far in this report two leaky cables have been used as the sensor in a guided radar system and targets have been detected, located or identified on the basis of the interaction between the target and the electromagnetic field between the cables. This configuration is well suited to perimeter surveillance since the detection zone is confined to the area around the cables. However, in principle, it should be possible to perform the same functions with a centrally located antenna and a single surrounding leaky cable. In effect, a distributed antenna is replaced with a point source radiator. The wave propagating from the central antenna couples into the leaky cable. A target in the vicinity of the cable or between the cable and the antenna influences the amount of coupling and therefore changes the signal monitored at one end of the cable. Through this change the target can be detected.

In a two cable system the location of the target can be determined by a technique similar to time delay reflectometry. R.F. energy is transmitted along the sensor in pulses. The target location is determined by the time delay between the pulse transmission and the appearance of the target vector. In the single cable short perimeter system a similar technique could be used with suitable modification to account for the fact that a spherical wavefront is being transmitted from a central antenna. Transmission of a simple continuous wave simplifies the processing system but eliminates the location capability for a perimeter of useful length. However, by a simple modulation technique the target location capability can be included in a CW system.

The purpose of the experiments reported in this section was to investigate the performance of leaky coaxial cables in a single cable system. Furthermore, a technique was investigated which would allow the location of the target to be determined even when operating in a CW mode.

Section 7.2 gives a brief analysis of the operation of the system and contains a discussion of the constraints on the proposed location technique. The hardware and software are described in Section 7.3. The experiments performed and the results are presented in Section 7.4. Section 7.5 presents a discussion of the effects of errors in the analog hardware on the accuracy of the system and Section 7.6 is a summary.

7.2 System Analysis

7.2.1 Basic Operation

The system to be analysed consists of an antenna placed in the centre of a perfect circle of leaky coaxial cable. The cable has a receiver connected to one end and a matched load connected to the other end. The antenna is connected to a transmitter which is producing a signal at a frequency f_o. The setup is shown in figure 7.1.

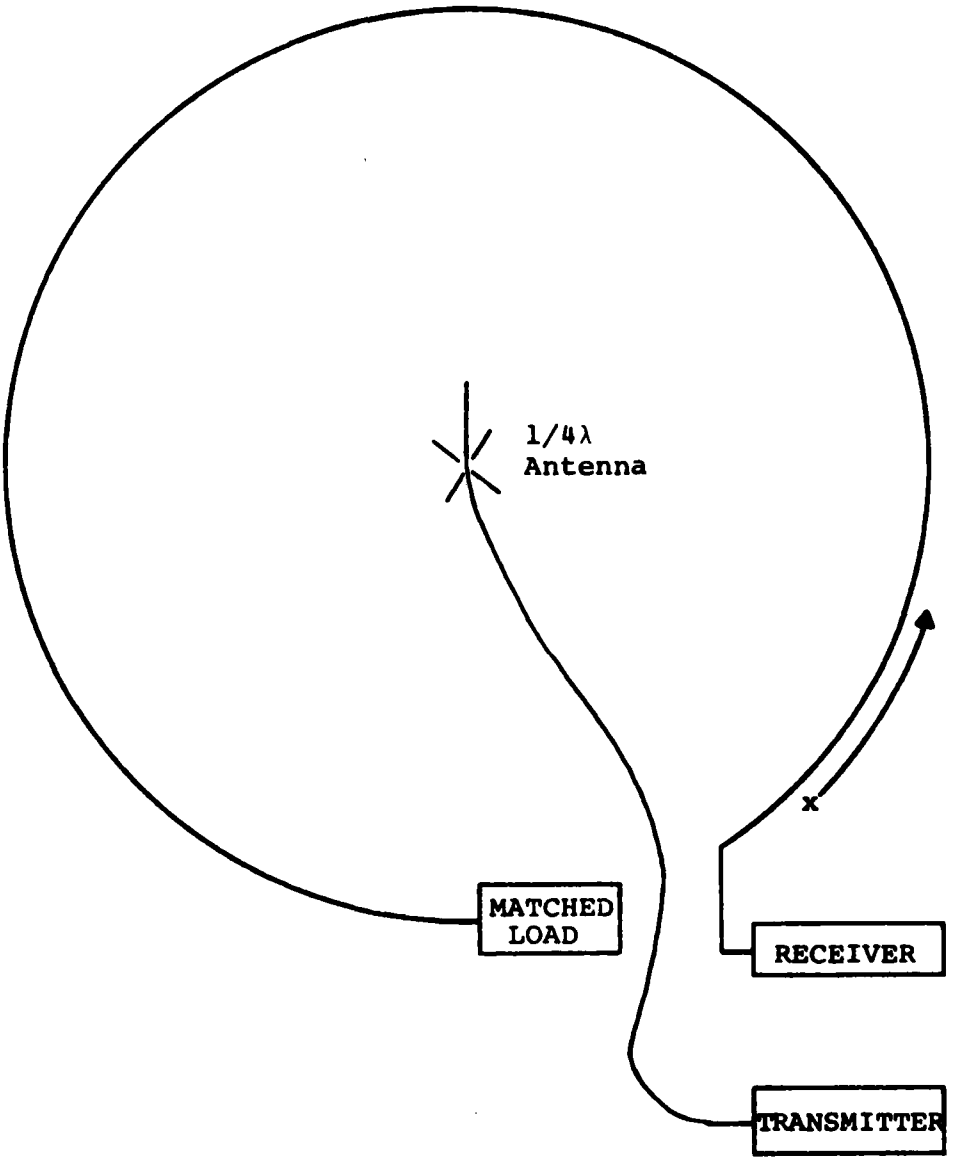

Figure 7.1: System Configuration

The electromagnetic field produced by the antenna is assumed to be symmetric with respect to azimuthal angle. Since the distance from the antenna to the cable is the same for all points on the cable, the phase of the signal at the cable is also the same for all points on the cable. A portion of the electromagnetic field at the cable is converted into a coaxial mode and propagates down the leaky cable to the receiver or to the load.

If a target enters the detection zone around the cable the field will change as will the amount of energy coupled into the cable. The change in voltage at the receiver can be shown to be: (see Appendix B)

$$V_T = \Delta M_x \sin(2\pi f_o t + \theta + \beta_x) \qquad 7.1$$

where

f_o is the carrier frequency

θ is a phase delay due to the propagation time from the antenna to the cable. It is constant for all points on the cable

β_x is a phase delay due to the propagation time along the coaxial cable from the targets' location to the receiver

ΔM_x is the change in the signal coupled into the cable at the location of the target

The original transmitted signal was assumed to be of the form $\sin(2\pi f_o t)$.

The presence of a target is indicated by $\Delta M_x \neq 0$

The phase term β_x is directly proportional to the distance along the cable from the target to the receiver

$$\beta_x = \frac{2\pi x f_o}{v_{coax}} \qquad 7.2$$

where x is the distance along the cable from the target to the receiver

v_{coax} is the velocity of propagation in the cable

The length of the cable over which unambiguous location is possible is restricted. This restriction is discussed in the next section.

7.2.2 Cable Length Restriction

The form of equations 7.1 and 7.2 places a severe restriction on allowable perimeter length for unambiguous target location. The phase term β_x must be less than π radians since

ΔM_x can be positive or negative and

$$\sin(2\pi f_o t + \theta + \beta_x) = -\sin(2\pi f_o t + \theta + \beta_x + \pi)$$

Thus

$$x \leq \frac{v_{coax}}{2f_o} = \frac{\lambda}{2} \qquad 7.3$$

λ = wavelength of the electromagnetic field in the coaxial cable

For example, for a perimeter of 125 m and $v_{coax} = 0.8c$ f_o must be less than 960 kHz. Standard radiax leaky cables are very inefficient at this low frequency.

7.2.3 Modulation Technique

A more suitable operating frequency for Radiax is in the VHF range (50 MHz to 150 MHz). If a carrier frequency in this range is chosen, the ability to locate targets can be maintained by modulating the carrier with a frequency chosen on the basis of the required perimeter length.

Double sideband-suppressed carrier modulation was chosen. The transmitted waveform is now

$$V = \sin(2\pi f_o t)\sin(2\pi f_m t)$$

where f_o is the carrier frequency

f_m is the modulation frequency

It can be shown by a simple extension of the analysis in Appendix B that the target vector now has the form

$$V_T = \Delta M_x \sin(2\pi f_o t + \theta + \beta_x)\sin(2\pi f_m t + \phi + \gamma_x) \qquad 7.4$$

The phase terms θ and ϕ are constants determined by the geometry of the system and do not influence the analysis. They will be ignored from this point on. Synchronous detection with appropriate filtering at both the carrier frequency and the modulation frequency yields four signals containing the desired target information

$$\Delta I_1 = \Delta M \sin\beta_x \sin\gamma_x$$
$$\Delta Q_1 = \Delta M \sin\beta_x \cos\gamma_x$$
$$\Delta I_2 = \Delta M \cos\beta_x \sin\gamma_x \qquad 7.5$$
$$\Delta Q_2 = \Delta M \cos\beta_x \cos\gamma_x$$

Target vector magnitude is given by

$$M_T = \sqrt{\Delta I_1^2 + \Delta Q_1^2 + \Delta I_2^2 + \Delta Q_2^2} \qquad 7.6$$

Target vector phase can be calculated from

$$\gamma_x = \tan^{-1}\left(\frac{\Delta Q_1}{\Delta I_1}\right) \qquad \sin\beta_x \neq 0$$
$$7.7$$
$$= \tan^{-1}\left(\frac{\Delta Q_2}{\Delta I_2}\right) \qquad \cos\beta_x \neq 0$$

The carrier frequency can be chosen high enough for efficient coupling into the coaxial cable and the modulation frequency low enough to provide unambiguous target location over the desired perimeter.

7.3 System Description

7.3.1 Hardware

A block diagram of the hardware used in the single cable system is shown in figure 7.2. The transmitter consisted of a 60 MHz carrier oscillator amplitude modulated by a 700 kHz modulation oscillator, and a five watt power amplifier.

The receiver consisted of two stages of synchronous detection each followed by the appropriate filtering. The first stage detector synchronously demodulated the 60 MHz carrier frequency. A hybrid was used to provide the 90° phase shift of the reference carrier signal for the quadrature mixer. The resulting in phase (I) and quadrature (Q) components from the first detector were filtered through a pair of 9 pole low-pass filters with a cut-off frequency of 700 kHz.

The I and Q components from the first detector were then separately processed by a pair of synchronous detectors using the 700 kHz modulation oscillator as the reference signal. In this case, specially cut delay lines were used

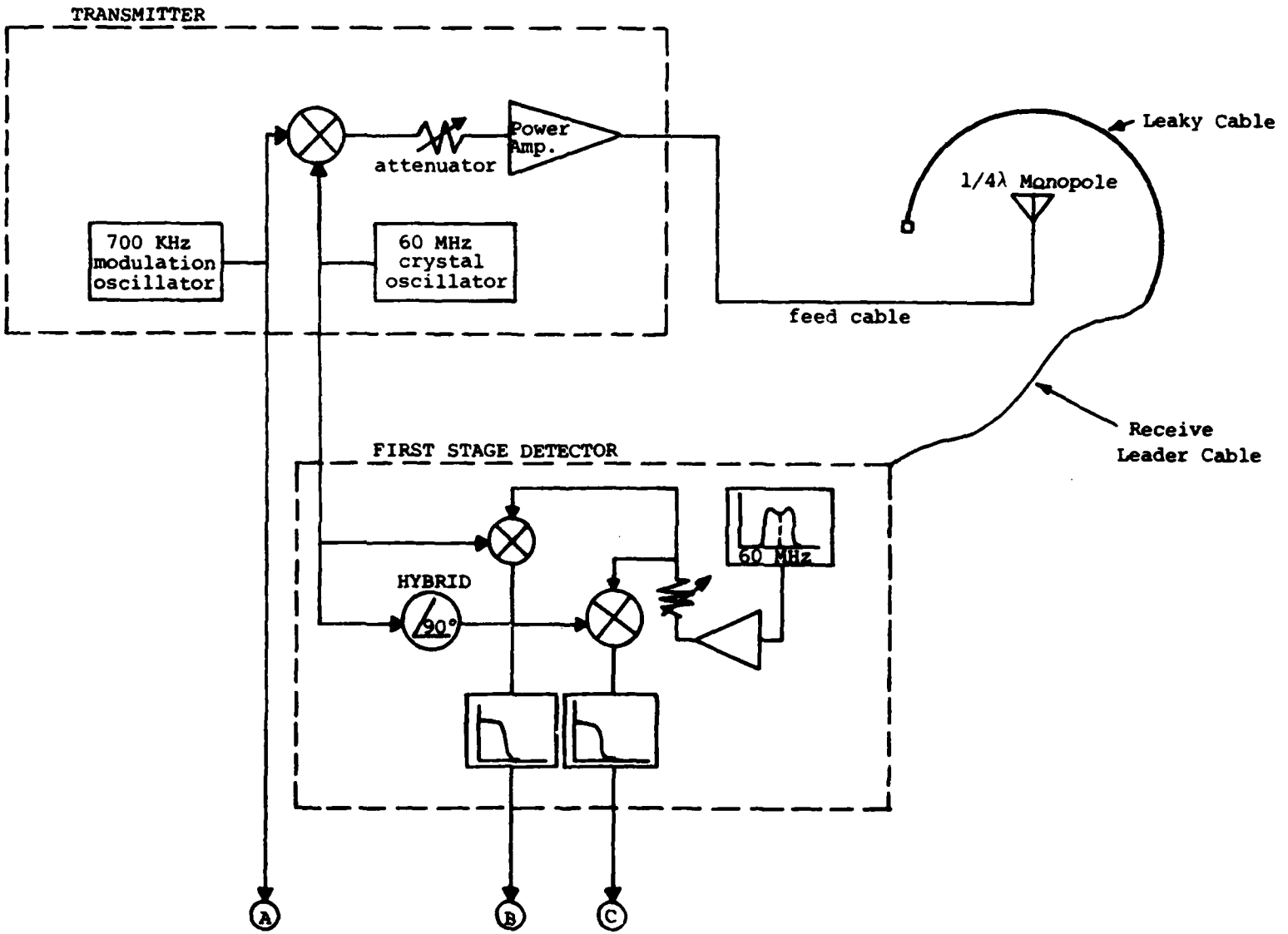

Figure 7.2: Hardware Block Diagram

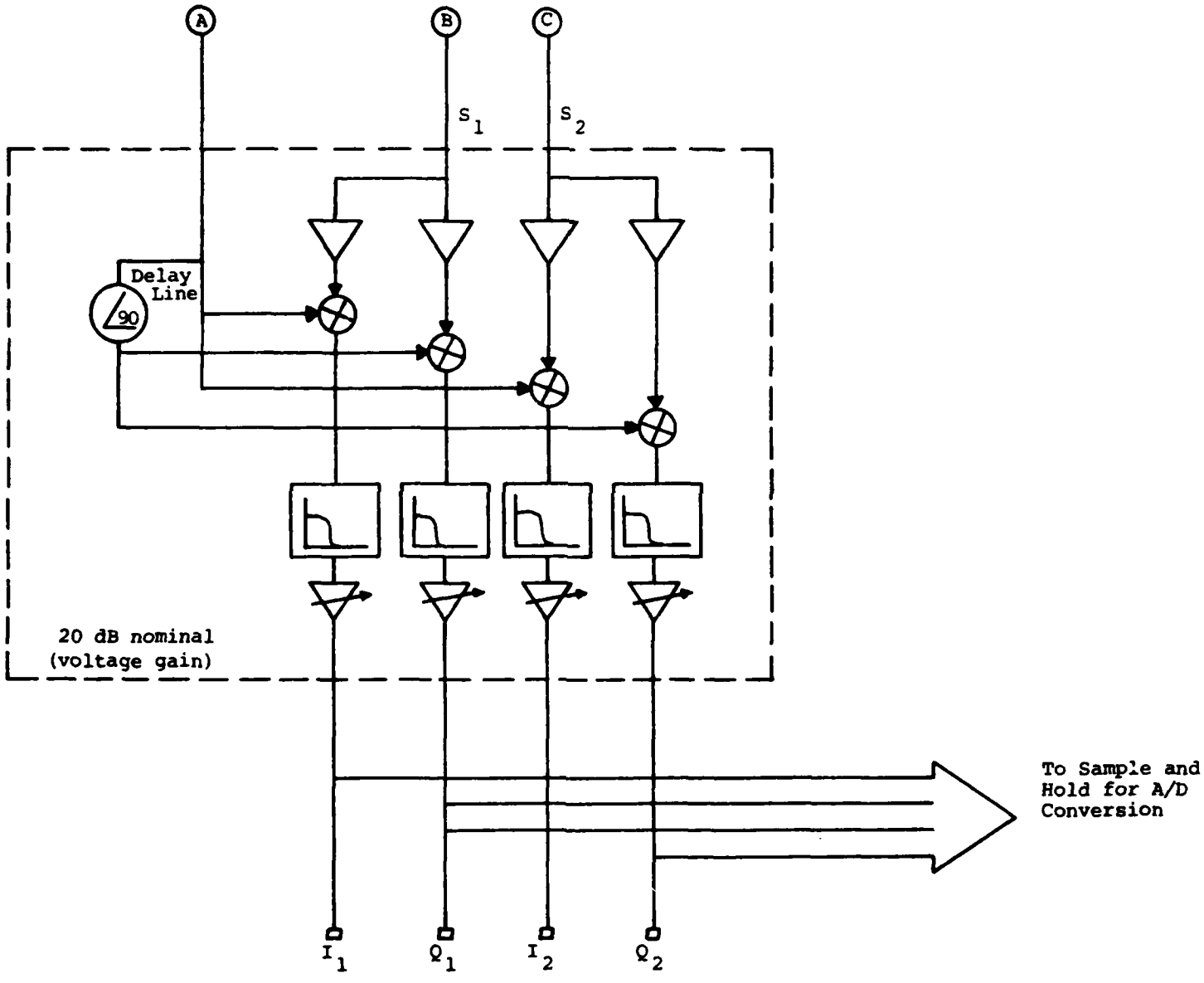

Figure 7.2: Analog Hardware Outline

to shift the reference oscillator by 90°. The four resulting signals were filtered by low pass filters having a cut-off frequency of 30 Hz and then sequentially sampled and converted to a digital representation. All four signals were digitized in 16 ms giving an effective profile sampling rate of 60 Hz.

7.3.2 Software

A flow diagram for the processing scheme is shown in figure 7.3. Each time sample of the return signal consisted of four numbers - digitized versions of I_1, Q_1, I_2 and Q_2. The initial value of each of these signals was used as the reference profile - the system response with no target present within the detection zone of the system.

The reference profile was subtracted from each subsequent sample of the profile to form a target response vector (ΔI_1, ΔQ_1, ΔI_2, ΔQ_2). The magnitude of the target response vector was then calculated $M = \sqrt{\Delta I_1^2 + \Delta Q_1^2 + \Delta I_2^2 + \Delta Q_2^2}$. If this magnitude was below a threshold level, chosen on the basis of system noise levels, it was assumed that no target was within the detection zone and the next profile sample was processed. If the target vector magnitude was greater than the threshold a comparison was made between M_1 and M_2 where $M_1 = \sqrt{\Delta I_1^2 + \Delta I_2^2}$ $M_2 = \sqrt{\Delta I_2^2 + \Delta Q_2^2}$. The location of the target was then calculated on the basis of a target phase $\gamma_x = \tan^{-1} \frac{\Delta Q_n}{\Delta I_n}$ where n = 1,2 depending upon which of M_1 or M_2 was largest.

7.4 Results

7.4.1 Standard Walk

Most of the measurements on the system were made by means of a standard walk in which a human target followed a fixed path around the protected perimeter. This path is shown in figure 7.4.

At the start of the experiment the target was well outside the detection zone assuring a reliable recording of the reference profile. The target crossed the cable at one end and walked at a constant velocity approximately 35 cm from the cable on the inside of the loop.

7.4.2 Experiments

A variety of experiments were performed with different system configurations. These are summarized in Table 7.1 Each experiment was performed a number of times and typical results will be discussed below.

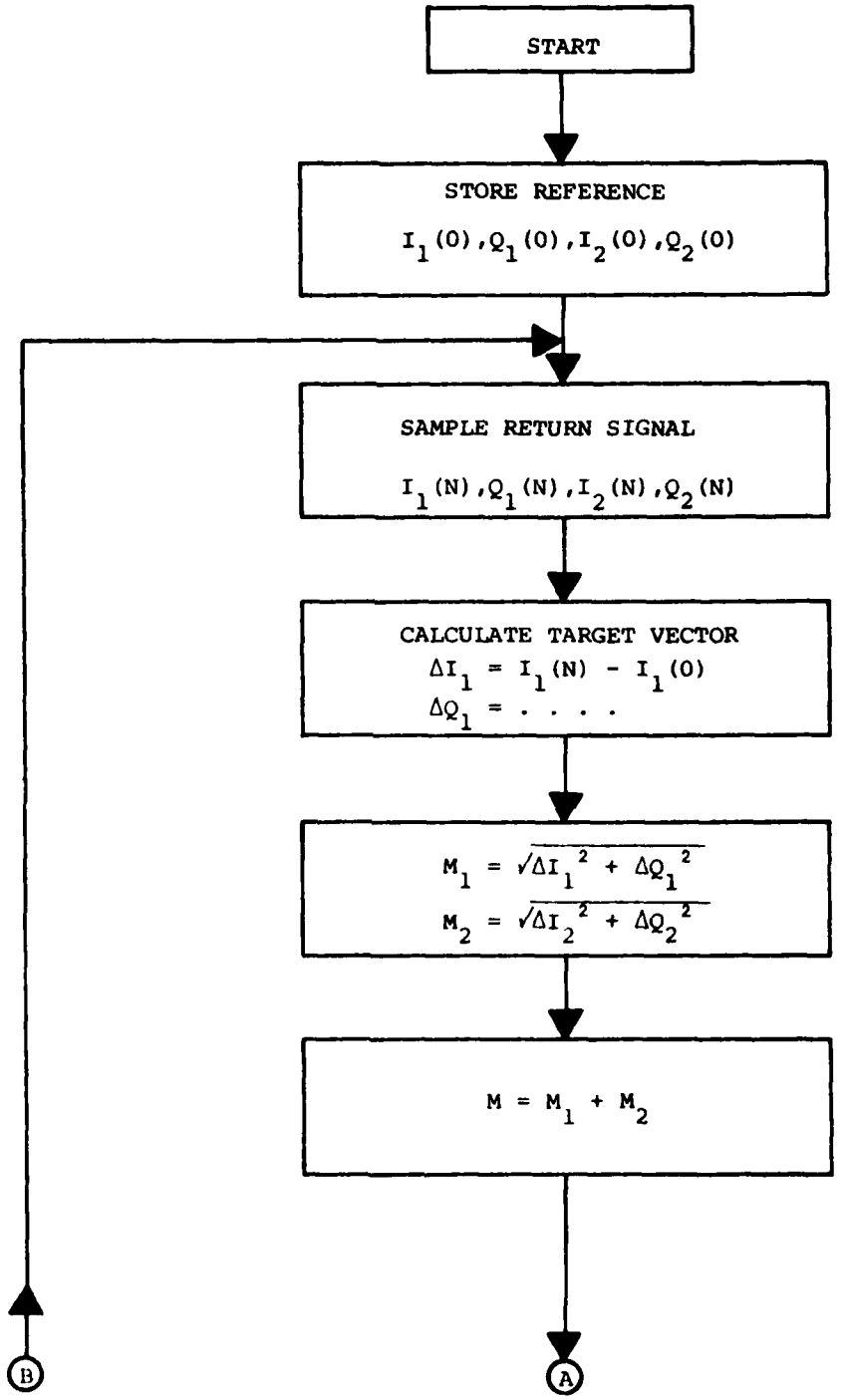

Figure 7.3: Processing Flow Diagram

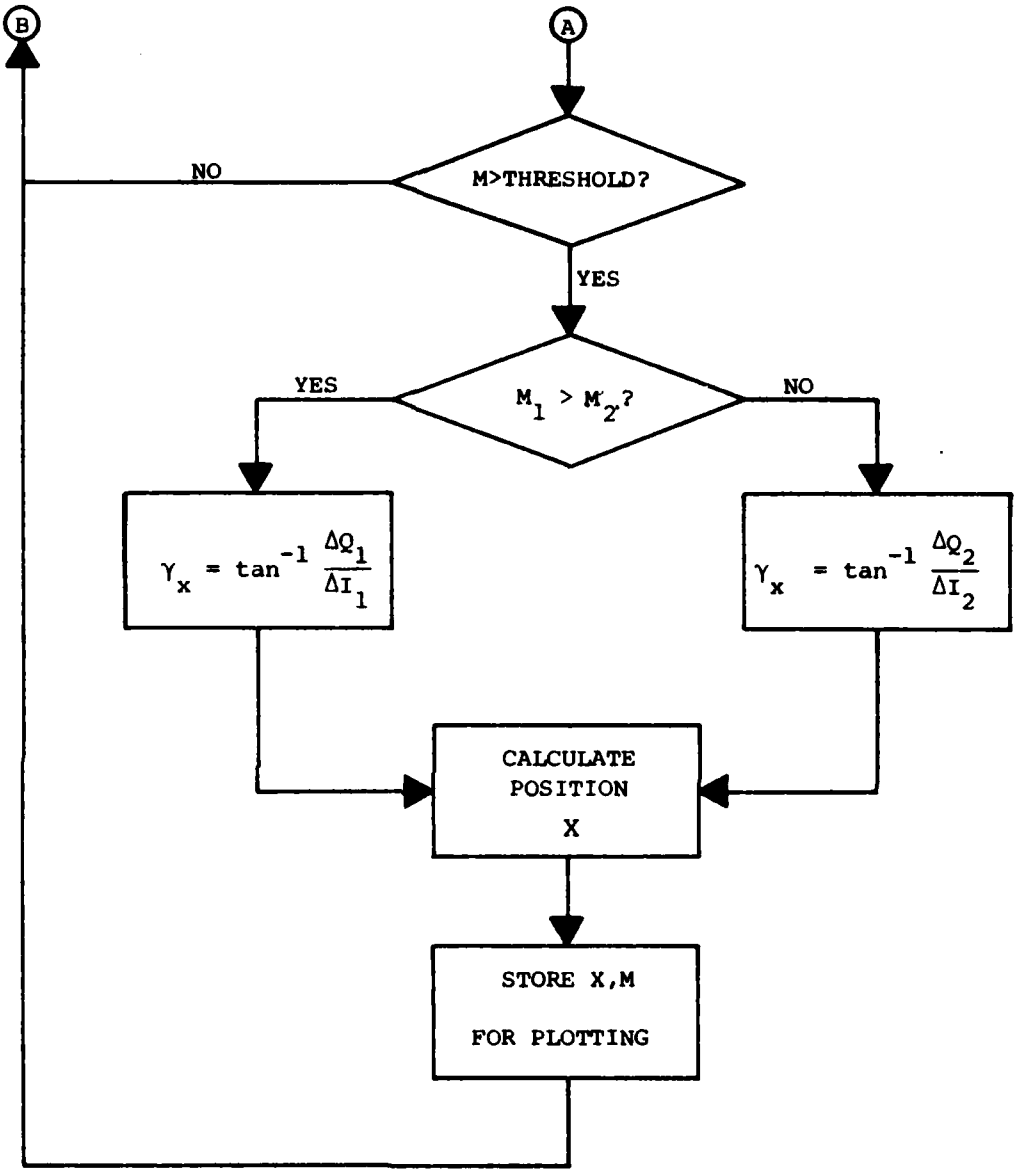

Figure 7.3: Processing Flow Diagram

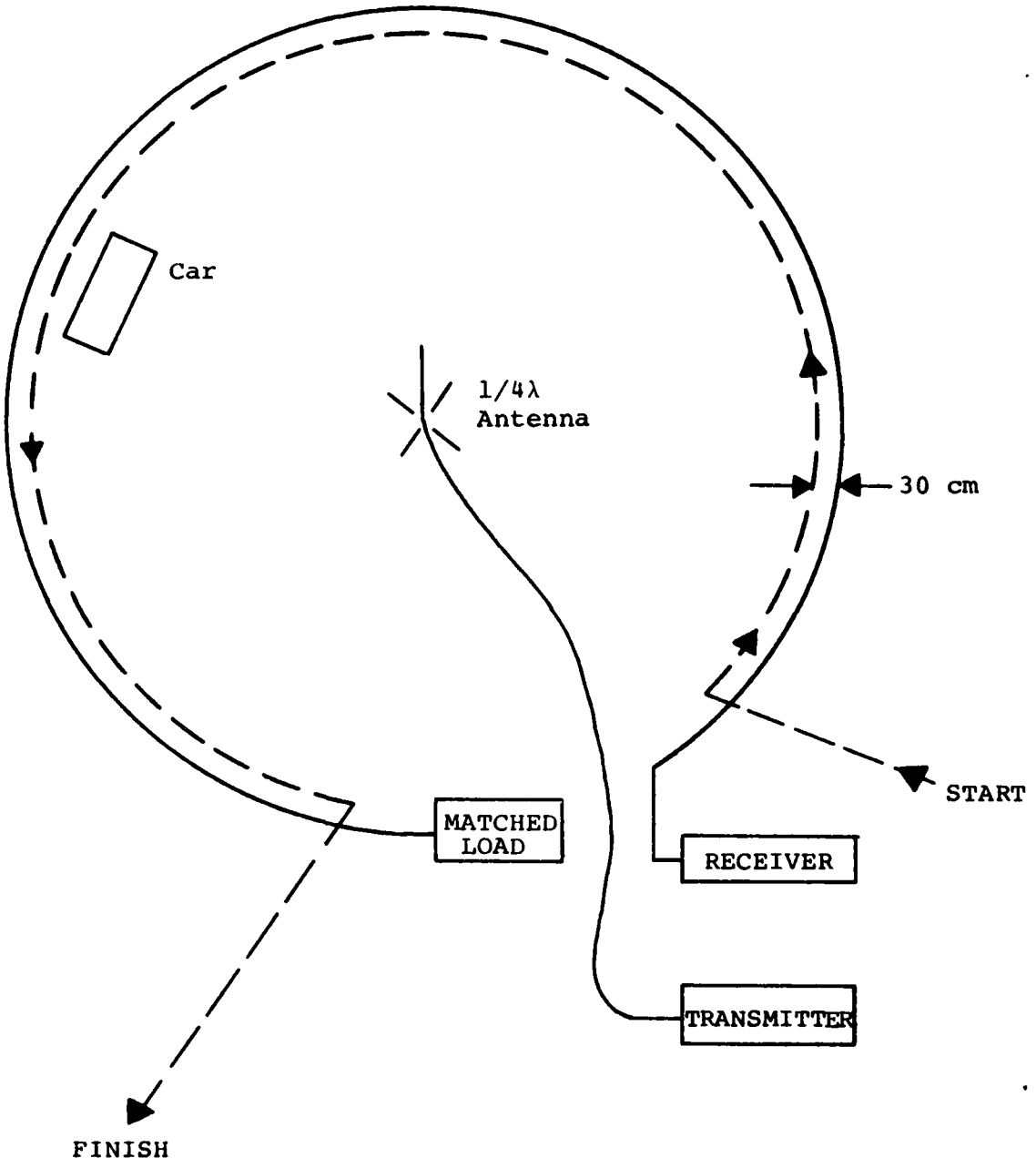

Figure 7.4: Standard Walk Path

Table 7.1

SUMMARY OF SINGLE CABLE EXPERIMENTS

Cable Type	Transmitter	Cable Position	Special Conditions
RX4-3	Antenna	ground	
	Cable	ground	
	Antenna	1 metre	
	Antenna	ground	large stationary target
	Antenna	ground	radial walk
RX4-1	Antenna	ground	
	Cable	ground	

7.4.3 Basic System Performance

In figure 7.5 are plotted the results of a typical standard walk experiment. An RX4-3 cable was used on the ground. The lower curve is a plot of the target vector magnitude Δm versus time. The upper curve is a plot of the calculated target positon versus time. The straight line is the best fit straight line to the data using a minimum root-mean-square error criterion. Marked on the graph is the peak value of the target response. The results plotted in figure 7.6 are for a similar experiment with the exception that an RX4-1 cable was used.

It is clear that the scheme for target location works well. The ripple on the target position plots results from differences in the gain of the amplifiers in the four channels and deviation from perfect quadrature in the synchronous detectors. This will be discussed further in section 7.5. The target vector magnitude plots are similar in detail with the exception that the target response for RX4-1 is 15 dB lower than that for RX4-3.

7.4.4 Performance with Cable as Transmitter

The reciprocity theorem implies that it should be possible to reverse the positions of the cable and the central antenna. Figure 7.7 is a plot of the results from a standard walk with the transmitter connected to the cable and the receiver connected to the central antenna. The performance is essentially the same as when the central antenna was used as the transmitter.

7.4.5 Elevated Cables

For a number of walks the cable was suspended by plastic clips on wooden stakes approximately 1 metre above the ground. Figure 7.8 shows the results of one such experiment. The most obvious change is in the target magnitude plot. Large, regularly spaced nulls appear where the system sensitivity becomes very low. At these nulls the target location response also becomes inaccurate.

The sensitivity nulls most likely occur because of interference between several modes of propagation along the cable. One mode would be a coaxial mode within the cable and a second mode would propagate between the outer conductor of the cable and the ground plane produced by the earth. These modes, propagating at different velocities, interfere to produce the senstivity nulls. Similar periodic sensitivity nulls have been observed in a normal two cable guided radar system when the cables were suspended in the air [13,14] and a theoretical, coupled-mode model has been used to determine the parameters which influence the spacing and depth of the nulls in a two cable system [15].

The decrease in location accuracy at the nulls is a result of the decreased signal-to-noise ratio at these points.

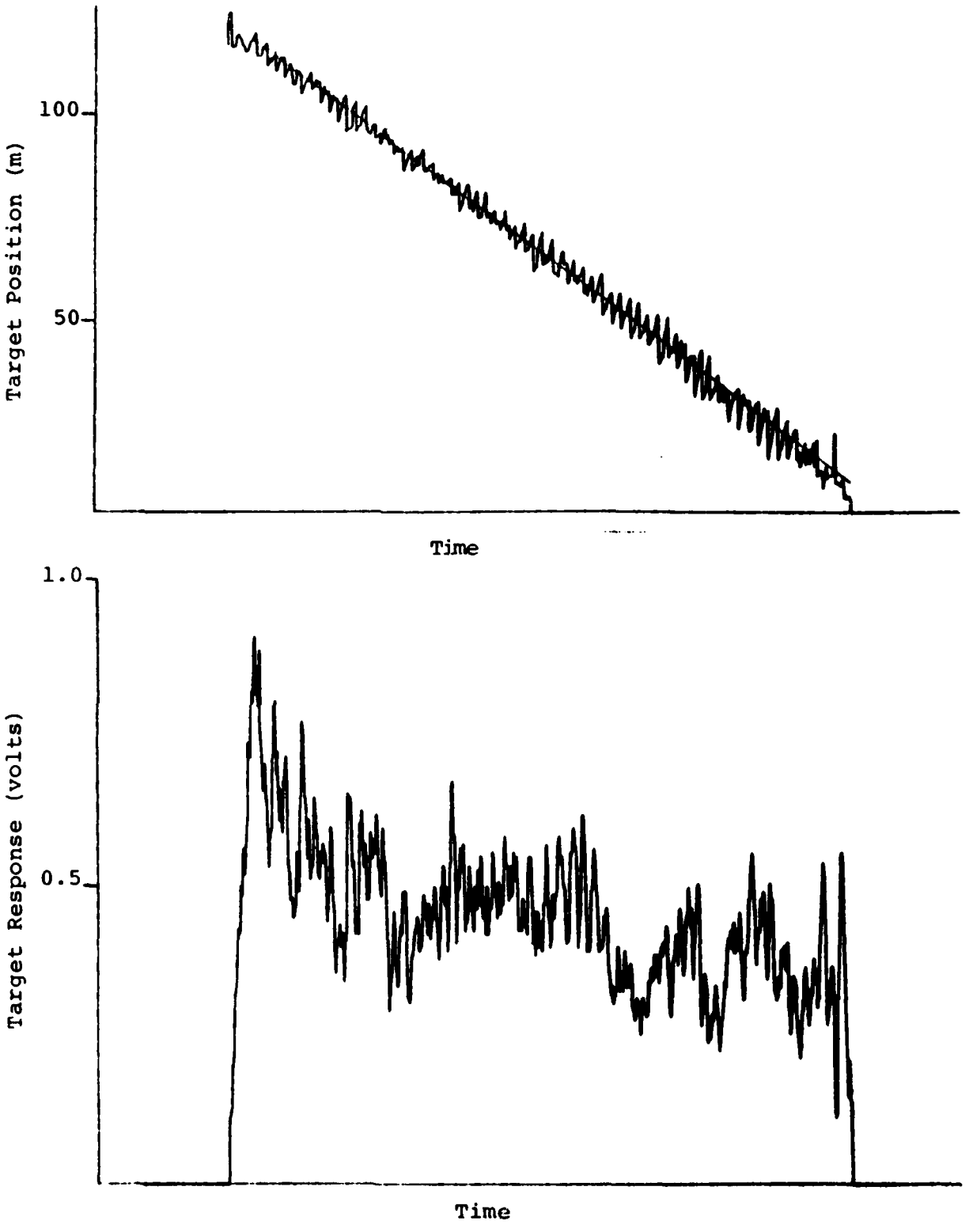

Figure 7.5: Typical Standard Walk - RX4-3
Maximum Response 0.9 volts

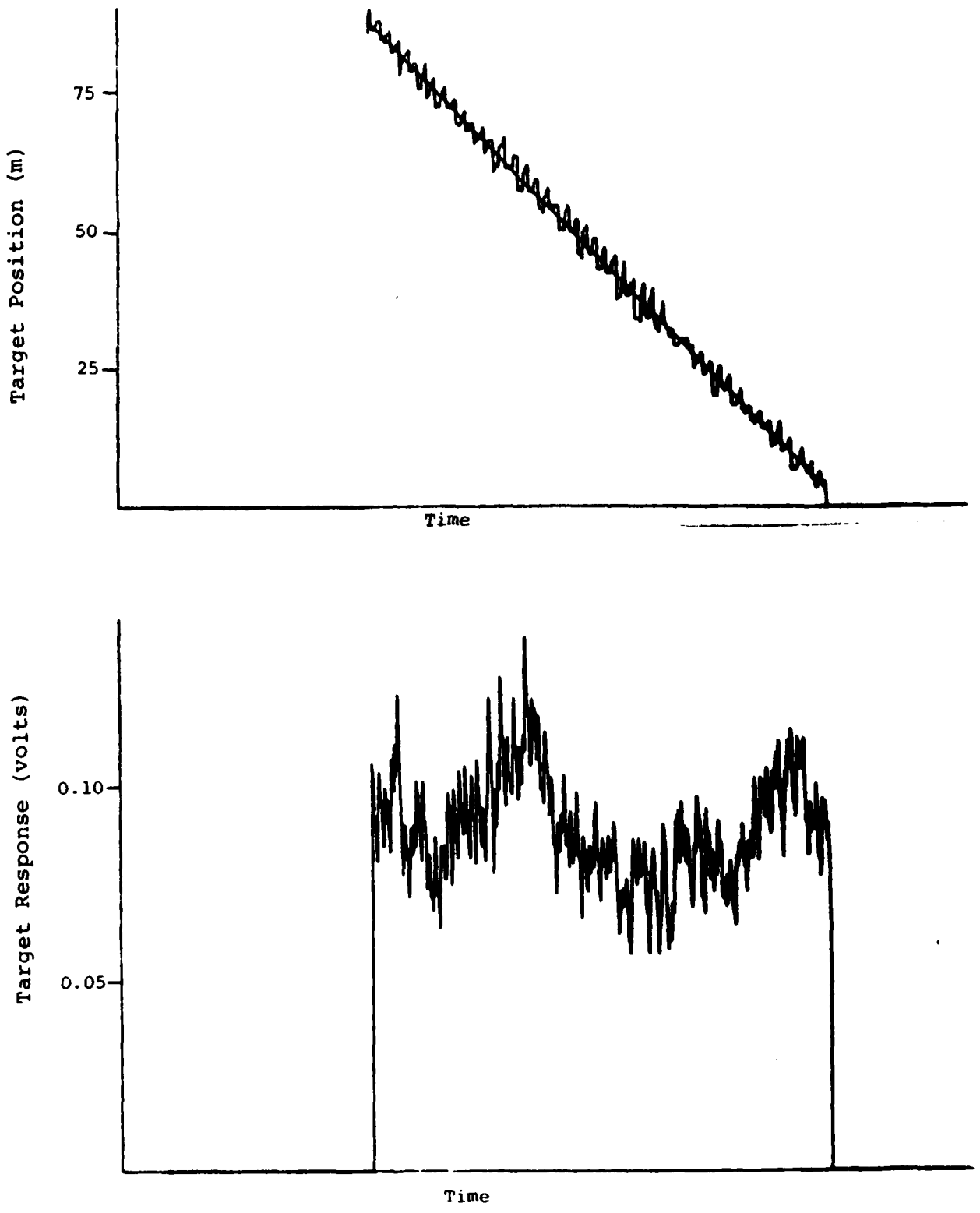

Figure 7.6: Typical Standard Walk RX4-1
Maximum Response 0.14 volts

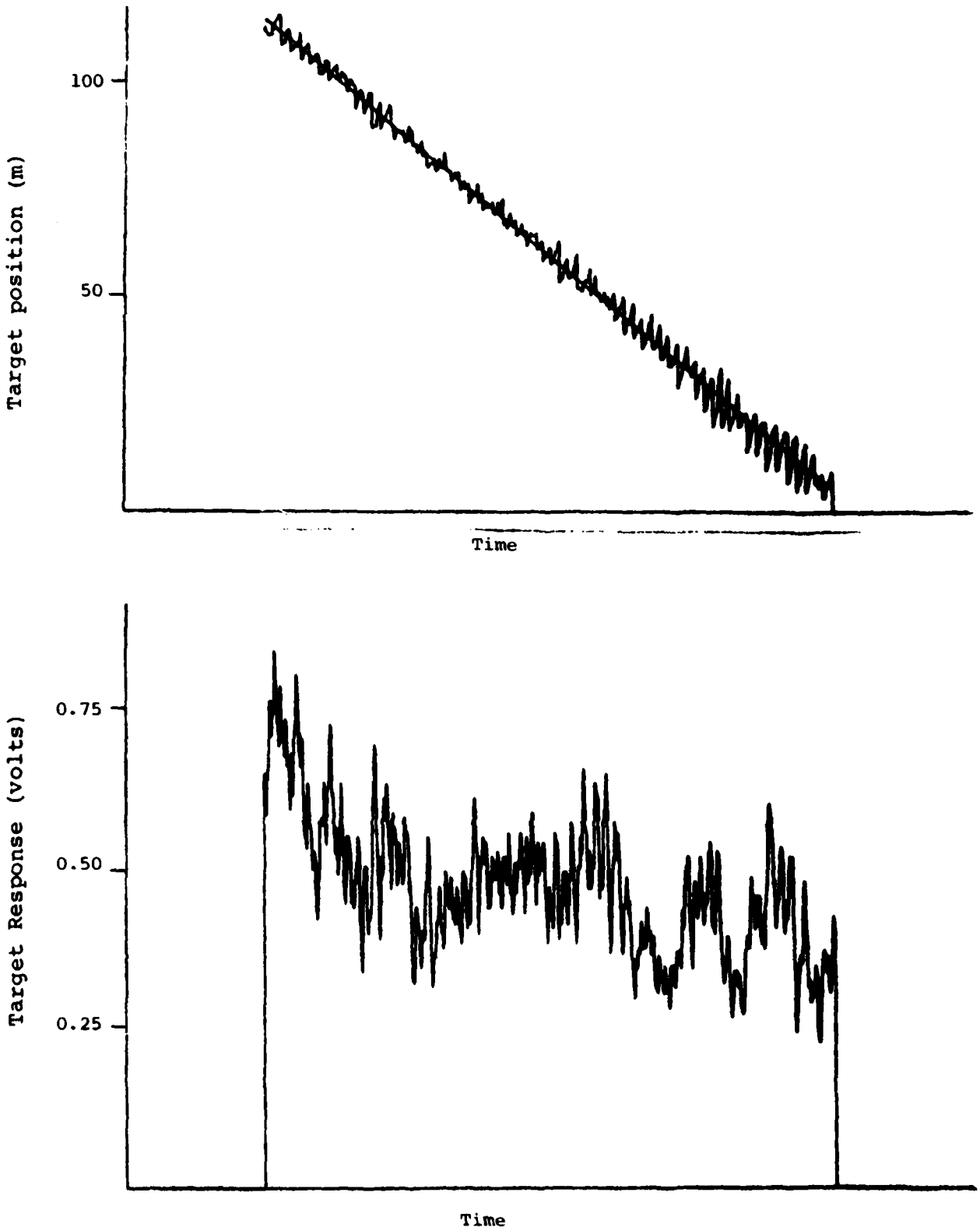

Figure 7.7: Cable as Transmitting Antenna
Maximum Response 0.84 volts

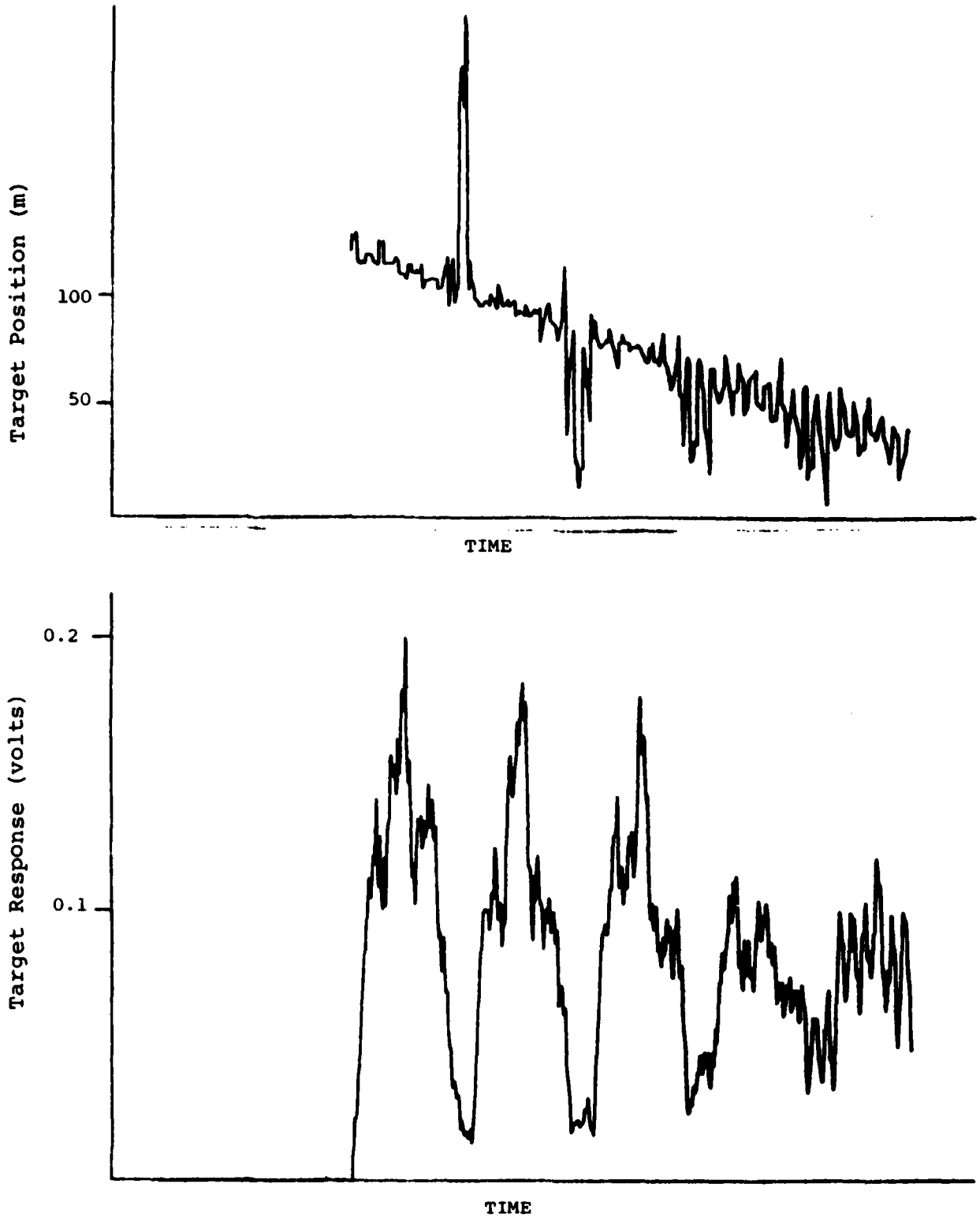

Figure 7.8 Cable Raised 1 Metre in Air
Maximum Response 0.2 volts

7.4.6 Performance with Large Stationary Obstacles

A series of experiments was performed to determine the influence of a large, stationary, metallic object (an automobile) on the performance of the system. The car was parked inside the loop of cable with the side of the car approximately 1-1/2 feet from the cable. The target's (a human) path was the same as in the standard walks with the target passing between the car and the cable.

A typical result is shown in figure 7.9. The overall system sensitivity was about the same as it would be with no obstacle present except when the target was "shadowed" by the car. At that point the sensitivity dropped by about 3 dB. The target location accuracy was not affected.

7.4.7 Radial Walks

The last experimental series involved a radial walk. The target started approximately 10 m outside the loop and walked directly towards the antenna. The target remained at the antenna for fifteen seconds, turned, and followed the same radial path back to the starting point. Figure 7.10 is a plot of typical data collected during such a radial walk.

The target is clearly visible in both the target response plot and the target location plot. As the target approached the antenna the sensitivity dropped below the threshold for detection chosen for this experiment (-8 dB). When close to the antenna the target again was detected although it was not accurately located. A very similar result was produced when the cable was connected to the transmitter.

7.5 System Simulation

7.5.1 Introduction

On the basis of the analysis of the system (section 7.3 and Appendix B) it is possible to simulate the return signal produced at the receiver when a target is within the detection zone of the system. Furthermore, the processing that occurs in the analogue portion of the receiver (see figure 7.3) can also be simulated. If the resulting digital representation of the signal is then processed by the normal target detection and location algorithm, it should be possible to determine the effects of errors in the analogue processing on the accuracy of target detection and location. This exercise has been carried out.

Under ideal conditions, with matched gains in all four analogue channels and exact 90° phase shifts in the synchronous detectors the algorithm output, with a simulated input signal is shown in figure 7.11. The only differences between these plots and the ideal straight line plots results from quantization error in the simulation and algorithm.

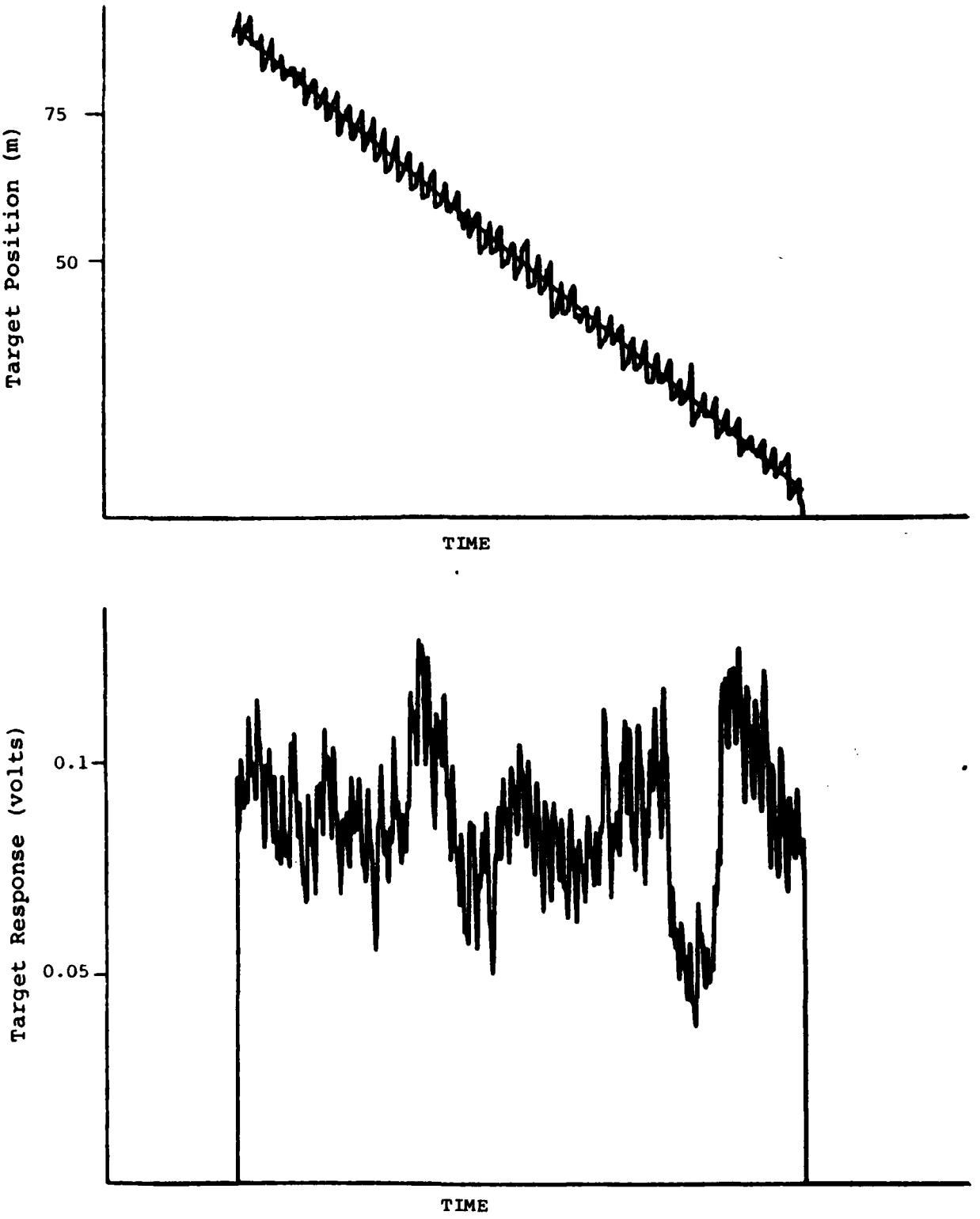

Figure 7.9 Response with Large Stationary Obstacle
Maximum Response 0.13 volts

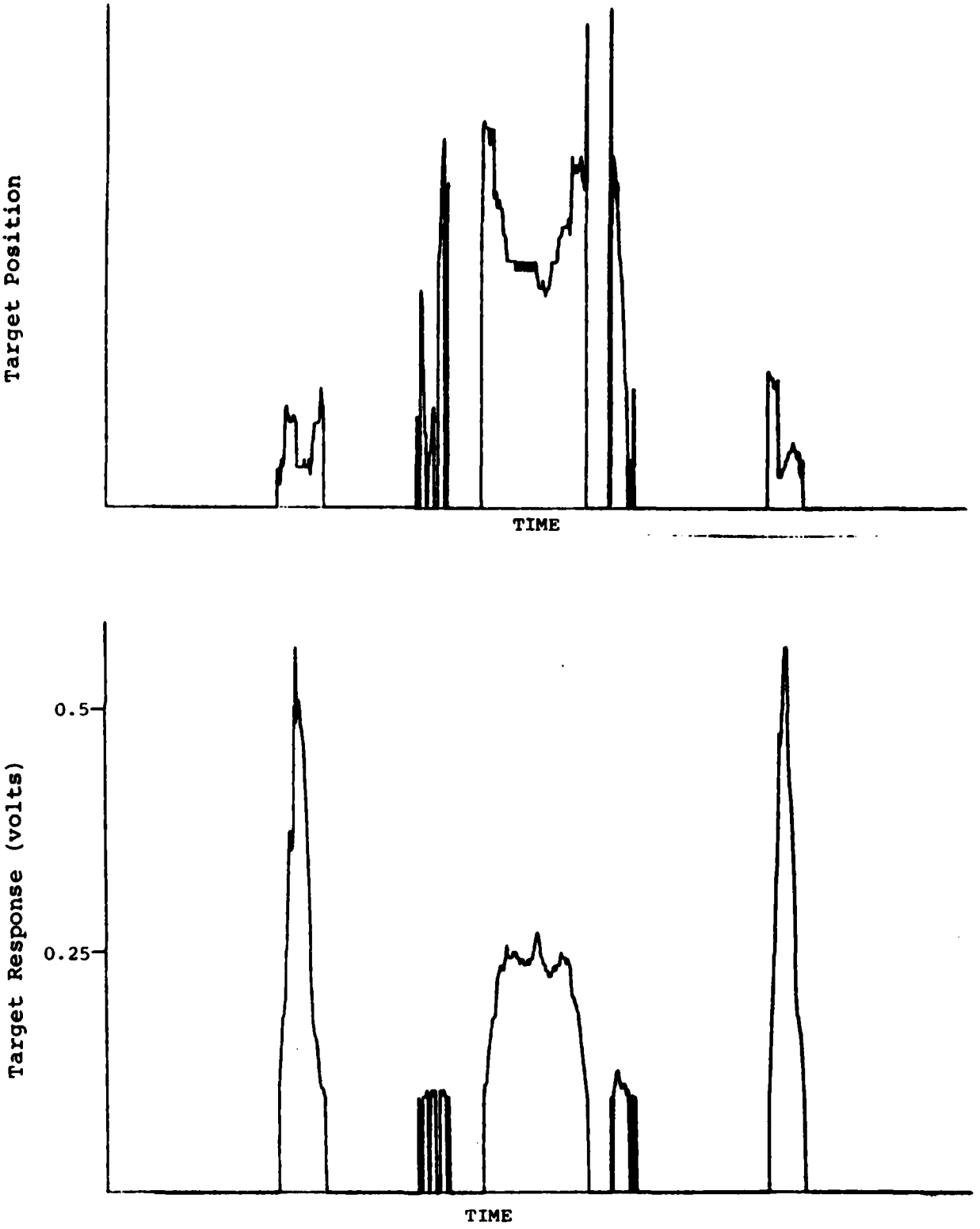

Figure 7.10: Radial Walk
Maximum Response 0.57 volts

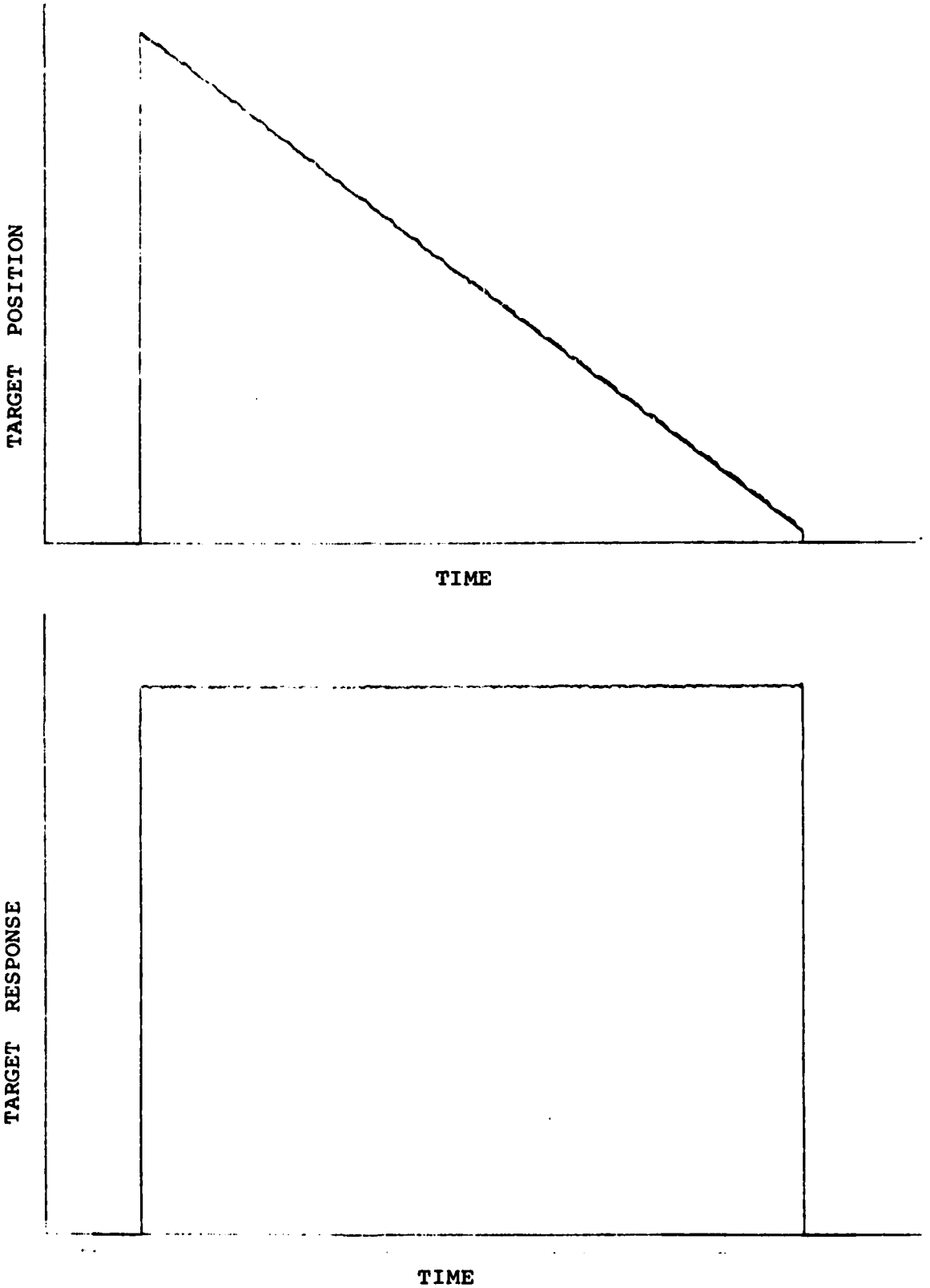

Figure 7.11 : Ideal System Response

7.5.2 Quadrature Error

A phase shift of other than 90° in the carrier detector will cause a change in two of the four signals produced by the analogue system. Equations 7.5 can be rewritten

$$\begin{aligned} \Delta I_1 &= \Delta M \sin(\beta_x+\alpha)\sin\gamma_x \\ \Delta Q_1 &= \Delta M \sin(\beta_x+\alpha)\cos\gamma_x \\ \Delta I_2 &= \Delta M \cos\beta_x \sin\gamma_x \\ \Delta Q_2 &= \Delta M \cos\beta_x \cos\gamma_x \end{aligned} \qquad 7.9$$

where α is the error in the quadrature oscillator.

Since target location is calculated either from $\Delta I_1/\Delta Q_1$ or $\Delta I_2/\Delta Q_2$ the location plot should show no dependance on carrier detector quadrature error. The error will, however, affect the target magnitude response. Figure 7.12 illustrates these points. For this simulation $\alpha = 10°$.

An error in the baseband detector would cause equations 7.5 to have the form

$$\begin{aligned} \Delta I_1 &= \Delta M \sin\beta_x \sin(\gamma_x+\delta) \\ \Delta Q_1 &= \Delta M \sin\beta_x \cos\gamma_x \\ \Delta I_2 &= \Delta M \cos\beta_x \sin(\gamma_x+\delta) \\ \Delta Q_2 &= \Delta M \cos\beta_x \cos\gamma_x \end{aligned} \qquad 7.9$$

where δ is the error in the baseband detector.

An error term will occur in both the target magnitude response curve and the target position curve. The form of the error is illustrated in figure 7.13. An error of 10° was included in the baseband quadrature oscillator.

7.5.3 Amplifier Gain Imbalance

Differences in the gain of the four system channels will affect both the target magnitude response and the target location accuracy. The precise effect of an error will depend upon which channels are miscalibrated.

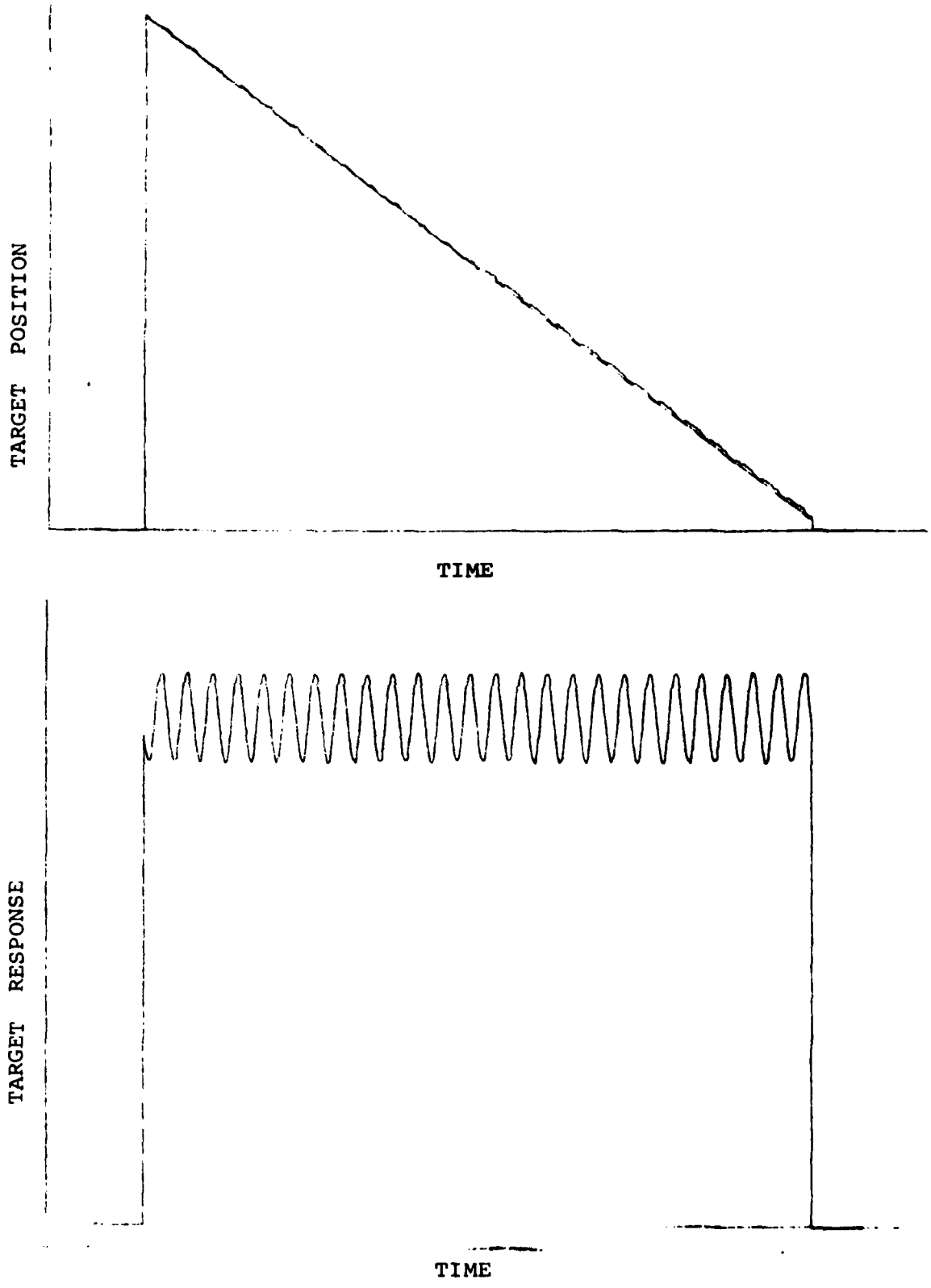

Figure 7.12: 10^{o} Error in Carrier Detector

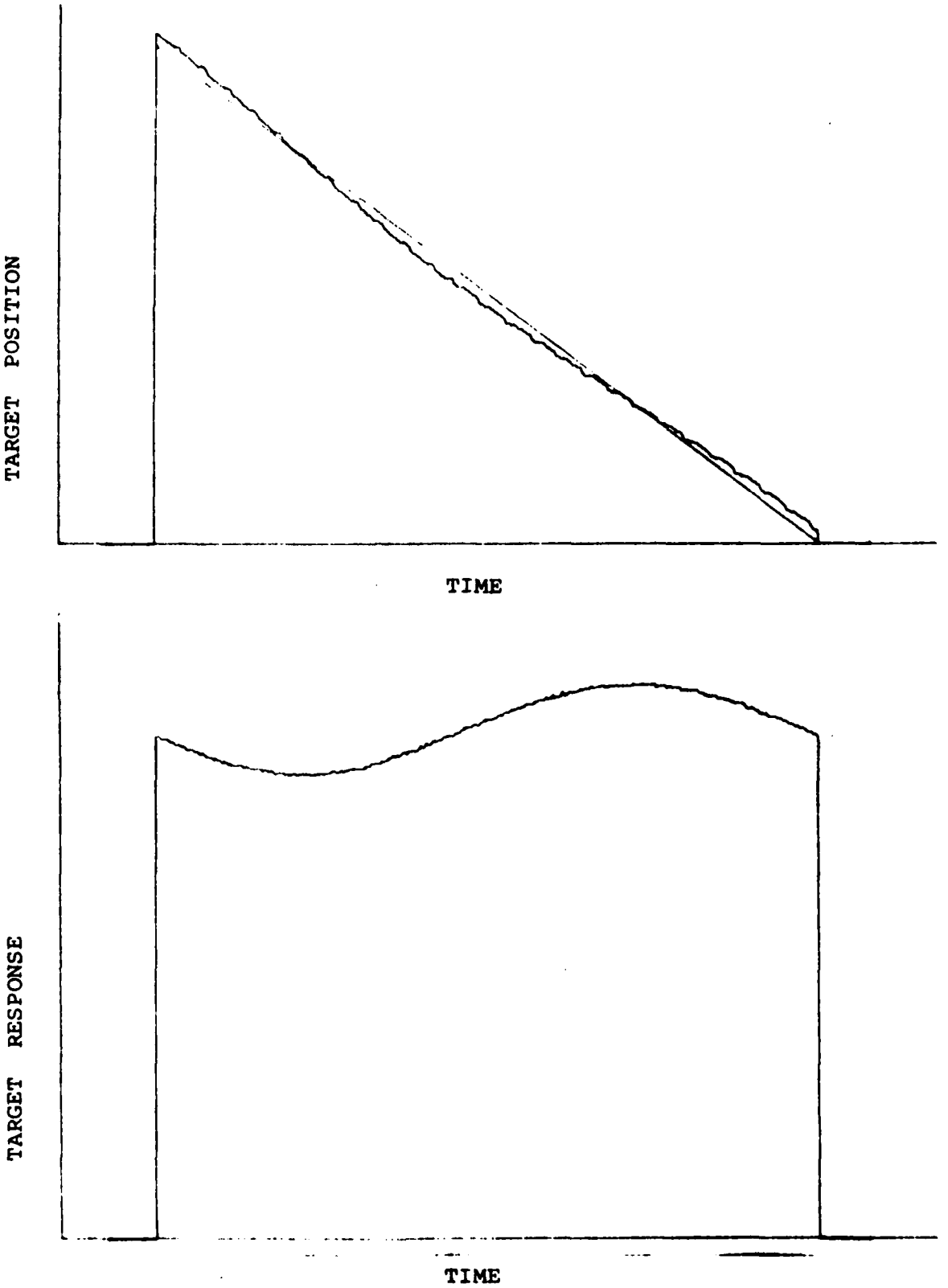

Figure 7.13 : 10° Error in Baseband Detector

Let $G_{\Delta I_n}$ = gain of the n^{th} I channel

$G_{\Delta Q_n}$ = gain of the n^{th} Q channel

If $G_{\Delta I_n} = G_{\Delta Q_n}$ $\quad n = 1,2$

but $G_{\Delta I_1} \neq G_{\Delta I_2}$

then the magnitude response curve will be affected but the target location plot will be correct since target location accuracy depends upon $\Delta I_n/\Delta Q_n$.

If $G_{I_n} \neq G_{Q_n}$ for either n = 1 or 2

then both the magnitude resoonse and the location accuracy will be influenced. The choice between calculating target position on the basis of $\Delta Q_1/\Delta I_1$ and $\Delta Q_2/\Delta I_2$ depends upon the ratio of M_1 and M_2 mentioned in section 7.3.2. As the target proceeds around the cable loop the algorithm will alternate between using the first pair of signals and the second pair of signals for position calculation. In a standard walk, therefore, the target position will appear to jump back and forth about an average position as the algorithm switches from using the first pair of signals to using the second pair.

Figure 7.14 shows the output of the algorithm when an error of 2 dB has been introduced into the gain of the ΔI_1 channel.

The errors introduced into the simulated analogue system in the examples shown in this section have been severe compared to what can be achieved in practice. From the results it would appear that neither the detection accuracy nor the location accuracy of the system is particularly sensitive to precise adjustment of system parameters.

7.6 Summary

It is clear, from the experiments reported in this section, that it is possible to replace one of the leaky coaxial cables in a standard guided radar system with a central antenna and still provide intrusion detection. When the cable is suspended in the air effects are seen which are similar to those in a two cable system due to interference between several modes of propagation of the energy along the cable. It should be possible to minimize these effects by the same techniques as have been suggested for a two cable system.

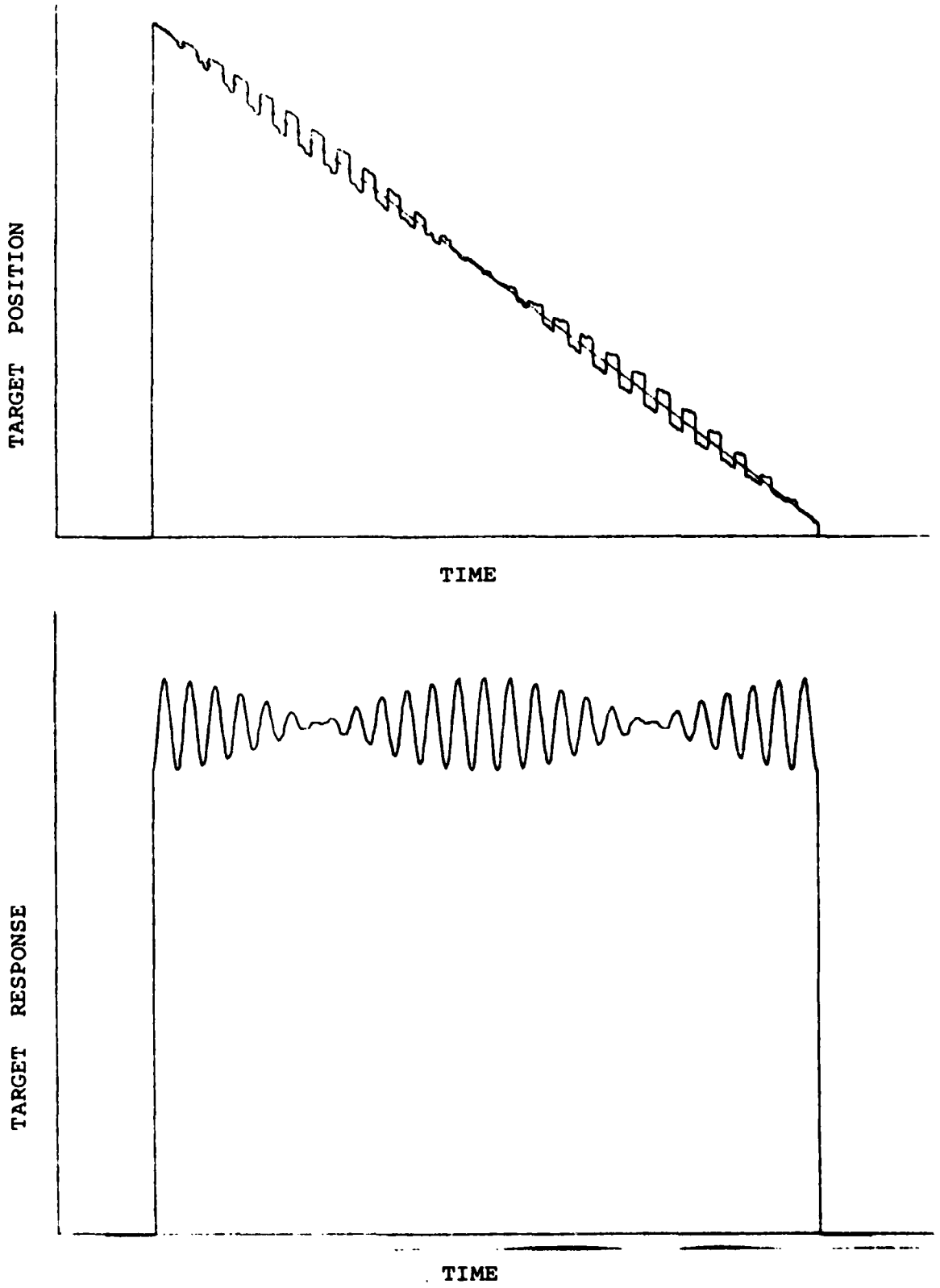

Figure 7.14 : Channel Gain Unbalance

No experiments were conducted with the leaky cable buried in the ground. However, based upon experience gained with a two cable system both with the cables buried and on the surface, no significant change in the performance would be expected if a buried cable were used.

The system can operate with either the cable or the antenna as the transmitting element. The target detection performance is similar in both cases. However, when the cable is used as the transmitting element, the field strength in the area surrounding the protected perimeter would be lower since a large portion of the transmitter power would be absorbed by the matched load. This would obviously be the best configuration in situations where several single cable detection systems must operate in close proximity to each other or where radiation from the intrusion detection system would interfere with other systems.

The feasibility of the proposed modulation scheme for allowing the measurement of location of an intrusion was successfully demonstrated. The maximum perimeter used was 125 metres, not because of any inherent restriction, but simply because of the available cable lengths. Perimeters of any circumference could be protected as long as the modulation wavelength was at least twice the circumference and the signal coupled into the cable was large enough to be detected. The accuracy of location is proportional to the accuracy of measurement of a phase angle and could be stated as being the appropriate constant fraction of a wavelength of the modulation signal. A higher modulation frequency therefore gives better location accuracy. The best choice of modulation frequency is the frequency having a wavelength which is twice the length of the protected perimeter. Since the location accuracy depends upon modulation wavelength, as long as a good signal to noise ratio were maintained no change in the location accuracy would be expected if the cable was buried.

Targets could be detected in the area between the cable and the antenna. Only a few preliminary experiments were performed to investigate the target detection characteristics within the loop. It appears that the target is detected within an annulus about the cable and when it is near the central antenna. Target location is accurate, however, only when the target is near the cable. More detailed experimentation would be required to determine whether it would be possible to track the target when it is within the protected perimeter.

The simple signal processing required for target detection and location and the necessity for having only one cable should allow the development of a practical microprocessor based portable short perimeter surveillance system.

8. SUMMARY

The work described in this report covers a number of quite different aspects of the performance of leaky coaxial cables in a variety of configurations. Advances have been made in a number of areas. These will be briefly summarized below.

8.1 Environmental Effects

The conditions of the ground around the leaky coaxial cables can influence their performance in a guided radar system. By far the most important environmental factor is moisture, either in the form of rain or snow. To determine the extent of the influence, long term monitoring of a stable guided radar installation must be undertaken. The results of such monitoring have been reported in Section 3 of this report. The winter and early spring seasons were chosen because the most significant changes in environmental conditions take place during that period.

Sensitivity changes of up to 15 dB were noted at any point on the sensor although the average range of sensitivity change was closer to 10 dB. The presence of large amounts of moisture decreased the sensitivity while small amounts enhanced sensitivity by 1 or 2 dB. The change in sensitivity was relatively uniform at all points along the cable.

Profile varied in the same way as sensitivity although to a greater extent. The maximum variation for any cell was 22 dB with the average being 13 dB. The variations of profile along the sensor were less uniform than the variations in sensitivity.

The noise in the system was relatively constant throughout the experimental period and was generated, in the main, in the receiver. The weather conditions, therefore, did not influence the system noise levels.

Continued long term monitoring of a guided radar installation would be required to more closely delimit the magnitude of the environmental effects since particular weather conditions occur only once or twice during a season. This monitoring should include automated measurement of soil temperature and relative moisture content. Also the results presented in this report were obtained from cables laid on the surface of the ground. The effects of weather would be expected to be different for buried cables. For example, a greater delay should occur between the onset of precipitation and an effect being noted in the profile or sensitivity. The time constants of the effects due to drying of the surface soil should also be different. A facility, such as the automated data logging system at the Queen's University field site would be required for adequate monitoring during rapidly changing conditions.

It is recommended that further monitoring of an installed leaky coaxial sensor be carried out to achieve some statistical significance in the results. This should

be done for a variety of cable installations including surface mounted and buried cables and perhaps including cables buried in soil, gravel and sand.

8.2 Velocity Measurement

The results presented have demonstrated that the velocity of a target moving longitudinally between the sensors can be measured, based upon the doppler shift in the return signal. The accuracy of the measurement depends upon system design. The velocities of two targets can be measured independently, assuming they are different from each other. In some situations different signal processing could be used to simplify the system. For example, if only one target is present, hard limiting and zero-crossing counting could replace the fourier transform operation presently used.

8.3 Target Classification

The experiments reported indicate that basic target classification can be performed using the return signal in a guided radar system. The classification is based upon the so-called target signature - the log-magnitude of the fourier transform of the target vector. Only rudimentary classification has been demonstrated and a large amount of work in this area remains to be done. The results of much of the work in target classification in normal radar systems can be applied directly to the leaky cable system although there are peculiarities of the guided radar system (non-uniform field distribution around the sensor, environmental effects) which require study directly within the guided radar context to assess their influence on target signatures and target classification.

The ability to classify targets, even broadly, has a significant effect on the false alarm rate of a deployed system. It would also allow an appropriate response to a detected intrusion. For these reasons, extension of the work reported here is highly recommended.

Only classification of targets moving longitudinally between the sensors was attempted. However, because of the decidedly non-uniform field distribution in the transverse plane in the vicinity of the cables it should be possible to produce a "signature" for a transverse crossing and, perhaps, classify on the basis of this signature. A study of this possibility is also recommended.

8.4 Single Cable System

The performance of a single cable system with a centrally located antenna was investigated. Such a system would be satisfactory for protecting relatively short perimeters. The system operated in a CW mode. However, a modulation technique was included which allowed the position of the intrusion to be measured.

The system performed well and its feasibility was thus demonstrated. The area used for the experiments was relatively clear of stationary obstacles (except when an obstacle was intentionally placed near the cable). The influence of stationary targets should be studied in some detail.

The processing involved in the system is such that it is possible to implement it on a microprocessor based system thus resulting in a compact and portable signal processing signal processing unit. In fact, a start has been made in this direction in a 4th year project performed last year at Queen's University. (This project was not funded by this contact.) An algorithm was developed for the M6800 microprocessor which demonstrated that the processing required could be done by a microprocessor. An extension of this work should be contemplated.

REFERENCES

1. N.A.M. Mackay and J.C. Beal, "The testing of leaky coaxial cables and their application to guided radar," Workshop Proc. Electromagnetic Guided Waves in Mine Environments, I.T.S., N.T.I.A., Department of Commerce, Boulder, Colorado, U.S.A. 80303, March 1978.

2. N.A.M. Mackay and J.C. Beal, "Electromagnetic aspects of guided radar," 19th General Assembly International Union of Radio Source (URSI), Helsinki, Finland, August 1978.

3. J.R. Wait, "Electromagnetic field analysis for a coaxial cable with periodic slots," IEEE Trans. on EM Compatibility, Vol. 19, pp. 7-13, Feb. 1977.

4. D.J. Gale and J.C. Beal, "Comparative testing of leaky coaxial cables by use of a two-cable cavity resonator," IEEE International MTT-S Symposium, Ottawa, Ontario, Canada, June 1978.

5. R.E. Patterson and N.A.M. Mackay, "A guided radar system for obstacle detection," IEEE Trans. Instrumentation and Measurement, Vol. IM-26, No. 2, pp. 137-143, June 1977.

6. R.E. Patterson, "Some aspects of a guided radar information processing system," M.Sc. Thesis, Queen's University, 1977.

7. M. Vinnins, "Digital aspects of a high-resolution guided radar system," M.Sc. Thesis, Queen's University, 1977.

8. J.W. Griffiths (ed.), "Signal Processing," Academic Press, London, 1973.

9. B. Gold, C. Rader, "Digital Processing of Signals," McGraw-Hill, New York 1969.

10. F.J. Harris, "On the use of windows for harmonic analysis with the discrete fourier transform," Proc. IEEE, Vol. 66, No. 1, pp. 51-83, Jan. 1978.

11. N.A. Mackay and A. Benjamin, "Guided radar for railway obstacle detection," Proc. Biennial CIGGT Seminar on Railway Research, Queen's University, Kingston, Canada, Jan. 29, 1978.

12. D.A. Winter et al, "Kinematics of normal locomotion - a statistical study based on T.V. data," Journal of Biomechanics, Vol. 7, No. 5, pp. 479-486, Sept. 1974.

13. T. Yamashita, R. Kotch, "Moving pattern of point of application of vertical resultant force during level walking," Journal of Biomechanics, Vol. 9, No. 2, pp. 93-99, Feb. 1976.

14. N.A.M. Mackay and J.C. Beal, "Guided radar for obstacle detection in ground transportation systems," Invited Paper, IEEE International AP-S Symposium, Washington, D.C., U.S.A., May 1978.

15. D.J. Gale, "Electromagnetic Evaluation of Leaky Coaxial Cables," M.Sc. Thesis, Queen's University, 1978.

16. N.A.M. Mackay, J.C. Beal, D.J. Gale, J.L. Mason, "Leaky Coaxial Cables for Obstacle Detection and Continuous-Access Guided Communications," AGARD Symposium on Special Topics in HF Propagation, Lisbon, Portugal, May 1979.

APPENDIX A

MONTHLY METEOROLOGICAL SUMMARIES

Environment Canada
Kingston Airport Office

January, February, March, April, 1979

Note: All readings are in metric units

Fisheries and Environment Canada / Pêches et Environnement Canada
Atmospheric Environment / Environnement atmosphérique

MONTHLY METEOROLOGICAL SUMMARY
SOMMAIRE MÉTÉOROLOGIQUE MENSUEL

MONTH/MOIS JANUARY / JANVIER 1979

AT/À KINGSTON "A" ONTARIO.

LAT: 44 ·13 'N LONG 76 · 36 'W ELEVATION/ALTITUDE: 93 METRES (ASL) / MÈTRES (NMM) STANDARD TIME USED/HEURE NORMALE UTILISÉE: EASTERN

DATE	TEMPERATURE / TEMPÉRATURE			DEGREE-DAYS / DEGRÉS-JOURS		REL. HUMIDITY / HUMIDITÉ REL.		THUNDERSTORM / ORAGE	PRECIPITATION / PRÉCIPITATIONS			SNOW ON GROUND / NEIGE AU SOL	WIND / VENT			BRIGHT SUNSHINE / INSOLATION EFFECTIVE
	MAXIMUM / MAXIMALE °C	MINIMUM / MINIMALE °C	MEAN / MOYENNE °C	HEATING / DE CHAUFFE BASE 18°C	GROWING / DE CROISSANCE BASE 5°C	MAXIMUM / MAXIMALE %	MINIMUM / MINIMALE %		RAINFALL / PLUIE (HAUTEUR) mm	SNOWFALL / NEIGE (HAUTEUR) cm	TOTAL PRECIP. / PRÉCIP. TOTALE mm	cm	AVERAGE SPEED / VITESSE MOYENNE km/h	PREVAILING DIRECTION / DIRECTION DOMINANTE	MAXIMUM SPEED AND DIRECTION / VITESSE MAXIMALE ET DIRECTION km/h	HOURS / HEURES
1	6.4	0.6	3.5	14.5		100	83		21.0		TR		19.4	S	S 44	
2	0.7	-7.6	-3.5	21.5		100	86		0.4	4.4	4.2	TR	14.6	W	W 24	
3	-8.0	-13.6	-10.8	28.8		93	59			8.0	4.0	3	28.9	W	W 44	7.1
4	-8.8	-12.8	-10.8	28.8		95	54			10.5	5.8	18	22.6	W	WNW 32	4.2
5	-8.2	-14.2	-11.2	29.2		90	59			.5	.5	20	21.1	W	WSW 32	7.9
6	-3.5	-12.5	-8.0	26.0		95	71			0.9	0.7	19	12.5	SW	WSW 30	4.1
7	-3.3	-7.4	-5.4	23.4		94	69			6.9	7.0	17	11.6	NE	SSW 26	
8	-4.8	-9.1	-7.0	25.0		88	45					20	11.8	N	N 17	1.7
9	-7.7	-13.0	-10.4	28.4		93	72			4.6	3.6	16	23.3	W	SW 41	
10	-9.5	-20.0	-14.8	32.8		98	63			TR	TR	19	7.1	NNW	W 13*	0.2
11	-11.0	-28.5	-19.8	37.8		100	64					18	8.2	SVRL	N 17*	6.0
12	-8.5	-14.3	-11.4	29.4		99	59			0.8	0.8	18	13.9	SVRL	S 26	3.9
13	-0.7	-11.7	-6.2	24.2		100	82		9.7	11.3	21.0	18	22.2	NE	NE 30	
14	3.3	-12.0	-4.4	22.4		100	66		10.0	TR	10.0	20	28.5	W	W 65	1.9
15	-8.2	-12.1	-10.2	28.2		88	59					16	21.0	W	W 37	8.0
16	-7.4	-15.9	-11.7	29.7		93	64			2.0	2.0	18	11.5	W	W 15	7.3
17	-13.5	-17.8	-15.7	33.7		94	65			13.4	13.0	16	19.3	NE	NE 30	
18	-13.8	-23.7	-18.8	36.8		95	64			0.8	0.8	30	13.8	N	N 28*	8.4
19	-17.0	-27.0	-22.0	40.0		94	67					30	6.5	ENE	ENE 20	2.8
20	-8.0	-17.4	-12.7	30.7		95	63		4.0	TR	4.0	30	20.5	ENE	ENE 28	
21	-4.0	-9.5	-6.8	24.8		98	79		4.0	12.4	16.4	35	23.8	NE	NNE 37	
22	-4.2	-10.4	-7.3	25.3		93	73			TR	TR	40	23.0	W	W 32	0.1
23	-1.0	-9.0	-5.0	23.0		94	77					37	10.5	SVRL	E 24	0.4
24	0.4	-8.4	-4.0	22.0		95	77		11.2	TR	11.2	31	22.0	ENE	ENE 30	
25	0.9	-2.6	-0.8	18.8		100	91		TR	27.2	29.0	45	M	M	NE 46	
26	4.0	0.0	2.0	16.0		95	82		0.2		0.2	30	M	M	NNW 22*	0.3
27	3.5	0.8	2.2	15.8		98	84					20	8.5	N	NNW 13	
28	2.5	0.1	1.3	16.7		97	78		1.0	1.0	2.0	18	15.1	NNW	NW 24	
29	-0.2	-6.5	-3.4	21.4		96	72			6.3	6.3	16	16.0	NW	NW 28	
30	-5.1	-8.1	-6.6	24.6		95	66			0.5	0.5	21	16.0	NW	W 28	0.2
31	-6.0	-12.5	-9.3	27.3		92	71			3.2	3.2	20	13.3	W	NNW 28	
				TOTAL	TOTAL			Total	TOTAL	TOTAL	TOTAL			PREVAILING	MAXIMUM	TOTAL
MEAN / MOYENNE	-4.5	-11.5	-8.0	807.0		95	70		61.3	114.7	167.0		15.7	W	W 65	64.5
NORMAL / NORMALE	-3.4	-11.7	-7.6	783.7					25.4	50.6	76.0		20.0	W		97.9

DEGREE-DAY SUMMARY – SOMMAIRE DE DEGRÉS-JOURS

BELOW 18°C / AU-DESSOUS DE 18°C	THIS YEAR / ANNÉE EN COURS	PREVIOUS YEAR / ANNÉE PRÉCÉDENTE	NORMAL / NORMALE	ABOVE 5°C / AU-DESSUS DE 5°C	THIS YEAR / ANNÉE EN COURS	PREVIOUS YEAR / ANNÉE PRÉCÉDENTE	NORMAL / NORMALE
TOTAL FOR MONTH / TOTAL DU MOIS	807.0	877.4	783.7	TOTAL FOR MONTH / TOTAL DU MOIS	0	0	0
ACCUMULATED SINCE JULY 1 / ACCUMULÉS DEPUIS LE 1er JUILLET	2420.7	2508.2	2302.7	ACCUMULATED SINCE APRIL 1 / ACCUMULÉS DEPUIS LE 1er AVRIL	1867.7	2271.3	1917.0

DAYS WITH TOTAL PRECIPITATION / JOURS AVEC PRÉCIPITATIONS TOTALES mm

0.2 OR MORE / OU PLUS	1.0 OR MORE / OU PLUS	2.0 OR MORE / OU PLUS	10.0 OR MORE / OU PLUS	50.0 OR MORE / OU PLUS
23	17	17	7	0

DAYS WITH SNOWFALL: / JOURS AVEC CHUTE DE NEIGE: cm

0.2 OR MORE / OU PLUS	1.0 OR MORE / OU PLUS	2.0 OR MORE / OU PLUS	10.0 OR MORE / OU PLUS	50.0 OR MORE / OU PLUS
18	13	12	5	0

UDC 551.509.1 (713.72) *Indicates more than one occurance of same wind speed but not necessarily same direction.

Subscription Price: $1.00 monthly, $10.00 per calendar year (January to December)
Prix d'abonnement: mensuel $1.00; annuel $10.00 (janvier à décembre)

00 0003-0000

COMPARATIVE RECORDS / RELEVÉS COMPARATIFS — Kingston Airport — MONTH / MOIS: JANUARY / JANVIER — 1979

TEMPERATURE/TEMPÉRATURE °C; PRECIPITATION/PRÉCIPITATION mm; RAIN/PLUIE mm; SNOW/NEIGE cm	THIS MONTH CE MOIS-CI		PREVIOUS YEAR ANNÉE PRÉCÉDENTE		NORMAL NORMALE	RECORD FOR THE MONTH RECORD POUR LE MOIS — HIGHEST MAXIMUM ABSOLU			LOWEST MINIMUM ABSOLU			YEARS OF RECORD PRECIPITATION
	VALUE RELEVÉ	DATE	VALUE RELEVÉ	DATE		VALUE RELEVÉ	DAY JOUR	YEAR ANNÉE	VALUE RELEVÉ	DAY JOUR	YEAR ANNÉE	
HIGHEST TEMPERATURE / TEMPÉRATURE LA PLUS ÉLEVÉE	6.4	01	4.9	8,9		15.0	4	1874	-25.6	14	1957	107
LOWEST TEMPERATURE / TEMPÉRATURE LA PLUS BASSE	-28.5	11	-22.1	10		7.2	4	1950	-33.3	30	1908	107
MEAN MONTHLY TEMPERATURE / TEMPÉRATURE MENSUELLE MOYENNE	-8.0		-10.3		7.6	-3.1		1967	-12.4		1970	20
TOTAL MONTHLY RAINFALL / HAUTEUR TOTALE MENSUELLE DE PLUIE	61.3		93,4		25.4	114.1		1937				106
TOTAL MONTHLY SNOWFALL / HAUTEUR TOTALE MENSUELLE DE NEIGE	114.7		95.8		50.6	133.9		1884	1.0		1933	106
TOTAL MONTHLY PRECIPITATION / PRÉCIPITATION TOTALE MENSUELLE	167.0		187.1		76.0	187.1		1978	13.7		1921	106
NO OF DAYS WITH MEASURABLE PRECIPITATION / NOMBRE DE JOURS AVEC PRÉCIPITATION MESURABLE	23		22									
GREATEST RAINFALL IN ONE DAY / HAUTEUR DE PLUIE MAXIMALE EN UNE JOURNÉE	21.0	01	41.0	26		41.0	26	1978				18
GREATEST SNOWFALL IN ONE DAY / HAUTEUR DE NEIGE MAXIMALE EN UNE JOURNÉE	27.2	25	15.0	19		35.6	30	1966				18
GREATEST PRECIPITATION IN ONE DAY / PRÉCIPITATION MAXIMALE EN UNE JOURNÉE	29.0	25	50.1	26		50.1	26	1978				18
MAXIMUM RAINFALL RECORDED IN: / HAUTEUR DE PLUIE MAXIMALE ENREGISTRÉE EN:												
5 MINUTES												
10 MINUTES												
30 MINUTES												
60 MINUTES												
24 CONSECUTIVE HOURS / HEURES CONSÉCUTIVES												
MEAN WIND SPEED (m.p.h.) / VITESSE MOYENNE DU VENT (m/h)	20.0		23.1		20.0	23.1		1978	8.2		1970	10
MAXIMUM SPEED (1 min.) (m.p.h.) / VITESSE MAXIMALE (1 min) (m/h)	W 65	14	SSW 74	26		SSW 74	26	1978	S 27	28	1970	10
MAXIMUM GUST SPEED (m.p.h.) / POINTE DU VENT MAXIMALE (m/h)	W 83	14	WSW 93	26		WSW 93	28 26	1977 1978	S 43	4	1973	10
TOTAL HOURS OF SUNSHINE / TOTAL DES HEURES INSOLATION	64.5		60.4		97.9	114.0		1970	60.4		1978	10
MEAN STATION PRESSURE (mb) / PRESSION MOYENNE À LA STATION (mb)	100.2		100.3		100.7	100.8		1974	99.8		1978	9
GREATEST STATION PRESSURE (mb) / PRESSION MAXIMALE À LA STATION (mb)	102.5	11	102.1	17		102.8	31	1973				9
LEAST STATION PRESSURE (mb) / PRESSION MINIMALE À LA STATION (mb)	99.4	26	95.1	26					95.1	26	1978	9

CLIMATOLOGICAL DATA FOR THE PAST 10 YEARS / DONNÉES CLIMATOLOGIQUES POUR LES 10 DERNIÈRES ANNÉES

YEAR ANNÉE	HIGHEST TEMP TEMP MAXIMALE	LOWEST TEMP TEMP MINIMALE	MEAN TEMP TEMP MOYENNE	RAINFALL HAUTEUR DE PLUIE	SNOWFALL HAUTEUR DE NEIGE	TOTAL PRECIP PRECIP TOTALE	HIGHEST PRECIP WITHIN ONE DAY PRÉCIP MAXIMALE EN UNE JOURNÉE	GREATEST SNOWFALL WITHIN ONE DAY NEIGE MAXIMALE EN UNE JOURNÉE	BRIGHT SUNSHINE HOURS HEURES INSOLATION	HEATING DEGREE DAYS DEGRÉS-JOURS DE CHAUFFE	COOLING DEGREE DAYS DEGRÉS-JOURS DE CONDITIONNEMENT		
1970	5.0	-28.3	-12.4	6.4	31.2	30.2	13.1	43	114.0	934.4			
1971	3.3	-30.0	-10.7	11.4	34.8	41.9	20.3	58	107.4	888.9			
1972	11.7	-25.0	-5.3	15.0	46.2	47.0	23.8	80	131.1	717.2			
1973	6.1	-26.1	-5.1	30.7	14.0	42.9	21.3	51	104.2	713.3			
1974	8.9	-23.3	-7.2	33.8	58.7	88.4	20.6	75	98.5	776.6			
1975	10.0	-25.0	-4.7	40.9	26.2	63.8	20.8	64	84.7	699.4			
1976	4.1	-31.2	-11.0	29.3	60.3	87.8	19.8	56	115.1	900.3			
1977	-1.8	-28.4	-11.9	0.0	98.4	86.5	19.1	85	92.4	926.4			
1978	4.9	-22.1	-10.3	93.4	95.8	187.1	23.1	74	60.4	877.4			
1979	6.4	-28.5	-8.0	61.3	114.7	167.0	15.7	65	64.5	807.0			

00 0063-0001

Fisheries and Environment Canada / Pêches et Environnement Canada
Atmospheric Environment / Environnement atmosphérique

MONTHLY METEOROLOGICAL SUMMARY
SOMMAIRE MÉTÉOROLOGIQUE MENSUEL

MONTH/MOIS FEBRUARY / FEVRIER 1979

AT/À KINGSTON "A" ONTARIO.

LAT 44 ° 13 ' N LONG 76 ° 36 ' W ELEVATION/ALTITUDE 93 METRES (ASL) / MÈTRES (NMM) STANDARD TIME USED / HEURE NORMALE UTILISÉE EASTERN

DATE	TEMPERATURE / TEMPÉRATURE			DEGREE-DAYS / DEGRÉS-JOURS		REL HUMIDITY / HUMIDITÉ REL		THUNDERSTORM / ORAGE	PRECIPITATION / PRÉCIPITATIONS			SNOW ON GROUND / NEIGE AU SOL	WIND / VENT			BRIGHT SUNSHINE / INSOLATION EFFECTIVE
	MAXIMUM MAXIMALE °C	MINIMUM MINIMALE °C	MEAN MOYENNE °C	HEATING / DE CHAUFFE (BASE 18°C)	COOLING / DE CROISSANCE (BASE 5°C)	MAXIMUM MAXIMALE %	MINIMUM MINIMALE %		RAINFALL / PLUIE (HAUTEUR) mm	SNOWFALL / NEIGE (HAUTEUR) cm	TOTAL PRECIP / PRÉCIP TOTALE mm	cm	AVERAGE SPEED / VITESSE MOYENNE km/h	PREVAILING DIRECTION / DIRECTION DOMINANTE	MAXIMUM SPEED AND DIRECTION / VITESSE MAXIMALE ET DIRECTION km/h	HOURS / HEURES
1	-9.8	-14.0	-11.9	29.9		89	63			2.2	1.8	23	19.8	WNW	W 24	7.8
2	-7.0	-14.6	-10.8	28.8		90	60			1.0	1.0	24	14.1	WNW	WNW 22	6.3
3	-10.0	-20.0	-15.0	33.0		85	50					22	6.2	W	NW 13	9.6
4	-4.0	-17.5	-10.8	28.8		95	75			2.8	2.4	21	20.3	SVRL	SW 37*	1.3
5	-9.0	-18.7	-13.9	31.9		89	56					24	27.6	W	W 32*	8.2
6	-14.2	-23.5	-18.9	36.9		85	52					24	9.5	W	W 17*	9.5
7	-9.4	-18.5	-14.0	32.0		96	53			2.0	2.0	24	19.5	NE	NE 32	1.9
8	-8.2	-19.0	-13.6	31.6		96	58			4.3	4.2	29	12.8	NW	N 32	3.1
9	-16.2	-26.5	-21.4	39.4		80	50					29	11.9	SVRL	N 22	9.5
10	-16.6	-29.2	-22.9	40.9		75	45					29	11.6	N	N 22	8.7
11	-20.4	-29.1	-24.8	42.8		73	47					29	6.9	SVRL	NNW 13*	9.7
12	-13.5	-30.2	-21.9	39.9		80	60			TR	TR	29	8.2	SVRL	S 15	8.1
13	-17.0	-28.1	-22.6	40.6		70	40					29	12.8	N	N 28	7.9
14	-18.0	-27.9	-23.0	41.0		78	45					29	5.9	SW	SW 15	5.9
15	-15.6	-22.0	-18.8	36.8		83	60			4.8	4.8	29	16.8	NNE	NNE 30	8.2
16	-14.9	-23.7	-19.3	37.3		74	45			2.0	2.0	35	21.0	NNE	N 30	8.7
17	-20.5	-28.1	-24.3	42.3		67	47					35	13.0	NNW	N 26	10.0
18	-15.5	-31.3	-23.4	41.4		79	49					35	7.9	NE	ENE 15	7.6
19	-7.4	-17.8	-12.6	30.6		100	76			4.0	2.0	39	8.1	SVRL	SW 15	6.6
20	-3.2	-13.3	-8.3	26.3		100	72					37	19.5	SW	SW 33*	7.4
21	3.5	-4.4	-0.5	18.5		100	71		5.2		5.2	35	20.7	S	SSW 46	0.2
22	1.6	-1.6	0.0	18.0		97	71		TR		TR	28	15.3	W	W 33*	
23	2.4	-2.0	0.2	17.8		100	71		14.6		14.6	20	22.4	SVRL	S 37	2.0
24	5.7	-5.7	0.0	18.0		100	65		1.0		1.0	15	17.7	N	NNE 37	
25	-3.4	-10.1	-6.8	24.8		75	53					11	30.9	NE	NE 46	5.7
26	-3.9	-7.0	-5.5	23.5		94	60		0.8	7.4	8.2	11	35.3	NE	ENE 46	
27	-0.6	-8.1	-4.4	22.4		95	85			2.8	2.8	17	15.4	NNE	NNE 37	
28	3.4	-9.6	-3.1	21.1		100	55					18	12.4	W	W 22	10.2
29																
30																
31																
MEAN / MOYENNE	-8.6	-17.9	-13.3	TOTAL 876.3	TOTAL	87	58	TOTAL	TOTAL 21.6	TOTAL 33.3	TOTAL 52.0		16.8	PREVAILING / DOMINANTE NE/W	DIRECTION SVRL 46	TOTAL 156.3
NORMAL / NORMALE	-2.4	-11.6	-6.9	698.5					26.4	38.4	64.8		18.2	W		119.0

DEGREE-DAY SUMMARY – SOMMAIRE DE DEGRÉS-JOURS

BELOW 18°C / AU-DESSOUS DE 18°C	THIS YEAR / ANNÉE EN COURS	PREVIOUS YEAR / ANNÉE PRÉCÉDENTE	NORMAL / NORMALE	ABOVE 5°C / AU-DESSUS DE 5°C	THIS YEAR / ANNÉE EN COURS	PREVIOUS YEAR / ANNÉE PRÉCÉDENTE	NORMAL / NORMALE
TOTAL FOR MONTH / TOTAL DU MOIS	876.3	806.4	698.5	TOTAL FOR MONTH / TOTAL DU MOIS	0	0	0
ACCUMULATED SINCE JULY 1 / ACCUMULÉS DEPUIS LE 1er JUILLET	3297.0	3314.6	3001.2	ACCUMULATED SINCE APRIL 1 / ACCUMULÉS DEPUIS LE 1er AVRIL	2887.7	2271.3	1917.0

DAYS WITH TOTAL PRECIPITATION / JOURS AVEC PRÉCIPITATIONS TOTALES mm

0.2 OR MORE / OU PLUS	1.0 OR MORE / OU PLUS	5.0 OR MORE / OU PLUS	10.0 OR MORE / OU PLUS	50.0 OR MORE / OU PLUS
13	13	10	1	0

DAYS WITH SNOWFALL / JOURS AVEC CHUTE DE NEIGE cm

0.2 OR MORE / OU PLUS	1.0 OR MORE / OU PLUS	5.0 OR MORE / OU PLUS	10.0 OR MORE / OU PLUS	50.0 OR MORE / OU PLUS
10	10	9	0	0

UDC 551.501.1 (713.72)

* Indicates more than one occurance of same wind speed but not necessarily the same direction.

Subscription Price: $1.00 monthly, $10.00 per calendar year (January to December) / Abonnement: mensuel $1.00; annuel $10.00 (janvier à décembre)

00 0080-0000

Reduce and print image area on 8½ x 11" good quality 20 lb. bond paper allowing for ½" right and left hand margins. (DO NOT OVER REDUCE).

Whenever possible, use both sides of paper, i.e. pages 1 and 2 back-to-back, etc.

Réduire l'air imprimée et la reproduire sur du papier bond 20 lb. de bonne qualité, format 8½ x 11", avec marge de ½ pouce à gauche et à droite. (NE PAS TROP RÉDUIRE).

Imprimer recto verso dans la mesure du possible (par exemple, pages 1 et 2 recto verso, etc.)

Revised February 1977

COMPARATIVE RECORDS
RELEVÉS COMPARATIFS

Kingston, Ontario

MONTH / MOIS: FEBRUARY / FEVRIER

19 79

	THIS MONTH / LE MOIS		PREVIOUS YEAR / ANNÉE PRÉCÉDENTE		NORMAL / NORMALE	RECORD FOR THE MONTH / RECORD POUR LE MOIS						YEARS OF RECORD / ANNÉES D'OBSERVATION
						HIGHEST MAXIMUM ABSOLU			LOWEST MINIMUM ABSOLU			
	VALUE RELEVÉ	DATE	VALUE RELEVÉ	DATE		VALUE RELEVÉ	DAY JOUR	YEAR ANNÉE	VALUE RELEVÉ	DAY JOUR	YEAR ANNÉE	
HIGHEST TEMPERATURE TEMPERATURE LA PLUS ÉLEVÉE	5.7	24	0.0	24		13.3	28	1954	-25.6	8	1934	107
LOWEST TEMPERATURE TEMPERATURE LA PLUS BASSE	-31.3	18	-24.2	4		6.7	10	1966	-35.6	17	1896	107
MEAN MONTHLY TEMPERATURE TEMPERATURE MENSUELLE MOYENNE	-13.3		-10.8		-6.9	-3.4		1957	-13.3		1979	107
TOTAL MONTHLY RAINFALL HAUTEUR TOTALE MENSUELLE DE PLUIE	21.6		0.0		26.4	94.7		1925				107
TOTAL MONTHLY SNOWFALL HAUTEUR TOTALE MENSUELLE DE NEIGE	33.3		16.1		38.4	121.7		1876	TR		1977	107
TOTAL MONTHLY PRECIPITATION PRECIPITATION TOTALE MENSUELLE	52.0		15.0		64.8	131.6		1971	2.0		1877	107
NO OF DAYS WITH MEASURABLE PRECIPITATION NOMBRE DE JOURS AVEC PRÉCIPITATION MESURABLE	13		8									
GREATEST RAINFALL IN ONE DAY HAUTEUR DE PLUIE MAXIMALE EN UNE JOURNÉE	14.6	23	0.0			31.2	28	1966				18
GREATEST SNOWFALL IN ONE DAY HAUTEUR DE NEIGE MAXIMALE EN UNE JOURNÉE	7.4	26	8.6	7		28.7	13	1971				18
GREATEST PRECIPITATION IN ONE DAY PRÉCIPITATION MAXIMALE EN UNE JOURNÉE	14.6	23	8.6	7		31.2	28	1966				23
MAXIMUM RAINFALL RECORDED IN HAUTEUR DE PLUIE MAXIMALE ENREGISTRÉE EN:												
5 MINUTES												
10 MINUTES												
15 MINUTES												
30 MINUTES												
60 MINUTES												
24 CONSECUTIVE HOURS HEURES CONSECUTIVES												
MEAN WIND SPEED (km/h) VITESSE MOYENNE DU VENT (km/h)	16.8		15.2		18.2	21.8		1971	15.2		1978	10
MAXIMUM SPEED (1 min) (km/h) VITESSE MAXIMALE (1 min) (km/h)	SVRL46		NNE 52	7		SW 72	28	1971	N/NE40		1973	10
MAXIMUM GUST SPEED (km/h) POINTE DU VENT MAXIMALE (km/h)	WSW 63 ENE	21 26	NNE 78	7		W 83	2	1976	SW 57	27	1973	10
TOTAL HOURS OF SUNSHINE TOTAL DES HEURES INSOLATION	136.3		166.1		119.0	166.1		1978	97.1		1971	31
MEAN STATION PRESSURE (kPa) PRESSION MOYENNE À LA STATION (kPa)	101.2		100.7		100.4	101.5		1973	100.1		1976	8
GREATEST STATION PRESSURE (kPa) PRESSION MAXIMALE À LA STATION (kPa)	103.6	17/ 18	102.7	4		103.6	17/ 18	1979				8
LEAST STATION PRESSURE (kPa) PRESSION MINIMALE À LA STATION (kPa)	99.1	1	99.2	24					97.2	4	1972	8

CLIMATOLOGICAL DATA FOR THE PAST 10 YEARS
DONNÉES CLIMATOLOGIQUES POUR LES 10 DERNIÈRES ANNÉES

YEAR ANNÉE	HIGHEST TEMP TEMP MAXIMALE	LOWEST TEMP TEMP MINIMALE	MEAN TEMP TEMP MOYENNE	RAINFALL HAUTEUR DE PLUIE	SNOWFALL HAUTEUR DE NEIGE	TOTAL PRECIP PRECIP TOTALE	MEAN SPEED VITESSE MOYENNE	GREATEST WIND VITESSE MAXIMALE	MEAN SUNSHINE HEURES INSOLATION	HEATING DEGREE DAYS DEGRÉS-JOURS DE CHAUFF	COOLING DEGREE DAYS DEGRÉS-JOURS DE CLIMATISATION		
1969	4.4	-10.9	-4.6	.5	17.5	17.5				627.2			
1970	4.4	-32.8	-7.7	50.0	61.0	105.4	17.2	SE 58	140.5	711.7			
1971	6.7	-25.6	-5.9	61.7	73.7	131.6	21.8	SW 72	97.1	665.6			
1972	5.0	-23.9	-8.7	29.2	73.4	89.7	18.6	W/SW 56	131.8	771.7			
1973	7.8	-26.7	-8.7	24.4	21.6	44.5	17.1	W/NE 40	136.8	746.1			
1974	6.7	-22.2	-8.6	29.0	21.3	49.8	17.1	W 56	155.6	738.8			
1975	5.6	-22.2	-5.7	30.2	42.4	70.6	17.4	SW 56	114.3	660.0			
1976	9.5	-26.2	-3.5	48.2	22.4	70.6	19.8	SW 46	110.6	622.6			
1977	6.8	-21.2	-6.5	18.8	12.9	30.9	20.2	SW 43	104.0	684.5			
1978	0.0	-24.2	-10.8	0.0	16.1	15.0	15.2	NNE 52	166.1	806.4			
1979	5.7	-31.3	-13.3	21.6	33.3	52.0	16.8	SVRL 46	156.3	876.3			

Revised January 1976

Fisheries and Environment Canada / Pêches et Environnement Canada
Atmospheric Environment / Environnement atmosphérique

MONTHLY METEOROLOGICAL SUMMARY
SOMMAIRE MÉTÉOROLOGIQUE MENSUEL

MONTH/MOIS MARCH / MARS 1979

AT/À KINGSTON AIRPORT, ONTARIO.

LAT 44 - 13 'N LONG 76° 36 'W ELEVATION ALTITUDE 93 METRES (ASL) MÈTRES (NMM) STANDARD TIME USED: HEURE NORMALE UTILISÉE EASTERN

DATE	TEMPERATURE TEMPÉRATURE			DEGREE DAYS DEGRÉS-JOURS		REL HUMIDITY HUMIDITÉ REL		THUNDERSTORM ORAGE	PRECIPITATION PRÉCIPITATIONS			SNOW ON GROUND NEIGE AU SOL	WIND VENT			BRIGHT SUNSHINE INSOLATION EFFECTIVE
	MAXIMUM MAXIMALE °C	MINIMUM MINIMALE °C	MEAN MOYENNE °C	HEATING DE CHAUFFE BASE 18°C	GROWING DE CROISSANCE BASE 5°C	MAXIMUM MAXIMALE %	MINIMUM MINIMALE %		RAINFALL PLUIE (HAUTEUR) mm	SNOWFALL NEIGE (HAUTEUR) cm	TOTAL PRECIP PRÉCIP TOTALE mm	cm	AVERAGE SPEED VITESSE MOYENNE km/h	PREVAILING DIRECTION DIRECTION DOMINANTE	MAXIMUM SPEED AND DIRECTION VITESSE MAXIMALE ET DIRECTION km/h	HOURS HEURES
1	3.2	-2.6	0.3	17.7		100	55		1.0	TR	1.0	14	19.3	ENE	NE 30	1.4
2	2.0	-2.0	0.0	18.0		100	87		7.0		7.0	11	12.4	SSE	SSE 28	
3	3.6	-0.5	1.6	16.4		97	82					10	MSG	SSE	MSG	8.1
4	5.4	1.0	3.2	14.8		100	88		10.2		10.2	6	22.1	SSE	S 33	0.8
5	5.6	0.0	2.8	15.2		100	75		9.2		9.2	2	15.0	S	W 24	
6	1.9	-0.3	0.8	17.2		100	90		2.0		2.0	2	4.8	C	WSW 13	
7	2.3	-0.3	1.0	17.0		100	81					2	6.3	SW	N 11	0.8
8	4.6	-0.1	2.3	15.7		93	68					2	9.1	N	N 17	
9	3.4	0.0	1.7	16.3		85	69		TR		TR	2	7.6	SVRL	ESE 19	3.6
10	2.6	-2.1	0.3	17.7		100	86		5.0		5.0	2	19.3	WSW	SE 35*	
11	-2.1	-8.6	-5.4	23.4		85	59					1	25.4	W	W 33	6.6
12	-2.8	-9.1	-6.0	24.0		83	36			0.2	0.2	1	24.2	W	NW 33	6.8
13	4.7	-9.6	-2.5	20.5		94	67		0.4		0.4	1	25.7	S	S 44	6.1
14	5.6	-10.8	-2.6	20.6		97	60		7.0	TR	7.0	TR	37.9	W	S 54	0.8
15	-7.4	-15.0	-11.2	29.2		70	49					TR	24.1	WNW	W 32	8.0
16	-1.6	-10.9	-6.3	24.3		90	70			0.4	0.4	TR	13.5	W	SW 26*	
17	3.0	-1.6	0.7	17.3		90	60					TR	6.7	SVRL	SE 19	4.4
18	5.7	-3.1	1.3	16.7		90	35					TR	15.1	NNE	NNE 26*	8.9
19	7.3	-3.2	2.1	15.9		87	47					TR	15.9	NE	NNE 28*	8.8
20	9.7	-2.2	3.8	14.2		81	47					TR	11.9	N	S 20	8.9
21	12.8	0.7	6.8	11.2	1.8	97	51					TR	12.7	SVRL	NE 28	9.6
22	6.7	-1.6	2.6	15.4		98	75						5.8	S	SSW 11	9.7
23	12.3	-0.4	6.0	12.0	1.0	95	50						15.5	SSE	SSE 28	9.4
24	12.1	4.8	8.5	9.5	3.5	95	62		0.5		0.5		23.4	SE	SE 32	
25	5.2	0.7	3.0	15.0		98	62		2.5		2.5		18.4	SW	SSW 26	0.4
26	0.7	-7.9	-3.6	21.6		96	52			TR	TR	TR	24.3	W	W 37*	0.5
27	0.4	-9.3	-4.5	22.5		65	39						23.7	W	W 30*	11.0
28	4.2	-8.7	-2.3	20.3		93	48						14.6	S	S 29	9.5
29	7.2	1.8	4.5	13.5		100	71		4.4		4.4		19.3	S	S 33*	0.6
30	6.5	3.2	4.9	13.1		100	91		8.6		8.6		15.2	ENE	ENE 26	
31	11.7	1.7	7.7	10.1	2.7	100	67		2.0		2.0		18.5	SW	WSW 35	1.5
				TOTAL	TOTAL			TOTAL	TOTAL	TOTAL	TOTAL			PREVAILING	MAXIMUM	TOTAL
MEAN MOYENNE	4.5	-3.1	0.7	536.5	9.0	93	64		60.8	0.6	61.4		16.9	W DOMINANTE	S 54	128.2
NORMAL NORMALE	3.1	-5.8	-1.3	597.9					37.3	26.7	64.0		19.5	W		145.3

DEGREE DAY SUMMARY – SOMMAIRE DE DEGRÉS-JOURS

BELOW 18°C AU-DESSOUS DE 18°C	THIS YEAR ANNÉE EN COURS	PREVIOUS YEAR ANNÉE PRÉCÉDENTE	NORMAL NORMALE	ABOVE 5°C AU-DESSUS DE 5°C	THIS YEAR ANNÉE EN COURS	PREVIOUS YEAR ANNÉE PRÉCÉDENTE	NORMAL NORMALE
TOTAL FOR MONTH TOTAL DU MOIS	536.5	679.8	597.9	TOTAL FOR MONTH TOTAL DU MOIS	9.0	0	2.6
ACCUMULATED SINCE JULY 1 ACCUMULÉE DEPUIS LE 1er JUILLET	3894.9	3994.4	3621.6	ACCUMULATED SINCE APRIL 1 ACCUMULÉE DEPUIS LE 1er AVRIL	1896.7	2271.3	1919.6

DAYS WITH TOTAL PRECIPITATION JOURS AVEC PRÉCIPITATIONS TOTALES: mm

0.2 OR MORE OU PLUS	1.0 OR MORE OU PLUS	2.0 OR MORE OU PLUS	10.0 OR MORE OU PLUS	50.0 OR MORE OU PLUS
15	11	10	1	0

DAYS WITH SNOWFALL JOURS AVEC CHÛTE DE NEIGE: cm

0.2 OR MORE OU PLUS	1.0 OR MORE OU PLUS	2.0 OR MORE OU PLUS	10.0 OR MORE OU PLUS	50.0 OR MORE OU PLUS
2	0	0	0	0

UDC 551.508.1 (713.72 • Indicates more than one occurance of same wind speed but not necessarily direction.

Subscription Price $1.00 monthly, $10.00 per calendar year (January to December)
Prix d'abonnement: mensuel $1.00, annuel $10.00 (janvier à décembre)

00 0083 9890

Reduce and print image area on 8½ x 11" good quality 20 lb. bond paper allowing for ½" right and left hand margins (DO NOT OVER REDUCE)

Whenever possible use both sides of paper, i.e. pages 1 and 2 back to back, etc.

Réduire et imprimer la zone d'image sur du papier bond 20 lb. de bonne qualité, format 8½ x 11" avec marge de ½ pouce à gauche et à droite (NE PAS TROP RÉDUIRE)

Imprimer recto verso dans la mesure du possible (par exemple, pages 1 et 2 recto verso, etc.)

COMPARATIVE RECORDS / RELEVÉS COMPARATIFS — KINGSTON ONTARIO — MONTH / MOIS: MARCH / MARS — 19 79

Temperature/Température °Celsius Precipitation/Précipitation Millimetres (mm) Rainfall/Hauteur de pluie Millimetres (mm) Snowfall/Hauteur de neige Centimetres (cm) Wind speed/Vitesse du vent Kilometres per hour/Kilomètres par heure (km/h) Station pressure/Pression à la station Kilopascals (kPa)	THIS MONTH / CE MOIS CI		PREVIOUS YEAR / ANNÉE PRÉCÉDENTE		NORMAL / NORMALE	RECORD FOR THE MONTH / RECORD POUR LE MOIS — HIGHEST MAXIMUM ABSOLU			LOWEST MINIMUM ABSOLU			YEARS OF RECORD / ANNÉES D'OBSERVATION
	VALUE / RELEVÉ	DATE	VALUE / RELEVÉ	DATE		VALUE / RELEVÉ	DAY / JOUR	YEAR / ANNÉE	VALUE / RELEVÉ	DAY / JOUR	YEAR / ANNÉE	
HIGHEST TEMPERATURE / TEMPÉRATURE LA PLUS ÉLEVÉE	13.7	31	6.4	31		19.4	28	1965	-18.9	1	1938	107
LOWEST TEMPERATURE / TEMPÉRATURE LA PLUS BASSE	-15.0	15	-20.5	5		8.3	30	1910	-28.9	3	1950	107
MEAN MONTHLY TEMPERATURE / TEMPÉRATURE MENSUELLE MOYENNE	0.7		-3.9		-1.3	2.9		1973	-5.7		1960	22
TOTAL MONTHLY RAINFALL / HAUTEUR TOTALE MENSUELLE DE PLUIE	60.8		53.4		37.3	129.8		1936	0.5		1962	105
TOTAL MONTHLY SNOWFALL / HAUTEUR TOTALE MENSUELLE DE NEIGE	0.6		28.8		26.7	89.7		1947	.5		1927	105
TOTAL MONTHLY PRECIPITATION / PRÉCIPITATION TOTALE MENSUELLE	61.4		86.0		64.0	153.4		1936	3.3		1915	105
NO OF DAYS WITH MEASURABLE PRECIPITATION / NOMBRE DE JOURS AVEC PRÉCIPITATION MESURABLE	15		12									
GREATEST RAINFALL IN ONE DAY / HAUTEUR DE PLUIE MAXIMALE EN UNE JOURNÉE	10.2	4	21.8	14		38.1	19	1975				18
GREATEST SNOWFALL IN ONE DAY / HAUTEUR DE NEIGE MAXIMALE EN UNE JOURNÉE	0.4	16	12.8	26		31.0	22	1977				18
GREATEST PRECIPITATION IN ONE DAY / PRÉCIPITATION MAXIMALE EN UNE JOURNÉE	10.2	4	22.3	26		38.1	19	1975				18
MAXIMUM RAINFALL RECORDED IN / HAUTEUR DE PLUIE MAXIMALE ENREGISTRÉE EN:												
5 MINUTES												
10 MINUTES												
15 MINUTES												
30 MINUTES												
60 MINUTES												
24 CONSECUTIVE HOURS / HEURES CONSÉCUTIVES												
MEAN WIND SPEED (km/h) / VITESSE MOYENNE DU VENT (km/h)	16.9		16.7		19.5	21.4		1970	16.7		1978	9
MAXIMUM SPEED (1 min.) (km/h) / VITESSE MAXIMALE (1 min.) (km/h)	S 54	14	W 65	19		W 65	19	1978	NE 45	28	1973	9
MAXIMUM GUST SPEED (km/h) / POINTE OU VENT MAXIMALE (km/h)	WNW 74	26	W 104	19		W 104	19	1978	NE 64	17	1973	9
TOTAL HOURS OF SUNSHINE / TOTAL DES HEURES INSOLATION	128.2		185.7		145.3	185.7		1978	75.6		1973	9
MEAN STATION PRESSURE (kPa) / PRESSION MOYENNE À LA STATION (kPa)	100.6		100.5		100.5	100.6		1973 1979	100.0		1971	9
GREATEST STATION PRESSURE (kPa) / PRESSION MAXIMALE À LA STATION (kPa)	102.7	15	102.6	25		102.7	15	1979				9
LEAST STATION PRESSURE (kPa) / PRESSION MINIMALE À LA STATION (kPa)	98.0	25	98.3	14					97.7		1971	9

CLIMATOLOGICAL DATA FOR THE PAST 10 YEARS / DONNÉES CLIMATOLOGIQUES POUR LES 10 DERNIÈRE ANNÉES

YEAR / ANNÉE	HIGHEST TEMP / TEMP MAXIMALE	LOWEST TEMP / TEMP MINIMALE	MEAN TEMP / TEMP MOYENNE	RAINFALL / HAUTEUR DE PLUIE	SNOWFALL / HAUTEUR DE NEIGE	TOTAL PRECIP / PRECIP TOTALE	MEAN WINDSPEED / VITESSE MOYENNE DES VENTS	GREATEST WINDSPEED / VITESSE MAXIMALE DES VENTS	HOURS OF SUNSHINE / HEURES INSOLATION	HEATING DEGREE DAYS / DEGRÉS-JOURS DE CHAUFFE	GROWING DEGREE DAYS / DEGRÉ JOURS DE CROISSANCE		
1969	7.8	-17.2	-1.9	48.0	21.1	61.0			164.8	612.8			
1970	6.7	-16.7	-2.6	32.3	13.0	49.8	21.4	SW 51	183.3	636.1			
1971	6.7	-17.2	-4.2	3.6	64.5	65.5	19.7	SW 64	135.0	681.7			
1972	7.2	-19.4	-4.8	46.2	18.5	103.9	19.4	S 51	118.6	676.1			
1973	15.0	-5.6	2.9	51.3	26.7	54.9	17.9	NE 45	75.6	465.6	13.3		
1974	13.9	-15.0	-2.8	42.2	20.3	93.7	20.2	S/SE 48	144.1	623.3	2.2		
1975	7.8	-18.9	-2.9	61.0	38.1	104.9	18.4	N 50	158.2	643.9			
1976	15.4	-19.2	-1.8	76.0	54.8	130.8	21.1	SW 59	123.4	612.4	2.3		
1977	17.4	-9.7	1.4	54.7	48.2	106.1	18.3	S/SW 41	150.9	514.9	13.7		
1978	6.4	-20.5	-3.9	53.4	28.8	86.0	16.7	W 65	185.7	679.8			
1979	13.7	-15.0	0.7	60.8	0.6	61.4	16.9	S 54	128.2	536.5	9.0		

00 0063-0001

Reduce and print image area on 8½ x 11" good quality 20 lb. bond paper allowing for ½" right and left bond margins. (DO NOT OVER REDUCE).

Whenever possible, use both sides of paper, i.e. pages 1 and 2 back-to-back, etc.

Réduire l'air imprimée et la reproduire sur du papier bond 20 lb. de bonne qualité, format 8½ x 11", avec marge de ½ pouce à gauche et à droite. (NE PAS TROP RÉDUIRE)

Imprimer recto verso dans la mesure du possible (par exemple, pages 1 et 2 recto verso, etc.)

Environment Canada / Environnement Canada
Atmospheric Environment / Environnement atmosphérique

MONTHLY METEOROLOGICAL SUMMARY
SOMMAIRE MÉTÉOROLOGIQUE MENSUEL

MONTH/MOIS APRIL / AVRIL 1979

AT/À KINGSTON AIRPORT ONTARIO.

LAT 44 · 13 °N LONG 76 · 36 °W ELEVATION/ALTITUDE 93 METRES (ASL) / METRES (NMM) STANDARD TIME USED/HEURE NORMALE UTILISÉE: EASTERN

DATE	TEMPERATURE / TEMPÉRATURE			DEGREE-DAYS / DEGRÉS-JOURS		REL HUMIDITY / HUMIDITÉ REL		THUNDERSTORM / ORAGE	PRECIPITATION / PRÉCIPITATIONS			SNOW ON GROUND / NEIGE AU SOL	WIND / VENT			BRIGHT SUNSHINE / INSOLATION EFFECTIVE
	MAXIMUM MAXIMALE °C	MINIMUM MINIMALE °C	MEAN MOYENNE °C	HEATING / DE CHAUFFE BASE 18°C	COOLING / DE CLIMATISATION BASE 18°C	MAXIMUM MAXIMALE %	MINIMUM MINIMALE %		RAINFALL / PLUIE (HAUTEUR) mm	SNOWFALL / NEIGE (HAUTEUR) cm	TOTAL PRECIP / PRÉCIP. TOTALE mm	cm	AVERAGE SPEED / VITESSE MOYENNE km/h	PREVAILING DIRECTION / DIRECTION DOMINANTE	MAXIMUM SPEED AND DIRECTION / VITESSE MAXIMALE ET DIRECTION km/h	HOURS / HEURES
1	4.9	0.2	2.6	15.4		90	66		TR		TR		21.5	NE	NNE 28	
2	6.3	3.7	5.0	13.0		100	85		23.6		23.6		24.3	SSE	S 39	
3	9.0	-1.3	3.9	14.1		97	44						18.8	W	WSW 30	6.0
4	7.2	-3.8	1.7	16.3		100	46		6.0	10.0	16.0		20.1	ENE	ENE 32*	0.8
5	4.0	0.3	2.2	15.8		100	70		4.0	2.0	6.0	2	28.4	WSW	WSW 46	
6	3.5	-3.7	-0.1	18.1		99	74		2.0	5.0	5.8	1	45.3	WSW	WSW 83	0.2
7	3.8	-3.8	0.0	18.0		80	40					TR	26.1	WNW	NW 32*	10.4
8	1.7	-7.0	-2.7	20.7		81	57					TR	11.9	SSW	SSW 24	7.2
9	0.4	-1.5	-0.6	18.6		99	57			13.2	13.2	TR	22.6	NE	NE 33	
10	8.9	-1.8	3.6	14.4		93	34					5	11.5	NW	NW 28*	11.5
11	5.0	-3.4	0.8	17.2		80	43					TR	11.5	NW	S 22	7.5
12	8.4	-1.0	3.7	14.3		85	37					TR	11.8	SVRL	NE 22*	3.7
13	12.4	3.3	7.9	10.1	2.9	84	44					TR	21.8	ENE	E 30	6.1
14	6.4	2.4	4.4	13.6		100	79		13.8		13.8		19.5	SVRL	S 33*	0.6
15	9.2	2.2	5.8	12.2	0.8	100	60		1.0		1.0		12.3	N	NNW 24	0.7
16	7.6	3.0	5.3	12.7	0.3	100	75		1.8		1.8		14.0	N	N 29	1.0
17	13.9	3.7	8.8	9.2	3.8	84	30						20.2	NNW	N 30	7.8
18	12.1	1.3	6.7	11.3	1.7	65	31						19.2	NNW	NNE 30	11.8
19	13.3	0.8	7.1	10.9	2.1	70	24						17.1	N	N 28	12.5
20	18.8	-0.4	4.2	13.8		90	48						10.3	N	SW 20	12.1
21	16.9	2.0	9.5	8.5	4.5	84	28						6.6	S	S 15	12.3
22	12.7	4.2	8.5	9.5	3.5	100	46		3.6		3.6		9.9	S	S 20*	7.8
23	15.6	4.8	10.2	7.8	5.2	93	37						13.3	S	SSW 28	11.9
24	16.2	1.7	9.0	9.0	4.0	95	49						7.1	S	S 13*	11.3
25	18.5	8.8	13.7	4.3	8.7	93	60		0.2		0.2		16.3	SSE	SSE 30	2.0
26	14.2	7.8	11.0	7.0	6.0	100	83		7.8		7.8		22.0	S	SE 32	
27	10.4	5.4	7.9	10.1	5.1	100	97		19.6		19.6		14.8	SVRL	W 26	
28	10.0	3.0	6.5	11.5	1.5	100	56						9.6	SW	W 19	4.0
29	8.2	2.5	5.4	11.6	0.4	97	65						15.8	SVRL	S 28	8.3
30	12.4	0.0	6.2	11.8	5.8	100	42		2.2		2.2		7.9	SVRL	NNW 28	9.4
31																
MEAN / MOYENNE	9.4	1.1	5.3	TOTAL 381.8	TOTAL 56.3	92	54	TOTAL	TOTAL 85.6	TOTAL 30.2	TOTAL 114.6		17.1	PREVAILING S/SVRL	GUSTIEST NSW 83	TOTAL 167.2
NORMAL / NORMALE	11.4	1.2	6.3	367.2	39.5				68.6	4.1	72.6		17.3	SW		174.8

DEGREE-DAY SUMMARY – SOMMAIRE DE DEGRÉS-JOURS

BELOW 18°C / AU-DESSOUS DE 18°C	THIS YEAR / ANNÉE EN COURS	PREVIOUS YEAR / ANNÉE PRÉCÉDENTE	NORMAL / NORMALE	ABOVE 5°C / AU-DESSUS DE 5°C	THIS YEAR / ANNÉE EN COURS	PREVIOUS YEAR / ANNÉE PRÉCÉDENTE	NORMAL / NORMALE
TOTAL FOR MONTH / TOTAL DU MOIS	381.8	417.1	367.2	TOTAL FOR MONTH / TOTAL DU MOIS	56.3	33.8	39.5
ACCUMULATED SINCE JULY 1 / ACCUMULÉE DEPUIS LE 1er JUILLET	4276.7	4411.5	3924.6	ACCUMULATED SINCE APRIL 1 / ACCUMULÉE DEPUIS LE 1er AVRIL	56.3	33.8	39.5

DAYS WITH TOTAL PRECIPITATION / JOURS AVEC PRÉCIPITATIONS TOTALES (mm)

0.2 OR MORE / OU PLUS	1.0 OR MORE / OU PLUS	2.0 OR MORE / OU PLUS	10.0 OR MORE / OU PLUS	50.0 OR MORE / OU PLUS
13	12	11	5	0

DAYS WITH SNOWFALL / JOURS AVEC CHUTE DE NEIGE (cm)

0.2 OR MORE / OU PLUS	1.0 OR MORE / OU PLUS	2.0 OR MORE / OU PLUS	10.0 OR MORE / OU PLUS	50.0 OR MORE / OU PLUS
4	4	4	2	0

UDC 551.508.1 (713.72 * Indicates more than one occurance of same wind speed but not necessarily the same direction.

Subscription Price: $1.00 monthly $10.00 per calendar year (January to December)
Prix d'abonnement: mensuel $1.00, annuel $10.00 (janvier à décembre)

00 0063 9890

Reduce print image area on 8½ x 14" good quality 20 lb. bond paper allowing for ½" right and left hand margins (DO NOT OVER REDUCE)

Whenever possible, use both sides of paper, i.e. pages 1 and 2 back to back, etc

Réduire l'aire imprimée et la reproduire sur du papier bond 20 lb. de bonne qualité (format 8½ x 14") avec marge de ½ pouce à gauche et à droite (NE PAS TROP RÉDUIRE)

Imprimer recto verso dans la mesure du possible (par exemple, pages 1 et 2 recto verso, etc.)

Revised February 1977

THIS PAGE IS BEST QUALITY PRACTICABLE FROM COPY FURNISHED TO DDC

A-8

COMPARATIVE RECORDS
RELEVÉS COMPARATIFS

Kingston Ont.

MONTH / MOIS: April /Avril

YEAR / AN: 79

		THIS MONTH LE MOIS CI		PREVIOUS YEAR ANNÉE PRÉCÉDENTE		NORMAL NORMALE	RECORD FOR THE MONTH RELEVÉ POUR LE MOIS						YEARS OF RECORD NOMBRE D'ANNÉES D'OBSERVATIONS
							HIGHEST MAXIMUM ABSOLU			LOWEST MINIMUM ABSOLU			
		VALUE RELEVÉ	DATE	VALUE RELEVÉ	DATE		VALUE RELEVÉ	DAY JOUR	YEAR ANNÉE	VALUE RELEVÉ	DAY JOUR	YEAR ANNÉE	
HIGHEST TEMPERATURE TEMPERATURE LA PLUS ÉLEVÉE		18.5	25	18.1	28		29.4	28	1962	-4.4	01 05	1923 1881	107
LOWEST TEMPERATURE TEMPERATURE LA PLUS BASSE		-7.0	8	-6.5	3		13.3	29	1878	-17.2	01	1923	107
MEAN MONTHLY TEMPERATURE TEMPERATURE MENSUELLE MOYENNE		5.3		4.1		6.3	8.1		1968	2.9		1972	22
TOTAL MONTHLY RAINFALL HAUTEUR TOTALE MENSUELLE DE PLUIE		85.6		63.4		68.6	121.7		1954	5.1		1879	105
TOTAL MONTHLY SNOWFALL HAUTEUR TOTALE MENSUELLE DE NEIGE		30.2		1.4		4.1	66.5		1885				105
TOTAL MONTHLY PRECIPITATION PRÉCIPITATION TOTALE MENSUELLE		114.6		64.8			136.1		1973	10.7		1881	105
NO. OF DAYS WITH MEASURABLE PRECIPITATION NOMBRE DE JOURS AVEC PRÉCIPITATION MESURABLE		13		8									
GREATEST RAINFALL IN ONE DAY HAUTEUR DE PLUIE MAXIMALE EN UNE JOURNÉE		21.6	2	17.6	20		40.6	19	1963				18
GREATEST SNOWFALL IN ONE DAY HAUTEUR DE NEIGE MAXIMALE EN UNE JOURNÉE		13.2	9	1.2	20		23.1	3	1975				18
GREATEST PRECIPITATION IN ONE DAY PRÉCIPITATION MAXIMALE EN UNE JOURNÉE		21.6	2	18.8	20		40.6	19	1963				38
MAXIMUM RAINFALL RECORDED IN HAUTEUR DE PLUIE MAXIMALE ENREGISTRÉE EN													
5 MINUTES													
10 MINUTES													
15 MINUTES													
30 MINUTES													
60 MINUTES													
24 CONSECUTIVE HOURS HEURES CONSÉCUTIVES													
MEAN WIND SPEED (km/h) VITESSE MOYENNE DU VENT (km/h)		17.1		17.8		17.9	18.9		1975	15.4		1972	9
MAXIMUM SPEED (1 min) (km/h) VITESSE MAXIMALE (1 min) (km/h)		W 80	6	S 41	01		W 80	19	1975	W 40	4,5	1972	9
MAXIMUM GUST SPEED (km/h) POINTE DU VENT MAXIMALE (km/h)		WSW 113	6	W 70	01		SW 96	19	1975	NE 54		1973	9
TOTAL HOURS OF SUNSHINE TOTAL DES HEURES INSOLATION		167.2		201.9		174.8	251.6		1970	176.9		1974	10
MEAN STATION PRESSURE (kPa) PRESSION MOYENNE A LA STATION (kPa)		100.4		100.3		100.3	100.5		1972 1977	100.2		1971	9
GREATEST STATION PRESSURE (kPa) PRESSION MAXIMALE A LA STATION (kPa)		102.7	12	102.4	3		102.4	5 3	1971 1978				9
LEAST STATION PRESSURE (kPa) PRESSION MINIMALE A LA STATION (kPa)		97.9	6	98.0	1					97.1	3	1975	9

CLIMATOLOGICAL DATA FOR THE PAST 10 YEARS
DONNÉES CLIMATOLOGIQUES POUR LES DERNIÈRES ANNÉES

YEAR ANNÉE	MAXIMUM TEMP TEMP MAXIMALE	MINIMUM TEMP TEMP MINIMALE	MEAN TEMP TEMP MOYENNE	RAINFALL HAUTEUR DE PLUIE	SNOWFALL HAUTEUR DE NEIGE	TOTAL PRECIP PRECIP TOTALE	MEAN SPEED OF HOURLY WINDS VITESSE MOYENNE DES VENTS	MAXIMUM SPEED (1 min) VITESSE MAXIMALE (1 min)	MEAN MONTHLY HOURS OF SUNSHINE MOYENNE MENSUELLE DES HEURES D'INSOLATION	MEAN MONTHLY HOURS OF CLOUDINESS MOYENNE MENSUELLE DES HEURES DE NUAGES	MEAN MONTHLY DEGREE DAYS MOYENNE MENSUELLE DES DEGRÉS-JOURS DE CHAUFFAGE
1969	20.0	-7.8	6.3	74.9	7.4	81.8			195.1	351.7	
1970	24.4	-7.2	5.8	50.8	13.5	63.8	17.2	N/W 48	251.6	363.2	59.4
1971	15.6	-8.9	3.6	28.5	1.8	30.2	18.1	W 45	188.6	427.2	17.2
1972	15.0	-11.3	2.9	39.1	11.9	50.6	15.4	W 49	208.0	448.9	10.6
1973	22.2	-6.1	6.1	126.8	9.9	136.1	18.2	NE 43	208.0	354.4	64.4
1974	21.7	-6.7	5.6	57.2	5.1	62.2	16.2	SW 54	176.9	470.0	53.3
1975	20.6	-7.8	3.1	34.3	34.8	69.1	19.9	SW 80	201.4	442.7	32.2
1976	24.7	-7.8	6.6	57.8	11.5	69.2	18.4	SW/W 41	226.6	341.6	76.3
1977	21.0	-9.3	5.2	58.2	2.8	60.6	17.0	W 46	228.0	304.4	58.5
1978	18.1	-6.5	4.1	63.4	1.4	64.8	17.8	S 41	201.9	417.1	33.8
1979	18.5	-7.0	5.3	85.6	30.2	114.6	17.1	WSW 83	167.2	381.8	56.3

00 0003 0001

Reduce and print image area on 8½ x 11" good quality 20 lb. bond paper allowing for 1" right and left hand margins *(DO NOT OVERREDUCE)*

Whenever possible, use both sides of paper i.e. page 1 and 2 back to back etc.

Réduire et imprimer la région image sur du papier bond 20 lb. de bonne qualité, formats 8½ x 11" avec marge de 1" gauche et à droite *(NE PAS TROP RÉDUIRE)*

Imprimer recto verso dans la mesure du possible (par exemple, pages 1 et 2 recto verso etc.)

APPENDIX B

Assume that the coupling from the external field into the coaxial cable takes place at only three discrete points around the circumference x, y and z. The signal from the antenna is $\sin(2\pi f_o t)$. Three voltage components will propagate in the leaky cable.

$$V_x(t) = X \sin(2\pi f_o t + \theta)$$

$$V_y(t) = Y \sin(2\pi f_o t + \theta) \qquad \text{B.1}$$

$$V_z(t) = Z \sin(2\pi f_o t + \theta)$$

where f_o is the carrier frequency

θ is a constant caused by the propagation time of the signal from the antenna to the cable

X,Y,Z are "coupling coefficients"

The coupling coefficients represent the proportion of the radiated field which is coupled into the coaxial cable at a particular point. In an ideal system with uniform sensitivity X, Y and Z would be equal.

The signal at the receiver is:

$$V_R(t) = X'\sin(2\pi f_o t + \theta + \beta_x) + Y'\sin(2\pi f_o t + \theta + \beta_y) + Z'\sin(2\pi f_o t + \theta + \beta_z) \qquad \text{B.2}$$

where X', Y' and Z' differ from X. Y and Z respectively, due to attenuation in the cable

β_x, β_y and β_z are phase terms caused by the propagation delay in the cable from the particular point to the receiver.

Assume that a target enters the detection zone at point X. The total receiver signal will now be

$$V_{RT}(t) = (X'+\Delta X')\sin(2\pi f_o t + \theta + \beta_x) + Y'\sin(2\pi f_o t + \theta + \beta_y) + Z'\sin(2\pi f_o t + \theta + \beta_z) \quad \text{B.3}$$

The change in received signal due to the presence of the target is

$$V_{RT} - V_R = \Delta X'\sin(2\pi f_o t + \theta + \beta_x) \quad \text{B.4}$$

In Section 7 $V_{RT} - V_R$ is referred to as the target vector V_T and $\Delta X'$ is given the symbol ΔM_X.

Appendix C

LIST OF PERSONNEL

Principal Investigators	Dr. J.L. Mason Dr. N.A.M. Mackay
Research Associates	Mr. D.J. Clarke Mr. A. Benjamin
Graduate Students	M. Woollam D. Ridding A. Benjamin
Research Assistant	B. Ross
Administrative Assistant	D.T. Kennedy

MISSION
of
Rome Air Development Center

RADC plans and executes research, development, test and selected acquisition programs in support of Command, Control Communications and Intelligence (C^3I) activities. Technical and engineering support within areas of technical competence is provided to ESD Program Offices (POs) and other ESD elements. The principal technical mission areas are communications, electromagnetic guidance and control, surveillance of ground and aerospace objects, intelligence data collection and handling, information system technology, ionospheric propagation, solid state sciences, microwave physics and electronic reliability, maintainability and compatibility.

Printed by
United States Air Force
Hanscom AFB, Mass. 01731

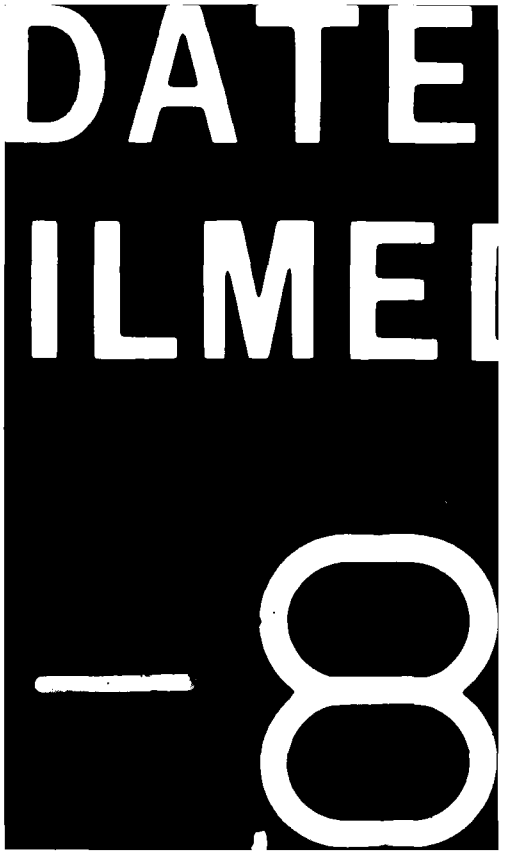
DATE
ILME
8